POLITECNICO DI MILANO
Department of Civil and Environmental Engineering
Doctoral Program in Environmental and Infrastructure Engineering


# Development of a multi-scale modeling system for urban air quality assessment: case study over the Milan area

Doctoral Dissertation of:
**Nicola Pepe**

Advisor:
**Prof. Giovanni Lonati**

Co-advisor:
**PhD Fulvio Amato**

Tutor:
**Ing. Guido Pirovano**

2018 - XXIX Cycle

# Contents

# Acknowledgements

Al Prof. Giovanni Lonati, per avermi proposto di iniziare questo nuovo percorso e accompagnato cercando sempre di migliorare le mie capacità attraverso critiche e buoni consigli. Grazie per avermi lasciato la libertà di agire secondo le mie idee, ascoltando però ogni mio dubbio in caso di necessità. Grazie per la sincerità e la schiettezza di questi anni. Grazie per le cose che mi ha insegnato e per quelle che, spero, mi vorrà ancora insegnare. Grazie per la confidenza, facendomi sentire uno della sua famiglia fin dall'inizio. Grazie per le risate, per le discussioni frivole su qualsiasi sport e per il Lego. Grazie per la passione che mette nel suo lavoro, alimentando di fatto anche la mia. Sarò sempre grato per tutto questo.

Al Politecnico di Milano per avermi concesso la possibilità di coltivare le mie passioni in questo triennio (2014-2017), mettendomi a disposizione tutti gli strumenti possibili e senza mai ostacolare il mio percorso. Un grazie particolare a Ruggero Tardivo per l'affiancamento sincero per tutte le pratiche di laboratorio.
Al centro di Ricerca sul Sistema Energetico (RSE), presso il quale ho svolto il mio dottorato e che ha finanziato la borsa di studio che mi ha permesso di portare avanti gli studi scientifici e confrontarmi con altre realtà che altrimenti non avrei mai potuto osservare

A Guido Pirovano, mio "tutor aziendale" in RSE che ha seguito ogni mio passo da quando sono entrato, formandomi sia dal punto di vista scientifico che umano. Grazie per l'entusiasmo coinvolgente, per la tua conoscenza messami a disposizione, per la correttezza, per l'umanità dimostratami e per tutti gli insegnamenti di questi anni.

Ai colleghi di RSE che hanno saputo con una parola di conforto o con una battuta, aiutarmi ad andare avanti sia nella mia vita privata che professionale. Grazie ai colleghi di ufficio Anna e Goffredo che mi hanno consigliato come se fossi un loro figlio. Grazie a tutti i ragazzi, Alessandra, Silvia, Filippo, Dario, Aberto, Andrea, Simone, Roberto, Federica, Carlo, Francesca, Houry, Paola

All'Agenzia Mobilità Ambiente Territorio di Milano che ha messo a disposizione le sue preziose risorse per poter svolgere le campagne di misure sulla risospensione del particolato in totale sicurezza. Un grazie particolato va a Marco Bedogni, per l'affiancamento tecnico e pratico a queste campagne, quanto mai indispensabile per la riuscita finale dell'attività sperimentale. Grazie per la sincerità, per la verità e per la simpatia che non mai è mancata nel nostro rapporto. Grazie per avermi mostrato tutta la passione per gli argomenti trattati

Al Dr. Fulvio Amato, per l'avermi dato fiducia e per il supporto economico nella realizzazione delle campagne di misura su Milano sulla risospensione stradale, facendomi sentire sempre coinvolto e parte integrante del progetto. Grazie per il supporto, per la disponibilità e per l'avermi mostrato tutto il tuo entusiasmo e passione per il tuo lavoro. Un grazie particolare anche al Dr. Elio Padoan per i preziosi suggerimenti durante le attività di campo e per la continua disponibilità

All'Istituto per la valutazione ambientale e la ricerca sull'acqua (IDAEA) del Consiglio Spagnolo per la Ricerca Scientifica (CSIC) per l'ospitalità e la gentilezza nel prestarmi tutte le attenzioni necessarie durante il soggiorno a Barcellona.

To Prof. Grazia Ghermandi (Università degli studi di Modena e Reggio Emilia) and Dr. Stijn Jansenn (Flemish Institute for Technological Research – VITO) for their precious contributions and advices in reviewing my final version of the PhD thesis.

Agli amici dell'università che mi hanno supportato durante queste percorso, aiutandomi e sopportandomi nei momenti in cui il morale non era dei migliori

Agli Amici Alessandro, Andrea, Michele, Daniele, Valentina e Sara per la presenza costante e incondizionata nonostante il tempo sottratto. Grazie per i momenti spensierati e le risate per aver reso più leggero questo percorso.

Alle mia grande famiglia distribuita su tutto lo stivale, sempre pronta ad incoraggiarmi.

Ai miei genitori Rosaria e Matteo, per avermi insegnato i valori del sacrificio e del lavoro. Grazie per non avermi mai fatto mancare nulla, per aver avuto sempre fiducia in me e per avermi sostenuto incondizionatamente nelle mie scelte. Grazie per avermi donato il valore della libertà.

A Sara, la persona più importante della mia vita. Hai portato la felicità nella mia esistenza rendendomi un uomo più completo. Il tuo supporto incondizionato ha portato serenità nei momenti più difficili. La tua forza è stata la mia forza.

# Abstract

In the last decades, air pollution become one of the main issues that affected modern society. Despite a progressive reduction of pollutant emissions, the state of air quality in some countries, including Italy, overcome limit thresholds, even though the constant growth of the world population and the related needs (transport, electricity and food). Air quality alteration is mainly due to emissions and meteorology. Emissions can be both natural (sea salt, saharian dust and resuspension) and anthropogenic (transport, residential heating and agriculture), while the local anemological regime (wind speed and direction) and the atmospheric stability conditions are the most important meteorological variables that can significantly influence atmospheric dispersion and therefore modify the air quality. The World Health Organization and a large number of medical studies confirmed that air pollution exposure is one of the causes of premature death in both adults and children. The ever-increasing attention to the problem led to an ever-increasing development of the chemical-physical processes knowledge that involve both primary and secondary pollutants and, consequently, the technologies to evaluate and mitigate it.

Particularly, Po Valley has always been affected by continuous exceeding of the thresholds, especially during winter time, for particulate matter (PM10 and PM2.5), determining a harmful situation for public health over the whole territory. Exceedances are mainly due to two factors: 1) high concentration of dust emission sources over an area strongly disadvantaged in terms of atmospheric dispersion, due to the weak exchange of air masses caused by Alps 2) very low wind speeds and frequent thermal inversions that favor the atmospheric stagnation of pollutants for shorter or longer periods.

Atmospheric modelling is one of the most suitable tools for studying the state of air quality and, above all, for estimating the energy scenarios and/or environmental policies impacts. The models that are usually used are: a) meteorological models b) chemistry and transport models; both run on different spatial scales, starting from the global one up to the local one, with a higher spatial resolution.

The main goal of this PhD, developed at the Research on the Energy System center (RSE), was to develop a new modeling tool able to estimate air pollution levels in a complex urban areas, considering local scale features (determined, for example, by the presence of roads with different traffic levels) as the larger-scale phenomena whose contributions are equally detectable. The modelling chain is composed by the meteorological model Weather and Forecast Research (WRF), the eulerian model of chemistry and transport at the regional scale Comprehensive Air Quality Model with Extensions (CAMx) and the Lagrangian model at local scale AUSTAL2000. The coupling of regional and local models derives from the inability of the former to work with high resolutions (typically greater than 1 km) and the lack in the second one, both of a chemical treatment of pollutions and contributions of sources located outside the local domain. Both regional and local phenomena (chemical and physical) are treated appropriately in order to obtain reliable estimates of concentrations over urban areas.
The hybrid modelling system was run over the whole Po Valley and in particular, over the city of Milan, the northern Italy metropolis with a daily people flow over 2 millions.

The first work of the three-year PhD program was focused on estimating the NOx concentration levels over a 1.6x1.6 km2 domain with a spatial resolution of 20 m, centered on Piazza del Duomo, for the whole year of 2010, both through the hybrid modelling system and the CAMx stand-alone apllication. The contribution generated by sources located outside the domain was estimated through a simulation over the metropolitan area of Milan, with a resolution of 1.7 km, nested into a domain covering the Po valley domain with 5 km grid step size.
By means of hybrid system, the double counting of emissions on the local domain was avoided thanks to the PSAT algorithm implemented within the CAMx code. PSAT allowed determining two distinct emissive areas: 1) the innermost one ("local") corresponding to the simulation domain 2) the whole area outside the local domain ("background"). Taking into account emissions over local domain by AUSTAL2000 and only background emissions for CAMx, the total concentrations was properly estimated.
The most important result achieved by the application of the hybrid modelling system was a more accurate reproducion of the concentration levels distribution over the local domain, with higher values on busiest road sections, also taking into account the presence of buildings. The overall performance of the hybrid modelling system did not see

significant improvements compared to the CAMx stand-alone approach during comparison with the observations at the two air quality stations located within local domain. Despite bias decreased of 6 and 8 ppb (12% and 13% of the observed annual average) respectively, at Senato and Verziere AQ stations, the correlation between the concentrations time series decreased about 2% at both stations. This worsening could be ascribed to the concentration peaks produced by AUSTAL2000 during atmospheric stability conditions occurred during the night. Results showed a lack of efficiency in considering some local scale features (e.g: urban canyon), indicating that both the temporal modulation and the spatial distribution of emissions should be improved.

The second work focused on source apportionment analysis, estimating the source categories and emissive areas contributions at an urban receptor located in Piazza del Duomo in Milan, by CAMx regional scale model. The analysis considered four pollutants: fine particulate matter (PM2.5), whose annual limit exceeded frequently during last years over the whole Po Valley, one of its primary components, the elemental carbon (EC), and a secondary one, the nitrate ion, (NO3-), and a gas, with a specific air quality threshold, the nitrogen dioxide (NO2), never evalutated before by this approach. The 11 emission categories represented the typical sources over the domain, including vehicular traffic (divided into 4 sub-categories: cars, light and heavy commercial vehicles and motorcycles), agriculture and residential heating (powered by biomass and with other fuels). The source apportionment analysis relied on 5 emissive regions: starting from a local domain, centered over Piazza del Duomo, we moved to the municipality of Milan, to the metropolitan area of Milan (Province), to the Lombardy region and finally to the whole Po Valley.

PM2.5 results showed a dishomogeneity in the spatial distribution of contributions, where more than 50% of the contributions was generated far away from the receptor of Piazza del Duomo (Lombardy region and the Po Valley area). Focusing on the emission sources, the most impactful were transports, which contributed for 28% to the PM2.5 annual average, and the biomass burning in residential heating, with a percentage contribution of 24%. The simulations for PM2.5 components highlighted completely opposite situation. Its primary component, elemental carbon, derives mainly from the local area and from sources near the receptor; the local and urban background sources generated 73% of the final concentration (60% due to the city and its metropolitan area). The

combination of transport and biomass burning contributions were again predominant, resulting in more than 80% of the final concentration. Conversely, about the secondary component, nitrate ion, the large part of contributions (more than 80%) were caused by emissive areas far away from receptor (Lombardy and the Po Valley areas) and only transports provided the most important contribution (43% of the total concentration) with almost the half part generated by heavy duty vehicles.

The results obtained for nitrogen dioxide showed the main role of emissions from metropolitan area of Milan (including the city itself), that contributed for about 60%. However, the local area effects (almost 10% of total concentration) were relevant even tough the number of sources were negligible if compared to the sources located over the metropolitan area of Milan. Transport sector was the main source, generating more than 70% of the total concentration over the whole year.

These results could be useful for supporting the evaluation of environmental scenarios both at local and regional level. However, since a validation of this tool was necessary, PM2.5 results were compared to the measures at Torre Sarca, in Milan, in 2013 in the framework of the AIRUSE project, led by Fulvio Amato, both at chemical speciation level and impact of the different sources, reconstructed by receptor models.

Similarly to previous work, the source apportionment analysis was also performed by the hybrid modelling system, considering only fine particulate matter and elemental carbon. The evaluation involved 3 urban receptors (high traffic exposure, urban park and residential area) in order to highlight the hybrid modelling system capabilities, and in particular AUSTAL2000, to capture some key features of the urban context.

As expected, the analysis of CAMx stand-alone results at 3 urban receptors did not showed relevant variations about concentration levels nor in their emission sources distribution. CAMx model was not able to evaluate the variability of an urban environment and generated similar results over the local domain. Conversely, hybrid modelling system led to a clear difference of both concentration levels and emission sources distribution. To better understand differences between hybrid modelling system and CAMx, only the contributions of local sources were analyzed. High traffic exposure receptor showed concentration levels 3 and 4 times higher respectively, at the residential and urban park site, both for PM2.5 and EC, regardless the period. Also the ratio between estimated concentrations for the residential and urban park sites was close to 2 throughout

the year and for both pollutants. Relevant discrepancies were also found between emission sources distributions: transport sector was the main source at the traffic site (if compared to residential heating), while at urban park site biomass burning reached an equal weight. Adding the contributions generated by other sources (located outside the local domain), these differences were appreciable but dampened, especially at the traffic receptor.

During the last period of the PhD and parallely to the model development, an experimental campaign was performed in order to study the particulate matter resuspension from road traffic. This experimental work, originally not contemplated in the research activity, relied on constant PM underestimation by the models and the lack of a deep characterization of the resuspension emission factors. These issues suggested two distinct experimental campaigns: 1) estimating the dust recharge rate on the road after a rainy event 2) estimating the impact of vehicle fleet composition and speed on resuspension emission factor. This experience was made possible thanks to the the instrumentation, specially developed in previous campaigns, and scientific support by Dr. Fulvio Amato and the his research group of the IDEA (Instituto Diagnostico Ambiental y Estudios del Agua) of Barcelona, and the precious collaboration by Marco Bedogni of the environmental and mobility agency of Milan (AMAT).

The first campaign took place between October 2016 and March 2017 with a sampler able to detect the silt load deposited over the road surface with a flow rate of 30 l/min on a quartz filter. Operationally, the filters were left in the climatic chamber for about 2 weeks in order to remove the residual moisture and weighed on a 5 precision digits balance.
In order to better characterize the recharge rate, it was necessary to intensify the sampling frequency since the end of the rainy event, 8 samplings during the first day, to arrive at a 1 sampling on the fifth day. Despite the numerous problems occurred during the campaign, only two suitable events for the gravimetric determination phase were captured. However, measures showed a logarithmic trend representin the phenomenon, with a rapid growth during the first hours after the rainy event reaching the maximum value after about 48 hours. To make the analysis and results more robust, it would be necessary to complete the database with other suitable rainy events.

The second campaign, carried out during the last months of PhD, focused on the estimation of a PM emission factor due to road traffic relied on vehicles types travelling on the road arch and their speed. The measurement campaign was divided into two parts, both with an exposure time of two weeks, considering the speed variation due to the installation of speed cameras. In order to obtain information on the effect of the different vehicle classes on resuspension, the experimental campaigns were conducted simultaneously along three different Milan roads (Via Parri, Via dei Missaglia and Via Ferrari).

The resuspended mass was captured by passive samplers installed on light poles positioned between the two carriageways or on the side of the road. For each road an array of three passive samplers were installed at different heights capturing lighter particles (higher samplers) and heavier ones (lower samplers). After the exposure period, passive samplers were collected and taken to the laboratory for a first phase of washing and collection of the PM mass on quartz filters and a second drying phase in the climatic chamber and final weighing.

The results obtained on Via dei Missaglia and Via Ferrari showed a reduction of the resuspended mass, correlated with a reduction of travelling speed, in the lower samplers, while on the higher ones the mass was similar. Data analyzed on Via Parri showed a substantial increase in the resuspended mass probably due by an incorrect position of passive samplers, too close to a guardrail. However, a construction site not foreseen during the second campaign made the experiment invalid.

# Sommario

Negli ultimi decenni l'inquinamento atmosferico è diventato uno dei principali problemi con il quale la società moderna si è dovuta confrontare. Nonostante una progressiva diminuzione delle emissioni in atmosfera degli inquinanti, contrapposta ad una crescita costante della popolazione mondiale e delle relative necessità (trasporto, energia elettrica e alimentazione), lo stato attuale di qualità dell'aria in alcuni paesi, tra cui l'Italia, non riesce a soddisfare i limiti normativi. Le cause che concorrono all'alterazione della qualità dell'aria sono sia di tipo emissivo che meteorologico. Le emissioni che insistono su un territorio possono essere sia di tipo naturale (sale marino, dust sahariano e risospensione) che antropogenico (trasporti, riscaldamento e agricoltura), mentre le caratteristiche del regime anemologico locale (velocità e direzione del vento) e le condizioni di stabilità dell'atmosfera sono tra le più importanti variabili meteorologiche in grado di influenzare sensibilmente la dispersione atmosferica e quindi di modificare lo stato di qualità dell'aria. L'organizzazione Mondiale della Sanità e un gran numero di studi medici hanno confermato che l'esposizione all'inquinamento atmosferico è una delle cause di morte prematura sia negli adulti che nei bambini. L'attenzione sempre crescente verso il problema ha perciò portato ad uno sviluppo sempre maggiore della conoscenza dei processi chimico-fisici che coinvolgono gli inquinanti sia di tipo primario che di tipo secondario e, conseguentemente, delle tecnologie per valutarlo e arginarlo.

In particolare, il bacino padano è da sempre interessato da continui superamenti dei limiti normativi, soprattutto nel periodo invernale, per il particolato atmosferico (PM10 e PM2.5) determinando una situazione particolarmente dannosa per la salute pubblica di tutto il territorio. Le cause di questi superamenti risiedono principalmente in due fattori: 1) un'elevata concentrazione delle sorgenti di emissione di polveri in un'area fortemente svantaggiata dal punto di vista della dispersione atmosferica per il debole ricambio delle masse d'aria determinato dalla cortina montuosa delle Alpi 2) velocità del vento molto basse e frequenti inversioni termiche, non aiutano la dispersione e, al contrario, favoriscono la stagnazione atmosferica degli inquinanti per periodi più o meno lunghi

La modellistica atmosferica rappresenta uno degli strumenti più adatti a studiare lo stato di fatto della qualità dell'aria e, soprattutto, per stimare gli impatti di possibili scenari di sviluppo energetico e/o di politiche di controllo dell'inquinamento atmosferico. I modelli che vengono solitamente utilizzati sono: a) modelli meteorologici b) modelli di chimica e trasporto; entrambi agiscono su scale spaziali diverse, a partire da quella globale fino ad arrivare a quella locale, con una risoluzione spaziale e un dettaglio sempre maggiori.

L'obiettivo di questo dottorato di ricerca, sviluppato presso il centro di Ricerca sul Sistema Energetico (RSE), è stato quello di sviluppare un nuovo strumento modellistico in grado di stimare i livelli di inquinamento in ambito urbano considerando, tanto le caratteristiche di un ambiente così eterogeneo dal punto di vista emissivo (determinato, ad esempio, dalla presenza strade con diverse intensità di traffico) quanto i fenomeni a più larga scala i cui effetti ricadono, anche con una certa intensità, a distanza di chilometri dal punto di emissione. La catena dello strumento modellistico è composta dal modello meteorologico Weather and Forecast Research (WRF), dal modello euleriano di chimica e trasporto a scala regionale Comprehensive Air Quality Model with Extensions (CAMx) e dal modello lagrangiano di diffusione a scala locale AUSTAL2000. L'esigenza di un accoppiamento del modello a scala regionale con quello a scala locale deriva dall'incapacità del primo di poter lavorare con risoluzioni elevate (tipicamente è opportuno operare con risoluzioni maggiori di 1 km) e dall'assenza nel secondo, sia di un modulo chimico che tenga conto delle reazioni in atmosfera che di informazioni sui contributi delle sorgenti poste al di fuori del dominio locale. In questo modo, ogni aspetto legato sia ai fenomeni regionali che locali di chimica e trasporto degli inquinanti viene trattato adeguatamente al fine di ottenere stime di concentrazioni in ambito urbano sempre più affidabili.
Il sistema modellistico ibrido è stato applicato sull'intero bacino padano e in particolare sulla città di Milano, metropoli del nord Italia con un flusso medio giornaliero di persone superiore a 2 milioni.

Il primo lavoro del percorso triennale di dottorato ha visto la stima dei livelli di concentrazioni di NOx su un dominio di 1.6x1.6 $km^2$ con una risoluzione spaziale di 20 m, centrato su Piazza del Duomo, per l'intero anno del 2010, sia attraverso il sistema modellistico ibrido sia tramite l'applicazione del solo modello CAMx. Il contributo delle

sorgenti localizzate al di fuori del dominio è stato calcolato attraverso una simulazione sull'area metropolitana di Milano, con una risoluzione di 1.7 km, innestata in un dominio che ha ricoperto l'intera pianura padana, in cui la simulazione ha una risoluzione di 5 km. Utilizzando il sistema ibrido, il doppio conteggio delle emissioni sul dominio di simulazione è stato evitato grazie all'algoritmo PSAT implementato all'interno del codice di CAMx, con il quale è stato possibile determinare due aree emissive distinte: 1) una più interna ("locale") corrispondente al dominio di simulazione 2) tutta l'area esterna al dominio di simulazione ("di fondo"). Considerando la parte emissiva locale stimata per AUSTAL2000 e solo quella dell'area più esterna stimata per CAMx, il contributo delle sorgenti locali non è stato conteggiato due volte.
Il risultato più importante raggiunto dall'applicazione del sistema ibrido è stato quello di ottenere una rappresentazione più accurata della distribuzione dei livelli di concentrazione sul dominio locale, con valori più elevati in corrispondenza dei tratti stradali più trafficati, anche tenendo conto inoltre degli effetti determinati dalla presenza degli edifici. In ogni caso, le prestazioni generali del sistema ibrido non hanno visto notevoli miglioramenti rispetto al semplice utilizzo del modello a scala regionale CAMx quando si sono confrontati i risultati modellistici con i valori di concentrazione rilevati nelle due stazioni di misura della qualità dell'aria presenti nel dominio locale. Nonostante lo scarto per la media annuale sia diminuito di 6 e 8 ppb (12% e 13% della media annuale osservata) rispettivamente nella stazione di Senato e Verziere, la correlazione tra le serie temporali delle concentrazioni è diminuita di circa il 2% in entrambe le stazioni. Questo peggioramento è stato causato dai picchi di concentrazione prodotti da AUSTAL2000 durante la notte, in condizioni di stabilità atmosferica. I risultati hanno mostrato inoltre una scarsa efficienza nel considerare alcune caratteristiche della scala locale (come le strutture a canyon urbano), indicando che tanto la modulazione temporale quanto la distribuzione spaziale delle emissioni devono essere oggetto di miglioramento.

Nel secondo lavoro si è affrontato il tema del ruolo delle sorgenti, stimando i contributi delle diverse categorie ed aree emissive ad un recettore urbano localizzato in Piazza del Duomo a Milano, attraverso l'utilizzo del modello a scala regionale CAMx. L'analisi si è focalizzata su quattro inquinanti: il particolato fine (PM2.5), il cui limite annuale è stato superato frequentemente negli ultimi anni su tutto il territorio del bacino padano, una sua componente primaria, il carbonio elementare (EC), e una secondaria, lo ione nitrato,

($NO_3^-$), ed infine su un gas oggetto di uno specifico limite di qualità dell'aria, il biossido di azoto ($NO_2$), mai studiato prima d'ora con questo tipo di approccio. Le 11 categorie emissive prese in esame rappresentano tutte le possibili sorgenti che insistono sul territorio, tra cui il traffico veicolare (diviso nelle 4 sottocategorie: autovetture, veicoli commerciali leggeri e pesanti e moto), l'agricoltura e il riscaldamento residenziale (alimentato con biomassa e con altri combustibili). L'analisi dei contributi è stata condotta anche su base areale, ed in particolare facendo riferimento a 5 regioni emissive: partendo da un dominio locale, centrato su Piazza del Duomo, si è passati al comune di Milano, all'area che corrisponde alla città metropolitana di Milano, all'intera regione Lombardia ed infine a tutto il bacino padano.

I risultati ottenuti per il PM2.5 hanno mostrato una disomogeneità nella distribuzione spaziale dei contributi, attribuendo più del 50% dei contributi alle sorgenti poste più lontano dal recettore di Piazza del Duomo, ovvero alle aree emissive della regione Lombardia ed al restante territorio della pianura padana. Concentrandosi sulle sorgenti emissive, le più impattanti sono risultate i trasporti, che contribuiscono per il 28% alla media annua di PM2.5, e la combustione della biomassa nel riscaldamento residenziale, con un contributo percentuale del 24%. Le simulazioni condotte per le due componenti del PM2.5 hanno evidenziato situazioni del tutto opposte. La sua componente primaria, il carbonio elementare, deriva principalmente dall'area locale e dalle sorgenti prossime al recettore; infatti la somma dei contributi di queste sorgenti arriva fino al 73% sulla concentrazione finale (il 60% causato dall'area della città metropolitana di Milano e dalla città stessa). La combinazione dei contributi dei trasporti e della combustione della biomassa si è rivelata ancora quella preponderante, arrivando a determinare più dell'80% della concentrazione finale. Al contrario, per la componente secondaria, il nitrato, si nota che la maggior parte dei contributi (più dell'80%) proviene dalle aree emissive più lontane dal recettore (regione Lombardia e bacino padano) e che il settore dei trasporti, da solo fornisce il contributo più importante, determinando il 43% della concentrazione totale con in particolare, circa il 20% del nitrato totale stimato al recettore di Piazza del Duomo determinato dai veicoli commerciali pesanti.

I risultati ottenuti per il biossido di azoto mostrano il ruolo principale delle emissioni dall'intera città metropolitana di Milano, compresa la città stessa, che complessivamente contribuiscono per circa il 60%. Tuttavia, particolarmente rilevante è anche l'effetto dell'area locale, che genera circa il 10% della concentrazione totale, nonostante il numero

di sorgenti sia nettamente inferiore rispetto a quelle che si può trovare nelle aree emissive del comune e della città metropolitana di Milano. I trasporti risultano essere la sorgente principale, generando più del 70% della concentrazione totale sull'intero anno.
I risultati di questa applicazione potrebbe essere di grande interesse e di supporto per la valutazione di ipotetici scenari ambientale sia a livello locale che regionale. In ogni caso, una validazione di questo strumento è necessaria e per questo motivo i risultati del PM2.5 sono stati confrontati con i dati osservati a Torre Sarca, a Milano, nel 2013 nel contesto del progetto AIRUSE, condotto da Fulvio Amato, sia a livello di speciazione chimica che di impatto delle diverse sorgenti, ricostruite attraverso l'utilizzo di modelli a recettore.

Analogamente a quanto svolto nel precedente lavoro, lo studio del ruolo delle sorgenti è stato condotto anche tramite l'applicazione del sistema modellistico ibrido, sviluppando la valutazione caso per il particolato fine e per il carbonio elementare. La valutazione ha interessato 3 tipologie di recettori urbani (elevata esposizione al traffico, parco urbano e zona residenziale) per evidenziare le capacità del sistema ibrido, ed in particolare della sua componente modellistica alla scala locale AUSTAL2000, di catturare alcune delle caratteristiche di un ambito eterogeneo come quello urbano.
Infatti, l'analisi dei risultati dell'applicazione di CAMx per la valutazione del ruolo delle sorgenti nei 3 recettori urbani non sono state evidenziate particolari variazioni nei livelli di concentrazione né tantomeno nella loro distribuzione, in termini di sorgenti emissivi. Il modello a scala regionale CAMx, non potendo lavorare a scale spaziali inferiori ad 1 km, non è stato in grado di valutare la variabilità di un ambito urbano ed ha generato un risultato in simile in tutti i recettori. L'applicazione del sistema ibrido ha portato invece ad una netta diversificazione sia dei livelli di concentrazione che dei singoli contributi. Per meglio comprendere le differenze fra il sistema ibrido e CAMx, sono stati analizzati solo i contributi delle sorgenti localizzate nel dominio locale. Il recettore posizionato in corrispondenza di un incrocio trafficato ha presentato livelli di concentrazione in media 3 e 4 volte più alti rispettivamente al sito residenziale e a quello localizzato nel parco, sia per il PM2.5 che per il EC, indipendentemente dal periodo. Anche il rapporto fra le concentrazioni stimate per il sito residenziale per quello urbano è prossimo a 2 durante tutto l'anno e per entrambi gli inquinanti. Importanti differenze sono state riscontrate anche fra i contributi delle diverse sorgenti, molto più elevati quello dei trasporti nel sito da traffico rispetto al riscaldamento, fino ad arrivare ad un sostanziale equilibrio nella

zona del parco urbano. Aggiungendo i contributi derivanti da tutte le altri sorgenti poste al di fuori del dominio locale, tali differenze sono state smorzate rimanendo tuttavia apprezzabili, soprattutto in corrispondenza del recettore da traffico.

Parallelamente alla parte di sviluppo modellistico, è stato possibile condurre durante l'ultimo periodo del dottorato, un lavoro sperimentale sul campo per lo studio del fenomeno di risospensione di polveri da traffico stradale. Tale lavoro sperimentale, originariamente non contemplato nell'attività di ricerca, ha trovato motivazione nella costante sottostima del particolato atmosferico da parte dei modelli e nella mancanza di una precisa caratterizzazione dei fattori di emissione di risospensione. Queste lacune hanno suggerito di condurre due campagne sperimentali distinte aventi come obiettivo: 1) la stima del rateo di ricarica delle polveri sul manto stradale dopo un evento piovoso 2) la stima del fattore di emissione delle polveri da risospensione dipendente dal tipo di flotta veicolare e al variare della velocità di percorrenza. Questa esperienza è stata possibile grazie al supporto scientifico ed alla strumentazione, appositamente sviluppata in precedenti campagne, messa a disposizione dal Dottor Fulvio Amato e dal gruppo di ricerca dell'IDAEA (Instituto Diagnostico Ambiental y Estudios del Agua) di Barcellona, e dalla preziosa collaborazione di Marco Bedogni dell'Agenzia Mobilità Ambiente Territorio di Milano.

La prima campagna di misura si è svolta tra ottobre 2016 e marzo 2017 con un campionatore in grado di aspirare lo strato di polvere creatosi sul manto stradale con una portata di 30 L/min e farlo depositare su un filtro posto al termine del campionatore. Operativamente, i filtri sono stati lasciati in camera climatica per circa 2 settimane per eliminare l'umidità residua e successivamente pesati su una bilancia con 5 cifre di precisione.
Al fine di caratterizzare al meglio il fenomeno di ricarica stradale, è stato necessario intensificare la frequenza dei campionamenti sin dal termine dell'evento piovoso, circa 8 durante il primo giorno, per arrivare ad effettuare un solo campionamento al quinto giorno. Nonostante le numerose problematiche sopraggiunte durante l'intera campagna, è stato possibile catturare solo due eventi idonei alla fase di determinazione gravimetrica dei filtri. In entrambi i casi però si è potuto notare il medesimo andamento logaritmico a saturazione del fenomeno, con una rapida crescita durante le prime ore dopo l'evento

piovoso per arrivare al massimo valore dopo circa 48 ore. Per rendere più robusta l'analisi e i risultati sarebbe necessario completare la base di dati con altri eventi piovosi idonei per il campionamento.

La seconda attività sperimentale, condotta proprio nei mesi conclusivi del dottorato, si è concentrata sulla stima di un fattore di emissione del particolato risospeso dal traffico stradale che dipendesse sia dalla tipologia di traffico veicolare transitante sull'arco stradale che dalla sua velocità di percorrenza. La campagna di misura è stata divisa in due parti, ognuna con un tempo di esposizione di circa due settimane, per considerare la variazione di velocità causata dall'installazione di limitatori di velocità (autovelox). Al fine di ottenere indicazioni sull'effetto delle diverse classi veicolari sulla risospensione, le due campagne di misura sono state condotte contemporaneamente lungo 3 strade di Milano diverse fra loro (Via Parri, Via dei Missaglia e Via Ferrari) sia per velocità di percorrenza che per composizione del traffico.
La massa risospesa è stata catturata da campionatori passivi installati su pali della luce posizionati al centro strada, fra le due carreggiate, o a bordo strada. Per ogni strada sono stati installati tre campionatori passivi a diverse altezze per catturare sia le particelle più leggere (campionatori più alti) sia quelle più pesanti (campionatori più bassi). Dopo il periodo di esposizione, i campionatori passivi sono stati raccolti e portati in laboratorio per una prima fase di lavaggio e raccolta del materiale depositatosi sui piattelli attraverso dei filtri in fibra di quarzo e una seconda fase di asciugatura in camera climatica dei filtri e pesatura finale della massa risospesa.
I risultati ottenuti sui tratti stradali di Via dei Missaglia e Via Ferrari hanno mostrato una riduzione della massa risospesa, correlata ad una riduzione della velocità di percorrenza, nei campionatori posizionati più in basso mentre su quelli più in alto la massa misurata è stata la stessa se non maggiore. I dati analizzati su Via Parri hanno mostrato un sostanziale aumento della massa risospesa, in controtendenza rispetto alle altre due strade, probabilmente causato da una scorretta posizione dei campionatori passivi, troppo prossimi ad un guardrail che ha impedito il corretto svolgimento dell'esperimento ma soprattutto all'inizio di un cantiere non previsto durante la campagna di misura post-autovelox che ha di fatto reso non valido l'esperimento.

# Acronyms

| Acronyms | Meaning |
|---|---|
| AQ | Air quality |
| AUS | Milan city center area |
| BB | Biomass burning factor |
| CAMx | Comprehensive Air Quality Model with Extensions |
| CTM | Chemical and Transport Model |
| EC | Elemental carbon |
| EEA | European Environment Agency |
| EF | Emission factor |
| EMEP | European Monitoring and Evaluation Program |
| HMS | Hybrid modelling system |
| IND | Industrial emission factor |
| IOA | Index of agreement |
| IR | Interquartile range |
| LOM | Lombardy region area |
| LSM | Local scale model |
| MAE | Mean absolute error |
| MB | Mean bias |
| MIL | Municipality of Milan |
| MIN | Mineral emission factor |
| NEX | Vehicle non-exhaust factor |
| OM | Organic matter |
| PMF | Positive Matrix Factorization |
| POA | Primary organic matter |
| POV | Po Valley area |

| | |
|---|---|
| PRO | Province of Milan – metropolitan area of Milan |
| PSAT | Particulate matte source apportionment technology |
| r | Correlation coefficient |
| RMSE | Root mean square error |
| SEA | Marine aerosol factor |
| SIA | Secondary inorganic aerosol |
| SM | Supplementary material |
| SNI | Secondary nitrate factor |
| SOA | Secondary organic matter |
| SSO | Secondary sulfate and organics factor |
| VEX | Vehicle exhaust factor |
| WHO | World health organization |
| WMO | World Meteorological Organization |
| WRF | Weather Research and Forecasting |

# 1. Introduction

World Health Organization (WHO) estimates 4.3 million deaths every year referable to air pollution exposure, in particular indoor exposition, in developing countries and middle income, of residential heating emissions (biomass burning, cook or other fuels combustion) through systems without any type of pollutant abatement. At the same time, 3.7 million deaths are linked to outdoor pollutant exposition. This phenomenon concerns all western European countries, United States and Australia region, notwithstanding all improvements achieved in terms of industrial and vehicular traffic emission reduction.

European Environmental Agency last estimate (2014) for Italy described more than 50 000 premature deaths caused by PM2.5 long term exposition, more than 17 000 caused by $NO_2$ long term exposition and almost 3 000 due to $O_3$.

Air pollution is not only an environmental issue, but also a social problem due to complexity of management and mitigation measures. Air pollutants can be emitted from anthropogenic sources and natural sources; they also can be emitted directly into the atmosphere (primary pollutants) and derived from chemical processes that involved precursors (secondary pollutants). Advection, diffusion, wet and dry deposition represent the principal physical phenomena that transport pollutants into the atmosphere, even far away from the emission point.

The last EEA report illustrated air quality concentrations field over EU cities for the main pollutants. Figure 1 shows the observed 90.4 percentile of PM10 over Europe during 2015. As can be noted, Po Valley region and middle-east Europe present the highest PM10 concentration levels. Focusing on Po Valley area, 90.4 percentiles values are always higher than PM10 threshold of 50 $\mu g/m^3$, indicating a critical situation in terms of maximum annual number of exceedances (35 days). Many papers addressed this issue and studied both local and regional meteorological phenomena and emission sources located over the domain. (Meroni et al, 2017, Squizzato et al, 2017, Pernigotti et al, 2013, Pepe et al, 2016)

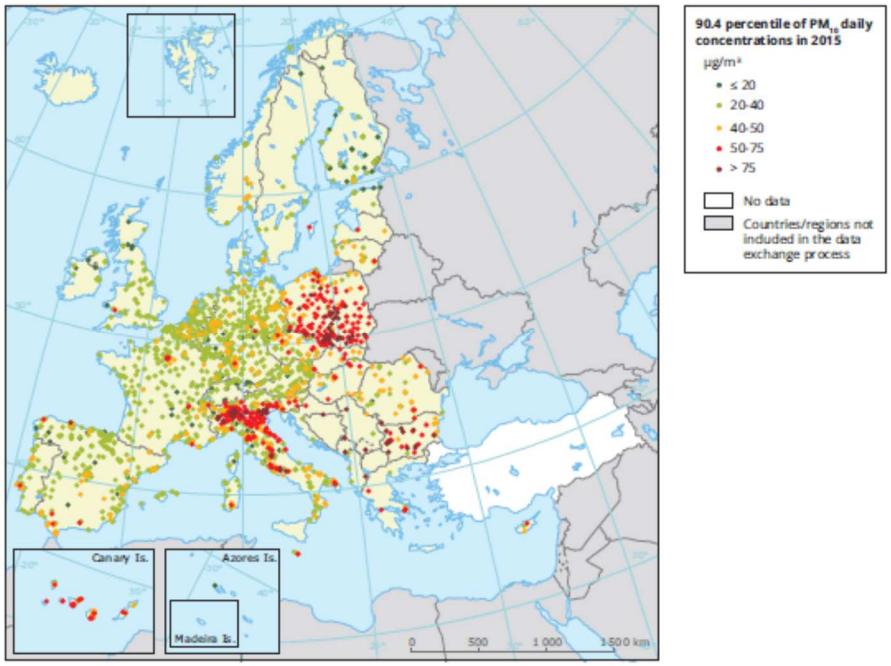


**Figure 1. Observed concentrations of PM10 in 2015. The map shows 90.4 percentile of the PM10 daily mean concentration, representing the 36$^{th}$ highest value in a complete series. It is related to the PM10 daily limit value, allowing 35 exceedances of the 50 µg/m$^3$ threshold over 1 year. Only stations with more than 75% of valid data have been included in the map.**

Similarly, even PM2.5 is analyzed over a large number of EU countries. Since the limited number of stations respect to PM10, dots indicated in Figure 2 are less dense. PM2.5 concentration spatial distribution reflects quite well what observed for PM10: higher concentrations over Po Valley region and east Europe too, while all other countries are under the limit threshold of 25 µg/m$^3$. PM2.5 exceedances concern a limited area of Po Valley region, focused on the northern Italy excluding Tuscany.

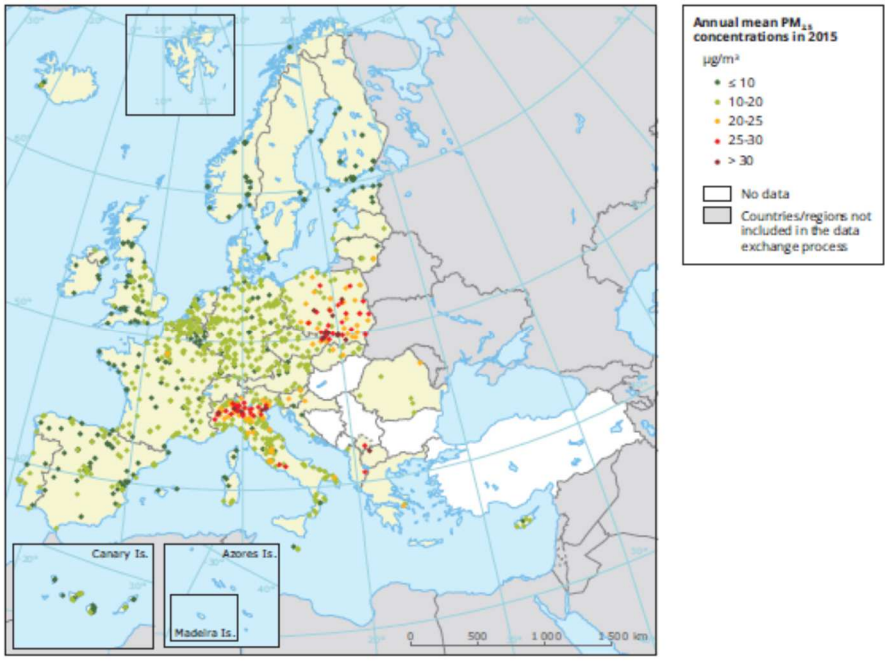


**Figure 2. Dark red and red dots indicate stations reporting concentrations above the EU annual limit value (>25 µg/m$^3$). Only stations with 75% of valid data have been included in the map**

Besides aerosols, gaseous pollutants as nitrogen dioxide, carbon monoxide or sulfur dioxide are analyzed. In Figure 3 are indicated NO2 observed annual mean concentrations over EU monitoring stations. Differently from PM concentrations, over Po Valley are not reached the EU maximum concentrations values, even though a critical situation persists. Highest concentration are measured within Germany.

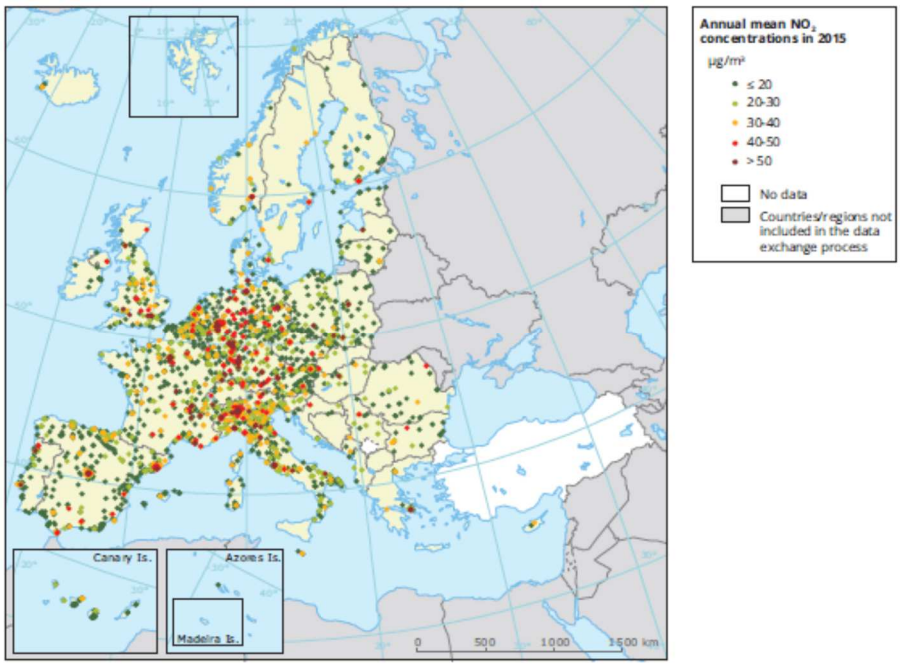


**Figure 3. Dark red and red dots indicate stations reporting concentration above EU annual limit value (> 40 µg/m$^3$). Only stations with 75% valid data have been included in the map.**

Observing coarse and fine particles and nitrogen dioxide measures, Po Valley regions is one the most polluted area within Europe. Not exclusively for this reason, European Parliament and the Council in 2008, adopted a new consolidated European Union Directive on ambient air quality and cleaner air for Europe (Directive 2008/50/EC – EC, 2008). The Air Quality Directive replaces the previous one, introducing new objectives concerning PM2.5 and the possibility of delaying the attainment of some limit values. In Figure 4 are listed target limits and limit values of pollutants presented in Air Quality Directive.

| Human health | Limit or target (a) value | | | | Time extension (c) | Long-term objective | | Information (b) and alert thresholds | |
|---|---|---|---|---|---|---|---|---|---|
| Pollutant | Averaging period | Value | Maximum number of allowed occurrences | Date applic-able | New date applicable | Value | Date | Period | Threshold value |
| $SO_2$ | Hour | 350 µg/m³ | 24 | 2005 | | | | 3 hours | 500 µg/m³ |
| | Day | 125 µg/m³ | 3 | 2005 | | | | | |
| $NO_2$ | Hour | 200 µg/m³ | 18 | 2010 | 2015 | | | 3 hours | 400 µg/m³ |
| | Year | 40 µg/m³ | 0 | 2010 | | | | | |
| Benzene ($C_6H_6$) | Year | 5 µg/m³ | 0 | 2010 | 2015 | | | | |
| CO | Maximum daily 8-hour mean | 10 mg/m³ | 0 | 2005 | | | | | |
| $PM_{10}$ | Day | 50 µg/m³ | 35 | 2005 | 2011 | | | | |
| | Year | 40 µg/m³ | 0 | 2005 (a) | 2011 | | | | |
| $PM_{2.5}$ | Year | 25 µg/m³ (a) | 0 | 2010 (d) | | 8.5 to 18 µg/m³ | 2020 | | |
| | | 20 µg/m³ (ECO) | | 2015 | | | | | |
| Pb | Year | 0.5 µg/m³ (a) | 0 | 2005 | | | | | |
| As | Year | 6 ng/m³ (a) | 0 | 2013 | | | | | |
| Cd | Year | 5 ng/m³ (a) | 0 | 2013 | | | | | |
| Ni | Year | 20 ng/m³ (a) | 0 | 2013 | | | | | |
| BaP | Year | 1 ng/m³ (a) | 0 | 2013 | | | | | |
| $O_3$ | Maximum daily 8-hour mean averaged over 3 years | 120 µg/m³ (a) | 25 | 2010 | | 120 µg/m³ | Not defined | 1 hour | 180 µg/m³ (b) |
| | | | | | | | | 3 hours | 240 µg/m³ |

**Figure 4. Limit values, target values, assessment thresholds, long-term objectives for the protection of human health listed in (EC, 2008).**

While previous directive relied on measurement for reporting and assessment, the new directive favors the use of Air Quality models coupled with measures. Even though models are considered an instrument more uncertain than measurements, they could be assumed as a tool able to recreate as close as possible the reality and all chemical/physical. There are three major reasons for using models, combined with monitoring for air quality assessment. Firstly, the spatial coverage of air quality stations is limited while modeling can cover completely the area without installing instruments; secondly, models could be applied for forecasting or to predict air quality as a result of emission scenarios (traffic reduction) or changing meteorological conditions; finally, through models could be possible to understand weights of the sources, processes and causes that determine air quality.

Obviously, models do not provide always solutions and are characterized by limitations. In particular, input requested by the models are not always available or easily acquired (emission and meteorological data). Even air quality and meteorological measures are not always available for testing modelling outcomes validity in order to accept or reject the model. Another limitation derived from the request of expert users for controlling and for

interpretation of model results. Finally, it is important highlighting that models are a detailed representation of real world through parameterization and limited processes description.

Nevertheless, models may be applied to a various application:

- assessment of the existing air quality, without replacing air quality measurements
- mitigation and planning for future air quality
- source apportionment analysis. Each application is ruled.

Assessment of existing air quality is possible only under certain conditions, in particular when concentrations are below the lower assessment threshold value, the model may be used alone for assessment. Models could be integrated with monitoring in different ways: for situations where exceedances are above the lower threshold limit, models may be in combination with measures while where exceedances are above the upper threshold value, models may be used to supplement monitoring data. Meaning of “combine” or “supplement” is not clarified, but supplement is intended that modelling is the secondary approach than measures. Last possible combination between modeling and monitoring is the “data fusion” or “data assimilation”. It means that the two datasets are combine to provide improved spatial concentration fields, through geometric means or statistical optimization methods. One of the most easy methods that could be applied is the multiple linear regression, where model concentrations are fitted to the available observations using least squares optimization.

Additionally to the assessment, Air Quality Directive states that when limit or target values are exceeded, an air quality plan is required from the Member States for the effected zone or agglomeration. This plan include longer-term air quality plan and short-term action plan regarding exceedances of alert thresholds. A cooperative air quality plan with other Member States is required for transboundary air pollution when it seen as a possible reason of exceedance. Air quality plans, following AQ Directive, is a plan to reduce the concentrations of pollutants that are in exceedance of the limit or target values. Reduction of pollutants levels are in most cases the result of reduced emissions of pollutant itself or of its precursors. Nevertheless, the complexity of atmospheric chemistry leads to non-linear reactions and sometimes a reduction of some pollutants could mean an increase of others. Modelling becomes a fundamental tool for developing air quality plans when the complexity of the problem growths, in particular when there are no evidences that caused exceedances of limit values, e.g. PM2.5 concentrations

where are involved sources located far away and other processes. This step can be easier when there is a clear source contributing the exceedance, e.g. road traffic or industrial activities. However, AQ Directive describes the main steps to follow.
Even though not directly written into the AQ Directive, source apportionment analysis is generally required in order to assess the causes of exceedances of air quality thresholds, contributions due to natural sources, re-suspended road material and salt. Since that setting up these processes everywhere could not be possible, air quality models, usually in combination with measures, could addressed this issue and became a valid methodology. Finally, source apportionment analysis constitutes an important part of any air quality assessment.

Following AQ Directive, models could be an important tool for assessing air quality where an air quality stations network is build up and where there is a lack of measurements. However, AQ Directive rules their utilization, trying to establish a priority order and avoiding that modeling becomes the only and the first instrument for air quality assessment.
Po Valley region, as described previously, presents in most cases concentration levels higher than limit threshold describing a critical situation that affects seriously human health. Modelling assessment is required by the AQ Directive even though observations network is quite extended over the entire northern Italy. Modeling can integrate actual observations with estimation values, e.g. where air quality stations are absent, but the main advantage derives from the source apportionment analysis. Through this methodology, it is possible to study and discover the contributions due to different sources. In a complex area as metropolitan area of Milan or generally northern Italy, source apportionment becomes a fundamental tool for assessment of air quality plans.

PhD thesis work is divided into two main parts: first part is focused on developing a hybrid modeling system able to reproduce air quality concentrations field over the urban context with higher resolution, while the second part relies on an experimental campaign in order to study the process of PM traffic resuspension and obtaining an estimate of emission factor.
The first part concerns the development of a modeling chain based on the meteorological model -WRF, the chemical and transport model CAMx, for regional scale modeling, and

the local scale model AUSTAL2000. The coupling of eulerian and lagrangian approach models allow deepening air quality assessment over restricted areas but with high grid step size resolution. Hybrid Modeling System (HMS) tries to tackle issues of regional and local scale model:

- CTMs are not able to simulate under 1 km of grid step size
- LSMs are not able to evaluate air quality concentrations at the regional scale

The first work with HMS evaluated NOx concentration level over urban local domain of 1.6x1.6 km2 within Milan city center with 20m grid step size. CAMx model run over two wider innermost domain, Italy and metropolitan area of Milan with respectively 15 km and 5 km grid step size, computing background concentrations for urban local domain.
Subsequently, we focused on PM2.5, EC, NO3- and NO2 source apportionment analysis over the Po Valley region. Through the developments introduced within the new version of CAMx (v6.30), it was possible evaluate contributions due to emissive regions besides usual emission sources. However, the key feature was the introduction of source apportionment analysis extended to gaseous pollutants. In particular, 11 emission source categories and 5 emissive regions were considered for source apportionment study. Finally, PM2.5 results were compared to an experimental campaign performed at Torre Sarca in 2013 in the AIRUSE+ project and to PMF factors.
After that, source apportionment analysis for PM2.5 and EC was performed by HMS. The main goal of the last work was to combine the accuracy of CAMx, concerning regional scale chemical processes, and the high performance of AUSTAL2000 within local scale domain in order to weight the contributions of the principal urban local sources, e.g. road traffic and residential and commercial heating.

During the last year and paralleling to modeling activities, two experimental campaigns were carried out. The main goal was to deepen the PM traffic resuspension processes within Milan urban context. Notwithstanding, different researches explored this phenomenon and tried to establish simple parameterization, numerical modeling needs further improvements. Thanks to collaboration of Fulvio Amato (CSIC-IDAEA), for technical and practical part, and Marco Bedogni (AMAT) for precious support during all the phases, we performed two experimental campaigns called “Direct measurements” and “Passive measurements”. The main goal of this activity was to estimate a PM traffic resuspension emission factor suitable for modeling. Direct measurement characterized

the dust load ($g/m^2$) over the street after a rainy event, following a fixed procedure by Amato. Many factors affected the road dust value hour by hour, however a typical phenomenon was discovered. The second experimental campaign focused on the estimation of emission factor of PM traffic resuspension. During two weeks of exposition, passive samplers installed on the light poles collected PM mass that was filtered and weighted for computing emission factors. Passive sampling campaigns were performed before and after the speed cameras installation over three different roads considering respectively speed and vehicular fleet composition effects.

# 2. Modelling chain setup

This chapter is focused on main parts of modeling system adopted for this PhD work and its geographical framework. In particular, description of singular components of the hybrid system will be addressed in terms of suitability for the aim of research. Overall performances will be evaluated over different spatial scales and for both gaseous and aerosols pollutants.

The hybrid modeling system (HMS) relies on two main components: the regional scale model CAMx and the local scale dispersion model AUSTAL2000. The modelling system also includes the Weather Research and Forecasting (WRF) meteorological model and the SMOKE emission model. Interactions between all models are shown in the flow chart of Figure 5. All models and tools implemented in the modelling chain relied on open source codes. The modelling system presents two main features:

- CTM and LSM input data consistency, i.e.: the two models share the same meteorological and emission data;
- Thanks to a source apportionment algorithm implemented in the chemical and transport model (CTM) the local sources' contribution is accounted for only by the local scale model (LSM), in order to avoid emissions double counting.

Chemical schemes are implemented into CAMx and cover an important role overall at the basin scale; conversely, at the local scale the correct quantification of the dispersion phenomena is more important in order to compute properly backlog events, key features concerning exposition levels within urban areas. Thanks to its LSM component the HMS can accurately reproduce the spatial pattern of emission sources and reconstruct the spatial variability of pollutants concentrations. Thus, for example, the HMS is helpful to define critical zones for urban pollution and to assess the impact of air quality control policies, as the introduction of "Low Emission Zone" (Hellison et al., 2013; Morfeld et al., 2014), popular in big cities of Germany and England and adopted also in Milan since a few years.

Models setup and details on the output of the HMS are given in the following paragraphs.

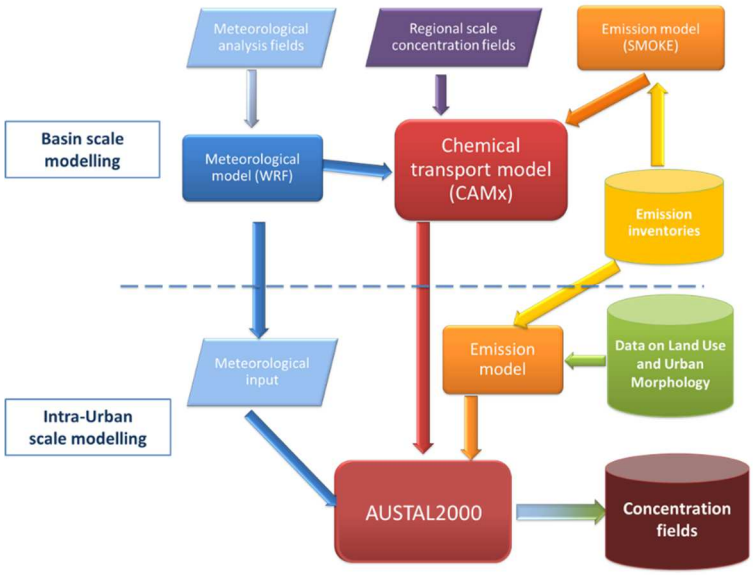


**Figure 5. Flow chart of the hybrid modelling system**

The meteorological model WRF v3.4.1 (Skamarock et al.,2008) was setup using 30 vertical layers, with the first one reaching about 25 meters from ground level; the top layer overcomes 15 km. Four horizontal nested grids were used, downscaling from a 3870x4140 $km^2$ domain covering Europe to a 1350x1530 $km^2$ domain over Italy, a 600x420 $km^2$ over the Po Valley and a 85x85 $km^2$ over a part of the Lombardy region, that covered the city of Milan. Each domain was gridded using different resolutions starting from 45 km as grid step down to 15 km, 5 km and 1.7 km for the last domain. Initial and boundary conditions were taken from ECMWF analysis fields at 0.5x0.5° grid size, both at ground level and at different pressure levels (http://old.ecmwf.int/products/data/archive/ECMWF_catalogue/index.html). Data included 3D and surface parameters (wind speed components, temperature, relative humidity), 2D surface parameters (sea level pressure and temperature, separating sea cells from ground ones), 2D static parameter of land sea mask and 3D soil parameters (temperature and water content) integrated on 4 ground layers (0-7 cm, 7-28 cm, 28 cm-1m, 1-2.55 m). Main physical settings within WRF included the Rapid Radiation Transfer Model (RRTM) radiation scheme (Iacono et al., 2008), Morrison double moment microphysics processes scheme (Morrison et al., 2009), Yonsei University PBL scheme (Hong et al., 2006), Grell 3D scheme for clouding creation (Grell et al., 2002) over European and Italian domain, Monin-Obukhov surface layer scheme (Monin and

Obukhov, 1954) and Noah land surface model (Chen and Dudhia, 2001). Analysis nudging of wind speed horizontal components, temperature and relative humidity was used in the WRF model with a nudging strength of $3x10^{-4}$. The classification system for land use was based on European database CORINE that counts 44 different categories (http://www.eea.europa.eu/), reclassified over 33 classes of USGS system. Particularly, CORINE adopts five different sub-categories of urban land use, from continuous urban fabric to discontinuous low-density urban fabric, that were linked to three USGS urban land use classes.

Two different versions of CTM were used during PhD thesis. Firstly, CAMx v5.60 model (ENVIRON, 2011) was used to simulate dispersion phenomena and chemical processes at regional scale, while CAMx v6.30 (ENVIRON, 2016) was used to perform high-detail source apportionment analysis during the final part of PhD. CAMx provided the concentration fields for the outer domains and background contributions for the local domain, better detailed below. CAMx was setup using the same horizontal grid structure as for WRF. CAMx vertical grid was defined collapsing the 27 vertical layers used by WRF into 14 layers in CAMx but keeping identical the layers up to 1 km above ground level; in particular, the first layer thickness was up to about 25 m from the ground like the corresponding WRF layer. The model was run only for the three innermost domains of WRF (Italy, Po Valley, Milan area), adopting the same grid step but slightly reduced dimensions to remove boundary effects. Details on the computational grids are reported in Table 1.

**Table 1. Lambert Conformal coordinates for nested domains in WRF and CAMx model**

| | *WRF (Europe)* | *WRF (Italy)* | *CAMx (Italy)* | *WRF (Po Valley)* | *CAMx (Po Valley)* | *WRF (Milan area)* | *CAMx (Milan area)* |
|---|---|---|---|---|---|---|---|
| SW X corner [km] | -2164.7 | -634.5 | -604.5 | -439.5 | -429.5 | -249.7 | -246.2 |
| SW Y corner [km] | -2358.2 | -1053.5 | -1023.5 | -108.5 | -98.5 | 66.8 | 69.8 |
| NE X corner [km] | 1705.3 | 715.5 | 685.5 | 160.5 | 150.5 | -164.7 | -167.8 |
| NE Y corner [km] | 1781.8 | 476.5 | 446.5 | 311.5 | 301.5 | 151.8 | 148.2 |
| DX-DY [km] | 45 | 15 | 15 | 5 | 5 | 1.7 | 1.7 |
| N cells X [n] | 86 | 90 | 86 | 120 | 116 | 51 | 47 |
| N cells Y [n] | 92 | 102 | 98 | 84 | 80 | 51 | 47 |

Homogenous gas phase reactions of nitrogen compounds and organic species were reproduced through CB05 mechanism (Yarwood et al., 2005). The aerosol scheme was based on two static modes (coarse and fine). Secondary inorganic compounds evolution was described by thermodynamic algorithm ISORROPIA (Nenes et al., 1998), while

SOAP (ENVIRON, 2011) was used to describe secondary organic aerosol formation. Meteorological input data were provided by WRF and were completed by OMI satellite data (http://toms.gsfc.nasa.gov), including ozone vertical content and aerosol turbidity. Vertical turbulence coefficients ($k_v$) were computed using O'Brien scheme (O'Brien, 1970), but adopting two different minimum $k_v$ values for rural and urban areas, so to consider heat island phenomena and increased roughness of built areas.

Emissions were derived from inventory data at three different levels: European Monitoring and Evaluation Programme data (EMEP, http://www.ceip.at/emission-data-webdab/emissions-used-in-emep-models/) available over a regular grid of 50x50 $km^2$; ISPRA Italian national inventory data (http://www.sinanet.isprambiente.it/it/sia-ispra/inventaria/disaggregazione-dellinventario-nazionale-2010) which provides a disaggregation for province; regional inventories data based on INEMAR methodology (INEMAR – ARPA Lombardia, 2015) for the four administrative regions in the Po Valley, which provide detailed emissions data at municipality level. Each emission inventory was processed using the Sparse Matrix Operator for Kernel Emissions model (SMOKE v3.5) (UNC, 2013) in order to obtain the hourly time pattern of the emissions. Temporal disaggregation was based on monthly, daily and hourly profiles deducted by CHIMERE model (INERIS, 2006) and EMEP model from Institute of Energy Economics and the Rational Use of Energy (IER) project named GENEMIS (Pernigotti et al., 2013). In order to avoid the double counting of the emissions placed inside the local domain, the source apportionment algorithm PSAT (Yarwood, 2004) implemented into CAMx was used. PSAT allowed keeping track of the contribution of different emission areas and source categories to the total pollutant concentration. For this application PSAT was setup to split the ambient concentrations resulting from the emissions of two Milan areas: innermost domain contribution and external domain contribution. The former contribution derives from the emissions belonging to the overlapping LSM-CTM urban domain, while the latter accounts for all the remaining sources, also including the CAMx parent domains.

This approach allows avoiding double counting of emission sources preserving physical and chemical consistency between the two models, in a simpler way than other methods requiring more simulations and assumptions (Stocker et al., 2014).

Initial and boundary conditions were taken from MACC-II system (http://www.gmes-atmosphere.eu/services/aqac/) that provides 3D global concentrations fields.

AUSTAL2000 v2.6.9 release was used as LSM within the modelling chain. AUSTAL2000 computational domain almost exactly overlapped one CAMx cell, covering a 1.6x1.6 km$^2$ urban area, including the main square of Milan city center, with 20 m grid step size is illustrated in Figure 6. The innermost domain is characterized by heterogeneous urban pattern: public parks, represented by green areas, and road arches separate the densely built up area. Based on the same emissions and meteorological parameters used by CAMx, AUSTAL2000 computed time series of concentrations generated by local sources enabling for the analysis of their spatial variability at high resolution within the urban domain. The vertical domain started from ground level up to 1500 m, adopting a variable-step grid: a 3m-step was used up to 60 m (i.e: twice the average height of the buildings), the top of the following three layers was set at 65 m, 100 m, 150 m, then a 100m-step was used from 200 m to 800 m and the top of the last three layers was set at 1000 m, 1200 m and 1500 m.

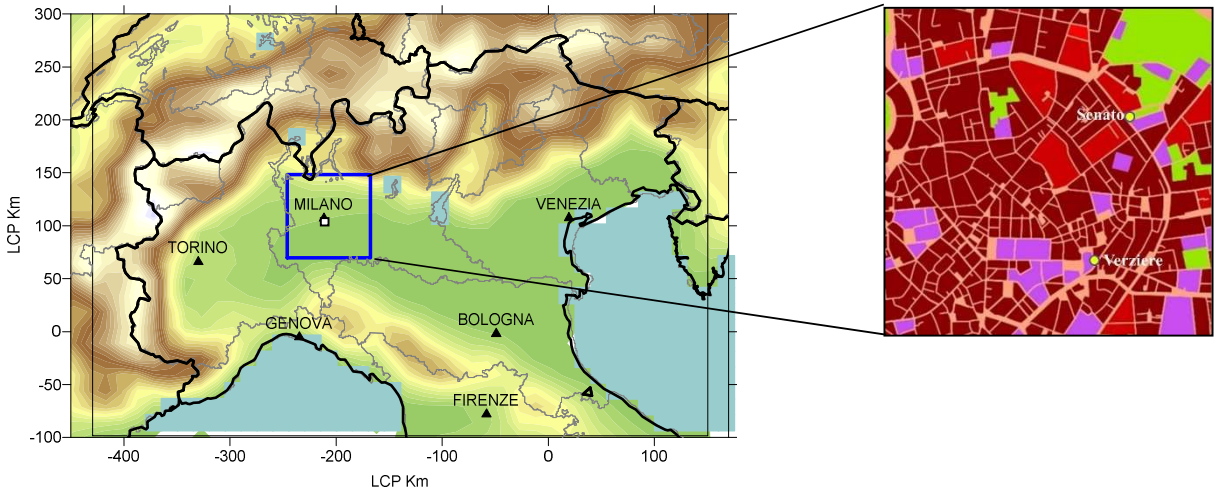


**Figure 6. Overview of Milan domain (left). View of AUSTAL2000 urban computational domain (right). Yellow dots represent the ARPA air quality stations included within the urban domain used for validation. Green areas represent public parks.**

Meteorological input variables for AUSTAL2000 (hourly data for Monin-Obukhov length, wind speed and direction) were provided by WRF and considered as representative of the non-disturbed flow; then the local wind field was calculated by the diagnostic wind field model TALdia, coupled with AUSTAL2000 and able to take into account the features of the urban built environment.

European land use atlas (http://www.eea.europa.eu/data-and-maps/data/urban-atlas), which provides information on the land cover composition according to the CORINE approach, was used to describe the presence of buildings in the urban domain. The cells covered at 99% by urban category land use, were considered as a building, with an assumed height of 30 meters based on the evidence of the average building height in Milan.

AUSTAL2000 used the same emission data as CAMx but with a more accurate spatial distribution that better mirrored the actual location of the sources and the release height. Namely, total emissions of the CAMx cell corresponding to the AUSTAL2000 urban domain were split among its cells based on proper 20x20 $m^2$ gridded information. For example, according to CAMx emission data, $NO_X$ emissions over the local domain were related only to domestic and commercial heating and to road transport. Domestic heating emissions were equally split among all the cells associated to buildings in the urban domain, lacking specific information on the energetic system and performance of the real buildings. Each building was associated to a stack represented as a point source at the building rooftop height. Traffic emissions were dealt with as ground-level linear sources, allocated with high accuracy within the domain exploiting the full potential of LSM model, and were proportionally split among all road arches in the local domain based on road network data provided by AMAT (http://www.amat-mi.it/it/documenti/dettaglio/16/). Emissions for each road have been computed as a weighted average of the total emissions within the local domain based on an aggregate street variable (ASV) given by the product of street length and vehicle number. AUSTAL2000 model operated considering $NO_X$ as an inert species. However, this limitation did not affect the results because of the very short atmospheric residence time within the local domain.

The modelling chain presents efficient features concerning computational time: 15 minutes/day with 8 core processors about CAMx outcomes while 4min/day about AUSTAL2000 outputs with single core. Physical and chemical processes are described and quantified although AUSTAL2000 treats all pollutants as inert.

The statistical parameters for model performance assessment included the mean bias (MB), mean absolute error (MAE), root mean square error (RMSE), index of agreement (IOA) and the correlation coefficient (r). The explicit definition of each parameter is reported in the S.M. section.

Meteorological fields were compared against surface observations proving that WRF was able to capture the temporal evolution of both the wind speed and direction over 2010. WRF Performance was evaluated considering the Po Valley and Milan area domain through two different observation networks: the World Meteorological Organization (WMO) and the Regional meteorological networks (ARPA). WRF provided similar performance for both networks; therefore, only the comparisons with ARPA data are shown in Figure 7 and Figure 8 for the Po valley and Milan area domain, respectively. Additionally, WRF performance results are available in the Figure S 1 and Figure S 2 of Supplementary Material (S.M.) for both ARPA and WMO network.

Year 2010 was characterized by a normal rise of specific humidity (mixing ratio) with a peak in the summer period, as temperature trend. Occasionally, quick decrease of temperature and mixing ratio were well captured by WRF over both domains during winter and summer months too. This is clearly proved by the values of the correlation index in Table 2 and Table 3 showing values higher than 0.95 for both parameters and domains.

**Table 2. List of statistics data for Q, T and WS for WRF validation analyzing ARPA stations.**

| | *Mixing ratio* | | *Temperature* | | *Wind speed* | |
|---|---|---|---|---|---|---|
| | *Po Valley* | *Milan area* | *Po Valley* | *Milan area* | *Po Valley* | *Milan area* |
| Num. Obs | 669929 | 94022 | 1388928 | 97864 | 664066 | 24427 |
| Mean OBS | 7.4 | 7.0 | 285.2 | 285.4 | 1.9 | 1.3 |
| Mean MODEL | 7.5 | 7.2 | 284.6 | 286.1 | 2.2 | 1.7 |
| CORR | 0.95 | 0.94 | 0.96 | 0.98 | 0.52 | 0.51 |
| Mean BIAS | 0.11 | 0.22 | -0.59 | 0.67 | 0.3 | 0.47 |
| MAE | 0.86 | 0.84 | 1.97 | 1.57 | 1.1 | 0.82 |
| IOA | 0.95 | 0.94 | 0.96 | 0.98 | 0.34 | 0.2 |
| RMSE | 1.2 | 1.23 | 2.68 | 2.01 | 1.48 | 1.1 |

**Table 3. List of statistics data for Q, T and WS for WRF validation analyzing WMO stations.**

| | *Mixing ratio* | | *Temperature* | | *Wind speed* | |
|---|---|---|---|---|---|---|
| | *Po Valley* | *Milan area* | *Po Valley* | *Milan area* | *Po Valley* | *Milan area* |
| Num. Obs | 227684 | 24495 | 228958 | 24688 | 168539 | 12747 |
| Mean OBS | 7.6 | 7.3 | 285.2 | 285.7 | 3.1 | 2.8 |
| Mean MODEL | 7.6 | 7.5 | 284.7 | 286.5 | 2.6 | 1.6 |
| CORR | 0.94 | 0.97 | 0.95 | 0.98 | 0.53 | 0.5 |
| Mean BIAS | -0.09 | 0.19 | -0.45 | 0.71 | -0.28 | -0.9 |
| MAE | 1.02 | 0.71 | 2.12 | 1.41 | 1.47 | 1.19 |
| IOA | 0.94 | 0.96 | 0.95 | 0.98 | 0.45 | 0.28 |
| RMSE | 1.46 | 0.97 | 3.05 | 1.86 | 2 | 1.52 |

Temperature over the Milan area domain was slightly overestimated over the whole year (BIAS = 0.67 deg and 0.71 deg), but the overall performance is better than the Po Valley domain, as stated by RMSE index, decreasing from 2.68 to 2.01 and from 3.05 to 1.86.
Focusing on ARPA stations, the observed annual wind speed distribution was correctly reproduced by WRF although a slight overprediction, higher for Milan area domain (BIAS=0.47 m/s) than Po Valley area (BIAS=0.3 m/s). Observed wind speed percentiles performed within Milan area domain were lower than wider domain, stressing critic situation for pollutants dispersion expected for Po Valley and urban domain.
Wind speed was constantly overpredicted over both domains but simulation for Milan area WRF showed an increased discrepancy in more windy conditions as shown by the $95^{th}$ percentile of the observed (2.67 m/s) and predicted (3.48 m/s) wind speed.

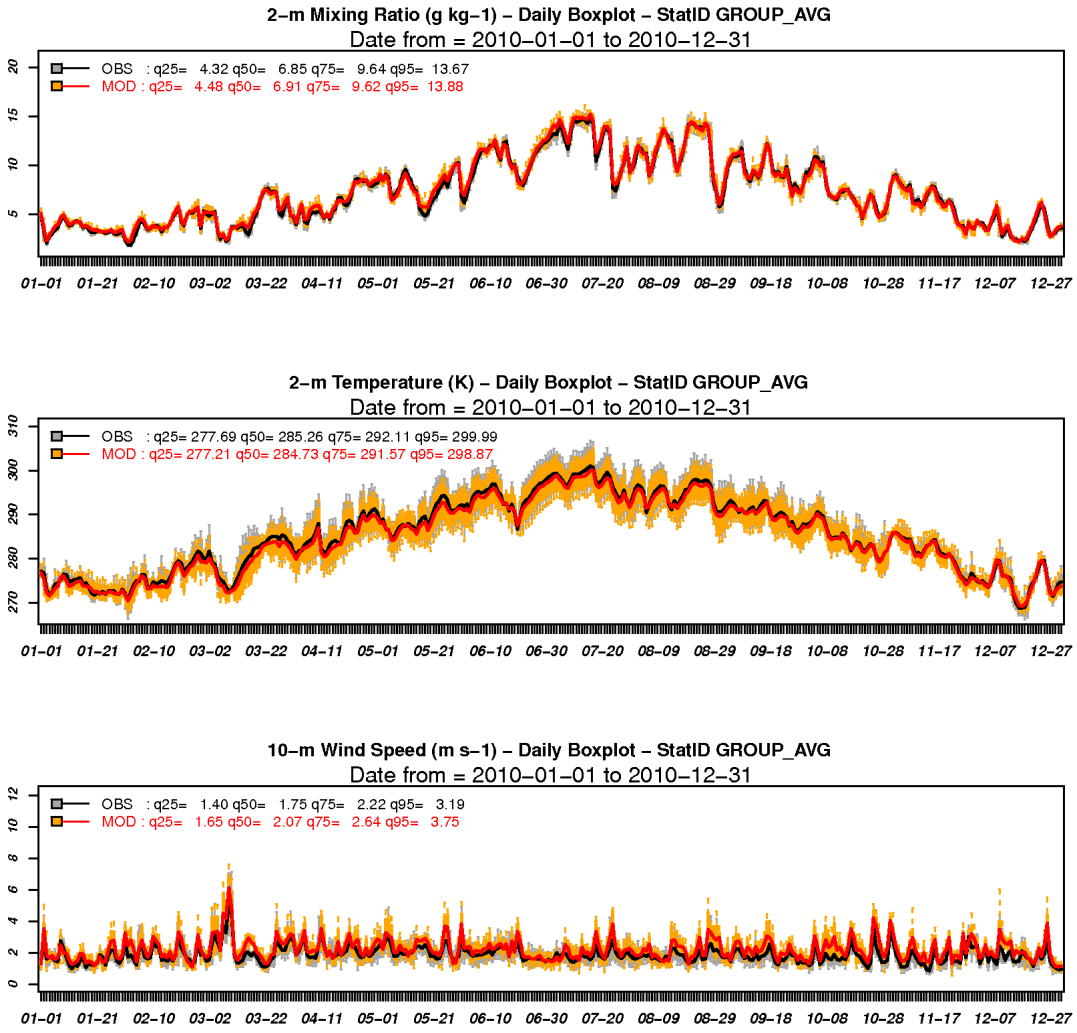


**Figure 7. Time series of the box and whisker plots for the daily distribution of the observed (black/grey) and computed (red/orange) values of mixing ratio, temperature and wind speed at 170 ARPA sites, computed over the Po valley domain for 2010. Bars show the interquartile range (IR), lines the median values, dashed vertical bars the (25th – 1.5 · IR) and the (75th + 1.5 · IR) value. Values for the 25th, 50th, 75th, and 95th quantiles of the whole yearly time series are reported too.**

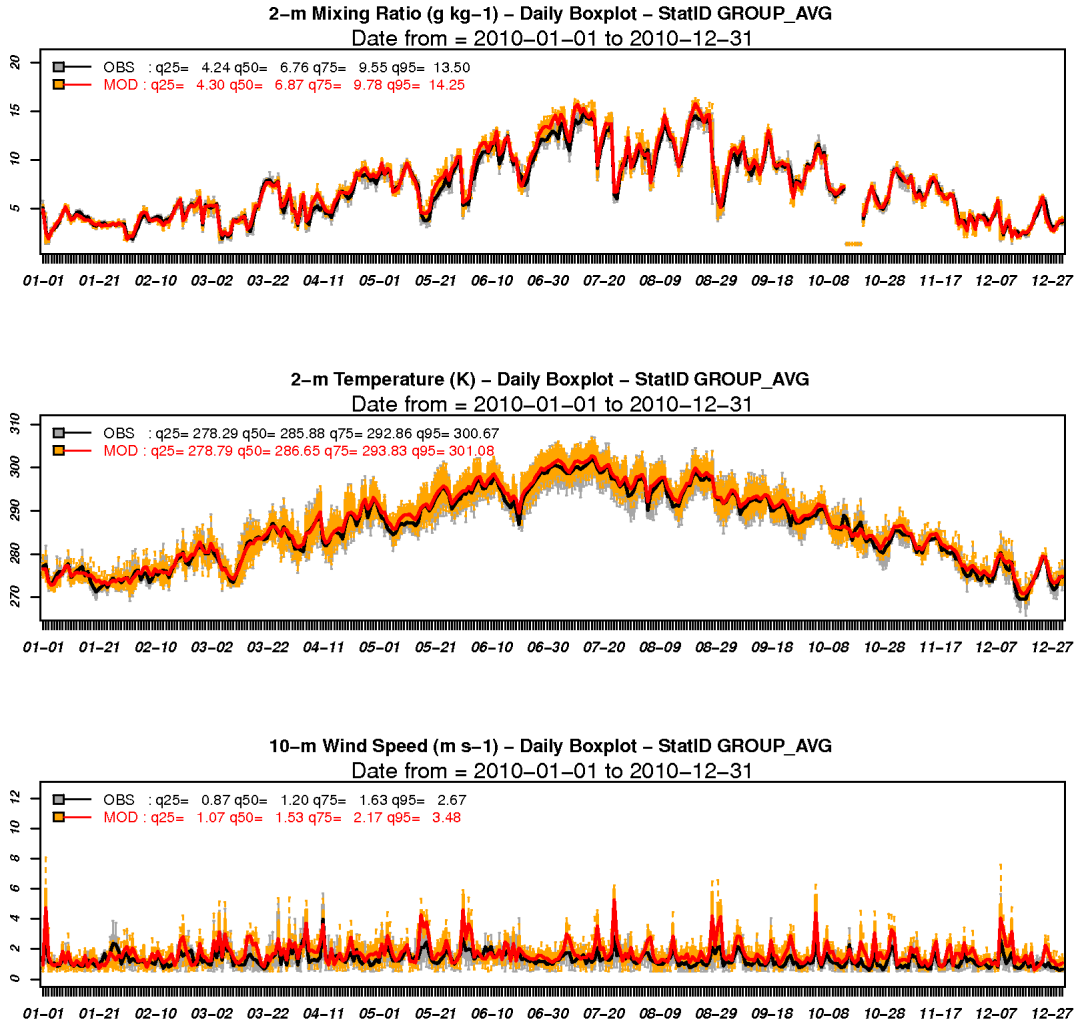


**Figure 8. Time series of the box and whisker plots for the daily distribution of the observed (black/grey) and computed (red/orange) values of mixing ratio, temperature and wind speed at 15 ARPA sites (only 3 sites for wind speed), computed over the Milan area for 2010. Bars show the interquartile range (IR), lines the median values, dashed vertical bars (25th – 1.5 · IR) and the (75th + 1.5 · IR) value. Values for the 25th, 50th, 75th, and 95th quantiles of the whole yearly time series are reported too.**

CAMx performance was computed over both Po Valley and Milan area domains. CAMx should reproduce the atmospheric behavior of all main pollutants, taking into account all relevant chemical processes. $NO_x$ performances were summarized in Table 4 comparing statistical indicators obtained for the two domains, but considering only urban and suburban air quality monitoring stations. Measurements at 20 urban sites and 8 sub-urban sites were available for the Milan area and at 97 urban sites and 43 sub-urban sites, also including the previous ones for the whole Po Valley domain. Observed mean concentration increased from 30 ppbV to about 40 ppbV zooming from the whole Po

Valley to the Milan area, due to the increasing strength of the anthropogenic emissions. Over both domains CAMx clearly underestimated the observed concentration, especially during the winter period, with an overall mean bias around 14 ppbV. As shown in Figure 9, regardless for the spatial resolution of the simulation, CAMx was able to reproduce the observed concentration for most of the summer months, but missing several of the severe episodes that took place on winter months, particularly January and December which caused a low correlation index. Indeed, the difference between modelled and observed time series became larger and larger in the upper tail of the distribution, as pointed out by the values of the three quartiles and of the 95$^{th}$ percentile reported in Figure 9.

The origin of $NO_X$ underestimation, mainly during the cold season, was not clearly identified, but it could be probably explained by the potential overestimation of the vertical mixing because horizontal dispersion was well captured by WRF model. Similarly, wind direction also could be a reason for the NOx underestimation but the error showed in S.M. in the Figure S 1 over the Milan area was not so relevant and homogenously distributed for different wind speed. Low wind speed, dry air and cold temperature that characterized principally the winter period in the Po valley, were often linked to strong inversion conditions with very low mixing heights, favoring pollutant accumulation, but direct measurements of mixing height were not available. However, focusing on peak events during the cold season, WRF slightly overestimated temperature and this could overestimate mixing layer height too. Similar performances are observed for the few rural stations available in the domain in S.M., in particular in Figure S 2 and Table S 1.

Additionally, it is worth noticing that CAMx provided the same performance for both the simulation domains, pointing out that the underestimation had not be ascribed to local scale effect (e.g. missing local sources), but to larger scale features not captured by the meteorological model.

**Table 4. Comparison of stand-alone CAMx model performance for NOx hourly concentrations computed for 2010 at urban and suburban AQ stations of Po Valley and Milan area domain.**

| | *Po Valley* | | *Milan area* | |
|---|---|---|---|---|
| | Observations | Model | Observations | Model |
| Mean [ppbV] | 29.7 | 14.9 | 39.4 | 26.5 |
| Standard Deviation [ppbV] | 35.1 | 17.5 | 46.4 | 24.0 |
| Number Observations [-] | 1173403 | | 237587 | |
| Correlation [-] | 0.45 | | 0.5 | |
| Mean Bias [ppbV] | -14.8 | | -13 | |
| Mean Error [ppbV] | 19.5 | | 23.2 | |
| Index_of_Agreement [-] | 0.56 | | 0.6 | |
| RMSE [ppbV] | 34.7 | | 42.3 | |

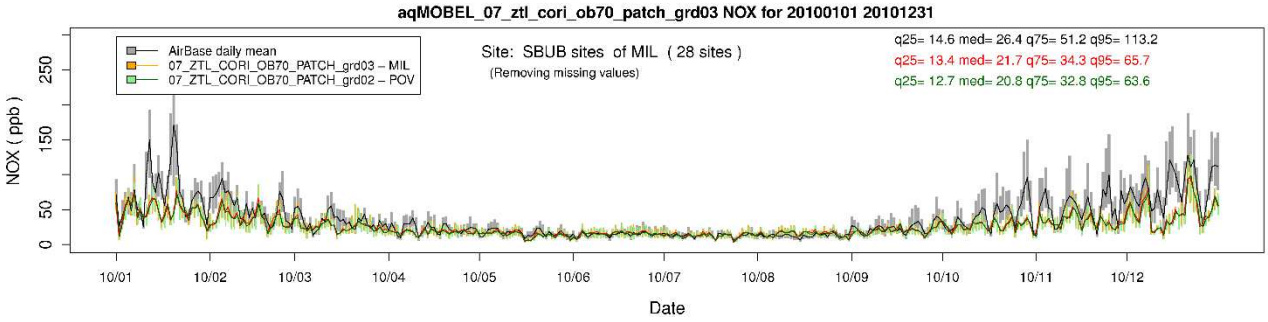


**Figure 9. Time series of the box and whisker plots for the daily distribution of the observed (black/grey) and computed values of NOx concentration (ppb) at Urban and Suburban monitoring sites of the Milan area domain for 2010. CAMx results at 5 km and 1.7 km resolution are displayed in red/orange and in green, respectively. Bars show the interquartile range, lines the median values. Values for the 25th, 50th, 75th, and 95th quantiles of the whole monthly time series are reported too.**

Similarly to NOx analysis, CAMx performances were investigated on aerosol pollutant too as PM10. Figure 10 and Table 5 showed respectively $PM_{10}$ time series of the daily average and the principal statistical indicators relied on suburban and urban air quality stations over Po Valley and Milan domains. Comparison between observations and modeling outcomes was focused only over Po Valley because, as confirmed by statistical indicators, higher resolution did not improve performances of model. As detected for NOx, PM10 was clearly underestimated during winter periods, in particular November, December and January while summer months were well simulated. The lower correlation indexes for Po Valley and Milan domains were caused by missed concentration peaks occurred during November and January. While observed concentrations exceeded PM10 threshold (50 $\mu g/m^3$), CAMx simulated levels under 30 $\mu g/m^3$ without evidencing increases. Discrepancies could be ascribed to two mains factors: meteorological variables were not well reproduced, in particular mixing height, and missed emission processes as PM traffic resuspension.

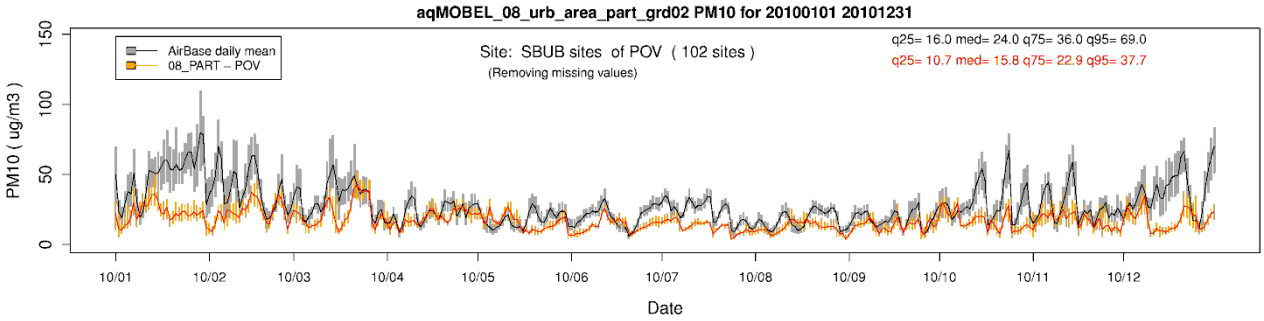


**Figure 10. Time series of the box and whisker plots for the daily distribution of the observed (black/grey) and computed (red/orange) values of $PM_{10}$ concentrations at 102 ARPA sites, computed over the POV domain for 2010. Bars show the interquartile range (IR), lines the median values, dashed vertical bars (25th – 1.5 · IR) and the (75th + 1.5 · IR) value. Values for the 25th, 50th , 75th, and 95th quantiles of the whole yearly time series are reported too**

The combination of these two factors produced low correlation values (0.44 and 0.42 respectively for Po Valley and Milan domain) if compared with NOx evaluation. Focusing on Index of Agreement, a slight reduction was observed for Milan domain.

**Table 5. Comparison of stand-alone CAMx model performance for $PM_{10}$ hourly concentrations computed for 2010 at Urban and Suburban AQ stations of Po Valley and Milan area domain**

| | *Po Valley* | | *Milan area* | |
|---|---|---|---|---|
| | Observations | Model | Observations | Model |
| Mean [µg/m$^3$] | 29.2 | 18.0 | 34.2 | 20.3 |
| Standard Deviation [µg/m$^3$] | 19.1 | 10.1 | 22.3 | 10.9 |
| Number Observations [-] | 34123 | | 6555 | |
| Correlation [-] | 0.44 | | 0.42 | |
| Mean Bias [µg/m$^3$] | -11.2 | | -13.9 | |
| Mean Error [µg/m$^3$] | 14.3 | | 17.2 | |
| Index_of_Agreement [-] | 0.56 | | 0.54 | |
| RMSE [µg/m$^3$] | 20.5 | | 24.6 | |

Overall, CAMx application presented quite good similar performances either for gaseous and aerosols pollutant regardless domain and grid step size; this aspect highlighted suitability of CAMx for coupling with LSMs for high-resolution air quality modeling and source apportionment analysis that enclosed both regional and local sources, taking into account regional scale dynamics as well as local scale ones.

## 2.1. Hybrid modeling system - NOx

The first part of thesis was focused on HMS application in order to assess hourly $NO_X$ concentrations over the Milan local domain showed in the right panel of Figure 6. Milan city center area combines different zones including parks, roads and buildings.

Following the hybrid approach, CAMx provided the background contribution that represented concentrations generated by sources located outside local domain, whilst AUSTAL2000 reproduced the hourly field concentration produced by the sources active in the innermost urban domain. The final $NO_X$ hourly concentration field at the Milan domain was computed adding the local scale concentration field to the CAMx background concentration. This approach avoided the double counting of local emissions that occurred generally when the LSM results for the local domain were simply superimposed to the regional scale results from CTM.

In order to illustrate the local meteorological situation and micro-environment, January 2010 wind rose was computed at two air quality stations located within the local domain. Figure 11 illustrated the location of air quality stations (Senato: 9,1974E, 45,4705N; Verziere: 9,1953E, 45,4633N); both were located in a kerbside position near trafficked streets and Senato station was classified as an urban canyon environment. Senato and Verziere were used because no meteorological monitoring sites were installed.

**Figure 11. Plant view of the two monitoring stations, circled in yellow. Senato site (left) and Verziere site (right).**

Wind roses obtained by TALdia, the meteorological pre-processor model, showed the different impact of buildings on local scale winds, reflecting key features of locations. In particular, the screen effect of the building "west" of Verziere site (Figure 12 – right), as well as the channeling effect of buildings along the city center ring road at Senato site (Figure 12 – left) were clearly highlighted. As mentioned before, at these sites no wind measurements were available, thus TALdia results could not be validated.

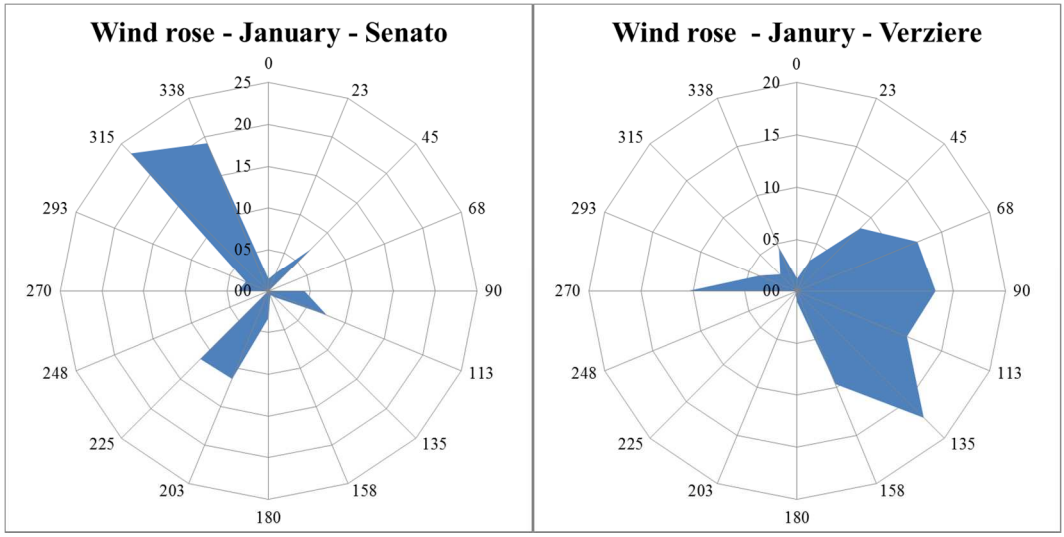


**Figure 12. January wind roses obtained by TALdia for two monitoring sites: Senato (left) and Verziere (right).**

AUSTAL2000 made possible the reconstruction of the urban structure of the city including buildings and all the obstacles that influence dispersion of pollutants. Figure 13 shows the $NO_X$ spatial distribution over the local domain as ground-level mean concentration for 2010.

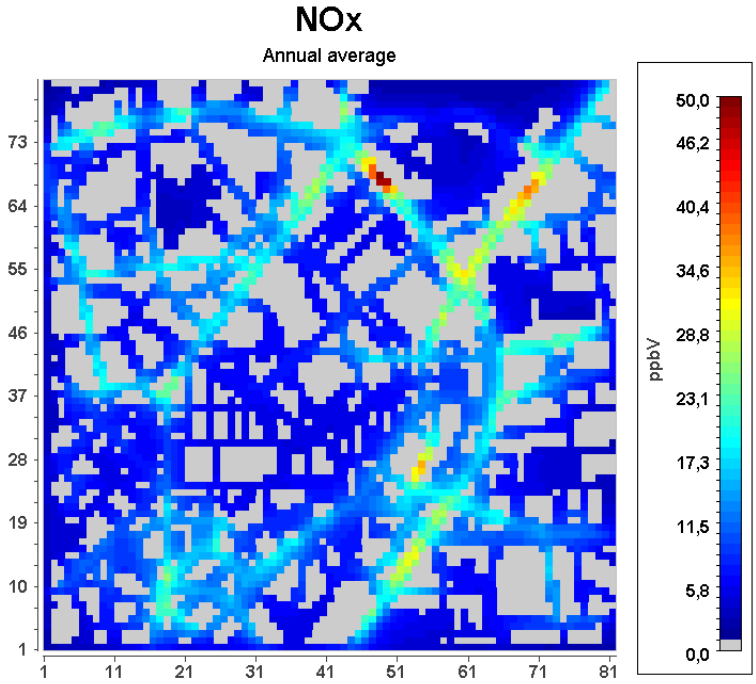


**Figure 13. AUSTAL2000 $NO_X$ mean concentration field for 2010 at ground level, computed as a vertical average along the first 24 meters (HMS_mean24m). Grey areas identify buildings.**

The mean concentration field pointed out the effect of traffic sources on main roads of the area, responsible for $NO_X$ levels as high as 40 ppbV near busy crossroads, as well as areas with lower levels, down to about 10 ppbV, far from busy streets. This result highlighted the LSM capability to reproduce the strong spatial variability of pollutants within urban areas, that cannot be captured by a CTM alone, that can provide only one mean concentration value over the same area.

An interesting feature of HMS was that the LSM output could be compared with the CTM local contribution (CAMx local), obtained through PSAT application, because both of them are produced starting from the same emissions sources. To this purpose, AUSTAL2000 vertical concentration profiles were averaged within the first 24 meters, in order to make them comparable to CAMx first layer output (up to around 25 meters). Then, in order to preserve LSM variability, the CAMx mean local concentrations were compared to the statistical distribution of the AUSTAL2000 concentrations, excluding cells with 0 values representing buildings or general obstacles.

Figure 14 showed the comparison between the mean estimations from CAMx (time series) and the box plots representing the distribution of daily mean $NO_X$ concentrations over all the urban domain from AUSTAL2000.

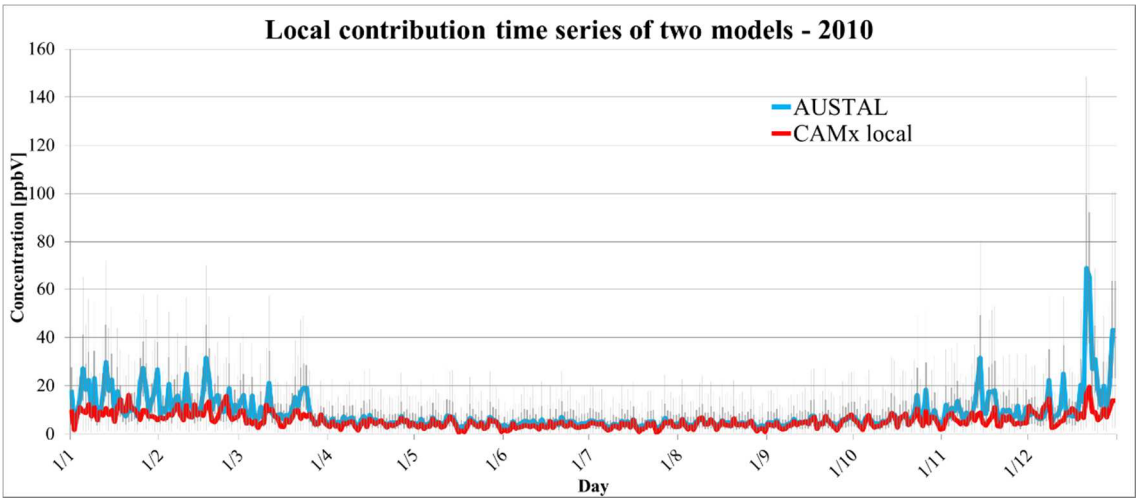


**Figure 14. Comparison between $NO_X$ daily concentrations for the urban domain computed by CAMx local (red line) and by AUSTAL2000. The latter is expressed as statistical distribution, with the blue line representing the median value of the spatial distribution, the blue box limits the 25$^{th}$ and 75$^{th}$ percentile of the distribution and the grey line the 5$^{th}$ and 95$^{th}$ percentile.**

The two models, relied on very different modeling approaches, were driven by the same meteorological input and the same emission data. CAMx local concentrations mostly

ranged between 0 and 20 ppbV while AUSTAL2000 showed several peaks ranging between 10 and 70 ppbV. However, models showed a rather good agreement, especially during summer when the estimated contribution from "local sources" was below 10 ppbV. Conversely, during other periods the whole distribution of AUSTAL2000 concentrations was higher than the CAMx local value, even though both the models tended to reproduce the same time pattern.

Model performances were affected mainly by atmospheric stability; this aspect was highlighted by the comparison between the daily pattern of local sources contributions illustrated in Figure 14 during a winter (January) and a summer month (June). In January, differences between models are related to first and last hours of the day, when AUSTAL2000 showed a more pronounced temporal variability than CAMx with two usual peaks corresponding to morning and late afternoon rush hours. Differently, CAMx simulated a slighter growth of concentrations on morning and evening rush hours and a flatter concentration time pattern over the whole day. Stratification of the atmosphere, more relevant for the LSM, drove AUSTAL2000 to emphasize backlog conditions, with a consequent increase of NOx concentration levels. Conversely, on daytime hours model results were very similar, but with CAMx mean values slightly higher.

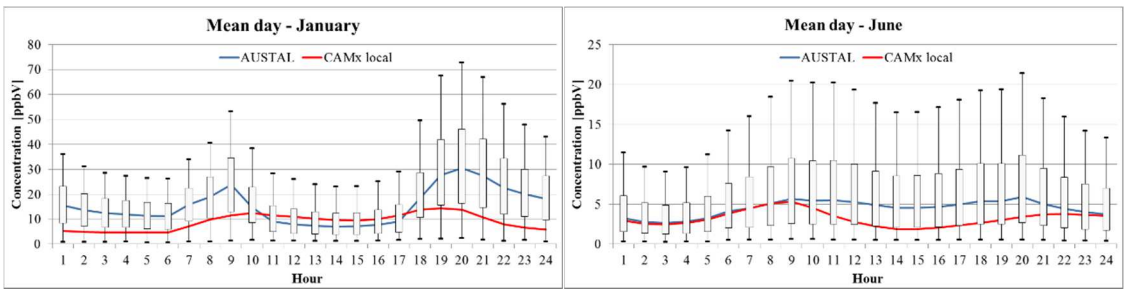


**Figure 15. $NO_X$ January (left) and June (right) mean day concentration. Red line represents CAMx local estimation. Blue line represents the median of AUSTAL2000 spatial distribution of the mean day concentrations, while the box's limits indicate 25$^{th}$ and 75$^{th}$ percentile and the vertical lines link the 5$^{th}$ and 95$^{th}$ percentile.**

Adding AUSTAL2000 outcomes to the background concentration computed by CAMx, it was possible to obtain the HMS estimation of the total $NO_X$ concentration, excluding double counting error. HMS output was compared with observations as well as with the results of the stand-alone CAMx run. HMS "total" $NO_X$ concentration required additional assumptions. Indeed, AUSTAL2000 results were available over a 3m-stepped vertical profile, observed values generally referred to 4 m above ground level, while CAMx

concentration represents the mean value for the first vertical layer. For this reason, at a first stage, the model performance evaluation was based on two different definition of the LSM concentration contribution: AUSTAL2000 contribution at 3 meters from the ground (HMS_3m) was used for comparison with measurements, which were sampled at a similar height; AUSTAL2000 average contribution of first 24 meters (HMS_mean24m) was used for comparison with CAMx estimation. In Figure 16 the observed time series (black line), stand-alone CAMx estimate (red line) and HMS values made by background contribution (blue area) and AUSTAL2000 contribution (green area) are plotted. The analysis referred to Verziere and Senato site, the two only monitoring sites available within the local domain.

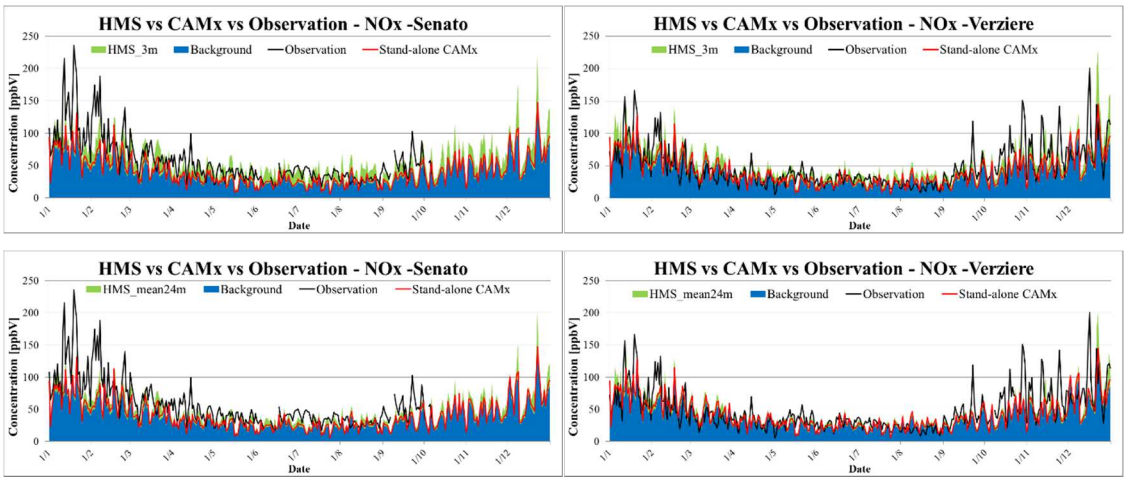


**Figure 16. Comparison of daily mean NOx concentrations observed and computed by the HMS, according to both definition, and stand-alone CAMx for Senato (left column) and Verziere site (right column). HMS concentration is obtained superimposing CAMx background concentration (in blue) with AUSTAL2000 local contribution (in green). AUSTAL2000 contribution in HMS time series is HMS_3m in top graphs and HMS_mean24m in bottom graphs. Stand-alone CAMx results are in red.**

The most important finding stemming from Figure 16 was that, in most cases, the total HMS concentration was mainly due to the background contribution, thus depending on the sources placed outside the local domain. The mean modeled contributions were summarized in Table 6, showing a background concentration around 36 ppbV. Local contributions at Senato site ranged between 4 ppbV for CAMx local up to 21 ppbV with AUSTAL2000 at 3m and between 4.9 and 18.1 at Verziere site. This result implied that the reconstruction of air quality levels within urban areas, required a modeling approach

able to consider the influence of sources placed near receptor point and far away from it too.

Table 7 reports the main statistical parameters summarizing model performance for both HMS outputs and for stand-alone CAMx output.

Higher traffic volume and particular local features which favored backlog conditions caused higher mean concentrations in Senato site than Verziere. Actually, Verziere street is a secondary road, less trafficked compared to Senato street, that is a stretch of the city center ring road with the aspect of an urban canyon. Therefore, in addiction to high local NOx emissions, there are also buildings surrounding Senato monitoring station, that emphasize backlog conditions rather than at Verziere site where, moreover, the wider open area favors the dispersion of local emissions. Neither stand-alone CAMx nor the HMS were able to capture this feature. All model configurations showed increasing concentrations from stand-alone CAMx to HMS_3m, but without relevant differences between the two sites. This suggests that both the difference in urban morphology and in the emission load were not well captured by the HMS, due to mainly by CAMx background contribution.

At both sites, the statistical indexes showed a general underestimation for CAMx stand-alone (negative bias: -20.8 at Senato, -6.5 at Verziere), but improved with HMS application. Bias decreased of almost 8 ppbV at Senato site using HMS vertical mean approach and of more than 16 ppbV with concentration at 3m, anyway still remaining negative (-4.4 ppbV); at Verziere site bias was still negative, reaching a value of -0.1 ppbV with HMS_mean24m, becoming positive with HMS_3m (6.7 ppbV). Correlation index showed a slight worsening for both HMS options with respect to CAMx: from 0.84 for CAMx down to 0.78-0.81 for HMS at Senato site, from 0.73 down to 0.71-0.72 at Verziere site. The opposite trend of bias and correlation index, as well as of index of agreement, points out that: i) the higher concentrations produced by HMS with respect to stand-alone CAMx reduced, on the average, the model underestimation; ii) the presence of several peaks produced by AUSTAL2000 during nighttime stable conditions worsened the reproduction of the temporal evolution of $NO_X$ concentrations.

Lower but extended improvement of statistical indexes following vertical mean profile than computing concentrations at 3m, could be explained by the significant backlog capability of LSM at ground-level during stable conditions (night-time); this aspect

confirmed that the HMS_mean24m results was the best solution between the two approaches.

**Table 6. Comparison among the modelled contributions to the yearly mean $NO_x$ concentration and corresponding standard deviations.**

| *Statistical Parameters* | *Milano Senato* | | | | *Milano Verziere* | | | |
|---|---|---|---|---|---|---|---|---|
| [ppbV] | *CAMx Background* | *AUSTAL2000 24m* | *AUSTAL2000 3m* | *CAMx local* | *CAMx Background* | *AUSTAL2000 24m* | *AUSTAL2000 3m* | *CAMx local* |
| Mean | 36.7 | 13.4 | 21.4 | 4.2 | 36,3 | 11.3 | 18.1 | 4.9 |
| St. Dev | 21.2 | 14.9 | 20.6 | 3.5 | 20.8 | 13.4 | 18 | 4 |

**Table 7. Statistical parameters of HMS and CAMx model performance for $NO_x$ at Senato and Verziere site.**

| *Statistical Parameters* | *Milano Senato* | | | | *Milano Verziere* | | | |
|---|---|---|---|---|---|---|---|---|
| | *Observ.* | *HMS_mean24m* | *HMS_3m* | *CAMx stand-alone* | *Observ.* | *HMS_mean24m* | *HMS_3m* | *CAMx stand-alone* |
| Mean [ppb] | 58.1 | 50.1 | 58.1 | 40.9 | 47.9 | 47.6 | 54.4 | 41.2 |
| St. Dev. [ppb] | 37.1 | 27.3 | 29.5 | 23.3 | 31.5 | 27.6 | 30.2 | 23.3 |
| BIAS [ppb] | | -12.2 | -4.4 | -20.8 | | -0.1 | 6.7 | -6.5 |
| MAE [ppb] | | 26.5 | 27.2 | 28.1 | | 24.9 | 27.1 | 23.9 |
| IOA [-] | | 0.92 | 0.92 | 0.93 | | 0.84 | 0.81 | 0.86 |
| RMSE [ppb] | | 40.9 | 41.6 | 42.2 | | 38.1 | 40.8 | 36.1 |
| CORR [-] | | 0.81 | 0.78 | 0.84 | | 0.72 | 0.71 | 0.73 |

The analysis of the entire period, illustrated in Figure 17, showed that all CAMx stand-alone distributions systematically underpredicted the measurements at both sites, especially at Senato site. Through HMS introduction, this aspect improved, but there were still relevant discrepancies, particularly for the highest percentiles. A better agreement with modelled data was observed at Verziere site, particularly for HMS_mean24m data. This point confirmed that HMS was able to add properly the local scale magnitude of $NO_X$ concentrations to background contribution, but not always to reproduce their temporal variability as confirmed by statistical indexes shown previously. At this site, we could also observe a very good agreement for stand-alone CAMx output up to the 50$^{th}$

percentile while a systematic underestimation for Senato site for all possible approaches, confirmed that specific local scale features were not captured. Indeed, we already pointed out that highest observed concentrations took place during very stable conditions when local scale accumulation processes, that cannot be captured by CAMx, were prevailing.

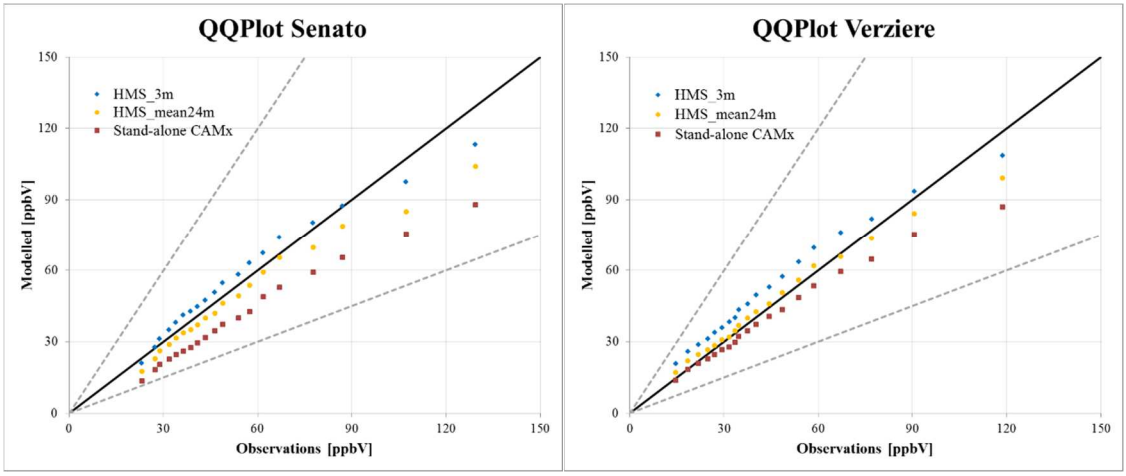


**Figure 17. Quantile-Quantile plot of the observed and modelled $NO_X$ daily concentrations at Senato (left) and Verziere (right) site, starting from 5$^{th}$ percentile up to 95$^{th}$ percentile with a step of 0.05.**

Even though underestimation persisted for highest percentiles after HMS application, the overall improvements will allow to capture a better level of exposure to pollutants of people living in high-density urban areas, particularly at hot spot sites, generally missed by larger scale model.

A further analysis of model performance was carried out considering the average weekly pattern and the mean day of modelled and observed $NO_X$ concentrations (Figure 18). The "day of the week" analysis showed an agreement between CAMx stand-alone approach and HMS during the decreasing trend among workdays and weekends, while the day-by-day variability was not reproduced quite well during January. The day-by-day variability as well as the absolute values of concentrations were quite well reconstructed during the summer month (June), especially at Verziere site that was not affected by morning rush hour peaks as at Senato site.

Figure 18 showed a negative bias at Senato site for January, across all weekdays. The discrepancy was mainly related to the strong underestimation of the morning peak and, as a consequence, of the ensuing daytime concentrations, as clearly pointed out by the mean day analysis in Figure 19. Other than to the emission pattern, the systematic under

prediction of $NO_X$ at Senato site, clear also during June, can be partly associated with an incorrect definition of the site's features as discussed before (e.g. street canyon character), that could not be captured by our modeling approach.

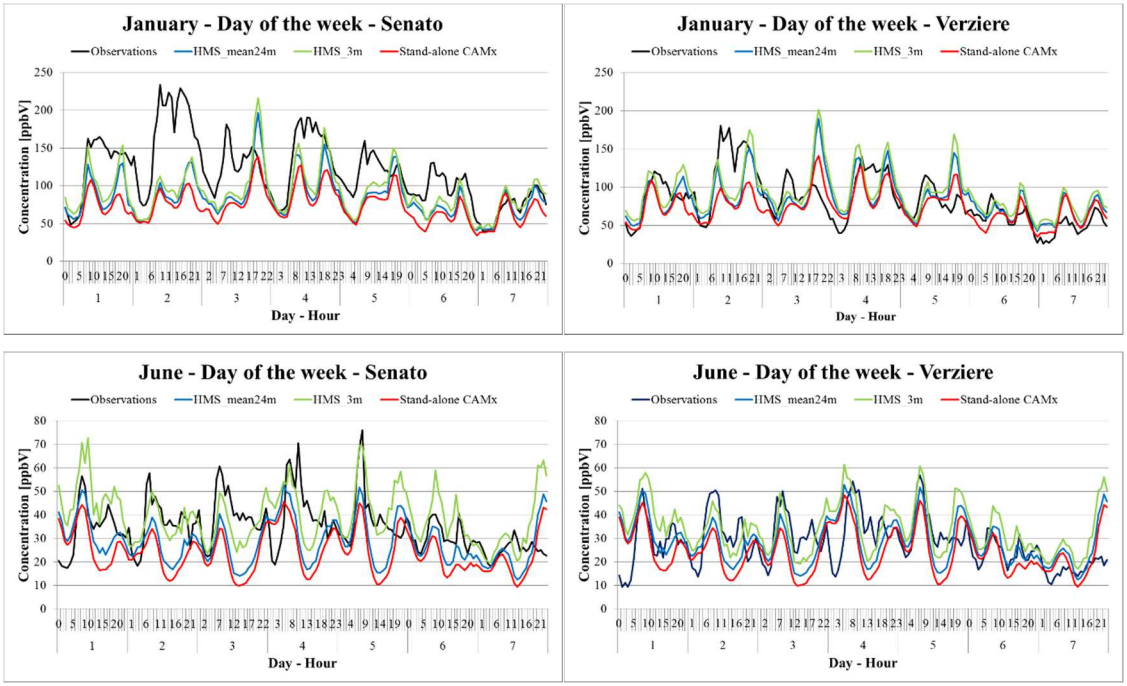


**Figure 18. Day of the week for January (top) and June (bottom) $NO_X$ concentrations at Senato (left) and Verziere (right) measurement site. Black line represents measure, red line indicates stand-alone CAMx concentrations, while green and blue line show HMS results. Day of the week ranges from Monday (1) to Sunday (7).**

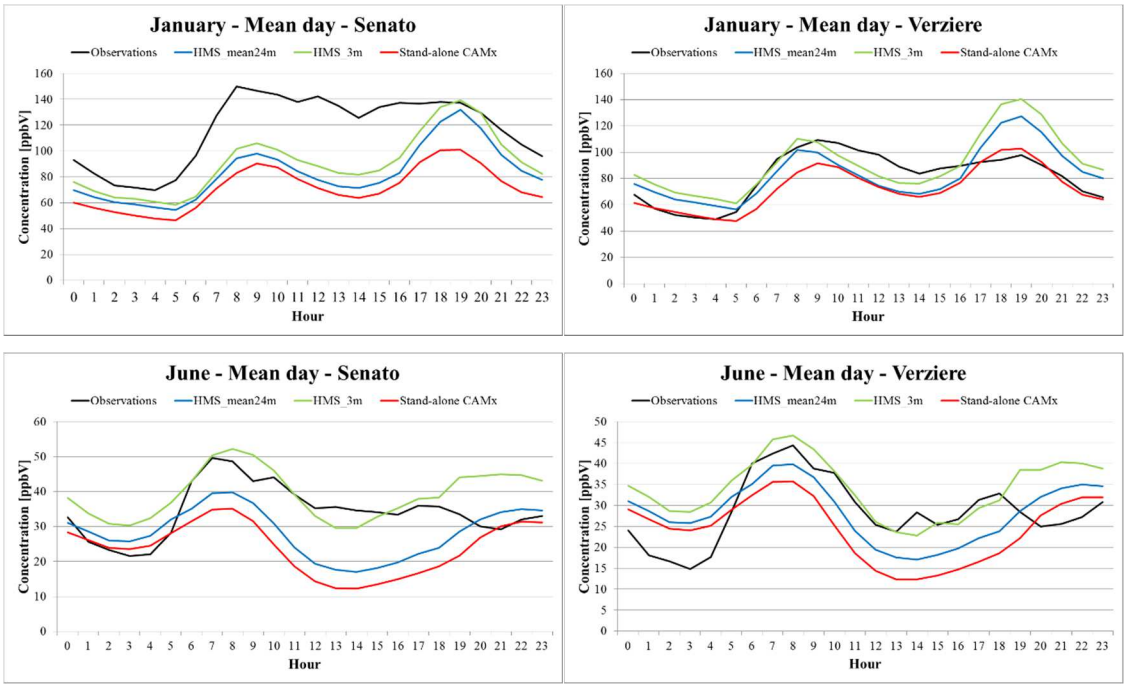


**Figure 19. Mean day for January (top) and June (bottom) NOx concentrations at Senato (left) and Verziere (right) measurement site. Black line represents measure, red line indicates stand-alone CAMx concentrations, while green and blue line show HMS results. Day of the week ranges from Monday (1) to Sunday (7).**

The HMS results showed in Figure 19 confirmed that the average day-time variability modeled was in compliance with observed concentrations, especially during the summer period when thermal and mechanical turbulence phenomena were more pronounced. In particular, the magnitude of NOx concentrations observed in the winter (from 60 ppbV to 100 ppbV) and summer period (from 15 ppbV to 40 ppbV) was correctly reproduced. However, the daily pattern was better reconstructed in the summer period than in the cold season.

HMS and CAMx stand-alone reproduced satisfactorily the morning and the evening peaks even if NOx concentrations were influenced significantly by the traffic modulation. Mechanical and relevant thermal turbulence during the warm season caused a lower evening peak, even though traffic modulation was similar to the cold season. This aspect was considered by both models (CAMx stand-alone and HMS).

Actually, the main discrepancy was related to the overestimation of the evening peak in January, and to a lesser extent in June, on both workdays and weekends, even up to about 30 ppbV.

Finally, the consistent overprediction suggested either a not good agreement between modelled and real modulation of traffic emissions or a too strong decrease of vertical

turbulence and mixing in the late afternoon. This latter phenomenon has been already highlighted by previous studies (Kim et al., 2015) and is related to the difficulty of meteorological model in taking into account the contribution of anthropogenic heating to energy balance within urban areas.

CAMx stand-alone and HMS approaches demonstrated following different approaches for air quality modelling, but at the same time to be valid solutions. Even though differences were presented between them, temporal variability, as showed in Figure 18 and Figure 19, was not affected by the two methods. Thus, the horizontal resolution, as well as the modelling method did not influence the temporal evolution of concentrations even though backlog capabilities of the models were different. Consequently, NOx temporal variability depends on emission temporal modulation and overall meteorological parameters, which remains unchanged between the two approaches.

## *2.2. CAMx source apportionment – PM2.5, EC, NO3- and NO2*

Particulate source apportionment algorithm (PSAT) implemented within newer version of CAMx (v6.30) was used to study the source emissions contributions and areal contributions too, in order to describe properly how each region affects itself and the surrounding areas. The key feature introduced with 6.30 version was the possibility to track the contributions generated by different areas and not only categories of PM gaseous precursors as $NO_2$. Besides investigating fine particulate matter ($PM_{2.5}$) and its components, both primary (EC) and secondary ($NO_3^-$), source apportionment analysis was focused on gaseous precursor ($NO_2$), whose contributions were undetectable by whatever CTM model or receptor model.

For this work, we defined 5 areas that reflected the concept of local, urban background and regional emission regions (see for example Lenschow, 2001 and the EU directive 2011/85/EU regarding e-reporting). We also constrained the definition of such regions to administrative boundaries in order to clearly link the pollution contribution to the corresponding administrative level (i.e. Municipality, Metropolitan area, Region, Country). The emission regions were shown for the two innermost computational domains, in Figure 20 labelled with different colors.

The wider area in yellow, named Po Valley (POV), included all sources between national and Lombardy region boundaries; in blue the Lombardy area (LOM), extending from the boundaries of Lombardy to those of the metropolitan area of Milan (formerly Province of Milan); in orange, the Metropolitan area of Milan (PRO), not including the municipality of Milan (MIL), the red area in Figure 20). The fifth area, the green one in Figure 20 bottom panel, represents a very local emission area within the Milan city center (AUS) where the receptor site is located.

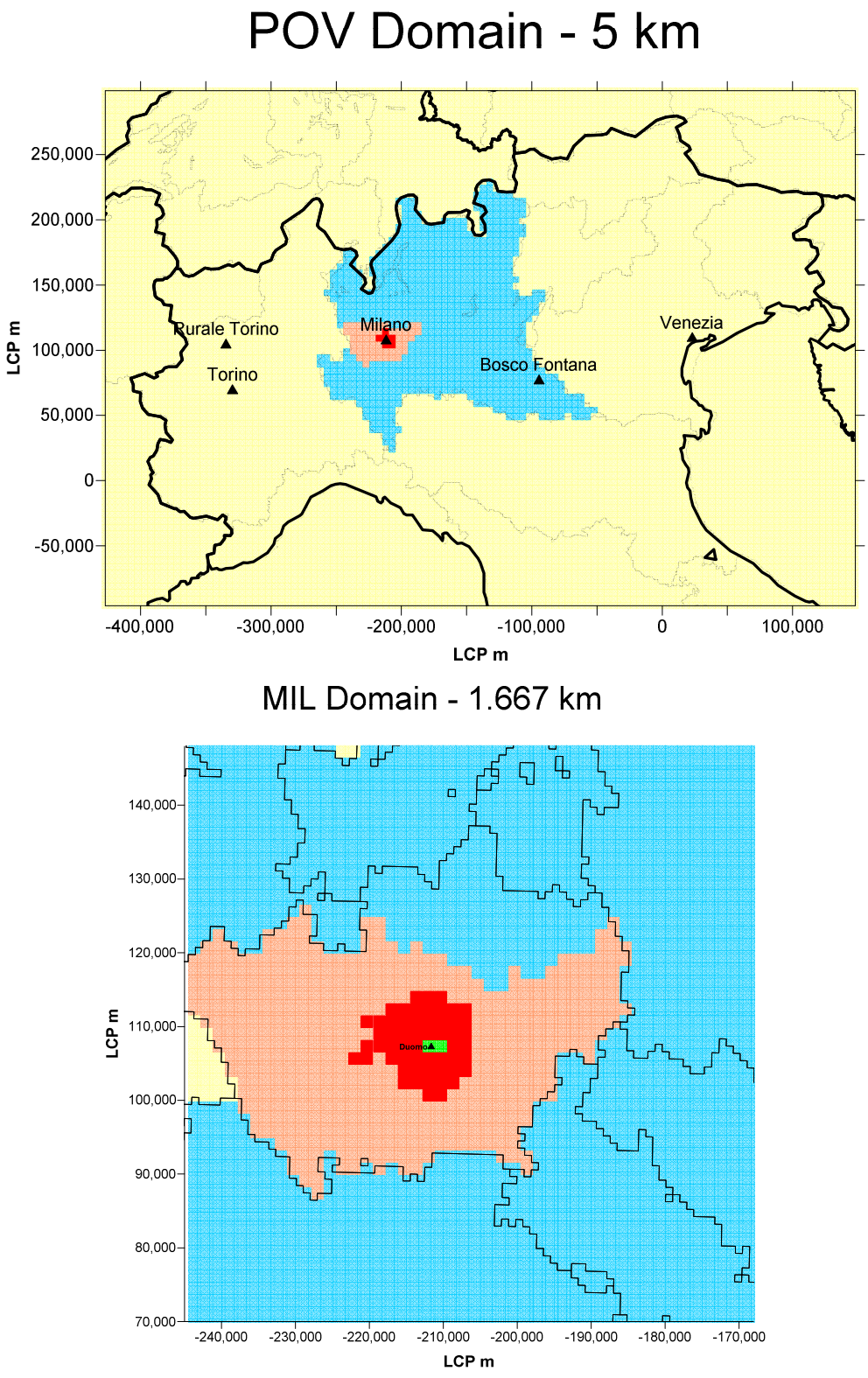


**Figure 20. Emissive regions within POV (5 km) and MIL (1.667 km) domains. In the top panel, some important cities over the Po Valley (Milan, Turin and Venice) are shown**

Accordingly to Lenschow's definition, emissions from POV and LOM regions were responsible for the regional background, those from PRO and MIL regions were

responsible for the urban background, those from the smallest region determined the very local contribution to the concentration levels in the center of Milan. Such a local contribution did not represent a street level contribution but it meant the smallest and closest emission region that could be defined with respect to the selected receptor.
Briefly, 11 emission source categories investigated were illustrated in Table 8

**Table 8. Source emission categories defined for CAMx/PSAT application**

| ***Label*** | ***Description*** |
|---|---|
| 01 ELE | Electrical energy production by industrial plants |
| 01 OTH | Industrial plants (no electrical energy production) |
| 02 BIO | Residential and commercial heating with biomass |
| 02 OTH | Residential and commercial heating with methane and gasoline (no biomass) |
| 07 AUT | Cars |
| 07 LEG | Light duty vehicles (weight < 3.5 tons) |
| 07 PES | Heavy duty vehicles (weight > 3.5 tons) |
| 07 MOT | Mopeds and motorcycles |
| 11 NAT | Natural sources –fires, volcanic eruptions, marine salt (only for Po Valley area) |
| EMEP | All sources located outside Italy. (no disaggregation on emission sources is provided) |
| OTHER | Other anthropogenic sources – agriculture, waste treatment, landfill, no streets transports |

This study evaluated contributions at a generic residential receptor located near Duomo cathedral. The area was characterized by moderated traffic volume, in particular taxy and private cars, and heating produced by commercial activities and private houses.
Through CAMx source apportionment the $PM_{2.5}$ mean annual concentration at Duomo station (about 18 $\mu g/m^3$) has been split by emission source categories, by emission regions, and by the combination of emission categories and regions. Modeled value was used as reference for all percentage data computed in this work.
In terms of region contributions (Figure 21a), both the regional (POV + LOM) and the urban background contribution (PRO + MIL) largely prevailed on the local contribution (AUS). Actually, POV and LOM regions, together with the long range transport (i.e.: contribution from sources located outside of POV computational domain) provided the largest contribution, overall accounting for about 53% of $PM_{2.5}$, the metropolitan area of Milan and its municipality, excluding the local sources, account for 38%, and the local contribution was responsible for less than 8%. Both primary and secondary nature of fine

particles that composed $PM_{2.5}$ were reflected by the similar contributions coming from urban background and local sources near to the receptor point and from the other sources located farther.

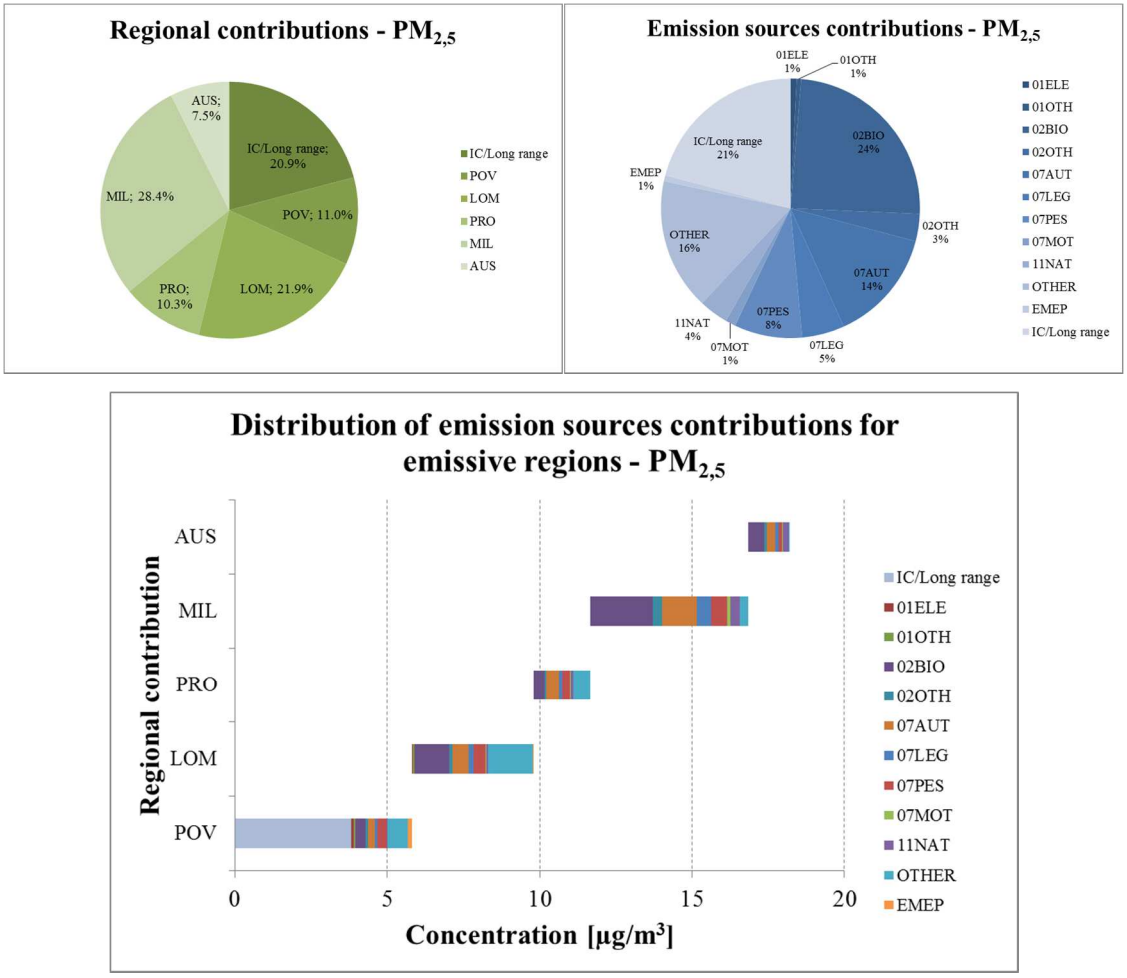


**Figure 21. $PM_{2.5}$ percentage distribution of emissive regions (17a, top-left) and emission sources categories (17b, top-right) contributions. (17c, bottom) is the regional absolute concentration distribution of each source activity contribution defined within CAMx/PSAT approach for $PM_{2.5}$**

In terms of source categories, road traffic, residential heating by biomass, and long range transport represented the most important sources for $PM_{2.5}$ with a total contribution of 73% (Figure 21b). The transport sector yielded the principal contribution (28%), with half contribution due to cars, 8% and 5% respectively due to heavy and light duty commercial vehicles, and 1% due to mopeds and motorcycles. Residential and commercial heating by biomass burning, accounted for 24%, resulting the second most important source for fine particles. Although the wood or pellet burning for residential heating was an activity not so used in a metropolitan city like Milan, the results was surprising and it will be addressed in the next chapters of the composite impact of both source emission regions

and categories. Long range transport was the third most impacting source (21%), followed by the OTHER category (i.e.: other anthropogenic sources like agriculture) that contributed up to 16%. Emissions from the non-biomass residential heating (3%), natural sources (4%) and industrial sources (2%) showed a minor impact, as the emission sources outside of Italy, but still included in the POV domain (EMEP emission category) that contributed for only 1%.

Contribution breakdown by region and emission category was synthesized in Figure 21c, showing that the highest contribution (4 $\mu g/m^3$) comes from long range transport from sources located outside the domain; the second highest contribution (2 $\mu g/m^3$) comes from biomass burning in MIL region and the third was given by the other anthropogenic sources in the LOM region.

Elemental carbon (EC) is a primary component of $PM_{2.5}$ directly emitted in atmosphere by combustion processes. As such, EC ambient concentration at receptor points is mainly driven by the contribution of local or short-range sources. At Duomo receptor, CAMx simulation estimated a mean annual EC level of 3.5 $\mu g/m^3$ for 2010. The geographic contribution analysis (Figure 22a) showed that more than 60% was due to urban background sources (MIL+PRO) and that the local sources (AUS) contributed for almost 13%. Nevertheless, the regional background contribution (POV+LOM) had a notable impact, reaching a total of 26% of the EC concentration when including also the long range transport. Focusing on source categories (Figure 22b), the transport sector represented the most impactful source for EC with a 55% share; in details, 26% came from cars, 15% and 13% were associated to heavy and light duty vehicles, respectively, while the contribution from mopeds and motorcycles was practically negligible (1%). Overall, the road source almost doubled the biomass burning, the second source for EC with 30%. The contribution from the other sources was rather limited: long range transport accounted for 5%, natural sources and the other anthropogenic sources for 4%, whilst EMEP sources and industrial processes did not impacted significantly on EC concentration level.

Figure 22c pointed out that the three most impacting sources were the traffic sector in the municipality of Milan (MIL) and in the Metropolitan area of Milan (PRO), that contributed respectively with 1.1 $\mu g/m^3$ (31%) and 0.28 $\mu g/m^3$ (8%) to EC level, and biomass burning in residential and commercial sources of the LOM region, which gave a 0.26 $\mu g/m^3$ contribution, similarly to the estimated share of traffic in the MIL area.

Overall, these three most impacting sources are responsible for almost 50% of the EC yearly mean concentration at Duomo receptor. Particularly, two of these sources were located in Milan metropolitan area boundaries highlighting the importance of urban sources, accordingly with the primary nature of this pollutant.

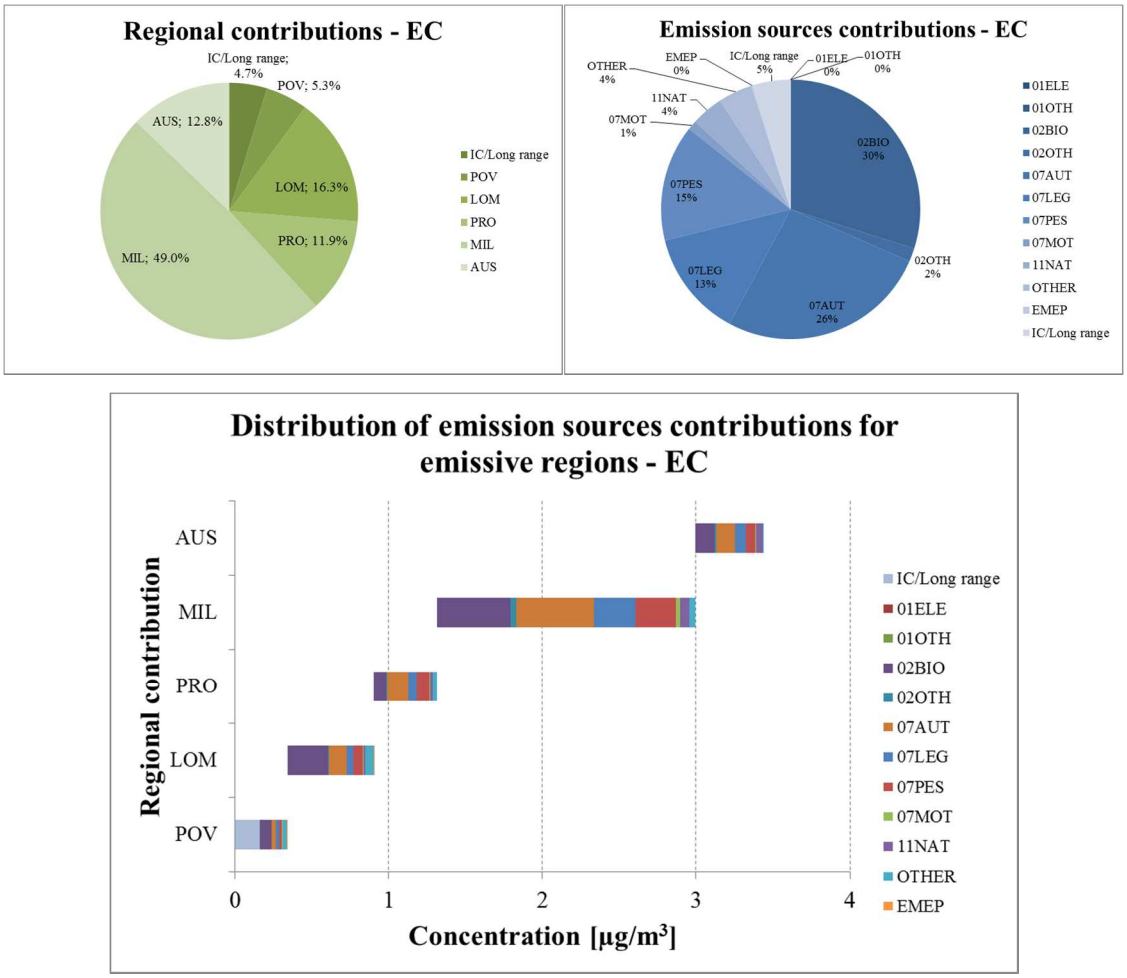


**Figure 22. EC percentage distribution of emissive regions (18a, top-left) and emission sources categories (18b, top-right) contributions. (18c, bottom) is the regional absolute concentration distribution of each source activity contribution defined within CAMx/PSAT approach for EC.**

Particulate nitrate is one of the secondary inorganic components of $PM_{2.5}$. For the Duomo receptor CAMx annual $NO_3^-$ level was 3.3 µg/m$^3$ in 2010.

$NO_3^-$ showed a deep different spatial distribution over the domain respect to EC as well as a different source contribution pattern. As shown in Figure 23a, the regional background contribution, given by long range transport, POV and LOM contributions, largely prevailed on all the other emissive regions. These sources determined 86% of the $NO_3^-$ annual mean concentration, with the remainder 14% totally due to urban background sources located in the Milan area (MIL + PRO). Emissions of the local area (AUS) gave

a negligible contribution (less than 1%). Overall, the local and short-range contribution, the most important for EC, had a limited role on the total concentration of this secondary component of $PM_{2.5}$. Almost 90% of total concentration was generated by sources far away from receptor point, presenting a homogeneous distribution among three contributions. In terms of source categories, the transport sector provided the largest contribution (43%), with heavy duty vehicles (20%) and cars (17%) yielding the highest share. Long range transport was responsible for 26%, the other anthropogenic sources for 16% and non-biomass residential and commercial combustion for 7%. Contributions from the other sources were evaluated 1-3% (Figure 23b).

Figure 23c pointed out the contributions of each source category by emission regions. The contribution originated from emission outside the POV domain (long range transport) was the highest (0.8 $\mu g/m^3$) among all region-and-category resolved contributions. The two other most impacting sources were transport in LOM and POV regions, with respectively 0.6 and 0.5 $\mu g/m^3$. All the sources related to urban background (MIL and PRO) and local region (AUS), generated a moderate contribution. Particularly, the contribution from all the sources within the urban area of Milan was less than 0.3 $\mu g/m^3$ and from the local area less than 0.15 $\mu g/m^3$.

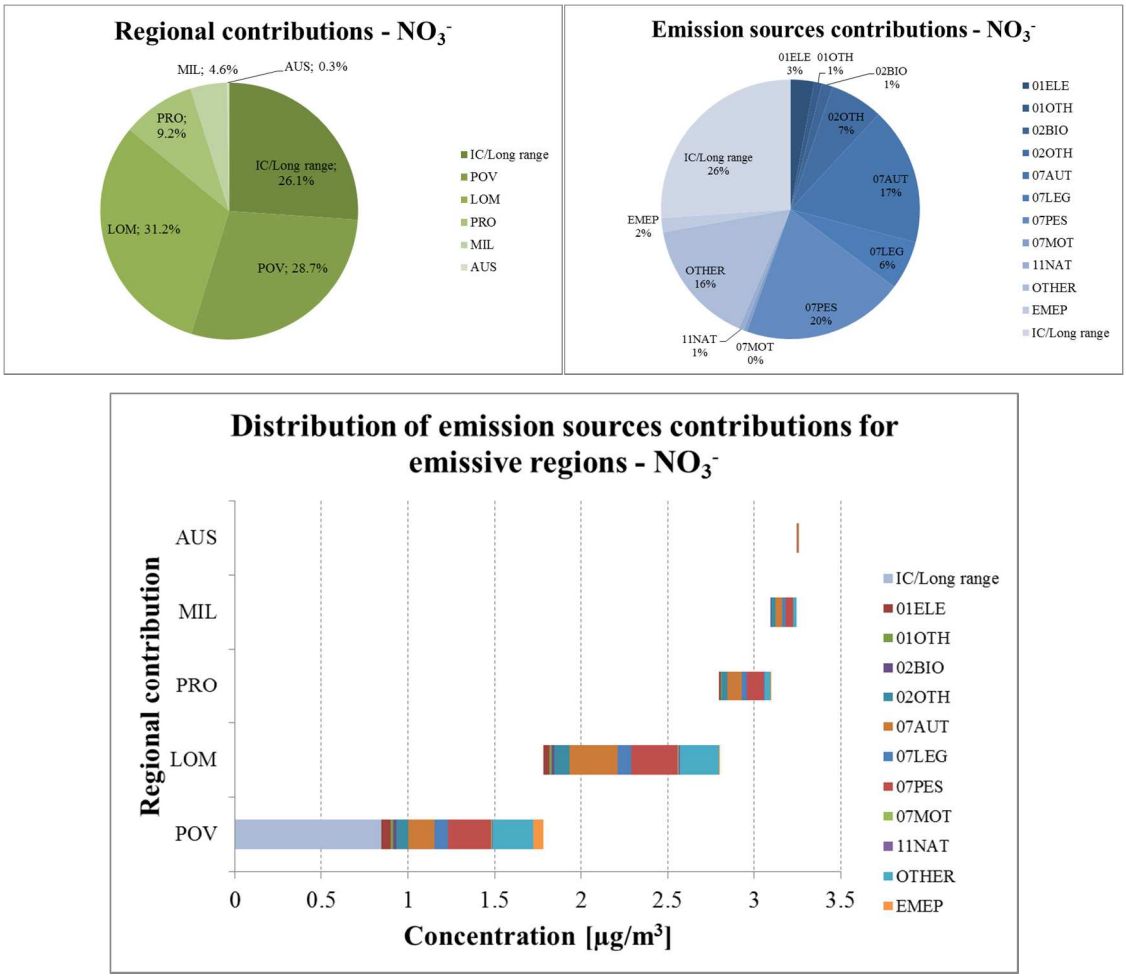


**Figure 23. $NO_3^-$ percentage distribution of emissive regions (19a, top-left) and emission sources categories (19b, top-right) contributions. (19c, bottom) is the regional absolute concentration distribution of each source activity contribution defined within CAMx/PSAT approach for $NO_3^-$**

The different contribution patterns obtained for EC and $NO_3^-$ were in agreement with the nature of these particulate components. The secondary origin of $NO_3^-$ was underlined by the higher contributions due to sources far away from the metropolitan area of Milan, as can be seen in Figure 24. Chemical reactions that produced secondary PM from gaseous precursors required adequate time scales, that favored their production far beyond the city boundaries. This fundamental aspect was demonstrated by contributions due to vehicular traffic. The local sources (AUS) of transport sector provided a negligible contribution to $NO_3^-$ at Duomo receptor. Moving far from the city area, the contribution due to transport sector to the nitrate fraction of PM gradually increased up to farther areas like POV where the 80% of the contribution to $PM_{2.5}$ at Duomo was related to $NO_3^-$. In particular, cars and heavy-duty vehicles that circulate in LOM area (0.5 µg/m$^3$) were more impacting than those circulate in Milan municipality (0.08 µg/m$^3$) and the nearer Metropolitan area (0.18 µg/m$^3$), even though all values are very low. Similar effects could be observed for

concentrations associated to cars and heavy-duty vehicles in POV area (0.4 µg/m$^3$). In first hypothesis, this aspect could be explained by a larger number of units of vehicles in LOM rather than in MIL but the correct answer relied on the origin of emission. The presence of ammonia, one of the gaseous precursors, combined with the large amount of NOx emissions generated the particulate nitrate that affected receptor points located farther away from emissive regions after transportation. As illustrated in the Figure 24 the other two emission categories (residential heating and other anthropogenic sources) detected the same behavior for the secondary component, higher in POV and LOM regions and lower or zero in AUS and MIL regions. Conversely, the pollution emitted directly in the atmosphere (EC) affected principally the contribution of sources located near the receptor point. Regarding road transport, almost 50% of road transport contribution of MIL area was due to EC as well as for AUS area. Either for residential and commercial heating, EC contribution showed an important role in MIL and AUS areas (20%). Regardless the total contribution related to each region, the "all emission categories" graph shown in figure below, presented the general distribution of primary and secondary components over a wide area. Including the long-range transport, EC growth was evident approaching regions near Duomo receptor point, while nitrate distribution was opposite. Farther regions presented an important contribution of particulate nitrate rather than elemental carbon.

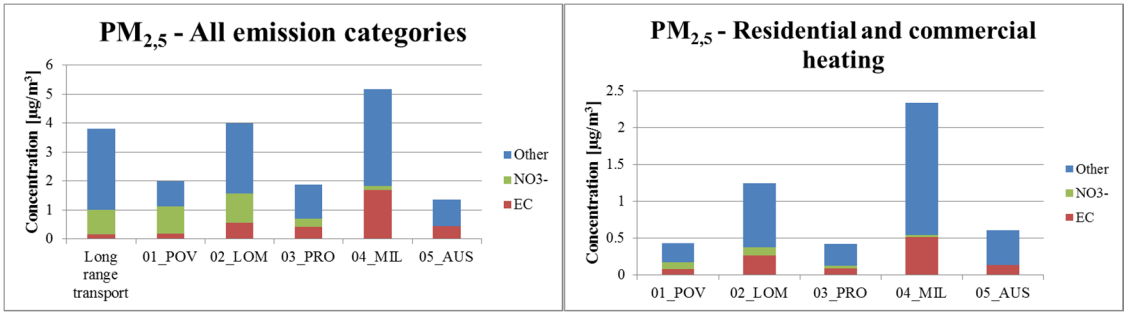

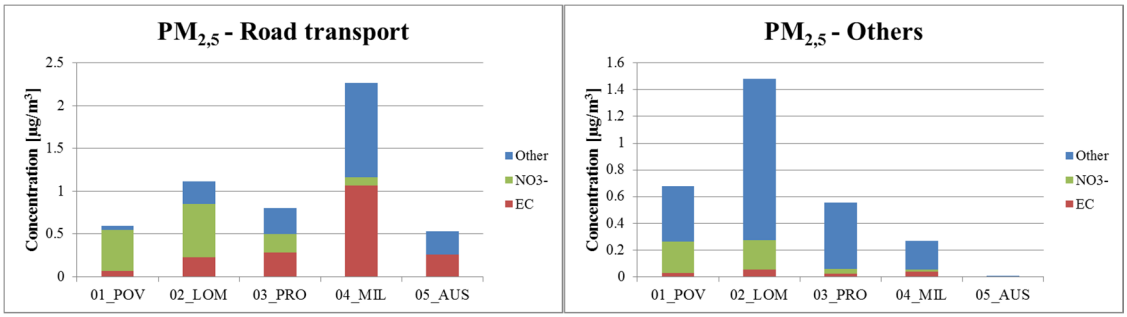


**Figure 24. $PM_{2.5}$ chemical profile of each emissive region contributions for specific source categories as residential heating (top-right), road transport (bottom-left), others (bottom-right) and all emission sources (top-left). The chemical species considered are elemental carbon (EC), particulate nitrate ($NO_3^-$) and all other compounds.**

Nitrogen dioxide is one of the gaseous precursors of nitrate particulate. At the Duomo receptor, the $NO_2$ yearly mean concentration estimated by CAMx for 2010 was 21 ppb. One of the RMs weaknesses was the difficulty to apportionment analysis either to gaseous pollutant like $NO_2$. Conversely this issue can be addressed by CAMx.

The panels of Figure 25 showed the relative contributions of regions, source categories, and geographically apportioned sources.

Overall, the urban background sources were responsible for about 70% of $NO_2$ concentration and considerably prevailed over the regional background sources (20%) and over the very local sources in proximity of the receptor point (10%). The urban background contribution was principally given by the emissions from the MIL region (51.8%), with only 18.1% from the metropolitan area of Milan (PRO). The regional background contribution was mainly determined by the LOM region (15.2%), with only minor contributions from POV region (3.2%) and long-range transport (1.3%). The AUS region provided a rather small contribution. However, considering the limited number of sources in this area with respect to the surrounding emission regions, the estimated 10% contribution stated that the local sources actually played a relevant role on $NO_2$ concentration at the receptor point and in urban areas in general.

Focusing on source categories, road transport, residential and commercial combustion, and the other anthropogenic sources determined 98% of $NO_2$ concentration, whilst natural sources, EMEP sources and long-range transport were practically negligible. The most impacting source was, by far, the road transport with a 72% share: 60% of $NO_2$ concentration came from heavy duty (31%) and cars (29%) emissions (largely composed by diesel cars), 11% from light duty vehicles, about 1% from mopeds and motorcycles. The incomplete combustion of diesel or gasoline produced a large amount of NO that

reacted immediately with the atmospheric oxidants like $O_3$, generating $NO_2$. Residential and commercial combustion, yielded an overall contribution of 17%, but almost totally due to fossil fuels (16%). The other anthropogenic sources category, namely industrial sources, gave a 9% contribution.

Figure 25c clearly showed that vehicular traffic in the municipality of Milan was the main source for $NO_2$ at Duomo receptor point. Road transport from the MIL region was responsible for 8 ppb, almost 40% of total $NO_2$ concentration. In details, cars and heavy-duty vehicles contributed at the same extent for 15%, that roughly corresponded 3 ppb. The impact of transport emissions from the surrounding regions was also significant, as traffic emissions from PRO and LOM regions, providing the second (13% - 2.8 ppb) and third (10% - 2.1 ppb) most relevant contributions.

The wide spatial distribution of source yielding a relevant contribution to $NO_2$ concentration at Duomo receptor, particularly for road transport, pointed out that coordination of local and regional policy was desirable in order to obtain visible reduction of $NO_2$ concentration levels.

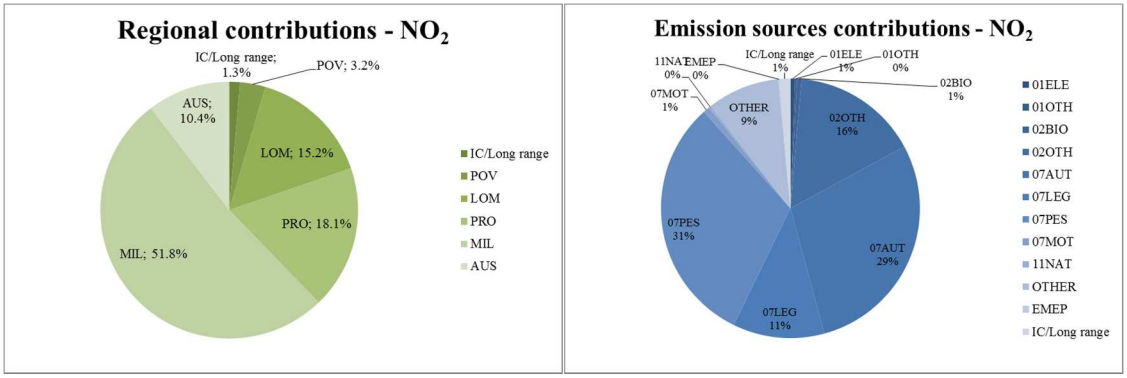


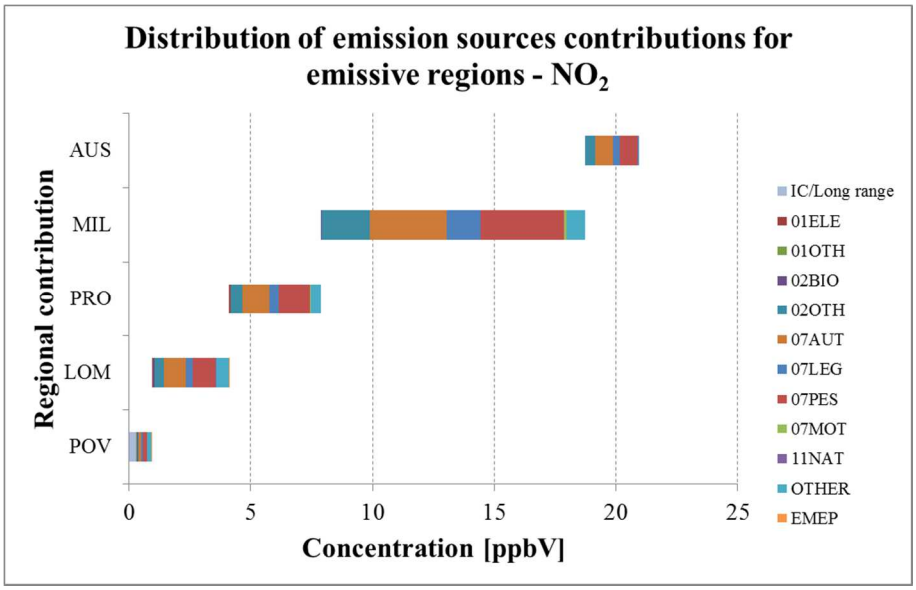

**Figure 25. $NO_2$ percentage distribution of emissive regions (21a, top-left) and emission sources categories (21b, top-right) contributions. (21c, bottom) is the regional absolute concentration distribution of each source activity contribution defined within CAMx/PSAT approach for $NO_2$.**

CAMx results for $PM_{2.5}$ chemical speciation and CAMx/PSAT results for $PM_{2.5}$ source apportionment were discussed in comparison with experimental data and Positive matrix Factoriziation (PMF) source apportionment from AIRUSE+ project (Amato et al, 2016). $PM_{2.5}$ data for 2013 from a one-year measurement campaign at Milano-Torre Sarca, an urban background site near Milan city center (about 5 km as crow fly distance from Duomo receptor) had been used for comparison purpose. Notwithstanding AIRUSE+ data and CAMx simulation output did not refer to the same period and receptor, the following analysis could be regarded as a validation of CAMx/PSAT results, at least qualitatively.

Reported $PM_{2.5}$ yearly mean concentration from gravimetric measurements at Milano-Torre Sarca (29.9 $\mu g/m^3$) was in agreement with automatic monitoring network data for another urban background site in Milan (30.7 $\mu g/m^3$). Table 9 summarized yearly mean concentrations of speciated $PM_{2.5}$ for AIRUSE+ and for CAMx simulation in this work. Other than the reference year and site, the two datasets also differed for the chemical species considered for mass closure. Actually, AIRUSE+ data mass closure was not complete, with 4.8 $\mu g/m^3$ not determined, likely due to water molecules of residual moisture, crystallization and formation water, and metal oxides. Conversely, these latter were considered in CAMx speciation as the primary elements generated by anthropogenic sources, labeled “other fine particles”.

Table 9 highlighted the strong difference in $PM_{2.5}$ concentration (29.9 $\mu g/m^3$ vs. 18.7 $\mu g/m^3$) that also held in a dry-basis comparison (25.1 $\mu g/m^3$ vs. 18.7 $\mu g/m^3$). Although the reference years and the sites were different, such missed concentration of 6.4 $\mu g/m^3$ could not be justified by a different yearly emission regime or meteorological conditions, thus confirming that CAMx tendentially underestimates the $PM_{2.5}$ mass.

According to AIRUSE+ data, organic matter (OM = POA + SOA) was the main component of $PM_{2.5}$, followed by secondary inorganic aerosol (SIA = nitrate + sulfate + ammonium), elemental carbon, soil fine dust and sea salt. Comparison with CAMx data pointed out relevant discrepancies for OM and EC, as well as a reasonably good agreement for SIA. OM was strongly underestimated by CAMx (5.1 $\mu g/m^3$ vs. 12 $\mu g/m^3$) due to an incorrect reconstruction of secondary organic aerosol (SOA), almost totally missed by the model (0.5 $\mu g/m^3$ vs. 8 $\mu g/m^3$). Troubles in properly estimating SOA through the SOA formation algorithm implemented in CAMx version used in this work

had been reported in literature (Pirovano et al., 2015; Meroni et al., 2017) Conversely, CAMx overestimated the primary fractions of $PM_{2.5}$: POA concentration was slightly overestimated (4.6 µg/m$^3$ vs. 4 µg/m$^3$) whereas EC at a larger extent, as CAMx result (3.4 µg/m$^3$) was almost twice as high as the measured concentration (1.6 µg/m$^3$). A better performance was observed for SIA, whose total concentrations were in good agreement, both in absolute (8.3 µg/m$^3$ vs. 9.5 µg/m$^3$) and relative terms (44% vs. 38% of $PM_{2.5}$ dry mass). More in details, ammonium was almost perfectly reproduced (2.0 µg/m$^3$ vs. 2.1 µg/m$^3$) whereas there were some discrepancies for sulfate and nitrate. Namely, CAMx overestimated sulfate (3.0 µg/m$^3$ vs. 1.8 µg/m$^3$), thus giving rise to a corresponding underestimation of nitrate (3.2 µg/m$^3$ vs. 5.7 µg/m$^3$). The minor components (sea salt and soil dust) did not reach remarkable concentration values in both datasets; however, CAMx tended to predict lower value for sea salt (0.2 µg/m$^3$ vs. 0.6 µg/m$^3$) and especially for soil dust (0.1 µg/m$^3$ vs. 1.8 µg/m$^3$)

**Table 9. $PM_{2.5}$ chemical speciation by AIRUSE+ measurement campaign and CAMx/PSAT output.**

| Species | AIRUSE+ (2013) | | This work (2010) | |
|---|---|---|---|---|
| | Concentration [µg/m$^3$] | % | Concentration [µg/m$^3$] | % |
| **Primary organic aerosol (POA)** | 4.0 | 16 | 4.6 | 24 |
| **Secondary organic aerosol (SOA)** | 8.0 | 32 | 0.5 | 2 |
| **Elemental carbon (EC)** | 1.8 | 7 | 3.4 | 18 |
| **Sulfate** | 1.8 | 7 | 3.0 | 16 |
| **Nitrate** | 5.7 | 23 | 3.2 | 17 |
| **Ammonium** | 2.1 | 8 | 2.0 | 11 |
| **Sea salt** | 0.6 | 2 | 0.2 | 1 |
| **Soil dust** | 1.2 | 5 | 0.1 | 1 |
| **Other fine particles (CAMx only)** | - | | 1.7 | 9 |
| **Total** | 25.1 | 100 | 18.7 | 100 |
| **Undetermined mass** | 4.8 | | - | |
| **Total** | 29.9 | | | |

The comparison between source apportionment results was not as straightforward as for speciated $PM_{2.5}$ because of the different output of the two approaches. PMF found a number of factors together with the related contribution and chemical profile. For AIRUSE+ dataset PMF found a 7-factor solution: relied on their profiles, these factors had been identified as vehicle exhaust (VEX) and non-exhaust (NEX), biomass burning

(BB), secondary nitrate (SNI), secondary sulfate and organics (SSO), marine aerosols (SEA), industrial emission (IND), and mineral emissions (MIN) with about 12% of the $PM_{2.5}$ mass still unapportioned.

Conversely, CAMx/PSAT output consisted of concentration values for each species and each source category considered. Thus, overall source contributions had to be reconstructed by adding the single $PM_{2.5}$ components generated by the different sources. CAMx/PSAT traffic factor was computed taking into account the related estimated concentrations for EC, POA and "other fine particles" and compared with VEX+NEX source form PMF. Similarly, biomass burning factor was defined as the sum of EC, POA and "other fine particles" produced by residential heating through biomass combustion. Sodium and chlorine concentrations estimated by CAMx/PSAT from the "Natural" emission category had been added in order to assess sea salt contribution, for comparison with SEA source from PMF. Because CAMx did not simulated soil dust emissions and industrial sources were not specifically tracked but simply included in the generic "other anthropogenic" source category, the comparison with the PMF factors MIN and IND was not possible.

For the secondary source, the comparison was not straight because the profiles of the SNI and SSO sources (the former mainly identified by nitrate and ammonium, the latter by sulfate and ammonium) were also characterized by the presence of organic carbon. Thus, altogether these sources accounted for SIA but also for a relevant amount of SOA. Additionally, even though they accounted for the most part of SIA, small sources of SIA were also associated by PMF to the other sources, but both also containing organic matter; thus, the sum of these factors also accounted for a fraction of the SOA. In practice, these two factors were also responsible for almost all of the SOA.

In spite of the difference in the modeling approaches, of year and receptor, and of the processes missed by CAMx, the results of source apportionment comparison were quite encouraging, especially for the primary sources. The traffic source was responsible for about 4 $\mu g/m^3$ (PMF: 4.3 $\mu g/m^3$; CAMx/PSAT: 3.6 $\mu g/m^3$), accounting for about 20% of $PM_{2.5}$. A good agreement was also observed for the biomass burning source too, with a mean concentration of 4.6 $\mu g/m^3$ (PMF: 5.1 $\mu g/m^3$; CAMx/PSAT: 4.3 $\mu g/m^3$) and a 24% a contribution. The lower contributions estimated by CAMx/PSAT might derive from the inclusion of fractions of SIA and SOA in the VEX+NEX and BB profiles by PMF. However, part of such might also derive from the low bias of CAMx for the total $PM_{2.5}$

mass that could be ascribed to meteorology, namely to the reduced dispersion of pollutants under strong inversion conditions in winter time, not correctly detected by the meteorological model. The mismatch on the contribution from secondary sources was essentially due to CAMx underestimation of SOA. However, if a SOA-free secondary source was computed out of PMF source profiles and contributions, the two values get much closer and confirmed the substantial agreement for the secondary inorganic source. This methodology needs further improvement in order to track SIA and SOA formation for their proper apportionment and to consider also the contribution of soil dust and resuspension. On the other hand, the main asset of CAMx/PSAT methodology is the possibility to localize the origin of pollution, also for the secondary aerosols and for the gaseous pollutants, providing additional and complementary information to PMF results. Once the results of the two modeling approaches are better reconciled, the combination of the piece of information coming from their concurrent implementation can improve the overall quality of source apportionment analysis. Local or regional air quality plans relied on such improved source apportionment analysis could help to assess the real health impacts of biogenic and anthropogenic sources over the domain and properly define intervention strategies for air quality.

## 2.3. Hybrid modeling system source apportionment – PM2.5 and EC

PhD last step, after comparison between CAMx/PSAT approach and PMF, was focused on HMS source apportionment application in order to detail this type of information over the urban local domain with higher resolution than CAMx stand-alone approach. This passage combines the strength of CAMx for regional atmospheric modeling, improved with PSAT method extended to gaseous precursors, with the accuracy presented by AUSTAL2000 about air quality modeling at local scale. This work was focused on PM2.5 and elemental carbon source apportionment analysis over urban local domain within Milan city center, coupling CAMx regional results and AUSTAL2000 outputs, considering only primary components.

Source apportionment analysis was conducted over three urban receptors representing different urban contexts: park site where no local sources affects mainly concentration

levels, residential site (Duomo site) where transports and residential heating were the most impactful sources and hot spot (traffic site) where traffic sector prevailed over other urban sources.
HMS source apportionment derived from off-line coupling of CAMx source apportionment over wider area representing regional and urban background sources and AUSTAL2000 source apportionment, excluding chemical processes, over restricted area that represented local sources.

Before to deal with main results of HMS source apportionment, in Figure 26 was illustrated the source apportionment comparison between CAMx and AUSTAL2000 over the local domain for $PM_{2.5}$. In order to compare eulerian and lagragian approaches, emission sources which affected local concentrations were equals. As cited before, private transports and residential heating were the most important emission categories that affect local urban concentrations. Focusing on March, the comparison pointed out the "flat" behavior of CAMx estimations notwithstanding urban receptors differed radically in terms of location, while AUSTAL2000 exalted properly the difference between them. $PM_{2.5}$ concentrations estimated by CAMx range from 1 $\mu g/m^3$ (park site) to 1.5 $\mu g/m^3$ (Duomo receptor) and were characterized by a strong influence of biomass burning which affected $PM_{2.5}$ levels more than 0.5 $\mu g/m^3$. Traffic sector generated always a concentration lower than 0.5 $\mu g/m^3$. The principal aspect relied on low sensibility of CAMx over a limited urban area: both $PM_{2.5}$ absolute values and distribution of contributions were quite similar between the three receptors. At opposite, AUSTAL described a relevant inhomogeneity between receptors due to different impact of local sources. Thus, traffic site concentration ($> 4 \mu g/m^3$) was more than four times higher than park site estimate (1 $\mu g/m^3$). As could be seen from Figure 26, traffic source, composed by cars, light and heavy-duty vehicles, mopeds and motorcycles, played an important role for the hot spot receptor located near crossroads, prevailing over residential heating; transports produced a contribution of 3 $\mu g/m^3$ that corresponded to the 63% of $PM_{2.5}$ urban level, while focusing on park site the residential heating became the most impactful source but with lower concentrations levels. During July, considering both models, concentration levels decreased two times than winter month and the distribution of emissions contributions changed radically. Regardless receptors locations, CAMx model estimated a concentration level lower than 0.5 $\mu g/m^3$ with a maximum in Duomo receptor

(0.5 µg/m$^3$). In the same locations, AUSTAL model described a spatial resolution more variable, starting from 0.25 µg/m$^3$ estimated at park site up to 2.2 µg/m$^3$ at traffic site. During summer, transport sector was recognized as the most impactful source with a percentage value higher than 90%. Notwithstanding two models were based on different approach, produced quite similar outcomes, in particular for park site and Duomo receptor. CAMx results could be assumed as concentrations levels visible in receptor points not affected by direct emissions. Conversely, at traffic site were estimated higher $PM_{2.5}$ concentrations levels and a different relative distribution of contributions due to a strong impact of traffic emissions.

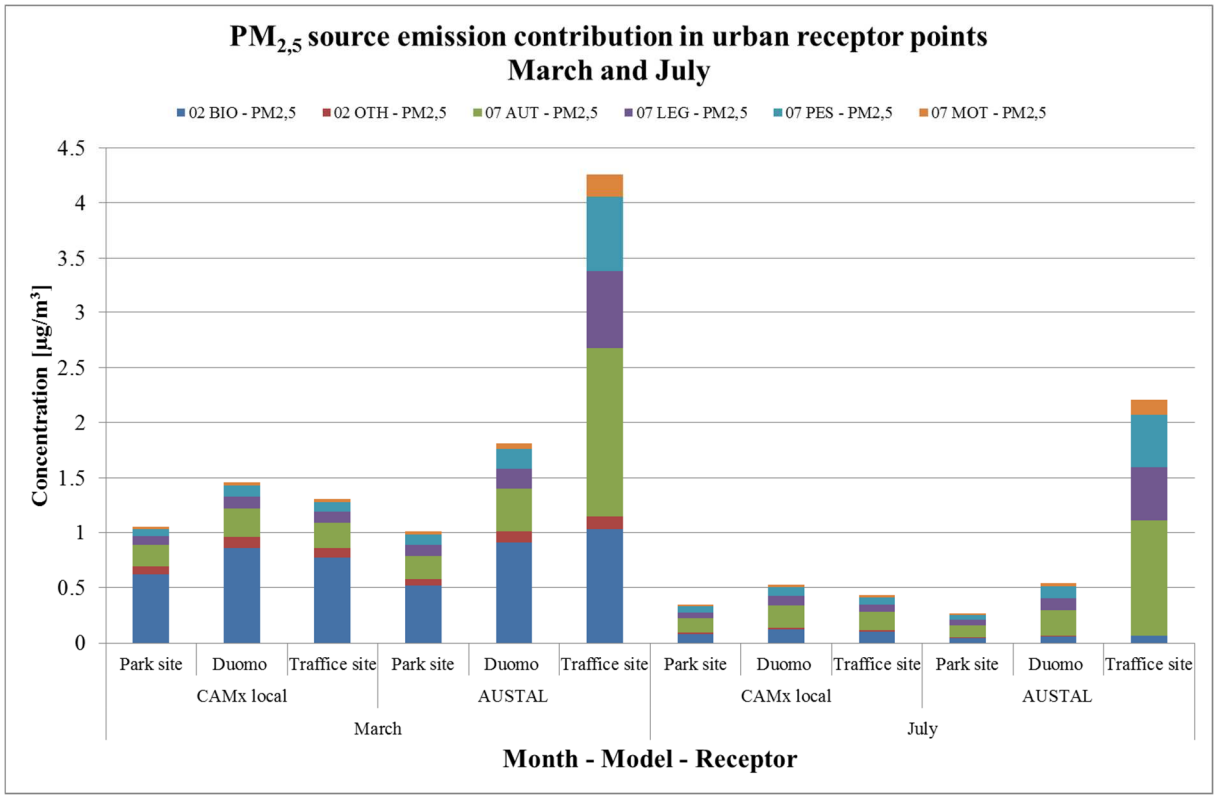


**Figure 26. PM2.5 source apportionment comparison between CAMx and AUSTAL at the urban receptors (park site, Duomo receptor and traffic site) over the Milan local domain for March (left part) and July (right part).**

As well as for $PM_{2.5}$, EC urban source apportionment analysis was illustrated in Figure 27. During March, CAMx model estimated a homogeneous concentration over all receptor points, starting from 0.3 µg/m$^3$ at park site to 0.4 µg/m$^3$ at Duomo receptor. Regardless site location, transport and residential and commercial heating contributed equally. Conversely, AUSTAL model reproduced a different concentration over the urban receptors. As expected, higher concentrations were estimated at the traffic site where EC

level reached about 2 µg/m$^3$, due to principally by transport and in particular cars that generated 0.8 µg/m$^3$, corresponding to the 40% of total concentration. At Duomo receptor, EC level decreased up to 0.6 µg/m$^3$, accordingly to a low traffic volume, while the contribution generated by residential heating was identical for both sites (0.2 µg/m$^3$). The lowest EC level (< 0.4 µg/m$^3$) was estimated at park site, where transport contributions were still the higher part while the residential heating generated a contribution lower than 0.1 µg/m$^3$. During July, elemental carbon concentrations were due totally to transports, in particular from cars that were the main component of urban traffic source, while the residential heating category did not affect final concentration. As for winter month, CAMx model showed similar EC concentration levels regardless the receptor location, while AUSTAL reproduced quite well the urban variability of EC levels. The lowest concentration was estimated at the park site while the highest over the traffic one.

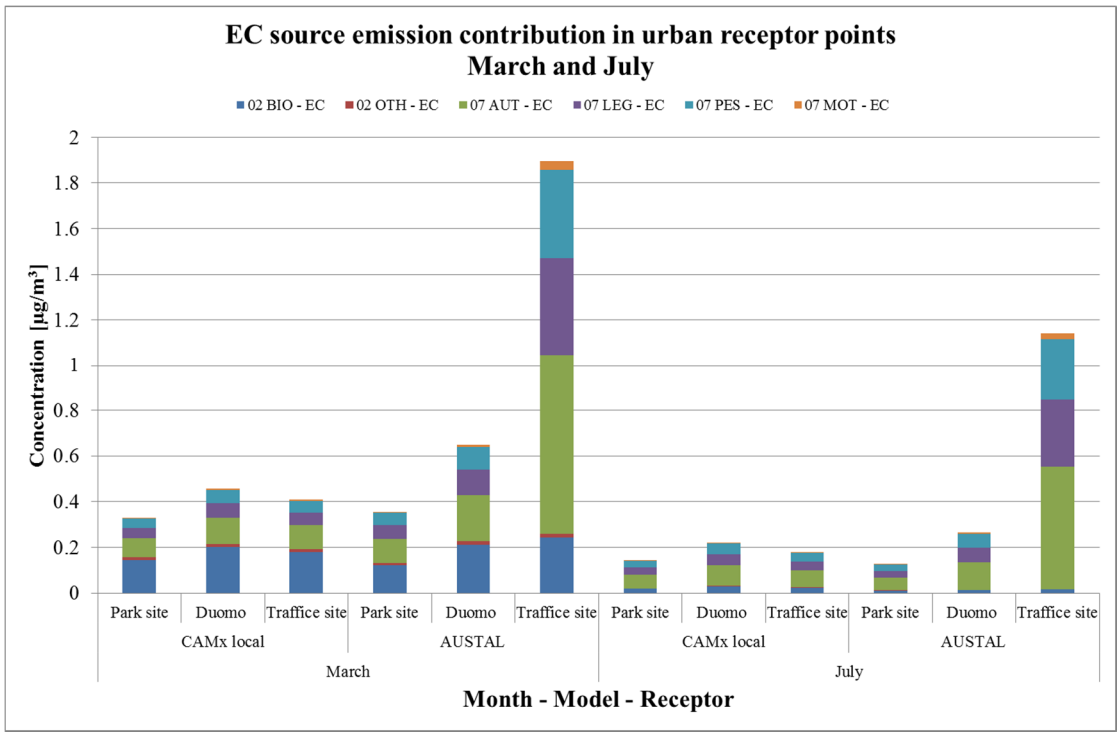


**Figure 27. EC source apportionment comparison between CAMx and AUSTAL at the urban receptors (park site, Duomo receptor and traffic site) over the Milan local domain for March (left panel) and July (right panel).**

$PM_{2.5}$ source apportionment results by HMS illustrated in Figure 28 pointed out the capability to reconstruct the sources contribution within an urban context, taking into account both local and regional sources.

Focusing on park site, HMS estimated more than 20 µg/m$^3$ during March, while during summer (July) the mean concentration level decreased under 10 µg/m$^3$. In March, long range transport (concentration contribution due to sources located outside the Po Valley domain) generated a contribution of about 5 µg/m$^3$ while MIL region was the most impactful area (7.5 µg/m$^3$), with 50% caused by biomass burning emission category. During July, biomass burning contribution was negligible while long range transport was still the highest. Focusing on the Duomo receptor, contribution derived from regions outermost the urban local domain (AUS) was identical to the previous receptor. The main difference was caused by AUSTAL outcomes, introduced with HMS, within AUS area. Even though emissive regime was quite different, mean concentrations were similar, in particular during summer month. Improvements due to the HMS were visible at the traffic site, focusing on the contributions generated by sources located within AUS domain. As can be seen from Figure 28, the concentrations due to the innermost sources were 5 µg/m$^3$ (during March) corresponding to 20% of final $PM_{2.5}$ level, while over the other receptors the percentage value decreased under 10%.

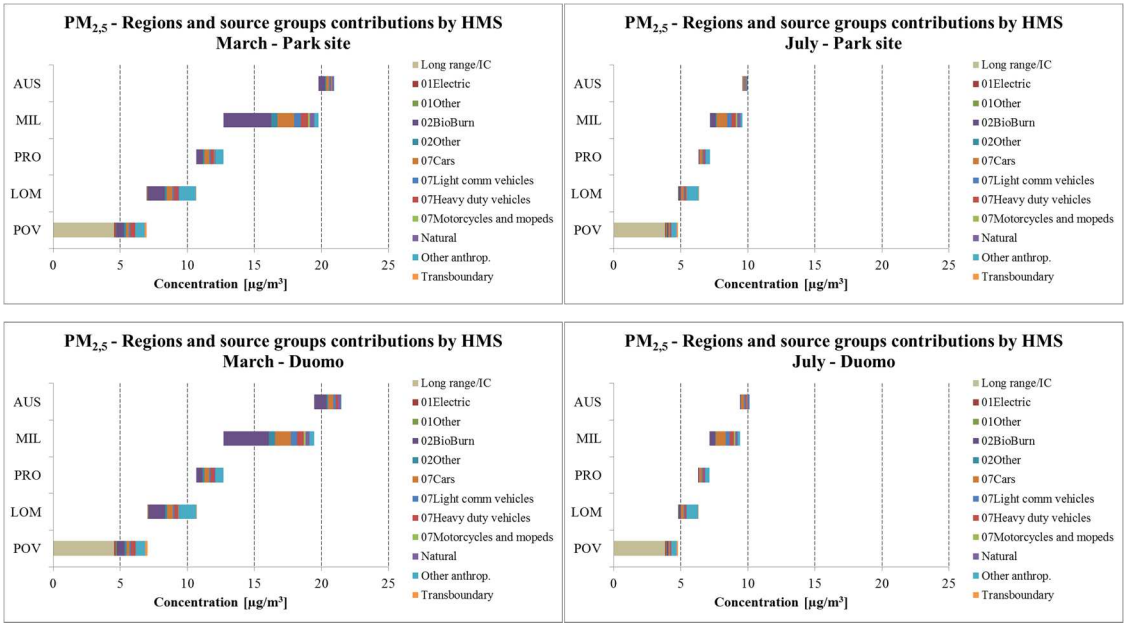

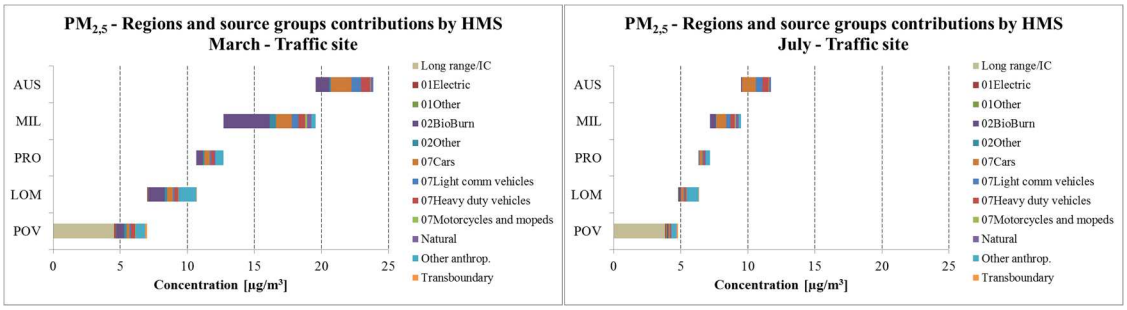


**Figure 28. PM2.5 source apportionment by HMS for park site, Duomo and traffic site during March and July**

Focusing on the summer month (July), $PM_{2.5}$ concentrations were quite low over all receptor points due to the absence of residential heating emission and pronounced atmospheric dispersion phenomena respect to the winter period. At park site, $PM_{2.5}$ level decreased up to 10 µg/m$^3$. The highest contribution was generated by POV region and the long-range transport represented the most impactful source between all emission sources for each area. Duomo receptor could be assimilated to park site for both final concentration level and source emission distribution. As discussed for March, hot spot receptor presented a totally different source emission distribution, although Po Valley was the most impactful region.

As illustrated in Figure 28, $PM_{2.5}$ primary and secondary behaviors were well represented during both periods: local and regional contributions were balanced in March, while during July prevailed secondary contribution represented by outer sources.

Figure 29 represented the source apportionment analysis of elemental carbon (EC) at the three urban receptors during March and July. Focusing on March, AUS region contribution was the only element of difference among receptors. As observed previously, main differences were due to lagrangian approach adopted within urban local area through AUSTAL model. At park site, EC concentration estimated reached almost 4 µg/m$^3$. The most impactful area was clearly MIL region. Road transports, combining car, light vehicles, heavy vehicles and motorcycles, was the source emission category that generated the higher contribution (more than 1 µg/m$^3$). Duomo receptor presented a similar contribution distribution even though AUS area affected final EC level for almost 1 µg/m$^3$. The most impactful source was again road transport. Hot spot receptor presented a contributions distribution totally different from park and Duomo site due to AUS sources. In this receptor, sources located near the traffic site determined a huge impact

for the final EC level reaching more than 5 µg/m$^3$. AUS area generated almost 2 µg/m$^3$ (about 40%), due totally to traffic sector with a high fingerprint of passenger cars.

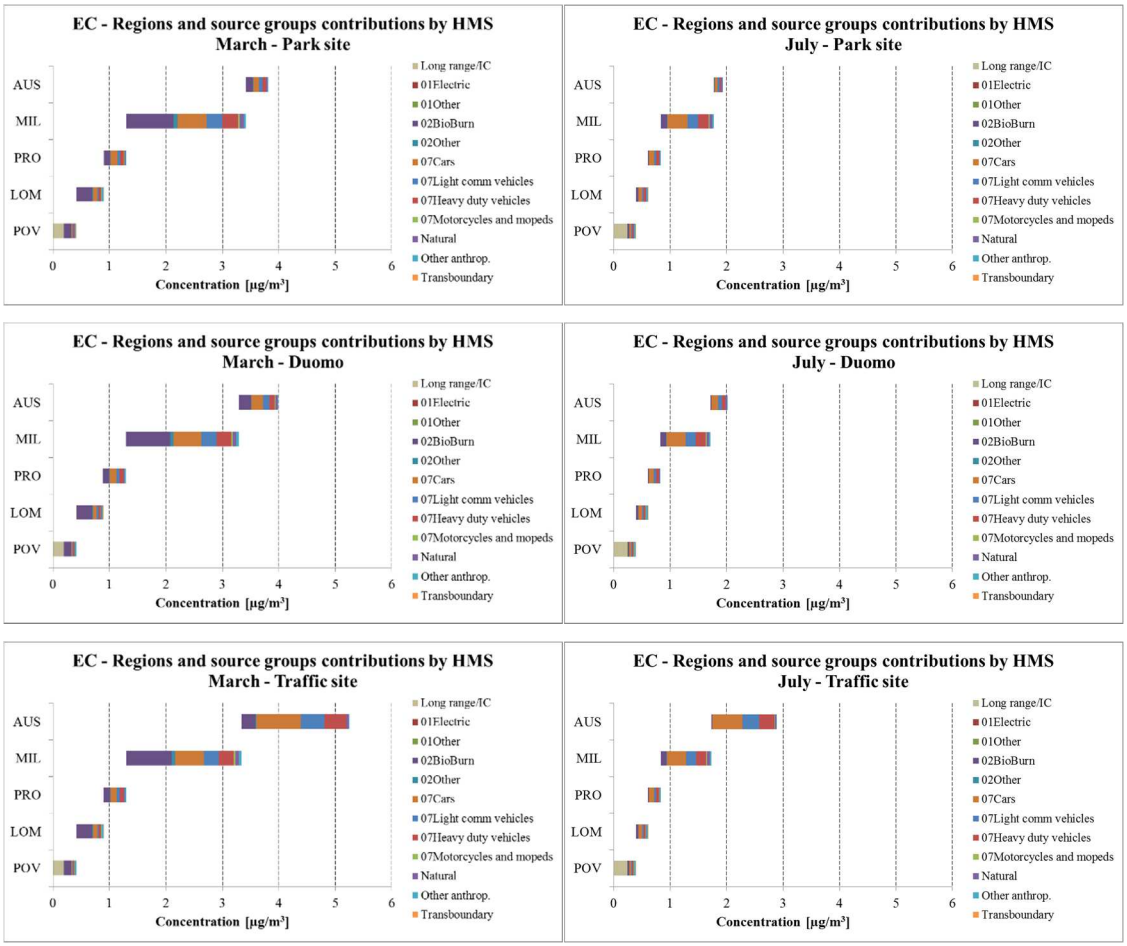


**Figure 29. EC source apportionment by HMS for park site, Duomo and traffic site during March and July**

Focusing on July, EC levels decreased until 2 µg/m$^3$ at park and Duomo receptor while over the traffic site reached almost 3 µg/m$^3$. Even though park and Duomo receptor were not directly affected by cars or other vehicles, traffic was still the most impactful source. Almost half of total concentration estimated in these two receptors was generated by MIL region and in particular, as described before, traffic source determined almost total contribution. Conversely, at traffic receptor the areal distribution of contributions was totally unbalanced to local sources. As illustrated in Figure 29, more than one third of total EC level estimated over traffic site was generated by AUS area. MIL area affected final EC level of about 1 µg/m$^3$ while the contribution due to sources located far away from receptor produced the remnant one third. As for AUS area, traffic source was the principal source considering the other regions

# 3. Experimental activities

In order to reduce PM underestimation, in particular during the winter period, was conducted an experimental campaign for estimating a site-dependent emission factor for PM resuspension due to transport sector. The aim of this work was to investigate an urban phenomenon which could be assumed as one of the reason of PM underestimation. As a matter of fact, some recent researches (Amato et al. 2017; Amato et al, 2012; Amato et al, 2009) pointed out as PM traffic resuspension could not be neglected within an urban context as whole metropolitan area of Milan. Therefore, two types of experimental campaign were carried out within Milan city area: direct and passive measurements.

## *3.1. Direct measurements*

The study of road dust resuspension was conducted by collecting samples directly from road pavement by sweeping sediment and either sieving or inducing resuspension in the laboratory and extracting PM10 through size selective inlets. However, these procedures and sample treatment are affected by the loss of the fine particles owing basically to the difficulties of collecting all deposited material and also to the electrostatic adhesion of particles to pincer/brush hairs and sieve meshes. New researches made by Amato et al, combined to the absence of a definitive sampling protocol, driven to the development of a new PM10 sampling device. A field resuspension chamber was developed for vacuuming in situ, with a flow rate of 25 l/min, the resuspended PM10 fraction onto filters. Road sediments were aspired from the pavement of active traffic lanes as showed in Figure 30, using a Becker pump powered by Honda field generator (located downwind respect to the sampling area). Particles were immediately resuspended in a Metacrylate deposition chamber and the particles small or light enough to be carried by air flow continued their journey through the system. After that, these particles entered a Negretti stainless steel elutration filter designed to allow passage to only PM10 material. At the end, these particles were collected on 47 mm diameter fiber quartz of Teflon membrane filters.


**Figure 30. Photos during collecting samplers in Via Tanzi.**

All particles with aerodynamic diameter higher than 10 μm were deposited in the Metacrylate chamber and along the elutration filter. Electrostatic adhesion caused some losses of particles minus than 10 μm. However, this loss could be considered negligible

respect to the traditional sampling losses. Thanks to collaboration of Fulvio Amato and its new sampling instrument, the resuspension campaigns were performed over Milan urban area, in particular at Via Tanzi, a road segment with a length of 200 m, one wide lane for each direction (could be possible to park one car alongside) and an Average Daily Traffic (ADT) of 5500 vehicles/day. Even though the traffic volume is quite moderate could not be compared to higher trafficated Milan roads, but was enough for our study.


**Figure 31. Overwiev of Milan city area (top) and a zoom over the street of interest. Red rectangular represents Via Tanzi**

Recent studies focused on the quantification of mass load (mg/m$^2$) collected at different sites (through the new protocol designed by Fulvio) and its temporal variability after a rainy event. Particularly, our research focused on silt load recovery rate after rainy event

combined with measure of albedo during sampling. Recovery rate relied on drying time, vehicles flow, air temperature and road material.

Notwithstanding a new and clear protocol, the difficulty was to collect road dust over the active part of the road due to the continue flow of vehicles. Thanks to road signs and help of second operator, sampling was performed during winter period. Sampling consisted in aspiration of half square meter (0.5 m2) for 15 min time-scheduled based on hours after the rainy event. The sampling protocol provided:

- 8 samplers just after the end of rainy event every hour
- 3 samplers every 3/4 hours
- 1 sample at third, fourth and fifth day

This procedure might be repeated four times during winter period for robustness of database.

Highest silt load ($mg/m^2$) values were measured after a long series of sunny days (five or six) and represented the maximum value that could be reached after the rainy event. Thus, reference value campaigns were performed in order to detect the reference value associated to the road.

After sampling, wet quartz filters (47 diameter) were conditioned under constantly the same conditions within a climatic camera (20º C and 50% HR) for 2 weeks. After conditioning, dried filters were weighted three times by means 1 µg sensitivity balance.

During the period 1/12/2016-31/7/2017 were performed only two campaigns due to some problems occurred while the sampler was available in Milan. First of all, limited rainy events between end of 2016 and first months of 2017 reduced possibility to measures, however a vacuum pump fault (no 30 l/min flow held constantly), breakdown of field generator and few suitable rainy events (e.g.: end of rain during Friday) did not allow to collect PM traffic resuspension as well as scheduled. Notwithstanding, Figure 32 and Figure 33 illustrated results of first experimental campaign held during February and the second one in July. Even though summer months were not considered optimal for sampling, a brief experimental campaign was conducted in order to test new instruments. As could be observed in Figure 32, the mobile dust load collected during July was doubled respect to January, pointing out the faulty vacuum pump used during the first campaign. Asymptotic value detected during February reached 0.2 $mg/m^2$ while during July reached 0.45 $mg/m^2$. A clear evidence of vacuum pump defect was indicated by sampling carried

at first hours after end of rainy event that explained the similar phenomenon but with a different intensity.

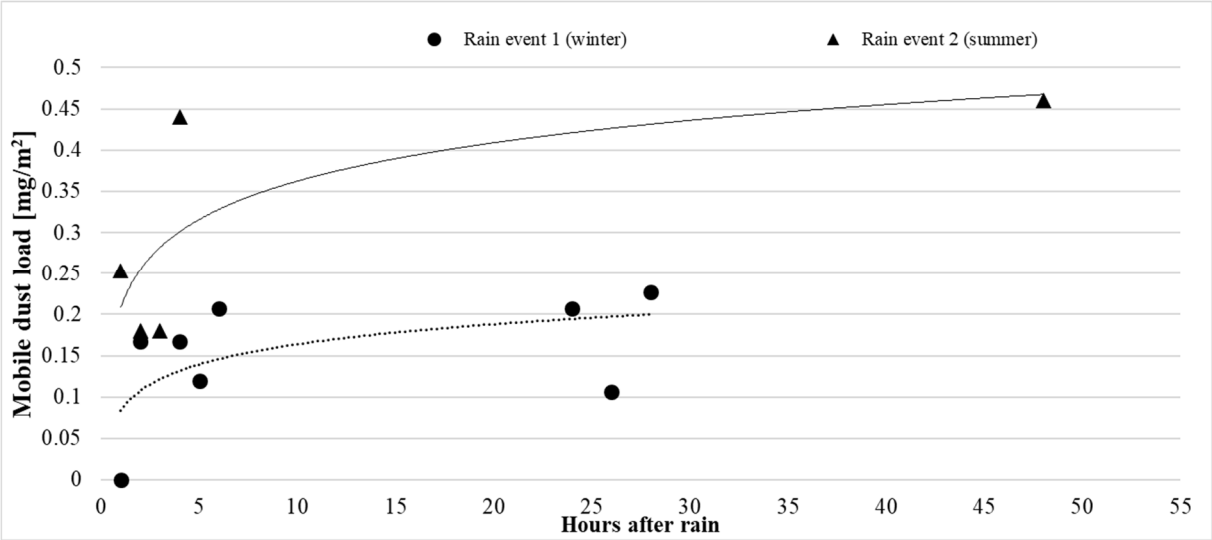


**Figure 32. Mobile dust load collected in Via Tanzi**

Figure 33 illustrated the normalized mobile dust load computed for February and July campaign. Independently by absolute values of dust load, an exponential law which explained physical phenomenon was computed for both campaigns, showing that the equilibrium value (resuspension and deposition were balanced) reached after 45 hours by the end of rainy event.

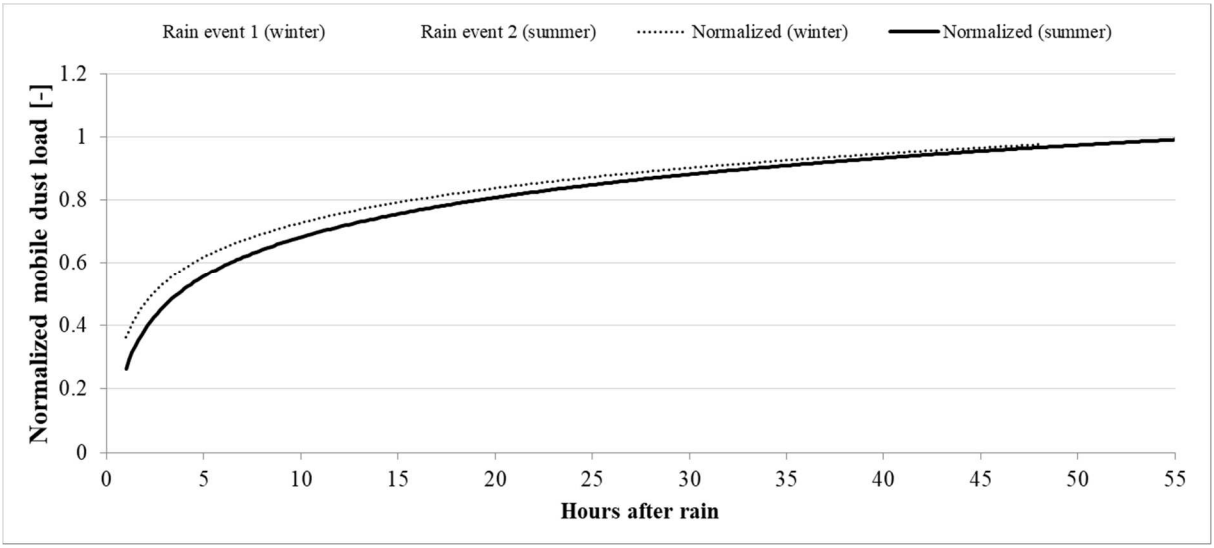


**Figure 33. Normalized mobile dust load collected in Via Tanzi**

In spite of two experimental campaigns, results were comparable to what discovered in Barcelona and Utrecht by Amato et al (2012). While climatological conditions of Barcelona allowed reaching equilibrium value after only 24 hours (e.g. stronger wind and higher temperatures), conversely in Utrecht after 76 hours due to high humidity values, that delayed road drying, and lower temperatures.

The last step of this study, delayed and not terminated due to problems occurred during sampling, will be the computation of PM traffic resuspension emission factors starting from measures of road dust. EFs will be inserted within emission inventories in order to evaluate correctly this phenomenon often underestimated or missed within inventories and, consequently, air quality simulations.

Despite comparable results between Milan and other cities, further analysis will be necessary. Completion of direct campaigns with, at least, two valid datasets will be fundamental for robustness of dataset, evaluation of correlation between albedo and silt load (started but not conclude) will help the investigation of drying phase after the rainy event, the study of correlation between traffic detailed flow and GRIMM measurements at kerbside will link traffic frequency peaks with concentration peaks.

## *3.2. Passive measurements*

Micro-scale vertical profiles of PM concentrations were investigated by means of the samplers utilized by (Orza et al, 2009) for estimating horizontal eolian sediment fluxes in PM traffic resuspended events, but in particular PM emission factors relied on speed and type of vehicle. Experimental campaigns held before and after speed cameras installation allowed studying the effect of speed for resuspension while tracking each vehicle (type – car, light, heavy, bus or motorcycle – and speed) an emission factor related to type could be computed. These samplers consisted of 15 cylindrical canisters of 6 cm height and 7 cm of inner diameter divided into three groups. The fifteen canisters, organized into three groups, were set in a vertical arrangement, separated by 1 cm each other. The canisters were crossed by a cylindrical steak that maintained the whole joined. A schematic representation of sampler position was illustrated in Figure 34.

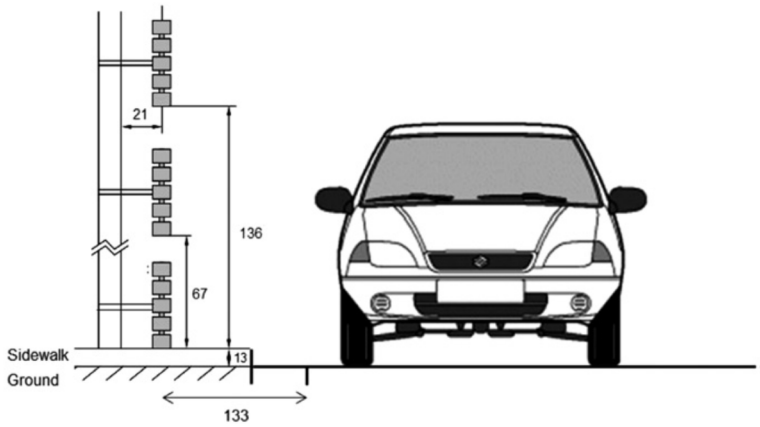


**Figure 34. Passive sampler installation**

Measures of distances between groups of canisters or from the ground were idealistic. Features of each site (distance from guardrail, obstacles or trees) determined distance of canisters from the ground. Next figures illustrated road sites in Milan where canisters were mounted. Exposition period of canisters was two weeks for both campaigns (before and after speed camera mounting) independently by climatological conditions.

Figure 35 showed roads interested of experimental campaigns. At Via dei Missaglia, canisters were mounted on a street lamp over the traffic island that separated two flow directions. Each direction was characterized by three lanes with a speed limit fixed at 50 km/h, but not respected by drivers; in fact, speed averaged measured with a speed and indicator Bresser 6x25 800m over three lanes was about 58 km/h, in particular over the third lane (the fastest) the speed was higher than 65 km/h. Speed camera installation reflected so much on driver's behavior that mean velocities decreased about 13% up to limit of 50 km/h.


**Figure 35. Sites where passive samplers were installed. From top-left, Via dei Missaglia (a), Via Ferrari (b) and Via Parri (c)**

Speeds measured at Via Ferrari were much higher respect to Via dei Missaglia. Even though roads were equal (three for each direction flow), the absence of traffic lights favored high velocities within the segment analyzed. Speed limit of 70 km/h was overcome over second and third lane; in particular the mean speed measured at third lane was 89 km/h, almost 20 km/h over the limit. Similarly to what happened at Missaglia street, speed camera mounting caused a clear reduction of velocities. Speed cameras affected positively the drivers to the point that mean velocity recorded at third lane was under the limit of 70 km/h (68 km/h) with a reduction of 23%. Also in the second lane, mean speed decreased from 74 km/h to 64 km/h while the first lane does not showed remarkable variations.

Unfortunately, vehicles speed at via Parri were not available due to incompatibility between monitoring site and instrument. Figure 36 showed exactly the localization of passive sampler that was mounted over a street lamp on the right side of the street while the previous ones were installed over the traffic island which separated traffic fluxes. The lateral position does not allowed measures of speed. Nevertheless, experimental campaign was conducted during the same period even though proximity to guardrail did not match with guidelines issued by Amato.

Via Parri was characterized by three lanes for each direction separated by one traffic island covered with grass and shrubberies. Figure 36 showed location of passive samplers and short distance from guardrail.

**Figure 36. Example of passive sampler installed in Via Parri**

The operation principle of the samplers is similar to that described by Wawda et al (1990) and Wagner and Leith (2000). The samplers were exposed to ambient air for passive collection of PM by deposition. First experimental campaign (before speed camera installation) started 30/06/2017 and passive samplers were removed after two weeks of exposition during 14/07/2017. Second campaign, just after speed cameras installation, started the 04/10/2017 and finished during 24/10/2017. A difference of 5 days between two campaigns occurred for rain fall last days of second exposition and the consequent drying phase of passive samplers.

An array of three samplers permitted obtaining the vertical profile of concentrations due to two opposite transport directions. Particles reached an equilibrium point through the combination of deposition and turbulent eddies that induced a rising movement of the particles. After exposition, passive samplers were dismounted and brought to the laboratory for weight.

Lab procedure followed was defined according to Fulvio Amato. Firstly, passive samplers were divided into singular canisters. Each one was filtered with 260 µm sieve using distilled water in order to remove all coarse material (small animals, blades of grass or pebbles). Resuspended material mixed with distilled water were collected and pour into a Buckner filter, modified with a little pump (few l/min) for forcing deposition of material over quartz filter. As descripted for direct measurements, quartz filter 47 mm diameter were used for final filtration. After Buckner filtration, wet filters were dried within climatic camera under controlled conditions of temperature (20 ºC) and humidity (50%) for at least 2 weeks. Finally, each filter was weighed three times for mass average computing. Figure 37 illustrated the different mass deposited over the filter based on distance from the ground, highlighted by the right photo where mass collected over lowest and highest canister were showed.

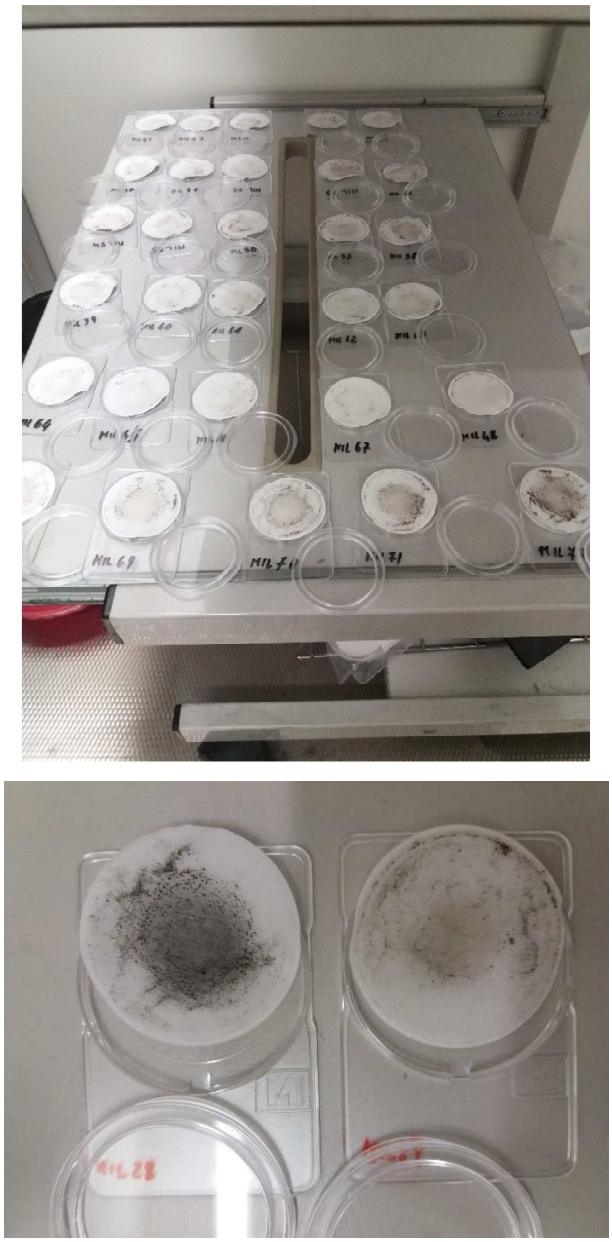

**Figure 37. Photos of wet filters during drying phase within climatic camera**

Figure 38 illustrated results of PM traffic resuspension campaigns conducted before and after speed camera installation. Apparently, there was not clear variation about PM mass deposited even though mean speeds decreased, in particular over the third lane which was typically the fastest. However, after a deep comparison between mass collected over each canister before and after speed camera, conclusions could be different. Focusing on Via dei Missaglia and considering all canisters, the mean reduction was about 140 µg, but the behavior of each group of five canisters could be independent by the others. Starting from the top, first and second group indicated an average mass increase of about 1 mg while at lowest group mass resuspended reduced more than 2 mg; in particular at the lowest

canister, PM mass decreased from 12.8 mg to 6.1 mg. Focusing on Via Ferrari, characterized by the same number of lanes but different average speed, PM vertical mass profile indicated an overall slight increase of about 1 mg. In detail, comparing the average mass at first group was observed a strong increase (more than 2 mg), as could be noted in Figure 38. Even though a different distribution, at medium group of canister PM mass deposited was quite similar for both cases. A difference was observed at the lowest group, where average mass measured after speed camera mounting decreased of about 200 µg.

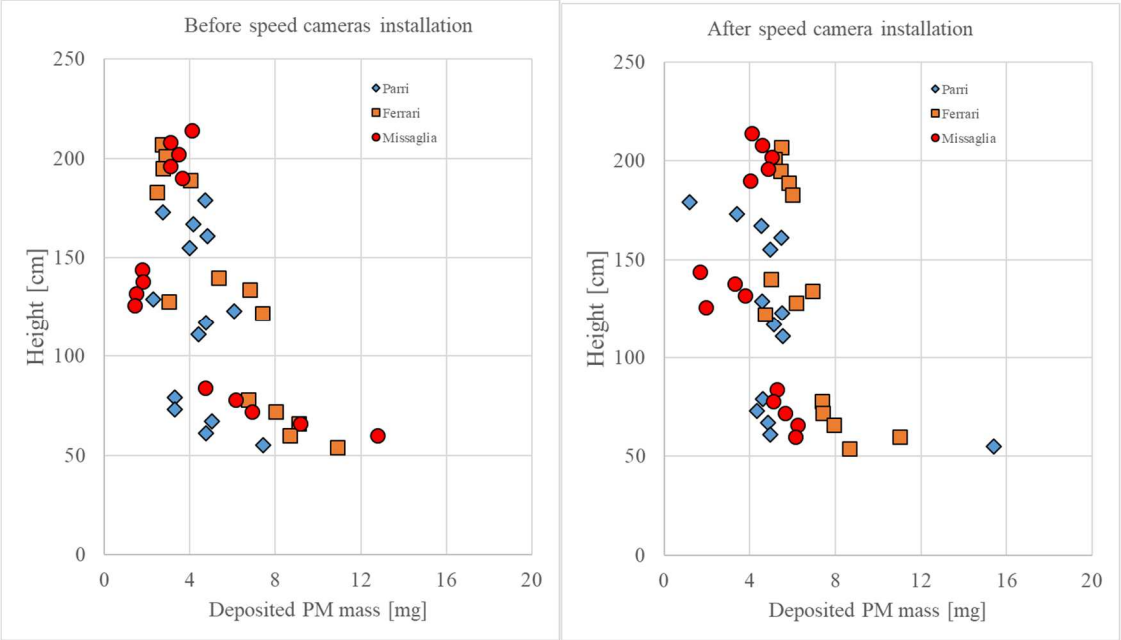


**Figure 38. PM resuspended mass vertical profile before (left) and after (right) speed camera installation for the three locations (Via dei Missaglia, Via Ferrari and Via Parri)**

Notwithstanding Via Parri location did not follow guidelines for installation, experimental campaign was conducted at the same way. Speed camera caused an average increment of 350 µg, distributed differently between canisters ground. The highest group was affected by a slight reduction (less than 0.2 µg) of PM deposited while at the other groups was observed an increment less than 1 mg. In particular, 0.8 mg and 0.6 mg for respectively second and third group. The last measure of PM deposition after speed camera installation was removed because considered too high if compared to the previous values.

Focusing on the most reliable datasets, Via dei Missaglia and Via Ferrari, a common feature could be noted. Both sites showed a reduction of PM resuspended mass at closer canister group to the ground, more pronounced in Via dei Missaglia even though speed

reduction due to speed cameras was lower. From this first analysis, relevant reduction of vehicular speeds could be affect positively PM traffic resuspension. Conversely to the speed variations, resuspended mass measured during second campaign at first and second group of canisters were higher respect to the campaign without speed limit. While mass increments observed in Via dei Missaglia and at the second group of Via Ferrari were limited (around 1 mg), the increment of 2 mg observed at the highest group in Via Ferrari could be ascribed to phenomena independent by lab procedures. Further insights will be necessary in order to study the site-specific physical phenomena of resuspension.

At the end of experimental activities, the deposition flux could be calculated by the terminal concentration $m_\infty$ divided by the deposition area A, and the sampling time (h) (Wagner and Leith, 2000):

$$J = \frac{m_\infty}{A * t} \tag{1}$$

where $m_\infty$ could be obtained by a least square fit of 15 canisters mass to an equation of the form of:

$$\frac{m - m_\infty}{m_0 - m_\infty} = \exp(-\frac{v_d}{D} z) \tag{2}$$

where $v_d$ is the deposition velocity, $D$ is an effective particle eddy diffusivity, $z$ is the height and $m_0$ and $m$ are the mass at height $z = 0$ and $z = z'$. The theoretical basis on which is based equation (2) can be found in Escrig et al. (2011), which assumes that the dry deposition of particulate matter is governed by diffusion-like and gravitational-like mechanisms (Pasquill, 1962). The value of minf could be used for calculating the deposition flux onto the $z = 0$ surface in equation (1). The average terminal concentration $m_\infty$ established the total emissions from traffic resuspesion during the whole period of passive collection. Consequently, an emission factor for traffic resuspesion could be estimated. Since that gravimetric determination finished the last day of PhD, the last part of emission factor calculation will be conclude in a second step in Barcelona. For this reason, EFs are not illustrated.

# 4. Supplementary Material

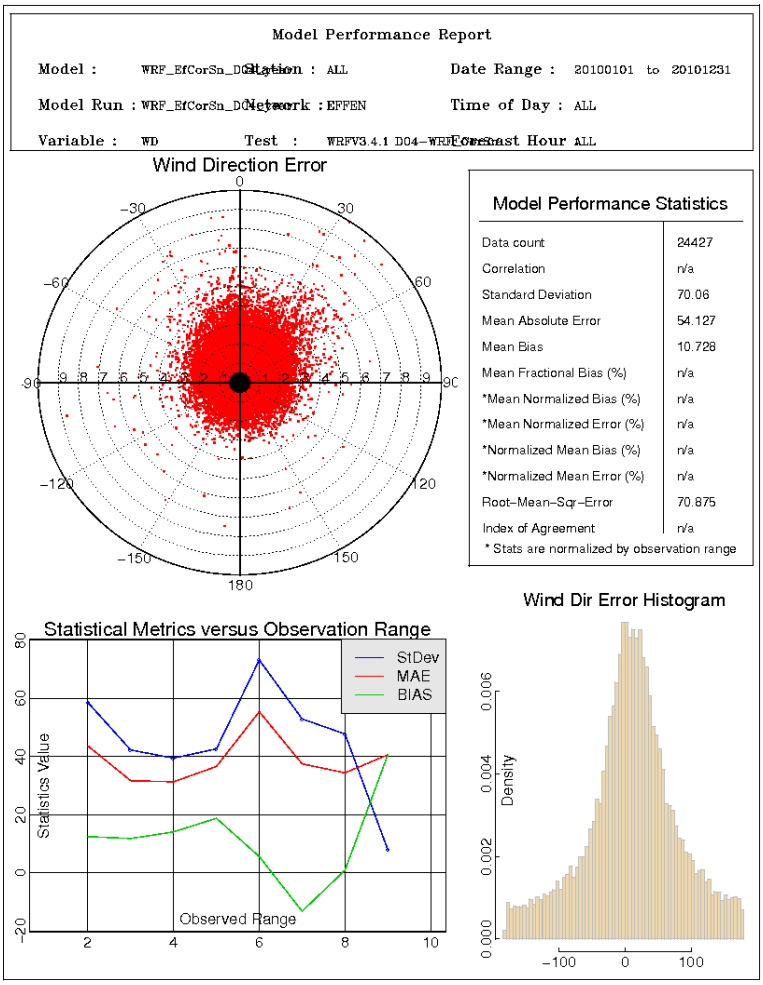


**Figure S 1. Evaluation of wind direction performance over Milan area in 2010. The scatter plot (top-left) presents the distribution of the wind direction error. The x-axis represents the wind speed and on the round axis there is the wind direction error. The table (top-right) lists the principal statistical parameters. The graph "Statistical Metrics versus Observation Ranges" (bottom-left) illustrates the BIAS, MAE and StDev trend for different wind speed. The histogram (bottom-right) shows the distribution of the wind direction error probability (x-axis: positive and negative wind direction error).**

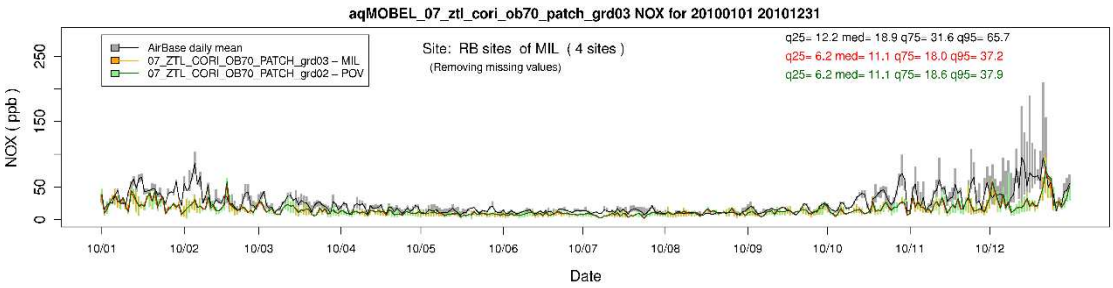


**Figure S 2. Time series of the box and whisker plots for the daily distribution of the observed (black/grey) and computed values of $NO_X$ concentration (ppb) at Rural monitoring sites of the Milan area domain for 2010. CAMx results at 5 km and 1.7 km resolution are displayed in red/orange and in green, respectively. Bars show the interquartile range, lines the median values. Values for the 25th, 50th, 75th, and 95th quantiles of the whole monthly time series are reported too.**

**Table S 1. Comparison of stand-alone CAMx model performance for $NO_X$ hourly concentrations computed for 2010 at rural AQ stations of Po Valley and Milan area domain.**

| | *Po Valley* | | *Milan area* | |
|---|---|---|---|---|
| | Observations | Model | Observations | Model |
| Mean [ppbV] | 16.5 | 10.3 | 26.1 | 14.1 |
| Standard Deviation [ppbV] | 19.6 | 10.9 | 28.8 | 15.7 |
| Number Observations [-] | 310495 | | 32262 | |
| Correlation [-] | 0.5 | | 0.4 | |
| Mean Bias [ppbV] | -6.2 | | -6.8 | |
| Mean Error [ppbV] | 10.2 | | 9.2 | |
| Index_of_Agreement [-] | 0.6 | | 0.6 | |
| RMSE [ppbV] | 18.4 | | 29 | |

# 5. Publications

## *Article 1*

Pepe N., Pirovano G., Lonati G., Balzarini A., Toppetti A., Riva G.M., Bedogni M.

## Development and application of a high resolution modelling system for the evaluation of urba air quality

Atmospheric Environment, (2016), 141, 297-311

Atmospheric Environment 141 (2016) 297–311

Contents lists available at ScienceDirect

Atmospheric Environment

journal homepage: www.elsevier.com/locate/atmosenv

# Development and application of a high resolution hybrid modelling system for the evaluation of urban air quality

N. Pepe [a, b, *], G. Pirovano [a], G. Lonati [b], A. Balzarini [a], A. Toppetti [a], G.M. Riva [a], M. Bedogni [c]

[a] RSE Spa, Via Rubattino 54, 20134 Milano, Italy
[b] Department of Civil and Environmental Engineering, Politecnico Milano, Milano 20133, Italy
[c] AMAT, Via T. Pini 1, 20134 Milano, Italy

## HIGHLIGHTS

- Hybrid modelling system developed at the urban local scale.
- Hourly model output at 20 x 20 m space resolution for urban area.
- Improvement in model bias despite slightly worsened time correlation.
- Weaknesses and strengths of the system are pointed out and discussed.
- Estimated NOX background accounted for about 75% in Milan area domain.

## ARTICLE INFO

Article history:
Received 4 February 2016
Received in revised form
21 June 2016
Accepted 27 June 2016
Available online 29 June 2016

Keywords:
Urban air quality
NOx
Hybrid modelling
CAMx
AUSTAL2000
Milan

## ABSTRACT

A hybrid modelling system (HMS) was developed to provide hourly concentrations at the urban local scale. The system is based on the combination of a meteorological model (WRF), a chemical and transport eulerian model (CAMx), which computes concentration levels over the regional domains, and a lagrangian dispersion model (AUSTAL2000), accounting for dispersion phenomena within the urban area due to local emission sources; a source apportionment algorithm is also included in the HMS in order to avoid the double counting of local emissions.

The HMS was applied over a set of nested domains, the innermost covering a 1.6 x1.6 km$^2$ area in Milan city center with 20 m grid resolution, for $NO_X$ simulation in 2010. For this paper the innermost domain was defined as "local", excluding usual definition of urban areas. WRF model captured the overall evolution of the main meteorological features, except for some very stagnant situations, thus influencing the subsequent performance of regional scale model CAMx. Indeed, CAMx was able to reproduce the spatial and temporal evolution of $NO_X$ concentration over the regional domain, except a few episodes, when observed concentrations were higher than 100 ppb. The local scale model AUSTAL2000 provided high-resolution concentration fields that sensibly mirrored the road and traffic pattern in the urban domain. Therefore, the first important outcome of the work is that the application of the hybrid modelling system allowed a thorough and consistent description of urban air quality. This result rep-resents a relevant starting point for future evaluation of pollution exposure within an urban context.

However, the overall performance of the HMS did not provide remarkable improvements with respect to stand-alone CAMx at the two only monitoring sites in Milan city center. HMS results were charac-terized by a smaller average bias, that improved about 6-8 ppb corresponding to 12-13% of the observed concentration, but by a lower correlation, that worsened around 1-3% (e.g. from 0.84 to 0.81 at Senato site), due to the concentration peaks produced by AUSTAL2000 during nighttime stable conditions. Additionally, the HMS results showed that it was unable to correctly take into account some local scale features (e.g. urban canyon effects), pointing out that the emission spatialization and time modulation criteria, especially those from road traffic, need further improvement.

Nevertheless, a second important outcome of the work is that some of the most relevant discrepancies between modelled and observed concentrations were not related to the horizontal resolution of the dispersion models but to larger scale meteorological features not captured by the meteorological model,

* Corresponding author. Present address: Via Rubattino 54, 20134 Milano, Italy.
E-mail address: nicola.pepe@polimi.it (N. Pepe).

http://dx.doi.org/10.1016/j.atmosenv.2016.06.071
1352-2310/

especially during winter period. Finally, the estimated contribution of the local emission sources accounted on the annual average for about 25-30% of the computed concentration levels in the innermost urban domain. This confirmed that the whole Milan urban area as well as the outside back-ground areas, accounting all sources outside the innermost domain, play a key role on air quality. The result suggests that strictly local emission policies could have a limited and indecisive effect on urban air quality, although this finding could be partially biased by model underestimation of the observed concentration.



## 1. Introduction

The impact assessment of environmental policies on air quality involves reactive pollutants, thus requiring chemical transport models (CTMs) and urban to regional domains, depending by the area of interest (Isakov et al., 2007; Denby et al., 2011; Martins, 2012). Urban areas are composed by heterogeneous elements and present densely built-up features, which can influence the spatial distribution of some pollutants such as NOx and $NO_2$, as well as the primary fraction of PM (EEA, 2015; Torras Ortiz and Friedrich, 2013). Due to their relatively low spatial resolution, CTMs cannot capture correctly the strong spatial gradients that can take place in urban areas, hampering a reliable evaluation of human exposure (Isakov et al., 2009; Batterman et al., 2014). The reconstruction of air quality variability within urban areas would require local scale models (LSMs); nevertheless LSMs alone are usually unable to reproduce chemical reactions and can not be applied over large domains (Stein et al., 2007; Lefebvre et al., 2011, 2013; Beevers et al., 2012; Isakov et al., 2014).

For all these reasons we developed an integrated hybrid modelling system (HMS) by combining the Comprehensive Air Quality Model (CAMx) with Extensions (ENVIRON, 2011), as chem-ical transport model, and the AUSTAL2000 (Janicke Consulting, 2014), as local scale model, according to a model nesting approach. The resulting HMS is a comprehensive and efficient modelling tool for urban air quality, capable of reconstructing the regional scale features of air pollution as well as the spatial vari-ability of concentrations within urban areas, taking into account the building structures and the detailed spatial distribution of the emissions at the urban scale. In particular, this work is intended to define a standardized modelling chain that can use the same emission inventories and land use datasets, as well as meteorolog-ical inputs, for the CTM and LSM components of the HMS.

A case-study application of the HMS concerning the metropol-itan area of Milan, with a specific focus over the city center, where the LSM was applied in cascade to the CTM in order to provide hourly NOx concentration for a high resolution urban grid (20 x 20 m) for 2010, is presented and discussed.

The paper firstly describes the conceptual structure and the elements of the HMS. The following section is devoted to the evaluation of the performance of the CTM part of the HMS. Then the results of the LSM application are presented and compared with the corresponding CTM outcomes. HMS results at the Milan urban domain are then compared with observations. Finally the evalua-tion of the spatial variability of the fine scale concentrations is presented and discussed.

## 2. Methods

### 2.1. The hybrid modelling system

The hybrid system relies on two main components: the regional scale model CAMx and the local scale dispersion model AUS-TAL2000. The modelling system also includes the Weather Research and Forecasting (WRF) meteorological model and the SMOKE emission model. Interactions between all models are shown in the flow chart of Fig. 1. All models and tools implemented in the modelling chain are based on open source codes. The modelling system has two main features:

- CTM and LSM input data consistency, i.e.: the two models share the same meteorological and emission data;
- solution to the double counting problem of local contribution, thanks to a source apportionment algorithm implemented in the CTM model the local sources' contribution is accounted for only by the LSM.

The modelling chain presents efficient features concerning computational time: 15 min/day with 8 core processors about CAMx outcomes while 4 min/day about AUSTAL2000 outputs with single core. Physical and chemical processes are described and quantified although AUSTAL2000 treats all pollutants as inert. Chemical schemes are implemented into CAMx, as described in setting section, and cover an important role overall at the basin scale; conversely, at the local scale the correct quantification of the dispersion phenomena is more important in order to compute backlog events, key features concerning exposition levels within urban areas. Thanks to its LSM component the HMS can accurately reproduce the spatial pattern of emission sources and reconstruct the spatial variability of pollutants concentrations. Thus, for example, the HMS is helpful to define critical zones for urban pollution and to assess the impact of air quality control policies, as the introduction of "Low Emission Zone" (Hellison et al., 2013; Morfeld et al., 2014), popular in big cities of Germany and En-gland and adopted also in Milan since a few years.

Models setup and details on the output of the HMS are given in the following paragraphs with specific reference to the case-study for $NO_X$ concentration in Milan city center.

### 2.2. WRF setup

The WRF model v3.4.1 (Skamarock et al., 2008) was setup using 30 vertical layers, with the first one reaching about 25 m from ground level; the top layer overcomes 15 km. Four horizontal nested grids were used, downscaling from a 3870 x 4140 $km^2$ domain covering Europe to a 1350 x 1530 $km^2$ domain over Italy, a 600 x 420 $km^2$ over the Po Valley and an 85 x 85 $km^2$ over a part of the Lombardy region, including the city of Milan. Each domain was gridded using different resolutions starting from 45 km as grid step down to 15 km, 5 km and 1.7 km for the last domain. Initial and boundary conditions were taken from ECMWF analysis fields at 0.5 x 0.5 grid size, both at ground level and at different pressurelevels (http://old.ecmwf.int/products/data/archive/ECMWF_ catalogue/index.html). Data included 3D and surface parameters

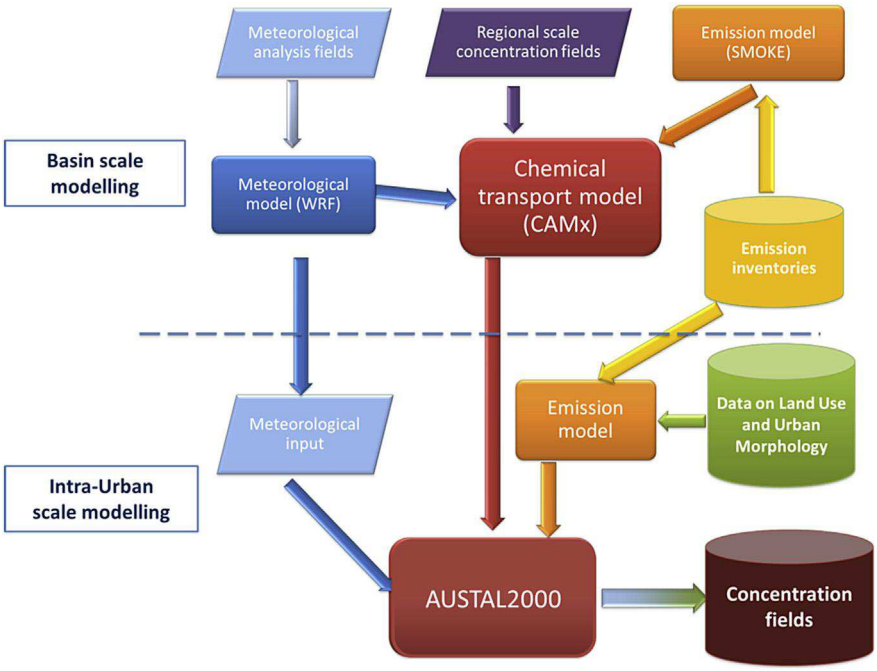


Fig. 1. Flow chart of the hybrid modelling system.

(wind speed components, temperature, relative humidity), 2D surface parameters (sea level pressure and temperature, separating sea cells from ground ones), 2D static parameter of land sea mask and 3D soil parameters (temperature and water content) integrated on 4 ground layers (0-7 cm, 7-28 cm, 28 cm-1m, 1-2.55 m). Main physical settings within WRF included the Rapid Radiation Transfer Model (RRTM) radiation scheme (Iacono et al., 2008), Morrison double moment microphysics processes scheme (Morrison et al., 2009), Yonsei University PBL scheme (Hong et al., 2006), Grell 3D scheme for clouding creation (Grell and Devenyi, 2002) over Eu-ropean and Italian domain, Monin-Obukhov surface layer scheme (Monin and Obukhov, 1954) and Noah land surface model (Chen and Dudhia, 2001). Analysis nudging of wind speed horizontal components, temperature and relative humidity was used in the WRF model with a nudging strength of 3 x 10 4. The classification system for land use was based on European database CORINE that counts 44 different categories (http://www.eea.europa.eu/), reclassified over 33 classes of USGS system. Particularly, CORINE adopts five different sub-categories of urban land use, from continuous urban fabric to discontinuous low-density urban fabric, that were linked to three USGS urban land use classes.

### 2.3. CAMx setup

CAMx v5.40 model (ENVIRON, 2011) was used to simulate dispersion phenomena and chemical processes at regional scale. CAMx provided the concentration fields for the outer domains and background contributions for the local domain, better detailed below. CAMx was setup using the same horizontal grid structure as for WRF. CAMx vertical grid was defined collapsing the 27 vertical layers used by WRF into 14 layers in CAMx but keeping identical the layers up to 1 km above ground level; in particular, the first layer thickness was up to about 25 m from the ground like the corre-sponding WRF layer. The model was run only for the three inner-most domains of WRF (Italy, Po Valley, Milan area), adopting the same grid step but slightly reduced dimensions to remove boundary effects. Details on the computational grids are reported in Table S1 of Supplementary materials section.

Homogenous gas phase reactions of nitrogen compounds and organic species were reproduced through CB05 mechanism (Yarwood et al., 2005). The aerosol scheme was based on two static modes (coarse and fine). Secondary inorganic compounds evolu-tion was described by thermodynamic algorithm ISORROPIA (Nenes et al., 1998), while SOAP (ENVIRON, 2011) was used to describe secondary organic aerosol formation. Meteorological input data were provided by WRF and were completed by OMI satellite data (http://toms.gsfc.nasa.gov), including ozone vertical content and aerosol turbidity. Vertical turbulence coefficients (kv) were computed using O'Bryan scheme (O'Brien, 1970), but adopting two different minimum kv values for rural and urban areas, so to consider heat island phenomena and increased roughness of built areas.

Emissions were derived from inventory data at three different levels: European Monitoring and Evaluation Programme data (EMEP, http://www.ceip.at/emission-data-webdab/emissions-used-in-emep-models/) vailable over a regular grid of 50 50 km2; ISPRA Italian national inventory data (http://www.sinanet.isprambiente.it/it/sia-ispra/inventaria/disaggregazione-dellinventario-nazionale-2010) which provides a disaggregation for province; regional inventories data based on INEMAR meth-odology (INEMAR e ARPA Lombardia, 2015) for the four adminis-trative regions in the Po Valley, which provide detailed emissions data at municipality level. Each emission inventory was processed using the Sparse Matrix Operator for Kernel Emissions model (SMOKE v3.5) (UNC, 2013) in order to obtain the hourly time pattern of the emissions. Temporal disaggregation was based on monthly, daily and hourly profiles deducted by CHIMERE model (INERIS, 2006) and EMEP model from Institute of Energy Economics and the Rational Use of Energy (IER) project named GENEMIS (Pernigotti et al., 2013).

In order to avoid the double counting of the emissions placed inside the local domain, the source apportionment algorithm PSAT (Yarwood et al., 2004) implemented into CAMx was used. PSAT allows keeping track of the contribution of different emission areas

and source categories to the total pollutant concentration. For this application PSAT was setup to split the ambient concentrations resulting from the emissions of two Milan areas: innermost domain contribution ("local") and external domain contribution ("back-ground"). The former contribution derives from the emissions belonging to the overlapping LSM-CTM urban domain, while the latter accounts for all the remaining sources, also including the CAMx parent domains. Therefore, in the context of this paper, "local" and "background" does not refer to the usual definition of the urban areas, but to the computational domains of the two modelling layers.

This approach allows avoiding double counting of emission sources preserving physical and chemical consistency between the two models, in a simpler way than other methods requiring more simulations and assumptions (Stocker et al., 2014).

Initial and boundary conditions were taken from MACC-II sys-tem (http://www.gmes-atmosphere.eu/services/aqac/) that pro-vides 3D global concentrations fields.

### 2.4. AUSTAL2000 setup

AUSTAL2000 v2.6.9 release was used as LSM within the modelling chain. AUSTAL2000 computational domain almost exactly overlapped one CAMx cell, covering a 1.6 x 1.6 km2 urban area, including the main square of Milan city center, with 20 m grid step size (Fig. 2). The innermost domain is characterized by het-erogeneous urban pattern: public parks (green area in the figure below) and road arches separate the densely built up area. Actually, the ring road is trafficked street during the all week-day. Based on the same emissions and meteorological parameters used by CAMx, AUSTAL2000 computed $NO_x$ time series of concentrations gener-ated by local sources enabling for the analysis of their spatial variability at high resolution within the urban domain. The vertical domain started from ground level up to 1500 m, adopting a variable-step grid: a 3 m-step was used up to 60 m (i.e: twice the average height of the buildings), the top of the following three layers was set at 65 m, 100 m, 150 m, then a 100 m-step was used from 200 m to 800 m and the top of the last three layers was set at 1000 m, 1200 m and 1500 m.

Meteorological input variables for AUSTAL2000 (hourly data for Monin-Obukhov length, wind speed and direction) were provided by WRF and considered as representative of the non-disturbed flow; then the local wind field was calculated by the diagnostic wind field model TALdia, coupled with AUSTAL2000 and able to take into account the features of the urban built environment.

European land use atlas (http://www.eea.europa.eu/data-and-maps/data/urban-atlas), which provides information on the land cover composition according to the CORINE approach, was used to describe the presence of buildings in the urban domain. The cells covered at 99% by urban category land use, were considered as a building, with an assumed height of 30 m based on the evidence of the average building height in Milan.

AUSTAL2000 used the same emission data as CAMx but with a more accurate spatial distribution that better mirrored the actual location of the sources and the release height. Namely, total NOX emissions of the CAMx cell corresponding to the AUSTAL2000 ur-ban domain were split among its cells based on proper 20 20 m2 gridded information. According to CAMx emission data, NOX emissions over the local domain were related only to domestic and commercial heating and to road traffic. Domestic heating emissions were equally split among all the cells associated to buildings in the urban domain, lacking specific information on the energetic system and performance of the real buildings. Each building was associated to a stack represented as a point source at the building rooftop height. Traffic emissions were dealt with as ground-level linear sources, allocated with high accuracy within the domain exploiting the full potential of LSM model. Total $NO_x$ traffic emissions were proportionally split among all road arches in the local domain based on road network data provided by AMAT (http://www.amat-mi.it/it/documenti/dettaglio/16/). Emissions for each road have been computed as a weighted average of the total emissions within the local domain based on an aggregate street variable (ASV) given by the product of street length and vehicle number. AUSTAL2000 model operated considering NOX as an inert species. However this limitation did not affect the results because of the very short at-mospheric residence time within the local domain.

### 2.5. Hybrid modelling system output

HMS was applied to assess hourly NOX concentration for the AUSTAL2000 computational domain showed in Fig. 2. In the hybrid approach CAMx provided the background contribution, whilst AUSTAL2000 reproduced the hourly field concentration generated only by the sources active in the innermost urban domain; the final NOX hourly concentration field at the Milan area domain was computed adding the local scale AUSTAL2000 concentration field to the CAMx background concentration. This approach avoided the double counting of local emissions that could occur when the LSM results for the local domain are simply superimposed to the regional scale results from CTM.

HMS results were compared with measurements at two air quality monitoring stations (Senato: 9,1974E, 45,4705N; Verziere: 9,1953E, 45,4633N) in the urban domain operated by the regional agency for environmental protection. Both stations are located in kerbside position near trafficked streets and Senato station is classified as an urban canyon environment. Fig. S2 in S.M. shows plan view of the two monitoring sites. In order to illustrate the local situation and micro-environments of both monitoring sites, the different impact of buildings on local scale winds is shown by the wind roses obtained by TALdia meteorological model for January 2010, reported in Fig. S3 in S.M. In particular, the screen effect of the building "west" of Verziere monitoring site (Fig. S4 e right), as well as the channeling effect of buildings along the city center ring road at Senato site (Fig. S4 e left) are clearly highlighted. However, because at these sites no wind measurements are available, TALdia results cannot be validated. Additionally, it was also possible to compare the HMS results with those simply produced by the CTM as a result of both the emissions inside and outside the urban domain (stand-alone CAMx).

The statistical parameters for model performance assessment included the mean bias (MB), mean absolute error (MAE), root mean square error (RMSE), index of agreement (IOA) and the cor-relation coefficient (r). The explicit definition of each parameter is reported in the S.M. section.

## 3. Results and discussion

### 3.1. WRF performance evaluation

Meteorological fields were compared against surface observa-tions proving that WRF was able to capture the temporal evolution of both the wind speed and direction over 2010. WRF Performance was evaluated considering the Po Valley and Milan area domain through two different observation networks: the World Meteoro-logical Organization (WMO) and the Regional meteorological net-works (ARPA). WRF provided similar performance for both networks; therefore, only the comparisons with ARPA data are shown in Figs. 3 and 4 for the Po valley and Milan area domain, respectively. Additional WRF performance results are available in the Table S2 and Table S3 of S.M. for both ARPA and WMO network.

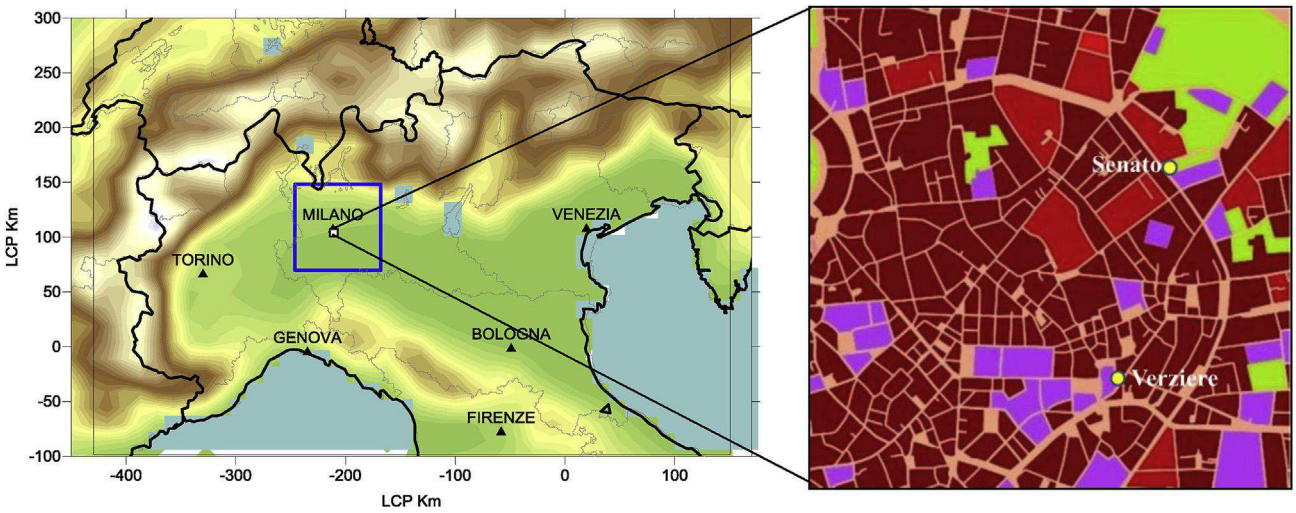


Fig. 2. Overview of Milan area boundary (left panel). View of AUSTAL2000 urban computational domain (right panel). Yellow dots represent the air quality stations included within the urban domain used for validation. Green areas represent public parks. (For interpretation of the references to colour in this figure legend, the reader is referred to the web version of this article.)

Year 2010 was characterized by a normal rise of specific hu-midity (mixing ratio) with a peak in the summer period, as tem-perature trend. Occasionally quick decrease of temperature and mixing ratio were well captured by WRF over both domains during winter and summer months too. This is clearly proved by the values of the correlation index (Table S2) showing values higher than 0.95 for both parameters and domains. Temperature over the Milan area domain was slightly overestimated over the whole year (BIAS = 0.67 deg), but the overall performance is better than the Po Valley domain, as stated by RMSE index, decreasing from 2.68 to 2.01. The observed annual wind speed distribution was correctly reproduced by WRF although a slight overprediction, higher for Milan area domain (BIAS = 0.47 m/s) than Po Valley area (BIAS = 0.3 m/s). Observed wind speed percentiles performed within Milan area domain were lower than wider domain, stressing critic situation for pollutants dispersion expected for Po Valley and urban domain.

Wind speed was constantly overpredicted over both domains but simulation for Milan area WRF showed an increased discrep-ancy in more windy conditions as shown by the 95th percentile of the observed (2.67 m/s) and predicted (3.48 m/s) wind speed.

### 3.2. Stand-alone CAMx performance evaluation

CAMx performance was computed over both Po Valley and Milan area domains. CAMx should reproduce the atmospheric behavior of all main gaseous and aerosol pollutants, taking into account all relevant processes ought to be available in the code. According to the aim of the work, in this paper only results con-cerning $NO_x$ concentration are presented and discussed.

Table 1 shows the comparison between statistical indicators over the two domains, considering only urban and suburban air quality monitoring stations. Measurements at 20 urban sites and 8 sub-urban sites were available for the Milan area and at 97 urban sites and 43 sub-urban sites, also including the previous ones for the whole Po Valley domain. Observed mean concentration increased from 30 ppbV to about 40 ppbV zooming from the whole Po Valley to the Milan area, due to the increasing strength of the anthropogenic emissions. Over both domains CAMx clearly underestimated the observed concentration, especially during the winter period, with an overall mean bias around 14 ppbV. As shown in Fig. 5, regardless for the spatial resolution of the simulation, CAMx was able to reproduce the observed concentration for most of the summer months, but missing several of the severe episodes that took place on winter months, particularly January and December which caused a low correlation index. Indeed, the dif-ference between modelled and observed time series became larger and larger in the upper tail of the distribution, as pointed out by the values of the three quartiles and of the 95th percentile reported in Fig. 5.

The origin of $NO_x$ underestimation, mainly during the cold season, was not clearly identified, but it could be probably explained by the potential overestimation of the vertical mixing because, as stated in the previous paragraph, horizontal dispersion was well captured by WRF model. Wind direction also could be a reason for the NOx underestimation but the error showed in S.M. in the Fig. S5 over the Milan area was not so relevant and homoge-nously distributed for different wind speed. Thus at basin scale, the effect of the wind direction error on discrepancies between ob-servations and model outputs was limited. Low wind speed, dry air and cold temperature that characterized principally the winter period in the Po valley, were often linked to strong inversion con-ditions with very low mixing heights, favoring pollutant accumu-lation, but direct measurements of mixing height were not available. However, focusing on peak events during the cold season, WRF slightly overestimated temperature and this could over-estimate mixing layer height too. Similar performances are observed for the few rural stations available in the domain in S.M., in particular in Fig. S6 and Table S4.

Additionally, it is worth noticing that CAMx provided the same performance for both the simulation domains, pointing out that the underestimation had not be ascribed to local scale effect (e.g. missing local sources), but to larger scale features not captured by the meteorological model.

### 3.3. CAMx and AUSTAL local concentration fields

AUSTAL2000 made possible the reconstruction of the urban structure of the city including buildings and all the obstacles that influence dispersion of pollutants. Fig. 6 shows the $NO_x$ spatial distribution over the local domain as ground-level mean concen-tration for 2010.

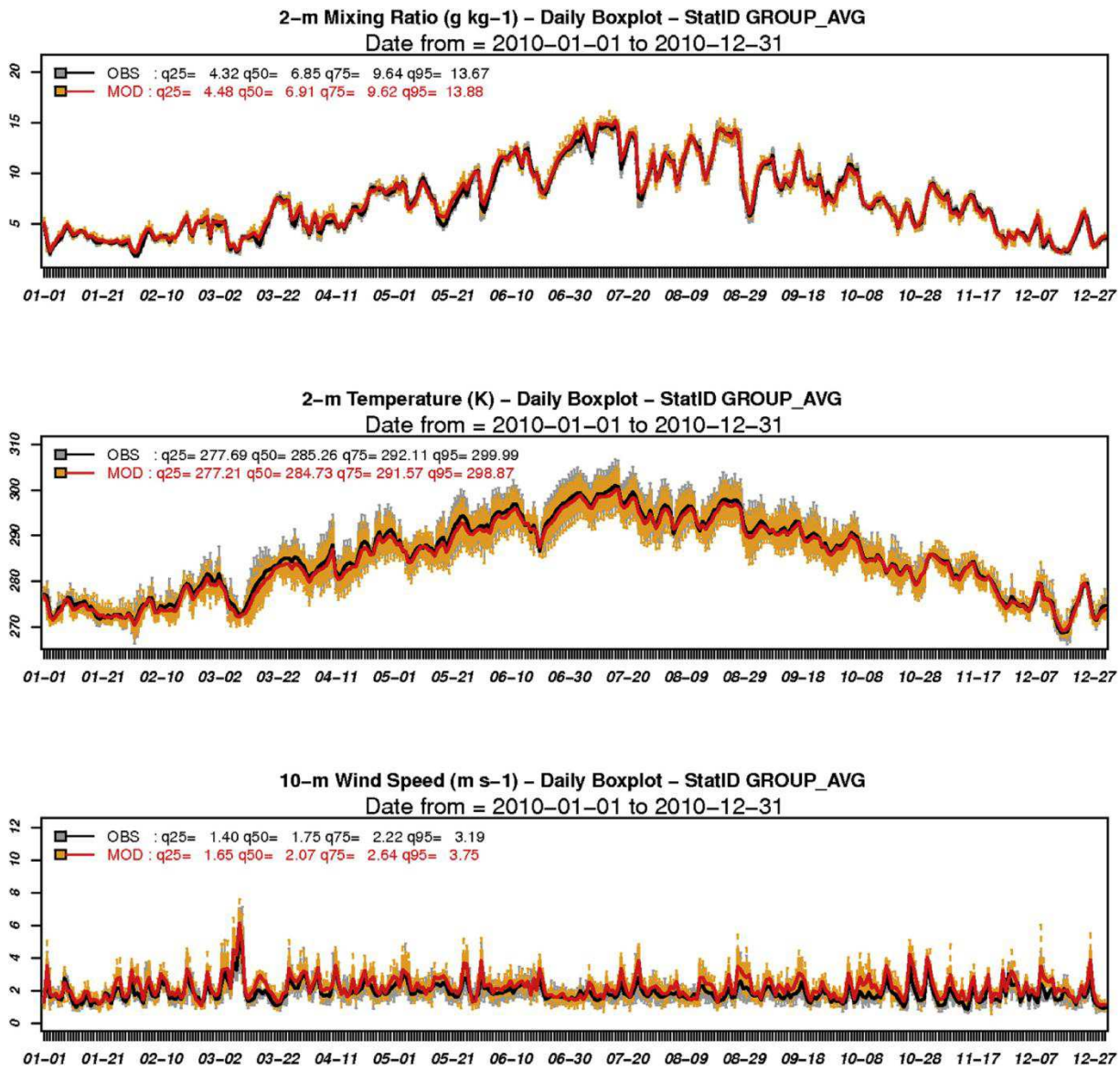


Fig. 3. Time series of the box and whisker plots for the daily distribution of the observed (black/grey) and computed (red/orange) values of mixing ratio, temperature and wind speed at 170 ARPA sites, computed over the Po valley domain for 2010. Bars show the interquartile range (IR), lines the median values, dashed vertical bars the (25th - 1.5 IR) and the (75th + 1.5 IR) value. Values for the 25th, 50th, 75th, and 95th quantiles of the whole yearly time series are reported too. (For interpretation of the references to colour in this figure legend, the reader is referred to the web version of this article.)

Such a mean concentration field points out the effect of traffic sources on main roads of the area, responsible for NOX levels as high as 40 ppbV near busy crossroads, as well as areas with lower levels, down to about 10 ppbV, far from busy streets. This result highlights the LSM capability to reproduce the strong spatial vari-ability of pollutants within urban areas, that cannot be captured by a CTM alone, that over the same area can provide only one mean concentration value.

An interesting feature of our HMS is that the LSM output can be compared with the CTM local contribution (CAMx local), obtained by PSAT application, because both of them are produced by the same emissions sources. To this purpose, AUSTAL2000 vertical concentration profiles were averaged within the first 24 m, in order to make them comparable to CAMx first layer output (up to around 25 m). Then, in order to preserve LSM variability, the CAMx mean local concentrations were compared to the statistical distribution of the AUSTAL2000 concentrations, excluding those cells representing a building or general obstacles.

Fig. 7 shows the comparison between the mean estimations from CAMx and the box plots representing the distribution of daily mean NOX concentrations over all the urban domain from AUS-TAL2000. In order to highlight the higher concentrations per-formed by AUSTAL2000, the scatter plot and the main statistical parameters from the two different local contributions were showed in Fig. S7 in S.M, based on the median value of AUSTAL2000 daily concentrations and CAMx local contribution.

The two models were driven by the same meteorological input and the same emission data but based on very different modelling approaches (CAMx is a eulerian model while AUSTAL2000 follows a lagrangian approach). CAMx local concentrations mostly ranged between 0 and 20 ppbV while AUSTAL2000 showed several peaks ranging between 10 and 70 ppbV. Nevertheless the models showed a rather good agreement in some periods, especially when the estimated contribution from “local sources” was below 10 ppbV

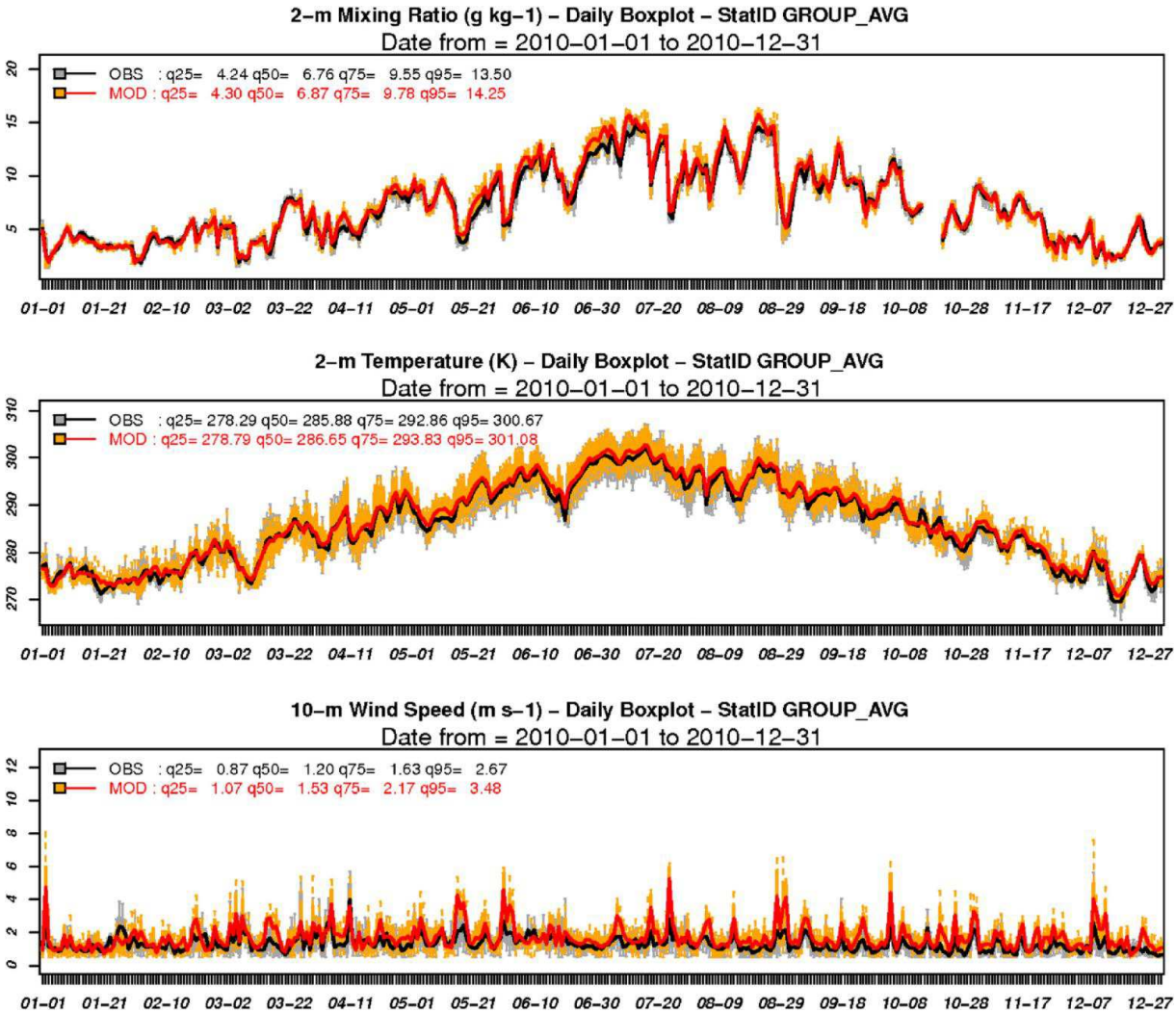


Fig. 4. Time series of the box and whisker plots for the daily distribution of the observed (black/grey) and computed (red/orange) values of mixing ratio, temperature and wind speed at 15 ARPA sites (only 3 sites for wind speed), computed over the Milan area for 2010. Bars show the interquartile range (IR), lines the median values, dashed vertical bars (25th - 1.5 IR) and the (75th + 1.5 IR) value. Values for the 25th, 50th, 75th, and 95th quantiles of the whole yearly time series are reported too. (For interpretation of the references to colour in this figure legend, the reader is referred to the web version of this article.)

Table 1
Comparison of stand-alone CAMx model performance for NOx hourly concentra-tions computed for 2010 at urban and suburban AQ stations of Po Valley and Milan area domain.

| | Po valley | | Milan area | |
|---|---|---|---|---|
| | Observations | Model | Observations | Model |
| Mean [ppbV] | 29.7 | 14.9 | 39.4 | 26.5 |
| Standard deviation [ppbV] | 35.1 | 17.5 | 46.4 | 24.0 |
| Number observations [ ] | 1,173,403 | | 237,587 | |
| Correlation [ ] | 0.45 | | 0.5 | |
| Mean bias [ppbV] | 14.8 | | 13 | |
| Mean error [ppbV] | 19.5 | | 23.2 | |
| Index_of_agreement [ ] | 0.56 | | 0.6 | |
| RMSE [ppbV] | 34.7 | | 42.3 | |

(e.g.: between April and October). Conversely, in some other pe-riods the whole distribution of AUSTAL2000 concentrations was higher than the CAMx local value, though both the models tended to reproduce the same time pattern. Other than to the different modelling approach, the discrepancy between the models can be related to different sensitivity to meteorological data.

The effect of atmospheric stability on model performance was highlighted by the comparison between the daily pattern of the computed “local sources” contributions (Fig. 8) for a winter a summer month. In January, differences between models are related to nighttime hours, when AUSTAL2000 showed a more pronounced temporal variability than CAMx with two peaks corresponding to morning and late afternoon rush hours. Differently, CAMx computed a slighter growth of concentrations on morning and evening rush hours and a flatter concentration time pattern over the whole day. Conversely, on daytime hours model results were very similar, but with CAMx mean values slightly higher. The model outputs largely differed on late evening hours, when the stratifi-cation of the atmosphere, more relevant for the LSM, drove AUS-TAL2000 to emphasize backlog conditions and consequently NOX concentration levels.

An additional analysis of the influence of winter meteorological conditions on concentration levels computed at Verziere and Senato site, the two air quality monitoring sites also used for model performance evaluation, is shown in Fig. S8. At both sites, the most part of hourly concentration events when the local sources' contribution estimated by AUSTAL2000 exceeded 50 ppbV

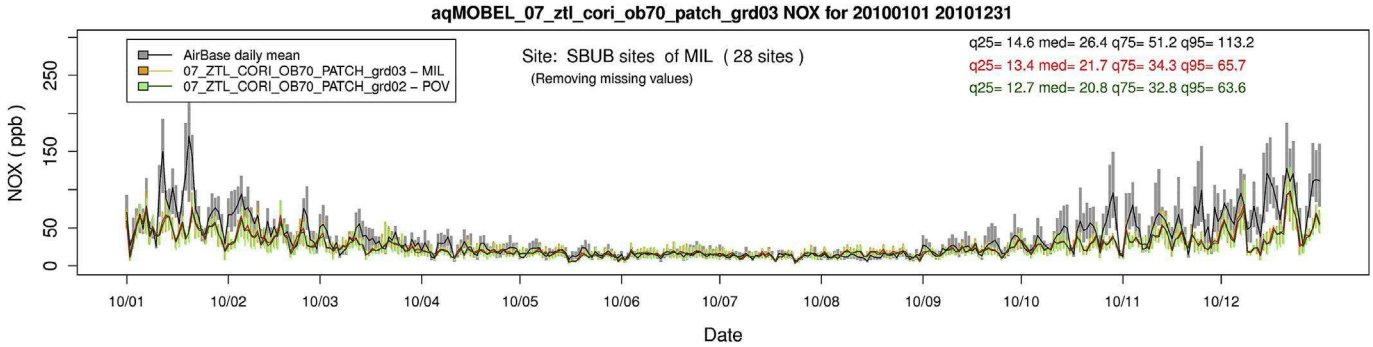


Fig. 5. Time series of the box and whisker plots for the daily distribution of the observed (black/grey) and computed values of NOx concentration (ppb) at Urban and Suburban monitoring sites of the Milan area domain for 2010. CAMx results at 5 km and 1.7 km resolution are displayed in red/orange and in green, respectively. Bars show the interquartile range, lines the median values. Values for the 25th, 50th, 75th, and 95th quantiles of the whole monthly time series are reported too. (For interpretation of the references to colour in this figure legend, the reader is referred to the web version of this article.)

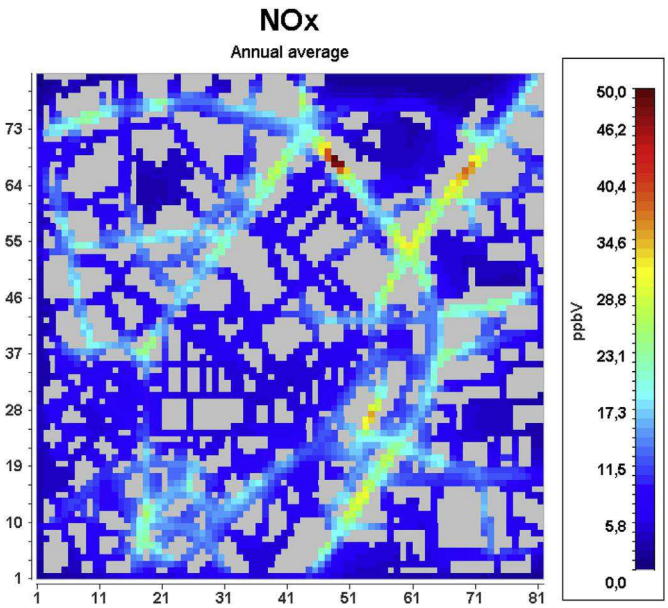


Fig. 6. AUSTAL2000 NOx mean concentration field for 2010 at ground level, computed as a vertical average along the first 24 m (HMS_mean24m). Grey areas identify buildings.

occurred under “critical conditions”, associated with wind speed lower than 1.5 m/s and Monin-Obhukov length in the 0.1-50 m range, thus representing stable atmospheric conditions.

The combined analysis of Fig. 8 and Fig. S8 points out that the “critical conditions” were prevailing during nighttime hours, when the absence of solar radiation favored the development of more stagnant conditions.

In June modelled concentrations are lower than winter for both models, as expected. CAMx and AUSTAL2000 showed a similar behavior during nighttime hours, while CAMx was lower than AUSTAL2000 during daytime. This results points out that CAMx is characterized by an enhanced vertical mixing during daytime hours of the warm season (Lonati et al., 2010).

### 3.4. Hybrid modelling system performance

Adding AUSTAL2000 output to the background concentration computed by CAMx, it was possible to obtain the HMS estimation of the total NOX concentration, without any double counting of local sources. HMS output was compared with observations as well as with the results of the stand-alone CAMx simulation. The definition of the HMS “total” NOX concentration requires additional as-sumptions. Indeed, AUSTAL2000 results are available over a 3 m-stepped vertical profile, observed values generally refers to 2 m above ground level, while CAMx concentration represents the

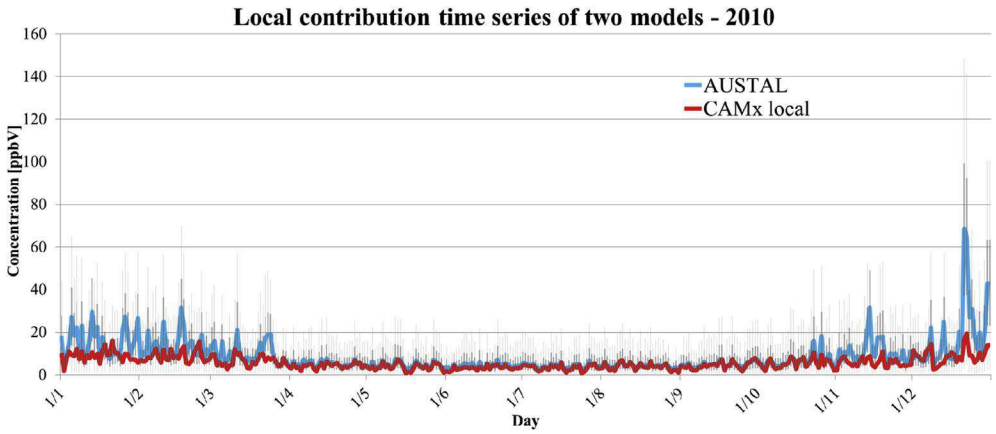


Fig. 7. Comparison between NOx daily concentrations for the urban domain computed by CAMx local (red line) and by AUSTAL2000. The latter is expressed as statistical distri-bution, with the blue line representing the median value of the spatial distribution, the blue box limits the 25th and 75th percentile of the distribution and the grey line the 5th and 95th percentile. (For interpretation of the references to colour in this figure legend, the reader is referred to the web version of this article.)

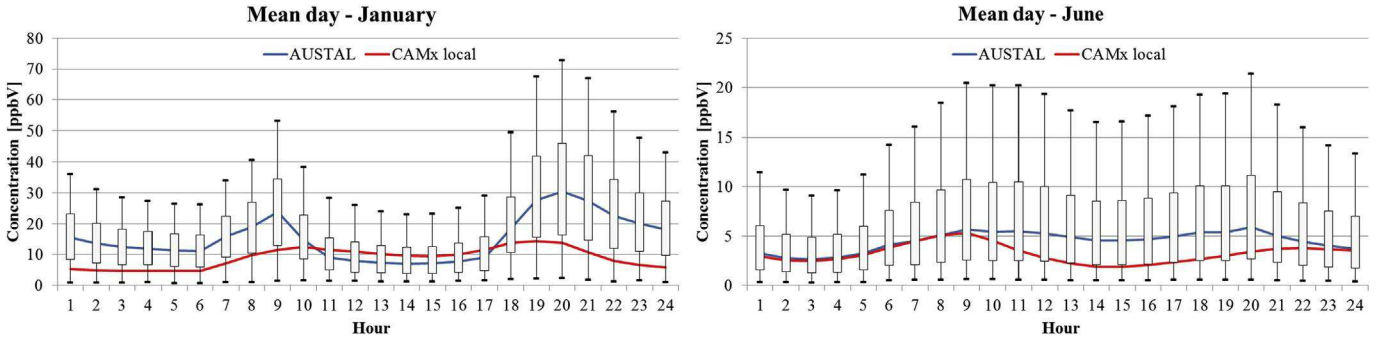


Fig. 8. NOx January (left) and June (right) mean day concentration. Red line represents CAMx local estimation. Blue line represents the median of AUSTAL2000 spatial distribution of the mean day concentrations, while the box's limits indicate 25th and 75th percentile and the vertical lines link the 5th and 95th percentile. (For interpretation of the references to colour in this figure legend, the reader is referred to the web version of this article.)

mean value for the first vertical layer. For this reason, at a first stage, the model performance evaluation was based on two different definition of the LSM concentration contribution: AUSTAL2000 contribution at 3 m from the ground (HMS_3m) was used for comparison with measurements, which are sampled at a similar height; AUSTAL2000 average contribution of first 24 m (HMS_mean24m) was used for comparison with CAMx estimation. In Fig. 9 the measured time series (black line), stand-alone CAMx estimate (red line) and HMS values made by background contri-bution (blue area) and AUSTAL2000 contribution (green area) are plotted. The analysis referred to Verziere and Senato site, the two only monitoring sites available within the local domain.

The first relevant finding stemming from Fig. 9 is that, in most cases, the total HMS concentration was mainly due to the back-ground contribution, thus depending on the sources placed outside the AUSTAL2000 local domain. The mean modelled contributions are summarized in Table 2, showing a background concentration around 36 ppbV. Local contributions at Senato site ranged between 4 ppbV for CAMx local up to 21 ppbV with AUSTAL2000 at 3 m and between 4.9 and 18.1 at Verziere site. This result implies that, first of all, the reconstruction of air quality levels within urban areas, even in an intensely emitting area like Milan city center, requires a modelling approach able to take into account the influence of sources placed over the whole urban context.

Table 3 reports the main statistical parameters summarizing model performance for both HMS outputs and for stand-alone CAMx output.

Both the observed annual mean concentration and the standard deviation of hourly concentrations at Senato site were higher than at Verziere site. The reason is probably related to local features of urban morphology as shown in Fig. S2 but also to the traffic load on the two streets. Actually, Verziere street is a secondary road, less trafficked compared to Senato street, that is a stretch of the city center ring road with the aspect of an urban canyon. Therefore, in addiction to high local NOx emissions, there are also buildings surrounding Senato monitoring station, that emphasize backlog conditions rather than at Verziere site where, moreover, the wider open area favors the dispersion of local emissions. Neither stand-alone CAMx nor the HMS were able to capture this feature. Indeed all the model configurations showed increasing concen-trations from stand-alone CAMx to HMS_3m, but without relevant differences between the two sites. This suggests that both the dif-ference in urban morphology and in the emission load were not well captured by the HMS.

At both sites the statistical indexes showed a general underes-timation for CAMx stand-alone (negative bias: 20.8 at Senato, 6.5 at Verziere), but improved with HMS application. Bias decreased of almost 8 ppbV at Senato site using HMS with AUSTAL2000 vertical average and of more than 16 ppbV with AUS-TAL2000 at 3 m, anyway still remaining negative (4.4 ppbV); at Verziere site bias was still negative, reaching a value of 0.1 ppbV with HMS_mean24m, but became positive with HMS_3m (6.7 ppbV). Correlation index showed a slight worsening for both HMS options with respect to CAMx: from 0.84 for CAMx down to 0.78-0.81 for HMS at Senato site, from 0.73 down to 0.71-0.72 at Verziere site. The opposite trend of bias and correlation index, as well as of index of agreement, points out that: i) the higher con-centrations produced by HMS with respect to stand-alone CAMx reduced, on the average, the model underestimation; ii) the pres-ence of several peaks produced by AUSTAL2000 during nighttime stable conditions worsened the reproduction of the temporal evolution of NOX concentrations.

The combined effect of both these aspects on model perfor-mance is supported by joint evaluation of the Index of agreement (IOA) and Root Mean Square Error (RMSE). Actually, with respect to stand-alone CAMx, the IOA computed for HMS options remained substantially unchanged at Senato site, where the worsening in correlation was compensated by the clear improvement in bias and a slight one in RMSE, especially for HMS_mean24m approach; differently at Verziere site IOA and RMSE showed a degraded per-formance, especially for HMS_3m.

In contrast with the improvements obtained for the BIAS, HMS_3m approach produced worst performance at both sites when IOA and CORR are considered. Conversely, HMS_mean24m shows less relevant improvements but extended to all the statis-tical performance indicators.

This aspect can be explained by the significant backlog capa-bility of LSM at ground-level during stable conditions (night-time), confirming the HMS_mean24m as best solution between the two approaches.

The analysis of the whole distribution of measured and modelled $NO_x$ time series showed that all CAMx stand-alone dis-tributions systematically underpredicted the measurements at both sites, especially at Senato site (Fig. 10 and Fig. S1 in S.M.). This behavior improved with the introduction of the HMS, but there were still relevant discrepancies, particularly for the highest per-centiles. A better agreement with modelled data was observed at Verziere site, particularly for HMS_mean24m data. This confirms that HMS was able to add properly the local scale magnitude of NOX concentrations to background contribution at this site, but not al-ways to reproduce their temporal variability as confirmed by sta-tistical indexes shown previously. At this site we could also observe a very good agreement for stand-alone CAMx output up to the 50th percentile while a systematic underestimation for Senato site, even

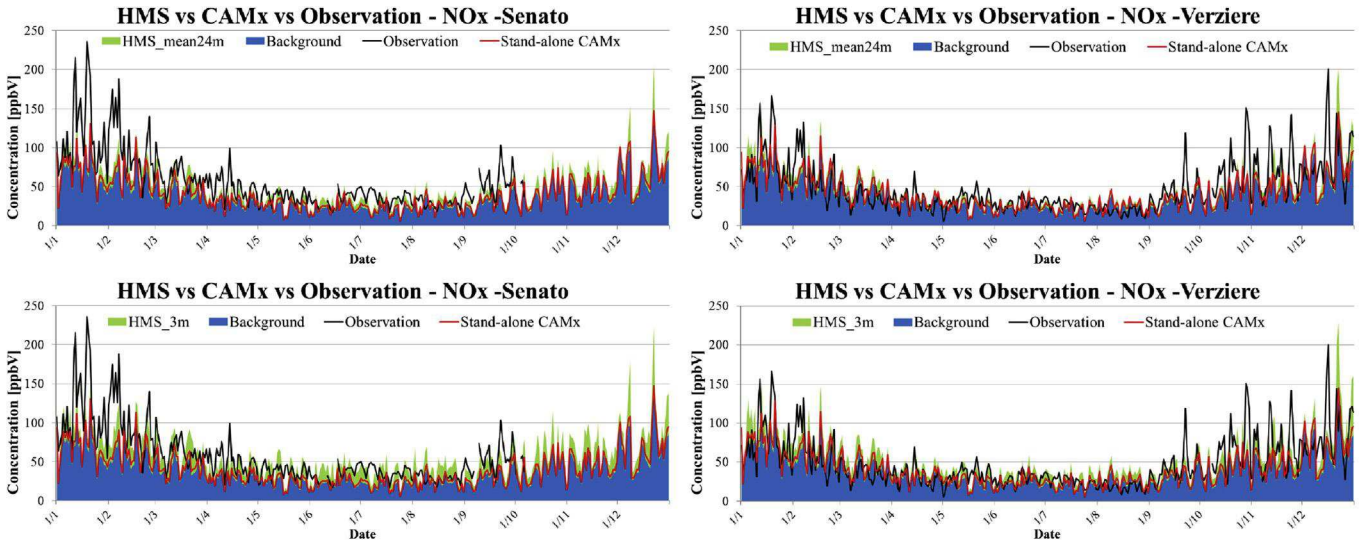


Fig. 9. Comparison of daily mean NOX concentrations observed and computed by the HMS, according to both definition, and stand-alone CAMx for Senato (left column) and Verziere site (right column). HMS concentration is obtained superimposing CAMx background concentration (in blue) with AUSTAL2000 local contribution (in green). AUSTAL2000 contribution in HMS time series is HMS_3m in top graphs and HMS_mean24m in bottom graphs. Stand-alone CAMx results are in red. (For interpretation of the references to colour in this figure legend, the reader is referred to the web version of this article.)

Table 2
Comparison among the modelled contributions to the yearly mean concentration and corresponding standard deviations.

| Statistical parameters | Milano Senato | | | | Milano Verziere | | | |
|---|---|---|---|---|---|---|---|---|
| [ppbV] | CAMx background | AUSTAL2000 24m | AUSTAL2000 3m | CAMx local | CAMx background | AUSTAL2000 24m | AUSTAL2000 3m | CAMx local |
| Mean | 36.7 | 13.4 | 21.4 | 4.2 | 36,3 | 11.3 | 18.1 | 4.9 |
| St. Dev | 21.2 | 14.9 | 20.6 | 3.5 | 20.8 | 13.4 | 18 | 4 |

Table 3
Statistical parameters of HMS and CAMx model performance at Senato and Verziere site.

| Statistical parameters | Milano Senato | | | | Milano Verziere | | | |
|---|---|---|---|---|---|---|---|---|
| | Observ. | HMS_mean24m | HMS_3m | CAMx stand-alone | Observ. | HMS_mean24m | HMS_3m | CAMx stand-alone |
| Mean [ppb] | 58.1 | 50.1 | 58.1 | 40.9 | 47.9 | 47.6 | 54.4 | 41.2 |
| St. Dev. [ppb] | 37.1 | 27.3 | 29.5 | 23.3 | 31.5 | 27.6 | 30.2 | 23.3 |
| BIAS [ppb] | | 12.2 | 4.4 | 20.8 | | 0.1 | 6.7 | 6.5 |
| MAE [ppb] | | 26.5 | 27.2 | 28.1 | | 24.9 | 27.1 | 23.9 |
| IOA [ ] | | 0.92 | 0.92 | 0.93 | | 0.84 | 0.81 | 0.86 |
| RMSE [ppb] | | 40.9 | 41.6 | 42.2 | | 38.1 | 40.8 | 36.1 |
| CORR [ ] | | 0.81 | 0.78 | 0.84 | | 0.72 | 0.71 | 0.73 |

though HMS_mean24m application, confirms that some specific local scale features were not captured by our modelling approach. Indeed, we already pointed out that highest observed concentra-tions took place during very stable conditions when local scale accumulation processes, that cannot be captured by CAMx, were prevailing.

Although the highest percentiles underestimation persists after HMS introduction, the overall improvements will allow to capture a better level of exposure to pollutants of people living in high-density urban areas, particularly at hot spot sites, generally missed by larger scale model.

A further analysis of model performance was carried out considering the average weekly pattern and the mean day of modelled and observed $NO_x$ concentrations (Fig. 11). The "day of the week" analysis shows that both HMS and stand-alone CAMx were able to capture the decreasing trend between workdays and weekends, especially in January, while failing in reproducing the day-by-day variability observed also during workdays. The origin of such variability, especially observed at Senato site, was not clearly identified and could not be properly reproduced with the current approach for emission processing, that used the same time pattern for all weekdays from Monday to Friday. The day-by-day variability as well as the absolute values of concentrations were quite well reconstructed during the summer month (June), especially at Ver-ziere site that was not affected by morning rush hour peaks as at Senato site.

Fig. 11 shows a negative bias at Senato site for January, across all weekdays. The discrepancy was mainly related to the strong un-derestimation of the morning peak and, as a consequence, of the ensuing daytime concentrations, as clearly pointed out by the mean day analysis in Fig. 12. Other than to the emission pattern, the systematic under prediction of $NO_x$ at Senato site, clear also during June, can be partly associated with an incorrect definition of the site's features as discussed before (e.g. street canyon character), that could not be captured by our modelling approach.

Notwithstanding the day-by-day temporal variability not

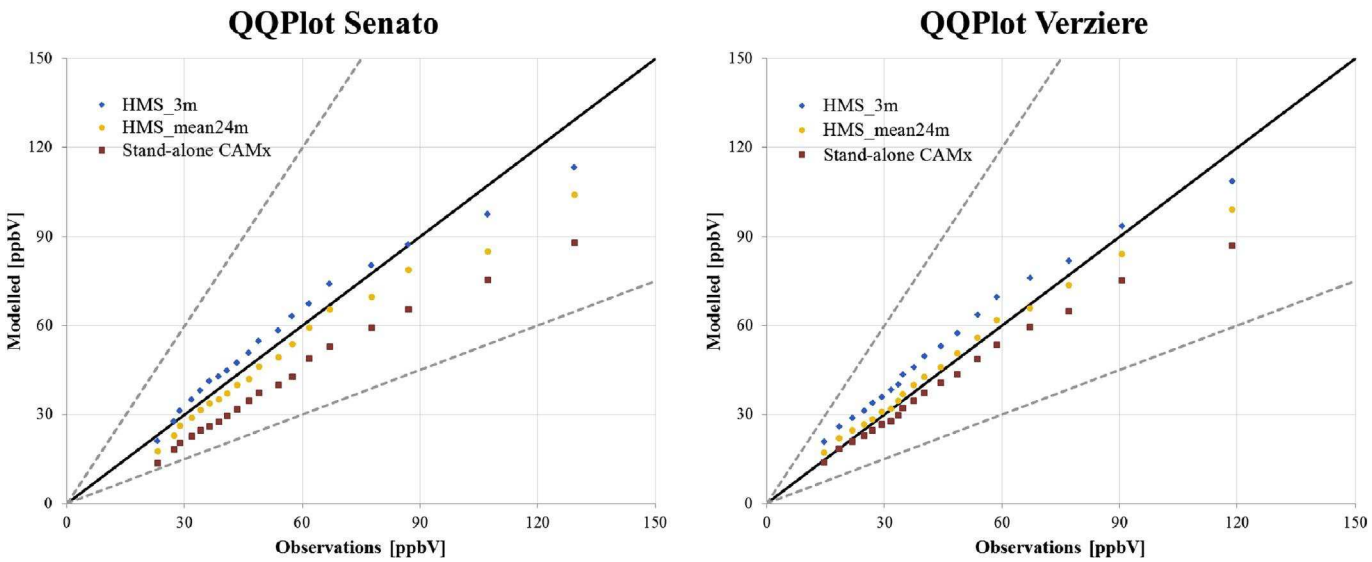


Fig. 10. Quantile-Quantile plot of the observed and modelled NOx daily concentrations at Senato (left) and Verziere (right) site, starting from 5th percentile up to 95th percentile with a step of 0.05.

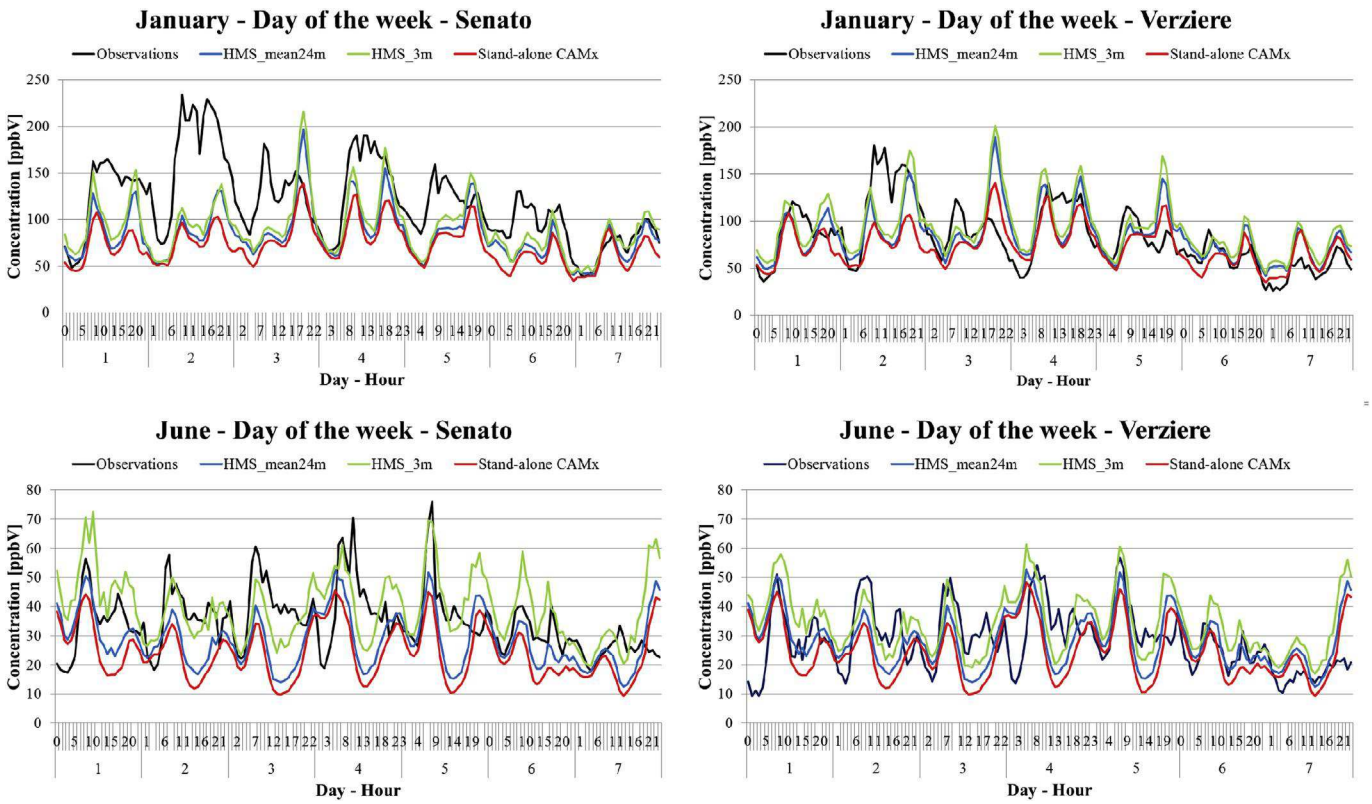


Fig. 11. Day of the week for January (top) and June (bottom) NOx concentrations at Senato (left) and Verziere (right) measurement site. Black line represents measure, red line indicates stand-alone CAMx concentrations, while green and blue line show HMS results. Day of the week ranges from Monday (1) to Sunday (7). (For interpretation of the ref-erences to colour in this figure legend, the reader is referred to the web version of this article.)

exactly reconstructed, the HMS (mean24m and 3m approach) re-sults showed in Fig. 12 confirmed that the average day-time vari-ability modelled was not much different from observed concentrations, especially during the summer period when thermal and mechanical turbulence phenomena were more pronounced than in winter time. In particular, the magnitude of NOx concentrations observed in the winter (from 60 ppbV to 100 ppbV) and summer period (from 15 ppbV to 40 ppbV) was correctly reproduced.

However, the daily pattern was better reconstructed in the summer period than in the cold season.

Indeed, traffic modulation and atmospheric conditions could influence significantly NOx concentrations during the hours of the day but CAMx stand-alone and especially HMS reproduce

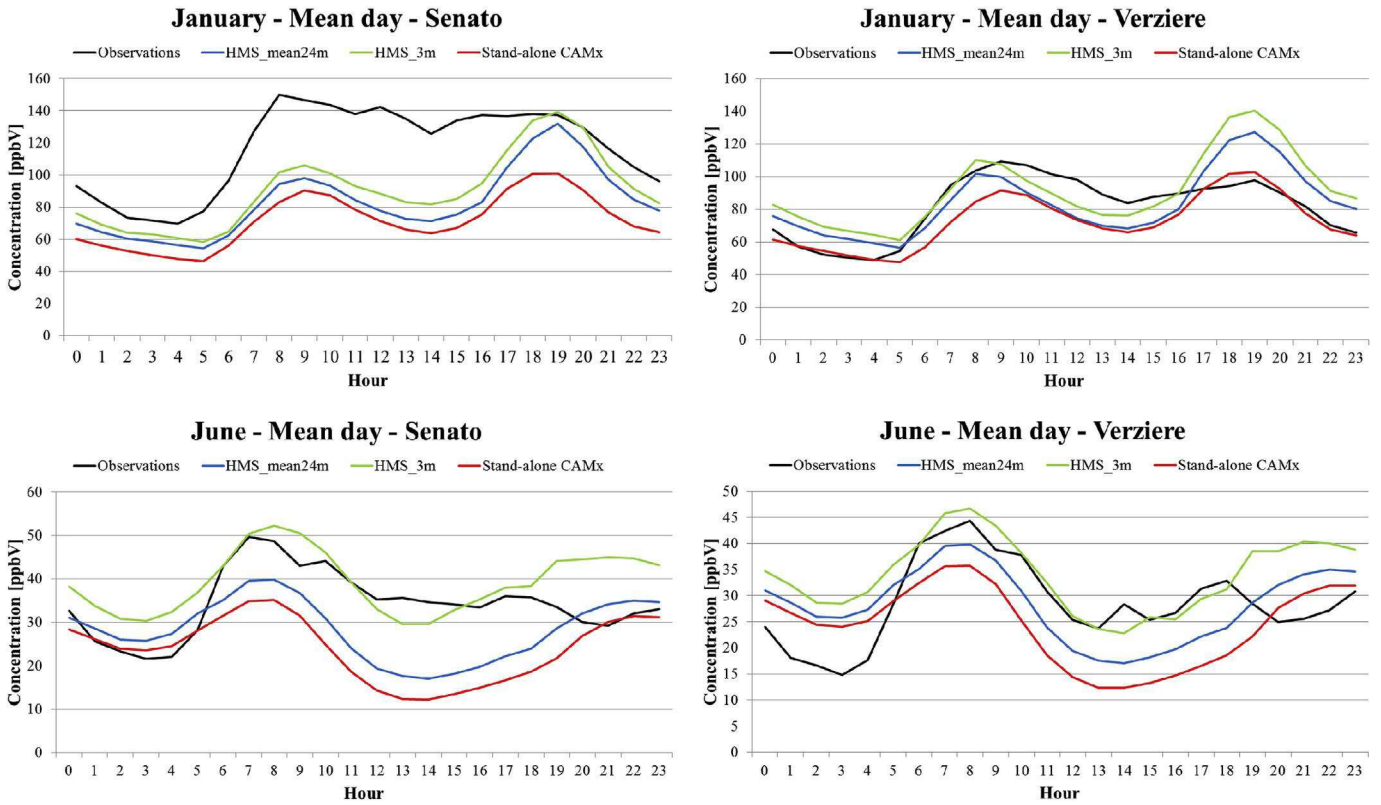


Fig. 12. Mean day for January (top) and June (bottom) NOx concentrations at Senato (left) and Verziere (right) measurement site. Black line represents measure, red line indicates stand-alone CAMx concentrations, while green and blue line show HMS results. Day of the week ranges from Monday (1) to Sunday (7). (For interpretation of the references to colour in this figure legend, the reader is referred to the web version of this article.)

satisfactorily the morning and evening peak, moreover during summer months. Mechanical and relevant thermal turbulence during the warm season caused a lower evening peak, even though traffic modulation was similar to the cold season. This aspect was considered by both models (CAMx stand-alone and HMS).

In particular, at Verziere site model outputs showed the smallest bias (Table 2), with the observed concentrations rather well captured, by HMS_mean24m on both summer and winter months.

Actually, the main discrepancy was related to the over-estimation of the evening peak in January, and to a lesser extent in June, on both workdays and weekends, even up to about 30 ppbV.

The consistent over prediction suggests either a not good agreement between modelled and real modulation of traffic emissions or a too strong decrease of vertical turbulence and mixing in the late afternoon. This latter phenomenon has been already highlighted by previous studies (Kim et al., 2015) and is related to the difficulty of meteorological model in taking into ac-count the contribution of anthropogenic heating to energy balance within urban areas.

CAMx stand-alone and HMS approaches resulted in solutions regarding concentration levels somewhat different but temporal variability as shown in Figs. 11 and 12 was not affect by the two methods. This aspect suggests that horizontal resolution as well as modelling method could either increase or decrease the backlog capability of the models, but they are less influent on temporal evolution. Consequently, NOx temporal variability depends on emission temporal modulation and overall meteorological param-eters, which remains unchanged between the two approaches.

Finally, as for as the “double counting” is concerned, results reported in Table 2 for the annual mean concentration and the inspection of the daily pattern of the contributions computed by CAMx and AUSTAL2000 at the two monitoring sites (Fig. 13) showed that the local sources’ contributions could not be consid-ered negligible. In particular, the CAMx local contribution (i.e. the potential “double counting”) was in the 5%-15% range of the daily mean concentration considering both sites and months. Thus, correctly the CAMx local contribution must be excluded from HMS outcome to have a more accurate model estimate. AUSTAL contri-bution was in the 15%-25% range for January while during June the range increased up to 30% as daily average.

## 4. Conclusions

A hybrid modelling system (HMS) was developed to provide hourly concentrations at the urban local scale. In this work the HMS was applied over a set of nested domains, the innermost covering a 1.6 1.6 km$^2$ area in Milan city center with 20 m grid step size. HMS is based on the combination of a meteorological model (WRF), a CTM eulerian model (CAMx), which computes concentration levels over the regional domains, and a lagrangian dispersion model (AUSTAL2000), which computes dispersion phenomena and relative concentrations, due to road traffic and domestic heating within the urban area. A source apportionment algorithm PSAT (Yarwood et al., 2004), is also included in the HMS in order to avoid the double counting of local emissions. PSAT is able to track contribution of different emission areas or source categories. In this application we split the NOx concentration level in two Milan emission areas’ contribution: innermost domain contribution (“local”) and external domain contribution (“background”). These two terms refer respectively to emission sources located within the

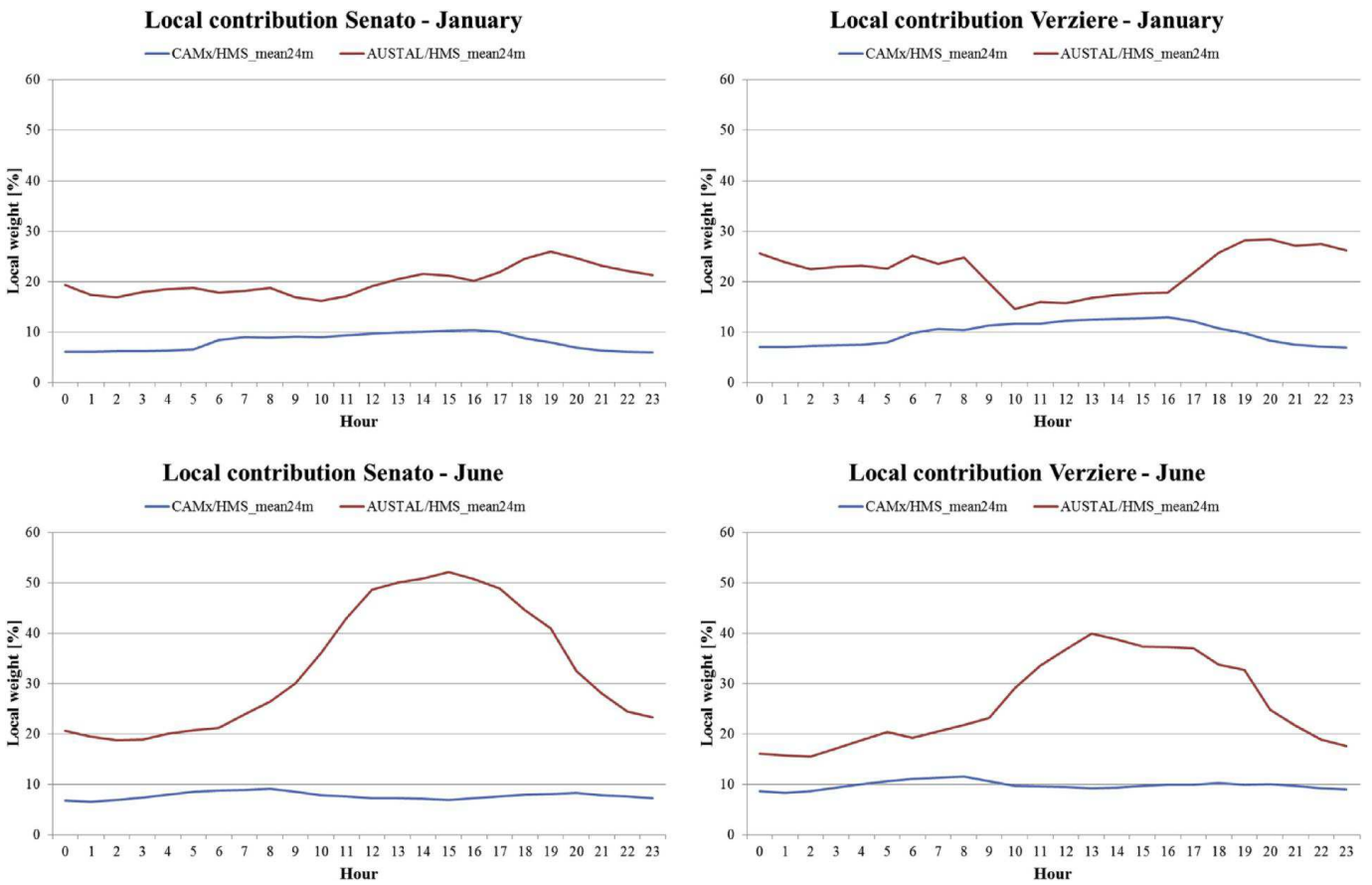


Fig. 13. Daily pattern of the percentage ratio between estimated local contributions and HMS_24m daily mean concentration, computed for CAMx local (blue) and AUSTAL2000 (red) at Senato (left) and Verziere (right) site for January (top) and June (bottom). (For interpretation of the references to colour in this figure legend, the reader is referred to the web version of this article.)

innermost domain and to all remaining sources outside. Limitedly to this application "local" and "background" does not refer to the usual definition of the urban areas, while to the computational domains of the two modelling layers. The performance of the model components of the HMS was thoroughly evaluated for both meteorology and air quality reconstruction at the basin and local scale.

WRF captured the overall evolution of the main meteorological features, but failing in reproducing some very stagnant situations, thus influencing the subsequent performance of regional scale model CAMx. Indeed, CAMx was able to reproduce the spatial and temporal evolution of $NO_x$ concentration over the whole regional and Milan area domain, with the exception of two severe episodes, characterized by observed concentrations higher than 100 ppb.

The local scale model AUSTAL2000 provided high-resolution concentration fields that sensibly mirrored the road and traffic pattern in the innermost urban domain. In spite of the different modelling approach, the local contributions estimated by CAMx and AUSTAL2000 were in good agreement, especially during day-time in the summer period when stronger dispersion conditions, due to increasing of height mixing layer, generate more homoge-nous concentrations over the first vertical layers. Conversely, AUSTAL2000 resulted in higher concentration levels on night hours due to pronounced backlog situations corresponding to atmo-spheric stratification phenomena.

According to the HMS the background contribution accounted on the average for about 70-75% of the computed concentration levels in the local domain, with the contribution of the local emission sources higher than the background only on particular events, mostly during atmospheric stability episodes (low wind speed and positive Monin-Obukhov length). This result, stating that $NO_x$ concentration levels within the inner part of the urban area could be mostly influenced by the contribution of sources outside the local domain, confirmed that in Milan the whole urban area as well as the outside background areas play a key role on air quality and that strictly local policies on urban emission sources could have a limited and indecisive effect. However, this finding could be partially biased by model underestimation of the observed concentration.

In spite of the interesting additional pieces of information pro-vided by HMS output about local scale modelling, namely con-cerning the detailed reconstruction of the spatial variability of $NO_x$ concentration, the overall performance of the HMS did not provide remarkable improvements with respect to stand-alone CAMx. Model validation relied on hourly $NO_x$ data collected for 2010 at the two only monitoring sites in the innermost simulation domain. Actually, with respect to stand-alone CAMx the HMS results were characterized by a smaller average bias as well as by a lower cor-relation, due to the concentration peaks produced by AUSTAL2000 during nighttime stable conditions that worsened the reproduction of the temporal evolution of $NO_x$ concentrations. Vertical averaging of HMS output data provided a slightly more robust performance, as averaging along the first atmospheric layers reduced the effect of the overestimated influence of stable and stagnant atmospheric

conditions.

The HMS provided rather similar results at both measuring sites, while observed values were clearly different, suggesting that some local scale features (e.g. the canyon effect at one site) still remain not correctly taken into account by the model or that the emission spatialization criteria, especially those from road traffic, need further improvement. Additionally, the analysis of the mean day concentrations highlighted that the HMS provided higher concen-trations during evening hours. Such systematic over prediction suggests either a not good agreement between the time modula-tion of modelled and real world emission or a too strong decrease of vertical turbulence in the late afternoon related to the difficulty of the meteorological model in taking into account the contribution of anthropogenic heating to energy balance within the urban area. However, a first important outcome of the work is that some of the most relevant discrepancies between modelled and observed concentrations were not related to the horizontal resolution of the dispersion models, but to larger scale meteorological features not captured by the meteorological model. Secondly, HMS output reduces the bias with observed NOx concentrations still keeping unaltered the time patterns (daily, weekly, monthly) of the CAMx model.

We have demonstrated that this hybrid approach for the prediction of pollutant concentrations in urban areas is promising, even though the performance of the HMS showed some limitations, partially due to some approximations in the local scale input data. Such limitations concerns, among others: the fixed height of the buildings, the width of the streets in relation to the grid step size, the domestic heating emissions partitioning, the split of traffic emission among the arches of the road network and to the value of the urban mixing layer height constrained by inherent model as-sumptions (Federal Ministry for Environment, 2002). In conclusion, the highly-resolved spatial and temporal scale of the HMS output can be used for refining human exposure and health impact assessment as well as for the assessment of the impact of energy and traffic policies on air quality at the regional and local scale.

Future work will also consider other pollutants, like particulate matter, a wider local domain in order to extent it to the entire urban area, and facing the abovementioned issues related to the input data for the local scale model.

## Acknowledgements

This work has been financed by the Research Fund for the Italian Electrical System under the Contract Agreement between RSE S.p.A. and the Ministry of Economic Development e General Directorate for Nuclear Energy, Renewable Energy and Energy Efficiency in compliance with the Decree of March 8, 2006. The authors would like also to acknowledge ARPA Lombardia for air quality and meteorological observations data, necessary to evaluate HMS and the models which composed it.

## Appendix A. Supplementary data

Supplementary data related to this article can be found at http://dx.doi.org/10.1016/j.atmosenv.2016.06.071.

## References

Batterman, S., Chambliss, S., Isakov, V., 2014. Spatial resolution requirements for traffic-related air pollutant exposure evaluations. Atmos. Environ. 94, 518e528.

Beevers, S.D., Kitwiroon, N., Williams, M.L., Carslaw, D.C., 2012. One way coupling of CMAQ and a road source dispersion model for fine scale air pollution pre-dictions. Atmos. Environ. 59, 47e58.

Chen, F., Dudhia, J., 2001. Coupling an advanced land-surface/hydrology model with the Penn State/NCAR MM5 modelling system. Part I: model description and implementation. Mon. Weather Rev. 129, 167e196.

Denby, B., Cassiani, M., de Smet, P., de Leeuw, F., Horalek, J., 2011. Sub-grid vari-ability and its impact on European wide air quality exposure assessment. Atmos. Environ. 45, 4220e4229.

EEA, 2015. EEA Technical Report 1. No 1/2006. Air pollution at street level in Eu-ropean cities. Available at: http://www.eea.europa.eu/publications/technical_ report_2006_1 (accessed 17.06.15.).

ENVIRON, 2011. CAMx (Comprehensive Air Quality Model with Extensions) User's Guide Version 5.4. ENVIRON International Corporation, Novato, CA.

Federal Ministry of Environment, Nature Conservation and Nuclear Safety, 2002. Technical Instructions on Air Quality Control e TA Luft, Germany.

Grell, G.A., Devenyi, D., 2002. A generalized approach to parameterizing convection combining ensemble and data assimilation techniques. Geophys. Res. Lett. 29 (14). Article 1693.

Hellison, R.B., Greaves, S.P., Hensher, D.A., 2013. Five years of London's low emission zone: effects on vehicle fleet composition and air quality. Transp. Res. Part D 23, 25e33.

Hong, S.-Y., Noh, Y., Dudhia, J., 2006. A new vertical diffusion package with an explicit treatment of entrainment processes. Mon. Weather Rev. 134, 2318e2341.

Iacono, M.J., Delamere, J.S., Mlawer, E.J., Shephard, M.W., Clough, S.A., Collins, W.D., 2008. Radiative forcing by long-lived greenhouse gases: calculations with the AER radiative transfer models. J. Geophys. Res. 113, D13103.

INEMAR e Arpa Lombardia, 2015. INEMAR, Emission Inventory: 2012 Emission in Region Lombardy e Public Review. ARPA Lombardia Settore Aria. Available at: http://www.inemar.eu/.

INERIS, 2006. Documentation of the Chemistry-transport Model CHIMERE [version V200606A]. Available at: http://euler.lmd.polytechnique.fr/chimere/.

Isakov, V., Irwin, J.S., Ching, J., 2007. Using CMAQ for exposure modelling and characterizing the subgrid variability for exposure estimates. J. Appl. Meteorol. Climatol. 46, 1354e1371.

Isakov, V., Lobdell, D.T., Palma, T., Rosenbaum, A., Ozkaynak, H., 2009. Combining regional- and local-scale air quality models with exposure models for use in environmental health studies. J. Air Waste Manag. Assoc. 59, 461e472.

Isakov, V., Arunachalam, S., Batterman, S., Bereznicki, S., Burke, J., Dionisio, K., Garcia, V., Heist, D., Perry, S., Snyder, M., Vette, A., 2014. Air quality modeling in support of the near-road exposures and effects of urban air pollutants study (NEXUS). Int. J. Environ. Res. Public Health 11, 8777e8793.

Janicke Consulting, 2014. AUSTAL2000. Program Description of Version 2.6, 2014-02-24. Technical Report. Federal Environmetal Agency, Janicke Consuluting, Germany.

Kim, Y., Sartelet, K., Raut, J.C., Chazette, P., April 2015. Influence of an urban canopy model and PBL schemes on vertical mixing for air quality modeling over Greater Paris. Atmos. Environ. ISSN: 1352-2310 107, 289e306. http://dx.doi.org/10.1016/j.atmosenv.2015.02.011.

Lefebvre, W., Vercauteren, J., Schrooten, L., Janssen, S., Degraeuwe, B., Maenhaut, W., de Vlieger, I., Vankerkom, J., Cosemans, G., Mensink, C., Veldeman, N., Deutsch, F., Van Looy, S., Peelaerts, W., Lefebre, F., 2011. Validation of the MIMOSA-AURORA-IFDM model chan for policy support: modeling concentra-tions of elemental carbon in Flanders. Atmos. Environ. 45, 6705e6713.

Lefebvre, W., Van Poppel, M., Maiheu, B., Janssen, S., Dons, E., 2013. Evaluation of the RIO-IFDM-street canyon model chain. Atmos. Environ. 77, 325e337.

Lonati, G., Pirovano, G., Sghirlanzoni, G.A., Zanoni, A., March 2010. Speciated fine particulate matter in Northern Italy: a whole year chemical and transport modelling reconstruction. Atmos. Res. 95 (4), 496e514.

Martins, H., 2012. Urban compaction or dispersion? An air quality modelling study. Atmos. Environ. 54, 60e72.

Monin, A.S., Obukhov, A.M., 1954. Basic laws of turbulent mixing in the ground layer of the atmosphere. Trans. Geophys. Inst. Akad. Nauk. USSR 151, 163e187.

Morfeld, P., Groneberg, D.A., Spallek, M.F., 2014. Effectiveness of Low Emission Zones: large scale of changes in environmental NO2, NO and NOx concentra-tions in 17 German cities. PLoS One 9, 8.

Morrison, H., Thompson, G., Tatarskii, V., 2009. Impact of cloud microphysics on the development of trailing stratiform precipitation in a simulated squall line: comparison of one- and two-moment schemes. Am. Meteorol. Soc. 137, 991e1007.

Nenes, A., Pilinis, C., Pandis, S.N., 1998. ISORROPIA: a new thermodynamic model for multiphase multicomponent inorganic aerosols. Aquat. Geochem. 4, 123e152.

O'Brien, J.J., 1970. A note on the vertical structure of the eddy exchange coefficient in the planetary boundary layer. J. Atmos. Sci. 27, 1213e1215.

Pernigotti, D., Thunis, P., Cuvelier, C., Georgieva, E., Gsella, A., De Meij, A., Pirovano, G., Balzarini, A., Riva, G.M., Carnevale, C., Pisoni, E., Volta, M., Bessagnet, B., Kerschbaumer, A., Viaene, P., De Ridder, K., Nyiri, A., Wind, P., 2013. POMI: a model inter-comparison exercise over the Po Valley. Air Qual. Atmos. Health. http://dx.doi.org/10.1007/s11869-013-0211-1.

Skamarock, W.C., Klemp, J.B., Dudhia, J., Gill, D.O., Barker, D.M., Duda, M.G., Huang, X.-Y., Wang, W., Powers, J.G., 2008. A Description of the Advanced Research WRF Version 3, NCAR Technical Note NCAR/TN-475þSTR, Boulder, Colorado.

Stein, A.F., Isakov, V., Godowitch, J., Draxler, R.R., 2007. A hybrid modeling approach to resolve pollutant concentrations in an urban area. Atmos. Environ. 47, 9410e9426.

Stocker, J., Hood, C., Carruthers, D., Seaton, M., Johnson, K., 2014. The development and evaluation of an automated system for nesting adms-urban in regional photochemical models. In: 13th Annual CMAS Conference, Chapel Hill, NC,

October 27e29, 2014.
Torras Ortiz, S., Friedrich, R., 2013. A modelling approach for estimating background pollutant concentrations in urban areas. Atmos. Pollut. Res. 4, 147e156.
UNC, 2013. SMOKE v3.5 User's Manual. Available at: http://www.smoke-model.org/ index.cfm.
Yarwood, G., Morris, R.E., Wilson, G.M., 2004. Particulate matter source apportionment technology (PSAT) in the CAMx photochemical grid model. In: Proceedings of the 27th NATO/CCMS International Technical Meeting on Air Pollution Modeling and Application. Springer Verlag.
Yarwood, G., Rao, S., Yocke, M., Whitten, G., 2005. Updates to the Carbon Bond Chemical Mechanism: CB05, Report, Rpt. RT-0400675, US EPA, Res. Tri. Park.

# *Article 2*

Pepe N., Pirovano G., Balzarini A., Toppetti A., Riva G.M., Amato F., Lonati G.

## Enhanced CAMx source apportionment analysis based on source categories and emissive regions: Milan urban receptor case study

To be submitted on Atmospheric Environment

**Enhanced CAMx source apportionment analysis based on source categories and emissive regions: Milan urban receptor case study**

N. Pepe[2], G. Pirovano[1], A. Balzarini[1], A. Toppetti[1], G.M. Riva[1], F. Amato[3], G. Lonati[2]

1 RSE Spa, via Rubattino 54 - 20134 Milano, Italy

2 Department of Civil and Environmental Engineering, Politecnico Milano, Milano, 20133, Italy

3 Institute of Environmental Assessment and Water Research (IDAEA-CSIC), 08034, Barcelona, Spain

**Corresponding author**: Nicola Pepe, E-mail: nicola.pepe@polimi.it, Via Gian Giacomo Gilino 9, 20128, Milano, Italy (Present address)

# ABSTRACT

Source apportionment analysis computed by the chemical and transport model (CTM) is considered, by the European government. as a valid method for deriving information about pollution sources and their contribution to ambient air quality level. The modeling chain proposed in this work is composed by the meteorological model (WRF) and the CTM (CAMx). PSAT, the Particulate matter Source Apportionment Technology algorithm, is implemented within the chemical model in order to track contribution of different sources located over the domain considering also the precursors gases for secondary PM. The simulation was computed over two nested domains, the innermost covering a 85x85 $km^2$ area in Po Valley region, mostly the metropolitan area of Milan, for primary and secondary pollutants in 2010 calendar year, while the wider domain covers totally the Po Valley region with a computational domain of 600x420 $km^2$. In particular the source apportionment analysis was focused on fine particulate ($PM_{2.5}$), elemental carbon (EC), particulate nitrate ($NO_3^-$) and dioxide nitrogen ($NO_2$). The new modeling system based on CAMx v6.3 is able to track effects due to emission categories (road traffic, biomass burning or agriculture) and source areas (local, urban background or regional background), defined by the users before running the simulation. Local areas could include sources located near the receptor point and within big city boundaries. The system provides the possibility to define independently each area as a function of the aim of the study. In this paper we defined 5 source areas starting from a urban local domain

which encloses a small number of sources, principally traffic and residential heating, up to the entire Po Valley region. WRF model captured the overall evolution of the main meteorological features, except for some very stagnant situations, thus influencing the subsequent performance of regional scale model CAMx. However, CAMx guarantees good performance for $PM_{2.5}$ and $NO_2$ comparing model output with measurements over the domains. Source apportionment analysis results over an urban receptor located near Duomo square are the following:

- Fine particles ($PM_{2.5}$) analysis shows an inhomogeneous distribution of contributions over the domain, centered over the regional background area that generates 53% of total concentration. Focusing on the sources, the most impactful are road transports (28%) and biomass burning (24%).
- For EC, local and urban background areas influence the final concentration for 73% (60% due to urban background sources) and biomass burning combined to transport effects generate a contribution of 85% (~ 3 $\mu g/m^3$).
- The nitrate ($NO_3^-$) estimated in Duomo receptor derived almost totally from regional background areas (> 80%) with transport that represents the higher contribution source (43% - 1.4 $\mu g/m^3$). Heavy duty vehicles influence for 20% the nitrate final concentration.
- Local area affects 10% the $NO_2$ concentration level in the urban receptor. The highest contribution comes from urban background sources (60%). Generally, the most impactful emission source is represented by transport sector (72%) with its high emission of NOx during the whole year.

CAMx/PSAT approach could be a valid instrument for assessment of local/regional air quality policies. However, validation is necessary, both for chemical reconstruction of PM species and source apportionment analysis. Through available measurement campaigns generated by the AIRUSE project (Amato et al, 2016), a comparison for CAMx/PSAT output was possible. In spite of the fact that different years were studied with the two methods, CAMx/PSAT tends to reconstruct quite well $PM_{2.5}$ components. The remarkable underestimation could be ascribed to missed processes as SOA formation, highest PM component over Po Valley region (Sandrini et al, 2014) and resuspension. Also the underestimation of stagnant conditions during winter periods from WRF model affects PM2.5 ambient levels. Finally, in this work we tried to recreate the PMF factor analysis through CAMx/PSAT output. Focusing on the comparison between

PMF and CAMx/PSAT outputs, best performances were reached for traffic and for biomass burning sources with comparable contributions and percentage distribution.

**Research Highlights**

- Source apportionment analysis with emission regions and categories by CAMx
- $PM_{2.5}$, elemental carbon, nitrate and $NO_2$ source apportionment
- $PM_{2.5}$ source apportionment comparison between CAMx/PSAT method and PMF receptor model

**Keywords**: source apportionment; CAMx; PSAT; source regions, Milan;

# 1. Introduction

During the last decades, air quality in high-density urban areas and rural lands as well, represented the main concern for the entire population in terms of exposition to pollutants, which could affect the human health with acute or chronic respiratory and cardiac diseases (WHO, 2016).

Air quality political strategies, combined with technological progress, could represent the key for the reduction of concentrations levels. The knowledge of the contribution of the different emission sources to the pollution level, split according different categories (e.g. transport, heating,…) and areas (e.g. local, urban and regional areas) can provide suitable information for environmental policies. The quantification of such contributions to the concentration level estimated by a model or measured by an air quality station is known as source apportionment. The use of source apportionment as instrument to investigate and support environmental strategies is indicated also in the 2008/50/EC European air quality directive.

Receptor Model (RM) techniques are widely used tools to estimate the contributions of the emission sources to the concentration levels of particulate matter (PM) and its components (Belis et al., 2013). Receptor models mainly rely on three statistical techniques (Belis et al., 2014): principal component analysis (PCA), chemical mass balance (CMB) and positive matrix factorization (PMF). Although these methods produce relevant outcomes for environmental strategies support, they present some weaknesses:

- This approach could be applied mainly for particulate matter, (e.g $PM_{10}$ and $PM_{2.5}$), while for detection of other pollutants contributions (e.g. $NO_2$, $SO_2$) the application of RMs is less straightforward and it is necessary to rely on other models.
- Despite of deep analysis of PM composition, RMs present limited capacities to track the origin of secondary PM whose precursors are often emitted by a wide range of sources
- The geographical origin of emission sources can be only partially detected. This evaluation can be more effective for sources with a specific chemical profile and localization.
- The source apportionment analysis conducted by RMs is site-dependent. The SA outcomes are valid only near the receptor point. Necessarily, further measurement campaigns must to be set in order to track emission contributions over wider areas.

  Alternative to RMs, source-oriented Chemical and Transport Model (CTMs) are widely used to conduct source apportionment analyses. In particular, CTMs like CAMx (Karamchandani et al, 2017; Wang et al,2017; Ciarelli et al, 2017), CMAQ (Buonocore et al, 2014; Appel et al, 2013; Zhang et al, 2014) and LOTOS-EUROS (Hamm et al, 2015; Mues et al, 2014; Curier et al, 2014) include specific tools allowing source apportionment analysis to be performed with a very effective approach. Similarly, CTMs present some drowbacks:

- Model reliability depend on emission inventory goodness provided by regional environmental agency or meteorological data estimated by diagnostic or prognostic meteorological model
- Secondary organic aerosols (SOA) are hardly to simulate and generally strongly underestimated

  Each emission source located over the domain can have a negligible or relevant role on pollution levels. It depends on many factors related to meteorological variables (wind intensity, direction or mixing layer height) as well as to the source category, such as: emission intensity, chemical profile or temporal modulation. In addition, from a policy point of view, it is very important to determine the spatial distribution of emission contribution to the total concentration.

  In this work we used the Comprehensive Air Quality Model with Extensions CAMx, (ENVIRON, 2016) which, by means of the embedded source apportionment algorithm PSAT (Yarwood et al., 2004), is able to track the contribution of different user defined

emission categories and regions (Pepe et al., 2016; Pirovano et al., 2015; Bedogni and Pirovano 2011).

The CTM application concerns the whole Milan urban area, while the analysis of the source apportionment was focused at one specific receptor point located in the city centre near the Duomo cathedral. This receptor is in a quite complex context due to presence of different sources as vehicular traffic, commercial activities and private houses. Additionally, overall orography and atmospheric chemistry increases the complexity of this area. CAMx/PSAT simulation covered the entire 2010 calendar year, focusing on ambient level of fine particulate ($PM_{2.5}$), elemental carbon (EC), nitrate particulate ($NO_3^-$) and dioxide nitrogen ($NO_2$) could be affected in different ways by emission sources located near or far away the receptor point.

In this work, the source apportionment analysis driven by CAMx tries to overcome weakness and limitations of RMs in order to improve SA results, detailing the different contributions of emission sources. The paper firstly describes the modeling chain and the new features of CAMx for a complete source apportionment analysis considering emission regions and source emission categories. The second section evaluates CAMx performances for $PM_{2.5}$ and $NO_2$ for urban, suburban and rural stations comparing air quality measurements data and estimation by the model. In the supplementary material (SM), $PM_{10}$ CAMx performance is evaluated too. After that, the annual mean source apportionment results focused on $PM_{2.5}$, EC, $NO_3^-$ and $NO_2$ is presented and discussed. Finally, CAMx results are discussed and compared to AIRUSE+ project outcomes, based on a PMF application of a Milan air quality campaign. The discussion illustrates strength and weakness of both approaches as well as improvements on aerosol process knowledge.

# 2. Methods

## 2.1. The modeling chain setup (WRF setup/performance and CAMx setup)

The modeling chain used for source apportionment analysis is composed by two main components: the Weather Research and Forecasting (WRF; Skamarock et al., 2008) meteorological model and the Comprehensive Air Quality Model (CAMx) model. The modelling system setup, also including the SMOKE emission model, is presented in Supplementary Material (SM) Figure S 3. Meteorological fields were reconstructed by

WRF model v3.4.1 (Skamarock et al., 2008) which was setup with 30 vertical layers, starting from the first one at 25 meters from the ground up to 15 km. Horizontally, 4 nested grids covering Europe, Italy, Po Valley, and the metropolitan area of Milan have been used; grid resolutions are 45 km, 15 km, 5 km and 1.7 km, respectively. WRF was driven by ECMWF analysis fields. Air quality simulations and source apportionment analysis were performed with CAMx v6.30 (ENVIRON, 2016). The CAMx simulation covered the two innermost domains of WRF but with a slight reduction of dimensions in order to remove boundary effects. The horizontal grid step size of Po Valley and Milan metropolitan area domains were the same as the WRF domain. Details on WRF and CAMx domains are showed in SM (Table S 2). The vertical structure of CAMx domain was divided into layers with different heights. Up to 1 km, CAMx vertical grid was identical to WRF grid.

Emissions were derived from inventory data at three different levels: European Monitoring and Evaluation Programme data (EMEP, http://www.ceip.at/emission-data-webdab/emissions-used-in-emep-models/) available over a regular grid of 50x50 $km^2$; ISPRA Italian national inventory data (http://www.sinanet.isprambiente.it/it/sia-ispra/inventaria/disaggregazione-dellinventario-nazionale-2010) which provides a disaggregation for province; regional inventories data based on INEMAR methodology (INEMAR – ARPA Lombardia, 2015). INEMAR, for the administrative regions of Lombardy, Veneto and Piedmont, which provide detailed emissions data at municipality level. Each emission inventory was processed using the Sparse Matrix Operator for Kernel Emissions model (SMOKE v3.5) (UNC, 2013) in order to obtain the hourly time pattern of the emissions.

Details on meteorological and emissions input data and chemical schemes adopted for this work are reported in Pepe et al. (2016), as well as the model validation phase for the 2010 calendar year comparing model results with measurements at meteorological and air quality stations.

## 2.2. Emission regions map

One of the new key features of CAMx/PSAT v6.30 used for this study is the possibility to setup different emission regions over the calculation grids. The goal was to track the contribution of different areas of the domain in order to describe properly how each region affects itself and the surrounding areas. We defined 5 areas that reflect the concept of

local, urban background and regional emission regions (see for example Lenschow, 2001 and the EU directive 2011/85/EU regarding e-reporting). We also constrained the definition of such regions to administrative boundaries in order to clearly link the pollution contribution to the corresponding administrative level (i.e. Municipality, Metropolitan area, Region, Country). The emission regions are shown for the two innermost computational domains, in Figure 20 labelled with different colors.

The wider area in yellow, named Po Valley (POV), includes all sources between national and Lombardy region boundaries; in blue the Lombardy area (LOM), extending from the boundaries of Lombardy to those of the metropolitan area of Milan (formerly Province of Milan); in orange, the Metropolitan area of Milan (PRO), not including the municipality of Milan (MIL), the red area in Figure 1). The fifth area, the green one in Figure 20 bottom panel, represents a very local emission area within the Milan city center (AUS) where the receptor site is located.

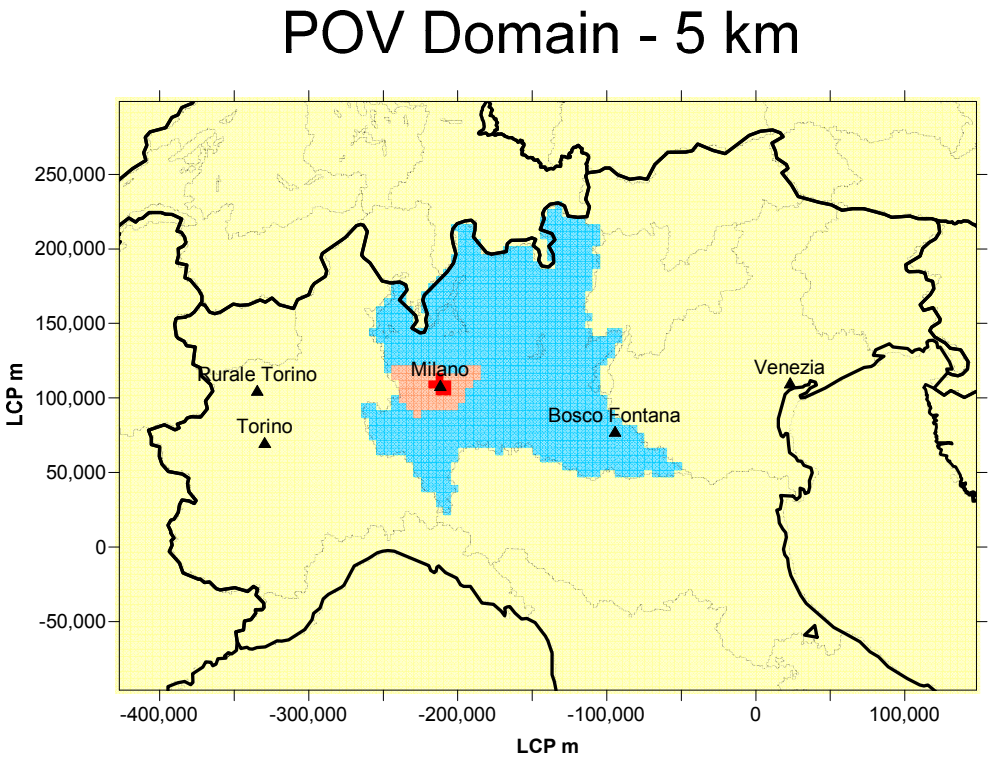

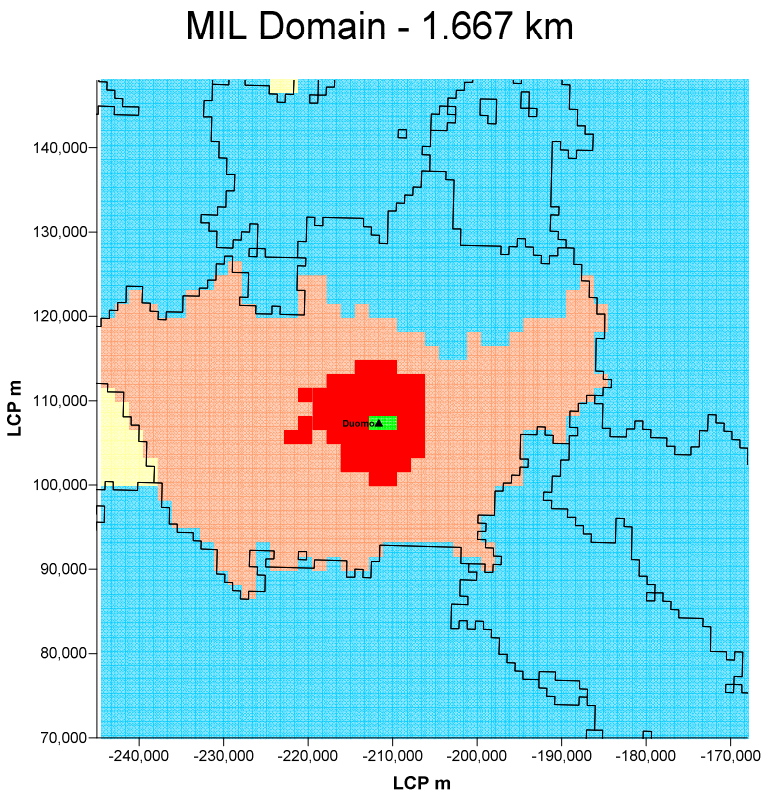


**Figure 39. Emissive regions within POV (5 km) and MIL (1.667 km) domains. In the top panel, some important cities over the Po Valley (Milan, Turin and Venice) are shown**

Accordingly to Lenschow's definition, emissions from POV and LOM regions are responsible for the regional background, those from PRO and MIL regions are responsible for the urban background, those from the smallest region determine the very local contribution to the concentration levels in the center of Milan. Such a local contribution does not represent a street level contribution, because it cannot be handled by a gridded model, but it takes into account the smallest and closest emission region that can be defined with respect to the selected receptor.

## 2.3. Emission categories

CAMx source apportionment analysis allowed also tracking the contribution according to a set of emissions categories. We defined the 11 source emission categories listed in Table 10.

**Table 10. Source emission categories defined for CAMx/PSAT application.**

| ***Label*** | ***Description*** |
|---|---|
| 01 ELE | Electrical energy production by industrial plants |
| 01 OTH | Industrial plants (no electrical energy production) |

| | |
|---|---|
| 02 BIO | Residential and commercial heating with biomass |
| 02 OTH | Residential and commercial heating with methane and gasoline (no biomass) |
| 07 AUT | Cars |
| 07 LEG | Light duty vehicles (weight < 3.5 tons) |
| 07 PES | Heavy duty vehicles (weight > 3.5 tons) |
| 07 MOT | Mopeds and motorcycles |
| 11 NAT | Natural sources –fires, volcanic eruptions, marine salt (only for Po Valley area) |
| EMEP | All sources located outside Italy. (no disaggregation on emission sources is provided) |
| OTHER | Other anthropogenic sources – agriculture, waste treatment, landfill, no streets transports |

These selected categories represent the main sources which generally affect the air quality in the Po Valley. In particular, we defined two emission groups for industrial plants, divided into electricity production (01 ELE) and no electricity production (01 OTH), and two emission groups for residential heating based on the kind of fuel (02 BIO, 02 OTH) in order to separate the biomass burning impact on air quality, which is typically interesting for for the Alpine regions. However, accordingly to national emission inventories, biomass burning is a relevant source also within the urban context of Milan. The road transport source was split it into four categories: cars, light and heavy duty vehicles, mopeds and motorcycles. The natural sources such as fires and sea salt are indicated as 11 NAT; the latter is considered only for the Po Valley geographical area. The OTHER category includes all the other anthropogenic sources within the Italian boundaries but not explicitly tracked in the previous categories, such as agriculture, waste treatment, landfill management and other ways of transport, as shipping or aviation. The EMEP category accounts for the contribution of the transboundary sources located outside of Italy but included in the Po valley domain. The last emission category, not included within Table 10, is the “Long range transport” and represents all contributions coming from north, south, east and west due to sources located outside the computational domain and from the top of the domain (boundary conditions – BC). These contributions were directly computed by CAMx in terms of final concentrations. Graphically, they will be a part of POV contribution, although their spatial origin is quite different.

# 3. Results and discussion

## 3.1. CAMx performance evaluation

CAMx performance was separately evaluated over both Po Valley and Milan metropolitan area domains. According to the aim of the work, in this paper results concerning $NO_2$ and $PM_{2.5}$ concentration are presented and discussed. $NO_2$ and $PM_{2.5}$ measurements for 2010 were provided by the stations of regional air quality networks. In particular, $NO_2$ and $PM_{2.5}$ data set were respectively composed by 144 and 40 urban and suburban stations, respectively. Figure 40 illustrates the daily comparison between CAMx output (orange line) and air quality stations observations (black line) for $NO_2$ and $PM_{2.5}$ over the Po Valley domain. The model shows a general underestimation of $NO_2$ concentration during the whole 2010, more pronounced in the winter months (December-January). As expected, also fine particulate is underestimated mainly during the winter months, while for the other months the model obtains better performance. Table 11 and Table 12 show the comparison between statistical indicators over the two domains, considering urban and suburban air quality monitoring stations. CAMx mean bias for $NO_2$ ranges between -40% and -22% moving from the Po Valley domain to the Milan area. $PM_{2.5}$ mean bias ranges between -34% and -30%. $NO_2$ correlation (r correlation), is approximately 0.3-0.4 over both domains, pointing out the difficulty of the model in reproducing the amplitude of both seasonal and weekly cycles of the observed concentrations. The index of agreement (IOA), which indicates the likelihood of model output respect to measurements, is a little bit higher than correlation because such index takes into account also the effect of the bias, that is rather low, in absolute value, for the most part of the year. Low correlation values are slightly influenced by the hourly integration time.

$PM_{2.5}$ simulation shows a better performance in terms of both correlation and index of agreement (about 0.53 and 0.63, respectively), with no relevant differences between the two computational domains, Actually, the model was able to correctly capture the temporal evolution of $PM_{2.5}$ from early spring to late fall but missed several severe episodes that took place in the winter months, particularly in January and December, thus causing a decrease in correlation index. The difficulty of the model in reproducing peak concentrations can be easily inferred looking at the difference between the statistical distribution of the modelled and observed time series that became larger and larger in the

upper tail of the distribution, as pointed out by the values of the three quartiles and of the 95$^{th}$ percentile reported in Figure 40.

The origin of the CAMx underestimation was extensively discussed in Pepe et al. (2016) with particular reference to $NO_X$, but similar conclusions can be drawn for $NO_2$ and $PM_{2.5}$. The discrepancies between measurements and observations occur mainly during the cold season and could be probably due to the potential overestimation of the vertical mixing. Generally, low wind speed, dry air and cold temperature are the factors that characterize the winter period in Po Valley region: often concurring with strong inversion conditions and with very low mixing heights, these factors favor pollutant accumulation, as confirmed in recent works (Squizzato et al, 2016; Pernigotti et al, 2014; Arvani et al, 2016).

Additional information on CAMx performance evaluation with respect to $PM_{10}$, EC (elemental carbon) and $NO_3^-$ (particulate nitrate) are available in S.M.. Figure S 4 and Table S 3 illustrate $PM_{10}$ model performance; time series comparison and statistical indexes revealed a worse performance than $PM_{2.5}$. The correlation and the IOA index presents lower values and during the summer period the discrepancy between measure and model output is more evident. Worsening in CAMx performance from $PM_{2.5}$ to $PM_{10}$ is mainly related to PM coarse fraction, due to some missing processes, such as dust resuspension, and was already observed in previous CAMx applications (Pirovano et al, 2012; Pernigotti et al., 2013). CAMx validation process at rural stations is reported in S.M. Figure S 5 and Tables S.3-S.5. Model performance improved for all the pollutants, proving that some of the discrepancies observed at urban and suburban sites can be probably ascribed to local scale processes. The influence of these processes on the observed concentrations cannot be captured at the adopted resolution, particularly with the larger grid step used over the Po Valley domain.

EC (elemental carbon) and $NO_3^-$ (particulate nitrate) output have been compared with observations at the EMEP monitoring site of Ispra, that is part of the European Monitoring and Evaluation Programme. Figure S 6 in S.M. illustrates concentrations time series and the principal statistical parameter trend during year 2010 for the Po Valley domain. Notwithstanding performance indexes were based on data from one monitoring station, this comparison provided some additional insights about model performance. Particularly, CAMx reproduced quite well EC and $NO_3^-$ behavior as confirmed by the bias index equal to 0.44 and 0.18 $\mu g/m^3$ respectively.

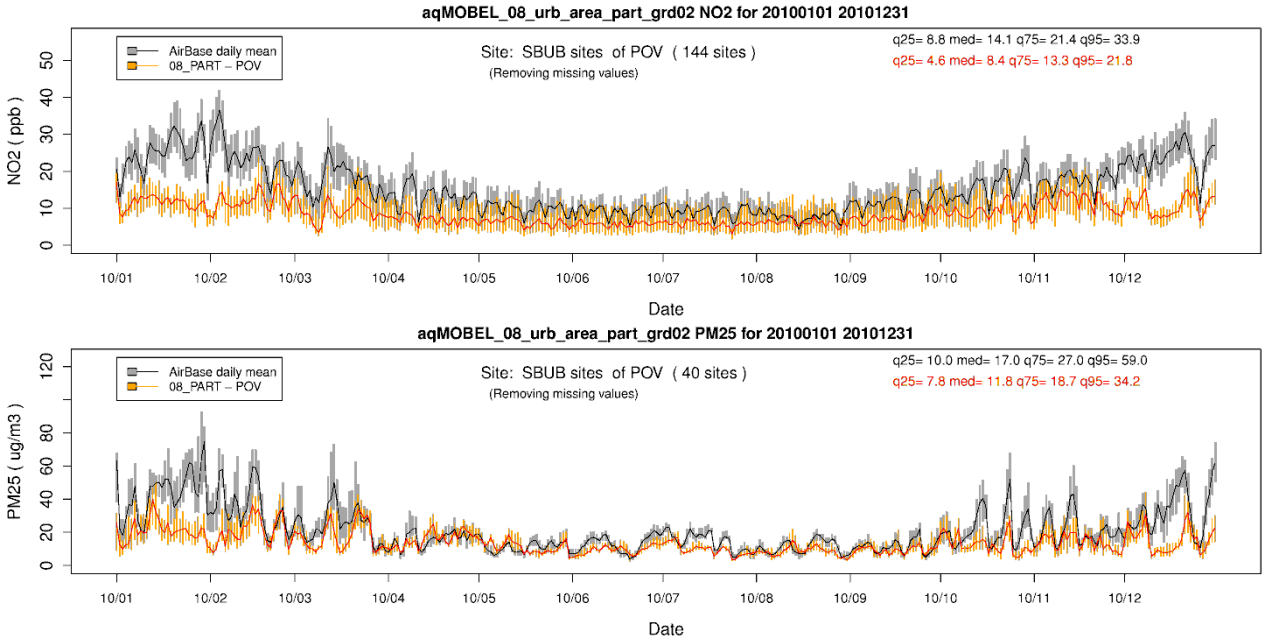


**Figure 40. Time series of the box and whisker plots for the daily distribution of the observed (black/grey) and computed (red/orange) values of $NO_2$ and $PM_{2.5}$ concentrations at respectively 144 and 40 ARPA sites, computed over the POV and MIL domains for 2010. Bars show the interquartile range (IR), lines the median values, dashed vertical bars (25th – 1.5 · IR) and the (75th + 1.5 · IR) value. Values for the 25th, 50th, 75th, and 95th quantiles of the whole yearly time series are reported too.**

**Table 11. Comparison of CAMx model performance for $NO_2$ hourly concentrations computed for 2010 at Urban and Suburban AQ stations of Po Valley and Milan area domain**

| | *Po Valley* | | *Milan area* | |
|---|---|---|---|---|
| | Observations | Model | Observations | Model |
| Mean [ppbV] | 16.2 | 9.7 | 19.8 | 15.5 |
| Standard Deviation [ppbV] | 11.8 | 8.3 | 14.0 | 9.8 |
| Number Observations [-] | 11659117 | | 238321 | |
| Correlation [-] | 0.39 | | 0.33 | |
| Mean Bias [ppbV] | -6.4 | | -4.4 | |
| Mean Error [ppbV] | 9.5 | | 10.7 | |
| Index of Agreement [-] | 0.59 | | 0.57 | |
| RMSE [ppbV] | 13.14 | | 14.8 | |

**Table 12. Comparison of CAMx model performance for $PM_{2.5}$ daily concentrations computed for 2010 at Urban and Suburban AQ stations of Po Valley and Milan area domain**

| | *Po Valley* | | *Milan area* | |
|---|---|---|---|---|
| | Observations | Model | Observations | Model |
| Mean [µg/m$^3$] | 22.0 | 14.6 | 27.3 | 19.1 |
| Standard Deviation [µg/m$^3$] | 16.9 | 9.7 | 19.9 | 11.2 |
| Number Observations [-] | 12890 | | 2369 | |
| Correlation [-] | 0.54 | | 0.52 | |
| Mean Bias [µg/m$^3$] | -7.4 | | -8.2 | |
| Mean Error [µg/m$^3$] | 10.5 | | 12.6 | |
| Index of Agreement [-] | 0.64 | | 0.63 | |
| RMSE [µg/m$^3$] | 16.1 | | 18.8 | |

## 3.2. Source apportionment output: Milan case study

In this work we focused on a singular receptor located within the urban city center, near Duomo cathedral. Duomo receptor identifies a residential area affected, in close proximity, by a moderate traffic level, at 90% composed by taxi, and a lot of commercial activities opened from the morning to the late evening. The most important emissions that affect the city center near the receptor are vehicular traffic and residential/commercial heating. As cited before, the biomass burning emission estimated by national inventories are not negligible although could not seem the principal emission source visible in the urban context.

The source apportionment analysis was focused on four pollutants: $PM_{2.5}$, EC, $NO_3^-$ and $NO_2$. $PM_{2.5}$ is actually one of the regulated pollutants of major concern, due to its health relevance and rather high average and episodic concentration levels, especially during the winter months. RMs were developed for source apportionment of PM, thus the comparison with CAMx SA analysis will be conducted for fine particles. Elemental carbon (EC) and nitrate ($NO_3^-$) present a different nature because while the first one is a primary compound, the particulate nitrate has a secondary origin. Thus, through the approach presented in this paper, it has been possible, firstly, to investigate the role of particles emitted directly into the atmosphere, again comparing CAMx findings to RMs results. Then we tried to overcome a RMs weakness developing a source apportionment analysis able to track the contribution of the different sources to a secondary pollutant. Finally, a gaseous pollutant as $NO_2$ was considered. As well as $PM_{2.5}$, it reached frequently higher concentrations during winter time but presented a wider monitoring stations network in order to control concentrations. As for secondary PM, CAMx/PSAT represents a step-forward in the understanding of $NO_2$ source apportionment. The CAMx model reconstructs the contribution of the different source on hourly basis, but in this paper the discussion of the results will be based only on annual mean concentrations, for the pollutants described before.

### 3.2.1. Particulate Matter ($PM_{2.5}$)

Through CAMx source apportionment the $PM_{2.5}$ mean annual concentration at Duomo station (about 18 $\mu g/m^3$) has been split by emission source categories, by emission regions, and by the combination of emission categories and regions. Modeled value is used as reference for all percentage data computed in this work.

In terms of region contributions (Figure 21a), both the regional (POV + LOM) and the urban background contribution (PRO + MIL) largely prevail on the local contribution (AUS). Actually, POV and LOM regions, together with the long range transport (i.e.: contribution from sources located outside of POV computational domain) provide the largest contribution, overall accounting for about 53% of $PM_{2.5}$, the metropolitan area of Milan and its municipality, excluding the local sources, account for 38%, and the local contribution is responsible for less than 8%. Both primary and secondary nature of fine particles that compose $PM_{2.5}$ are reflected by the similar contributions coming from urban background and local sources near to the receptor point and from the other sources located farther.

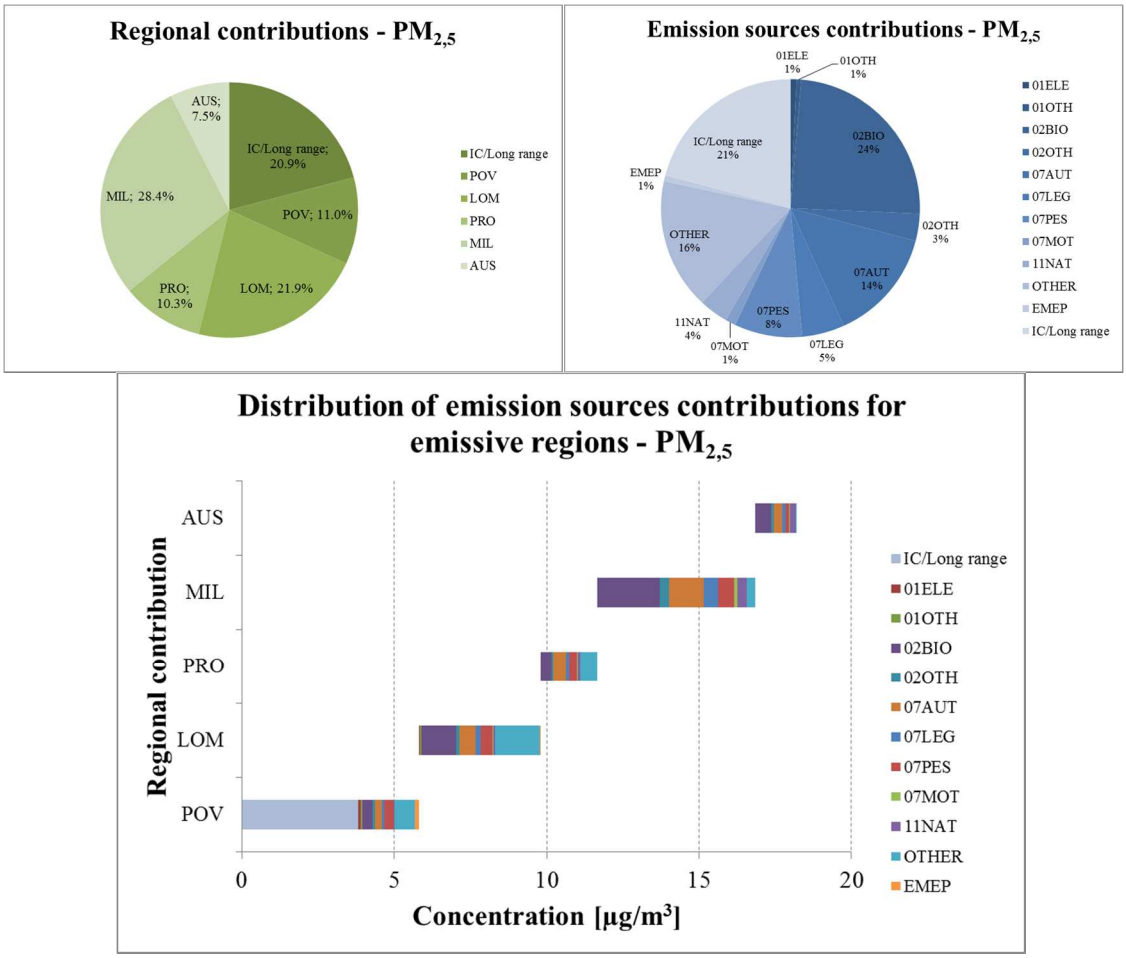


**Figure 41. $PM_{2.5}$ percentage distribution of emissive regions (3a, top-left) and emission sources categories (3b, top-right) contributions. (3c, bottom) is the regional absolute concentration distribution of each source activity contribution defined within CAMx/PSAT approach for $PM_{2.5}$**

In terms of source categories, road traffic, residential heating by biomass, and long range transport represent the most important sources for $PM_{2.5}$ with a total contribution of 73% (Figure 21b). The transport sector yields the principal contribution (28%), with half contribution due to cars, 8% and 5% respectively due to heavy and light duty commercial vehicles, and 1% due to mopeds and motorcycles. Residential and commercial heating by biomass burning, accounts for 24%, resulting the second most important source for fine particles. Although the wood or pellet burning for residential heating is an activity not so used in a metropolitan city like Milan, the results is surprising and it will be addressed in the next chapters of the composite impact of both source emission regions and categories. Long range transport is the third most impacting source (21%), followed by the OTHER category (i.e.: other anthropogenic sources like agriculture) that contributes up to 16%. Emissions from the non-biomass residential heating (3%), natural sources (4%) and industrial sources (2%) show a minor impact, as the emission sources outside of Italy, but still included in the POV domain (EMEP emission category) that contribute for only 1%.

Contribution breakdown by region and emission category is synthesized in Figure 21c, showing that the highest contribution (4 µg/m$^3$) comes from long range transport from sources located outside the domain; the second highest contribution (2 µg/m$^3$) comes from biomass burning in MIL region and the third is given by the other anthropogenic sources in the LOM region.

### 3.2.2. Elemental Carbon (EC) and Nitrate ($NO_3^-$)

Elemental carbon (EC) is a primary component of $PM_{2.5}$ directly emitted in atmosphere by combustion processes. As such, EC ambient concentration at receptor points is mainly driven by the contribution of local or short-range sources. For the Duomo receptor CAMx simulation estimated a mean annual EC concentration of 3.5 µg/m$^3$ in 2010. The geographic contribution analysis (Figure 22a) shows that more than 60% is due to urban background sources (MIL+PRO) and that the local sources (AUS) contribute for almost 13%. Nevertheless, the regional background contribution (POV+LOM) has a notable impact, reaching a total of 26% of the EC concentration when including also the long range transport. Regarding the contribution from the source categories (Figure 22b), the transport sector represents the most impactful source for EC with a 55% share; in details, 26% comes from cars, 15% and 13% are associated to heavy and light duty vehicles, respectively, while the contribution from mopeds and motorcycles is practically negligible (1%). Overall, the road source almost doubles the biomass burning, the second source for EC with 30%. The contribution from the other sources is rather limited: long range transport accounts for 5%, natural sources and the other anthropogenic sources for 4%, whilst EMEP sources and industrial processes do not impact significantly on EC concentration level.

Figure 22c points out that the three most impacting sources are the transport sector in the municipality of Milan (MIL) and in the Metropolitan area of Milan (PRO), that contribute respectively with 1.1 µg/m$^3$ (31%) and 0.28 µg/m$^3$ (8%) to EC concentration, and biomass burning in residential and commercial sources of the LOM region, which gives a 0.26 µg/m$^3$ contribution, very similar to the estimated share of traffic in the MIL region. Overall, these three most impacting sources are responsible for almost 50% of the EC yearly mean concentration at Duomo receptor. In particular, two of these sources are located in Milan metropolitan area boundaries highlighting the importance of urban sources, accordingly with the primary nature of this pollutant.

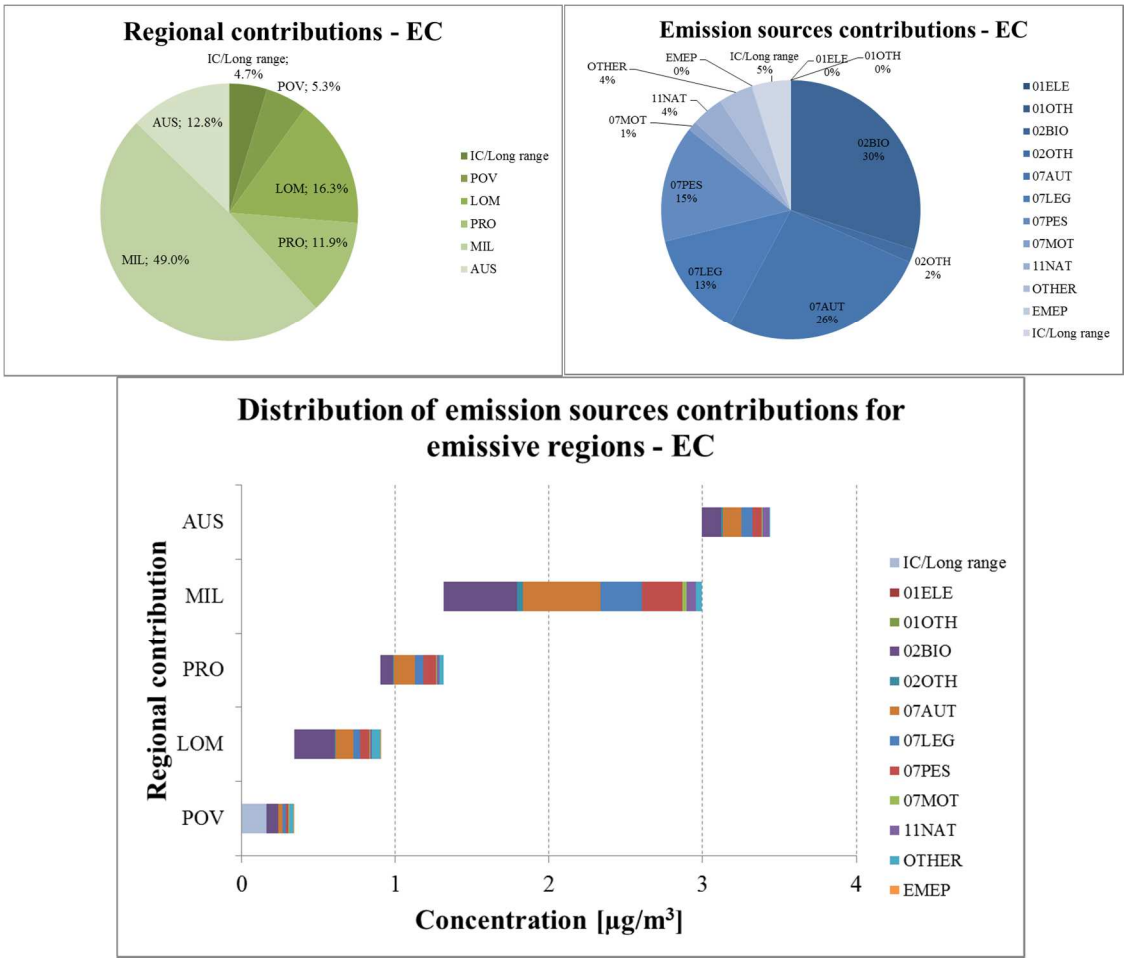


**Figure 42. EC percentage distribution of emissive regions (4a, top-left) and emission sources categories (4b, top-right) contributions. (4c, bottom) is the regional absolute concentration distribution of each source activity contribution defined within CAMx/PSAT approach for EC.**

Particulate nitrate is one of the secondary inorganic components of $PM_{2.5}$. For the Duomo receptor CAMx simulation estimated a mean annual $NO_3^-$ concentration of 3.3 µg/m$^3$ in 2010.

$NO_3^-$ shows a different spatial distribution over the domain with respect to EC as well as a different source contribution pattern. As shown in Figure 23a, the regional background contribution, given by long range transport, POV and LOM contributions, largely prevails on all the other emissive regions. These sources determine 86% of the $NO_3^-$ mean annual concentration, with the remainder 14% totally due to urban background sources located in the Milan area (MIL + PRO). The emissions of the local area (AUS) give a negligible contribution (less than 1%). Overall, the local and short-range contribution, the most important for EC, has a limited role on the total concentration of this secondary component of $PM_{2.5}$. Almost 90% of total concentration is generated by sources far away from receptor point, presenting an homogeneous distribution among three contributions.

In terms of source categories, the transport sector provides the largest contribution (43%), with heavy duty vehicles (20%) and cars (17%) yielding the highest share. Long range transport is responsible for 26%, the other anthropogenic sources for 16% and non-biomass residential and commercial combustion for 7%. Contributions from the other sources are in the order of 1-3% (Figure 23b).

Figure 23c points out the contributions of each source category by emission regions. The contribution originated from emission outside the POV domain (long range transport) is the highest (0.8 µg/m$^3$) among all region-and-category resolved contributions. The two other most impacting sources are transport in LOM and POV regions, with respectively 0.6 and 0.5 µg/m$^3$. All the sources related to urban background (MIL and PRO) and local region (AUS), generate a moderate contribution. In particular, the contribution from all the sources within the urban area of Milan is less than 0.3 µg/m$^3$ and from the local area less than 0.15 µg/m$^3$.

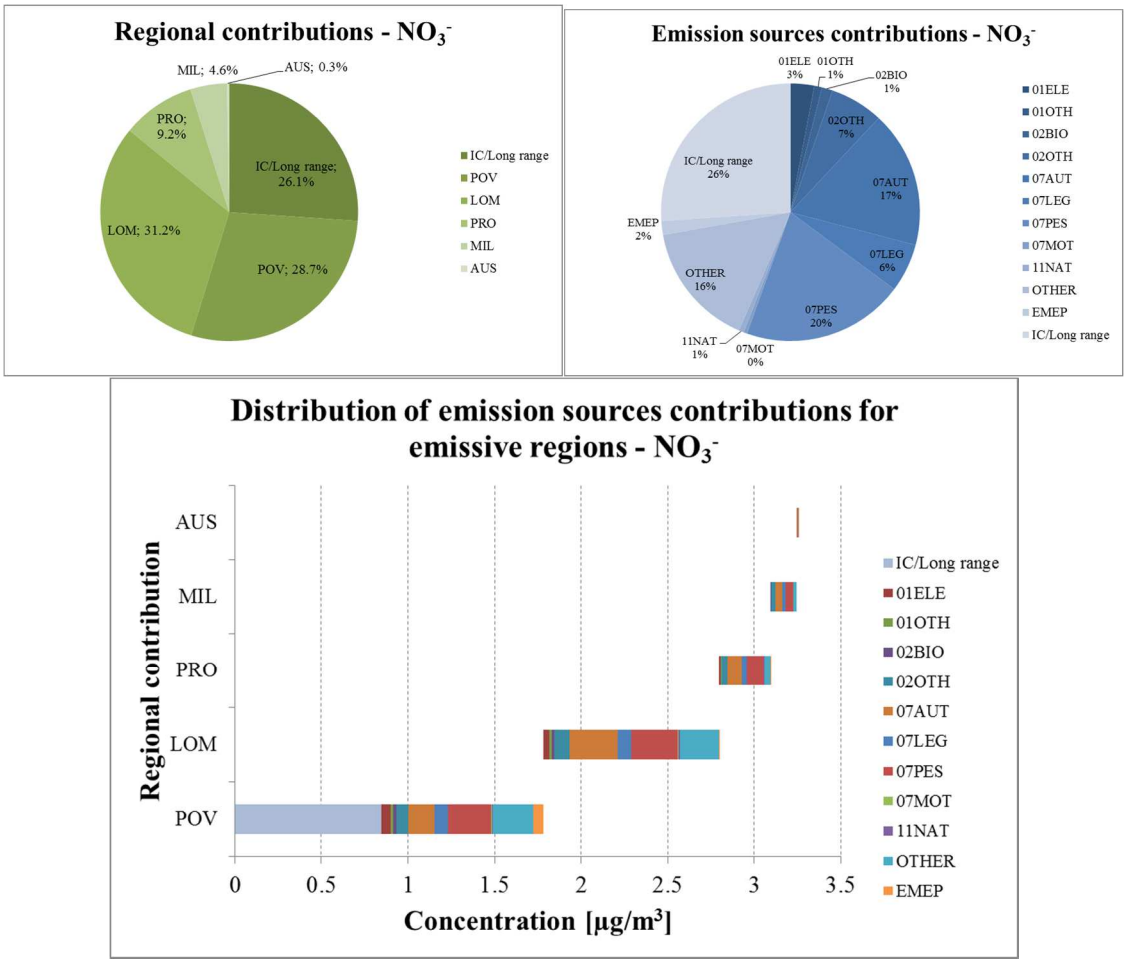


**Figure 43. $NO_3^-$ percentage distribution of emissive regions (5a, top-left) and emission sources categories (5c, top-right) contributions. (5c, bottom) is the regional absolute concentration distribution of each source activity contribution defined within CAMx/PSAT approach for $NO_3^-$**

The different contribution patterns obtained for EC and $NO_3^-$ are in agreement with the origin of these PM components. The secondary nature of $NO_3^-$ is underlined by the higher contributions due to sources far away from the metropolitan area of Milan, as can be seen in Figure 24. Figure 24.Chemical reactions that produce secondary PM from gaseous precursors require adequate time scales, that favor their production far beyond the city boundaries. This fundamental aspect is demonstrated by contributions due to vehicular traffic. The local sources (AUS) of transport sector provides a negligible contribution to $NO_3^-$ at Duomo receptor. Moving far from the city area, the contribution due to transport sector to the nitrate fraction of PM gradually increases up to farther areas like POV where the 80% of the contribution to $PM_{2.5}$ at Duomo is related to $NO_3^-$. In particular, cars and heavy duty vehicles that circulate in LOM area (0.5 $\mu g/m^3$) are more impacting than those circulate in Milan municipality (0.08 $\mu g/m^3$) and the nearer Metropolitan area (0.18 $\mu g/m^3$). Similar effects could be observed for concentrations associated to cars and heavy duty vehicles in POV area (0.4 $\mu g/m^3$). In first hypothesis, this aspect could be explained by a larger number of units of vehicles in LOM rather than in MIL but the correct answer relies on the origin of emission. The presence of ammonia, one of the gaseous precursors, combined with the large amount of NOx emissions generate the particulate nitrate that affects receptor points located farther away from emissive regions after transportation. As illustrated in the Figure 24 the other two emission categories (residential heating and other anthropogenic sources) detect the same behavior for the secondary component, higher in POV and LOM regions and lower or zero in AUS and MIL regions. Conversely, the pollution emitted directly in the atmosphere (elemental carbon) affects principally the contribution of sources located near the receptor point. Regarding road transport, almost 50% of road transport contribution of MIL area is due to EC as well as for AUS area. Either for residential and commercial heating, EC contribution shows an important role in MIL and AUS areas (20%). Regardless the total contribution related to each region, the “all emission categories” graph shown in figure below presents the general distribution of primary and secondary components over a wide area. Including the long range transport, EC growth is evident approaching regions near Duomo receptor point, while nitrate distribution is opposite. Farther regions present an important contribution of particulate nitrate rather than elemental carbon.

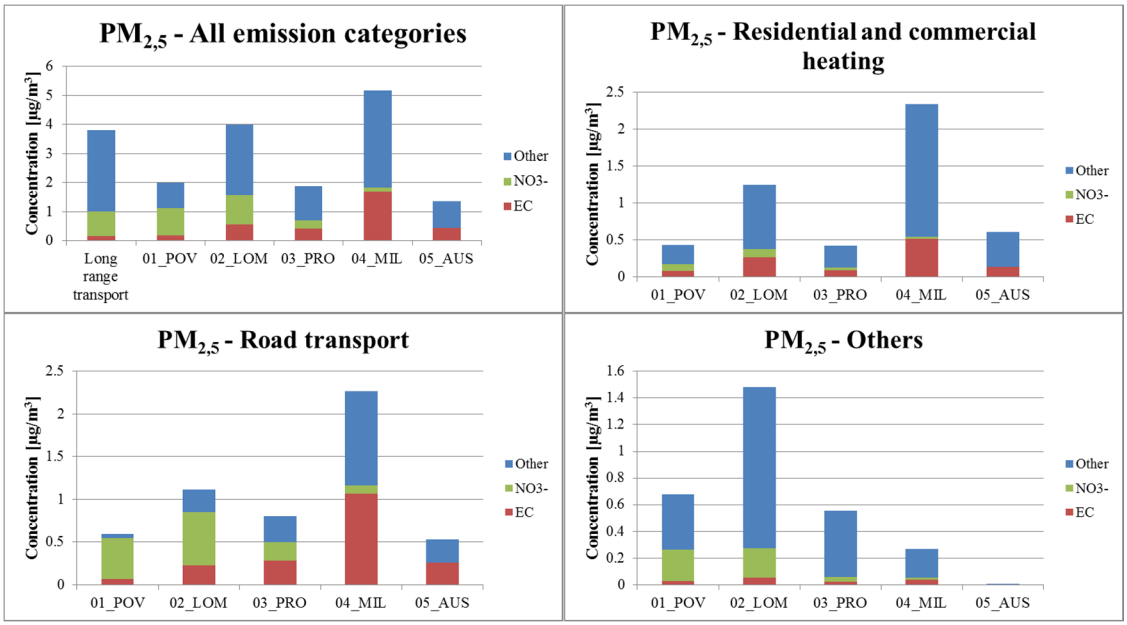


**Figure 44. $PM_{2.5}$ chemical profile of each emissive region contributions for specific source categories as residential heating (top-right), road transport (bottom-left), others (bottom-right) and all emission sources (top-left). The chemical species considered are elemental carbon (EC), particulate nitrate ($NO_3^-$) and all others compounds.**

## 3.2.3. Nitrogen dioxide ($NO_2$)

Nitrogen dioxide is one of the gaseous precursors of nitrate particulate. At the Duomo receptor, the $NO_2$ yearly mean concentration estimated by CAMx for 2010 is 21 ppb. As discussed in the first part of this work, one of the RMs weaknesses is the difficulty to apportionment analysis either to gaseous pollutant like $NO_2$. Conversely this issue can be addressed by CAMx.

The panels of Figure 25 show the relative contributions of regions, source categories, and geographically apportioned sources.

Overall, the urban background sources are responsible for about 70% of $NO_2$ concentration and considerably prevail over the regional background sources (20%) and over the very local sources in proximity of the receptor point (10%). The urban background contribution is principally given by the emissions from the MIL region (51.8%), with only 18.1% from the metropolitan area of Milan (PRO). The regional background contribution is mainly determined by the LOM region (15.2%), with only minor contributions from POV region (3.2%) and long range transport (1.3%). The AUS region provides a rather small contribution. However, considering the limited number of sources in this area with respect to the surrounding emission regions, the estimated 10%

contribution states that the local sources actually play a relevant role on $NO_2$ concentration at the receptor point and in urban areas in general.

Focusing on source categories, road transport, residential and commercial combustion, and the other anthropogenic sources determine 98% of $NO_2$ concentration, whilst natural sources, EMEP sources and long range transport are practically negligible. The most impacting source is, by far, the road transport with a 72% share: 60% of $NO_2$ concentration comes from heavy duty (31%) and cars (29%) emissions (largely composed by diesel cars), 11% from light duty vehicles reach only the 11%, about 1% from mopeds and motorcycles. The incomplete combustion of diesel or gasoline produces a large amount of NO that reacts immediately with the atmospheric oxidants like $O_3$, generating $NO_2$. Residential and commercial combustion, yields an overall contribution of 17%, but almost totally due to fossil fuels (16%). The other anthropogenic sources category, namely industrial sources, give a 9% contribution.

Figure 25c clearly shows that vehicular traffic in the municipality of Milan is the main source of $NO_2$ at Duomo receptor point. Actually, road transport from the MIL region is responsible for 8 ppb, that is almost 40% of total $NO_2$ concentration. In details, cars and heavy duty vehicles contribute at the same extent for 15%, that roughly corresponds 3 ppb. The impact of transport emissions from the surrounding regions is also significant, as traffic emissions from PRO and LOM regions provide the second and third most relevant contributions, the former with a 13% share (2.8 ppb), the latter with a 10% (2.1 ppb).

The wide spatial distribution of source yielding a relevant contribution to $NO_2$ concentration at Duomo receptor, particularly for road transport, points out that coordination of local and regional policy is desirable in order to see visible reduction of $NO_2$ concentration levels.

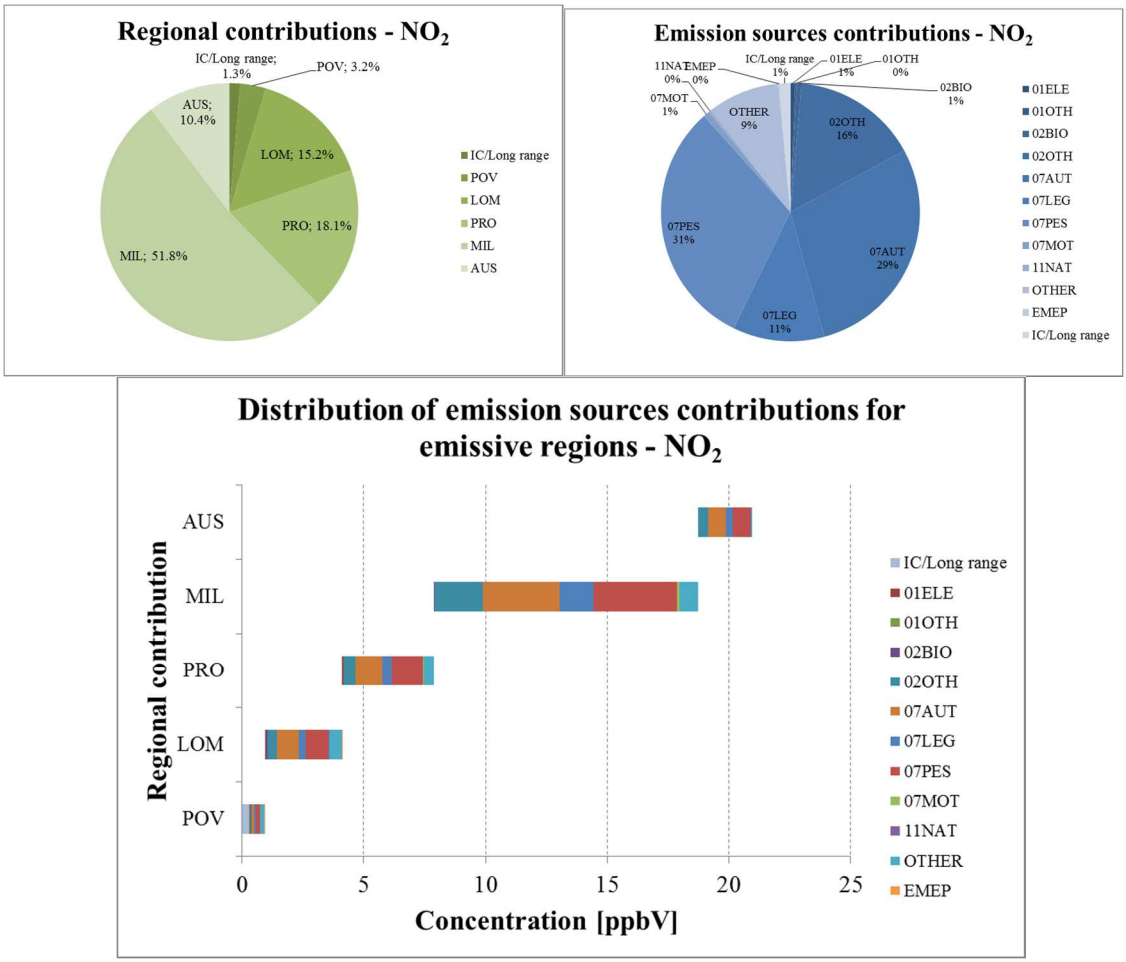


**Figure 45. $NO_2$ percentage distribution of emissive regions (7a, top-left) and emission sources categories (7b, top-right) contributions. (7c, bottom) is the regional absolute concentration distribution of each source activity contribution defined within CAMx/PSAT approach for $NO_2$.**

# 4. Discussion

CAMx results for $PM_{2.5}$ chemical speciation and CAMx/PSAT results for $PM_{2.5}$ source apportionment are discussed in comparison with experimental data and Positive matrix factoriziation (PMF) source apportionment from AIRUSE+ project (Amato et al, 2016). $PM_{2.5}$ data for 2013 from a one-year measurement campaign at Milano-Torre Sarca, an urban background site near Milan city centre (about 5 km as crow fly distance from Duomo receptor) have been used for comparison purpose. Notwithstanding AIRUSE+ data and CAMx simulation output do not refer to the same period and receptor, the following analysis can be regarded as a validation of CAMx/PSAT results, at least qualitatively.

Reported $PM_{2.5}$ yearly mean concentration from gravimetric measurements at Milano-Torre Sarca (29.9 $\mu g/m^3$) is in agreement with automatic monitoring network data for another urban background site in Milan (30.7 $\mu g/m^3$). Table 9 summarizes yearly mean concentrations of speciated $PM_{2.5}$ for AIRUSE+ and for CAMx simulation in this work. Other than the reference year and site, the two datasets also differ for the chemical species considered for mass closure. Actually, in AIRUSE+ data mass closure was not complete, with 4.8 $\mu g/m^3$ not determined, likely due to water molecules of residual moisture, crystallization and formation water, and metal oxides. These latter, conversely are considered in CAMx speciation as the primary elements generated by anthropogenic sources, labeled "other fine particles".

Table 9 highlights the strong difference in $PM_{2.5}$ concentration (29.9 $\mu g/m^3$ vs. 18.7 $\mu g/m^3$) that also holds in a dry-basis comparison (25.1 $\mu g/m^3$ vs. 18.7 $\mu g/m^3$), CAMx estimated concentration 6.4 $\mu g/m^3$ lower than measured one. Although the reference years and the sites are different, such missed concentration of 6.4 $\mu g/m^3$ can not be justified by a different yearly emission regime or meteorological conditions, thus confirming that CAMx tendentially underestimates the $PM_{2.5}$ mass.

According to AIRUSE+ data, organic matter (OM = POA + SOA) is the main component of $PM_{2.5}$, followed by secondary inorganic aerosol (SIA = nitrate + sulfate + ammonium), elemental carbon, soil fine dust and sea salt. Comparison with CAMx data points out relevant discrepancies for OM and EC, as well as a reasonably good agreement for SIA. OM is strongly underestimated by CAMx (5.1 $\mu g/m^3$ vs. 12 $\mu g/m^3$) due to an incorrect reconstruction of secondary organic aerosol (SOA), almost totally missed by the model (0.5 $\mu g/m^3$ vs. 8 $\mu g/m^3$). Troubles in properly estimating SOA through the SOA formation algorithm implemented in CAMx version used in this work have been reported in literature (Pirovano et al., 2015; Meroni et al., 2017) Conversely, CAMx overestimates the primary fractions of $PM_{2.5}$: POA concentration is slightly overestimated (4.6 $\mu g/m^3$ vs. 4 $\mu g/m^3$) whereas EC at a larger extent, as CAMx result (3.4 $\mu g/m^3$) is almost twice as high as the measured concentration (1.6 $\mu g/m^3$). A better performance is observed for SIA, whose total concentrations are in good agreement, both in absolute (8.3 $\mu g/m^3$ vs. 9.5 $\mu g/m^3$) and relative terms (44% vs. 38% of $PM_{2.5}$ dry mass). More in details, ammonium is almost perfectly reproduced (2.0 $\mu g/m^3$ vs. 2.1 $\mu g/m^3$) whereas there are some discrepancies for sulfate and nitrate. Namely, CAMx overestimates sulfate (3.0 $\mu g/m^3$ vs. 1.8 $\mu g/m^3$), thus giving rise to a corresponding underestimation of nitrate (3.2

µg/m$^3$ vs. 5.7 µg/m$^3$). The minor components (sea salt and soil dust) do not reach remarkable concentration values in both datasets; however CAMx to predict lower value for sea salt (0.2 µg/m$^3$ vs. 0.6 µg/m$^3$) and especially for soil dust (0.1 µg/m$^3$ vs. 1.8 µg/m$^3$).

**Table 13. $PM_{2.5}$ chemical speciation by AIRUSE+ measurement campaign and CAMx/PSAT output.**

| Species | AIRUSE+ (2013) | | This work (2010) | |
|---|---|---|---|---|
| | Concentration [µg/m$^3$] | % | Concentration [µg/m$^3$] | % |
| **Primary organic aerosol (POA)** | 4.0 | 16 | 4.6 | 24 |
| **Secondary organic aerosol (SOA)** | 8.0 | 32 | 0.5 | 2 |
| **Elemental carbon (EC)** | 1.8 | 7 | 3.4 | 18 |
| **Sulfate** | 1.8 | 7 | 3.0 | 16 |
| **Nitrate** | 5.7 | 23 | 3.2 | 17 |
| **Ammonium** | 2.1 | 8 | 2.0 | 11 |
| **Sea salt** | 0.6 | 2 | 0.2 | 1 |
| **Soil dust** | 1.2 | 5 | 0.1 | 1 |
| **Other fine particles (CAMx only)** | - | | 1.7 | 9 |
| **Total** | 25.1 | 100 | 18.7 | 100 |
| **Undetermined mass** | 4.8 | | - | |
| **Total** | 29.9 | | | |

The comparison between source apportionment results is not as straightforward as for speciated $PM_{2.5}$ because of the different output of the two approaches. PMF finds a number of factors together with the related contribution and chemical profile. For AIRUSE+ dataset PMF found a 7-factor solution: based on their profiles, these factors have been identified as vehicle exhaust (VEX) and non-exhaust (NEX), biomass burning (BB), secondary nitrate (SNI), secondary sulfate and organics (SSO), marine aerosols (SEA), industrial emission (IND), and mineral emissions (MIN) with about 12% of the $PM_{2.5}$ mass still unapportioned.

Conversely, CAMx/PSAT output consists of concentration values for each species and each source category considered. Thus, overall source contributions have to be reconstructed by adding the single $PM_{2.5}$ components generated by the different sources. CAMx/PSAT traffic factor was computed taking into account the related estimated concentrations for EC, POA and "other fine particles" and compared with VEX+NEX source form PMF. Similarly, biomass burning factor was defined as the sum of EC, POA and "other fine particles" produced by residential heating through biomass combustion.

Sodium and chlorine concentrations estimated by CAMx/PSAT from the "Natural" emission category have been added in order to assess sea salt contribution, for comparison with SEA source from PMF. Because CAMx did not simulated soil dust emissions and industrial sources were not specifically tracked but simply included in the generic "other anthropogenic" source category, the comparison with the PMF factors MIN and IND was not possible.

For the secondary source the comparison is not straight because the profiles of the SNI and SSO sources (the former mainly identified by nitrate and ammonium, the latter by sulfate and ammonium) are also characterized by the presence of organic carbon. Thus, altogether these sources account for SIA but also for a relevant amount of SOA. Additionally, even though they account for the most part of SIA, small sources of SIA are also associated by PMF to the other sources., but both also containing organic matter; thus, the sum of these factors also account for a fraction of the SOA. In practice, these two factors are also responsible for almost all of the SOA.

In spite of the difference in the modeling approaches, of year and receptor, and of the processes missed by CAMx, the results of source apportionment comparison are quite encouraging, especially for the primary sources. The traffic source is responsible for about 4 $\mu g/m^3$ (PMF: 4.3 $\mu g/m^3$; CAMx/PSAT: 3.6 $\mu g/m^3$), accounting for about 20% of $PM_{2.5}$. A good agreement is also observed for the biomass burning source too, with a mean concentration of 4.6 $\mu g/m^3$ (PMF: 5.1 $\mu g/m^3$; CAMx/PSAT: 4.3 $\mu g/m^3$) and a 24% a contribution. The lower contributions estimated by CAMx/PSAT may derive from the inclusion of fractions of SIA and SOA in the VEX+NEX and BB profiles by PMF. However, part of such may also derive from the low bias of CAMx for the total $PM_{2.5}$ mass that could be ascribed to meteorology, namely to the reduced dispersion of pollutants under strong inversion conditions in winter time, not correctly detected by the meteorological model WRF. The mismatch on the contribution from secondary sources is essentially due to CAMx underestimation of SOA. However, if a SOA-free secondary source is computed out of PMF source profiles and contributions, the two values get much closer and confirm the substantial agreement for the secondary inorganic source.

Therefore, excluding missed processes, principally SOA formation, CAMx/PSAT model detects correctly the principal source contributions to $PM_{2.5}$. Nevertheless, this methodology needs further improvement in order to track SIA and SOA formation for their proper apportionment and to consider also the contribution of soil dust and

resuspension. On the other hand, the main asset of CAMx/PSAT methodology is the possibility to localize the origin of pollution, also for the secondary aerosols and for the gaseous pollutants, providing additional and complementary information to PMF results. Once the results of the two modeling approaches are better reconciliated, the combination of the piece of information coming from their concurrent implementation can improve the overall quality of source apportionment analysis. Local or regional air quality plans based on such improved source apportionment analysis could help to assess the real health impacts of biogenic and anthropogenic sources over the domain and properly prioritize intervention strategies for air quality.

**Table 14. Comparison of $PM_{2.5}$ Source apportionment analysis conducted by two approaches: PMF and CAMx/PSAT. Percentage distribution and absolute concentration values are expressed for each emission factor.**

| | AIRUSE+ (2013) | | This work (2010) | |
|---|---|---|---|---|
| | Concentration [µg/m$^3$] | % | Concentration [µg/m$^3$] | % |
| **Vehicle Exahust (VEX)** | 1.8 | 6 | 3.6 | 19 |
| **Vehicle non-exhaust (NEX)** | 2.5 | 8 | | |
| **Biomass burning (BB)** | 5.1 | 17 | 4.3 | 23 |
| **Salt (SEA)** | 0.4 | 1 | 0.2 | 1 |
| **Industrial (IND)** | 1.4 | 5 | not tracked | |
| **Mineral (MIN)** | 1.5 | 5 | not tracked | |
| **Secondary nitrate (SNI)** | 8.9 | 30 | 8.7 | 46 |
| **Secondary sulfate (SSO)** | 5.6 | 19 | | |
| **Not apportioned** | 2.6 | 9 | - | |
| **Total** | 29.8 | | 18.7 | |

# 5. Conclusions

The modeling chain based on the combination of the meteorological model (WRF) and the chemical and transport model (CAMx) was developed for source apportionment (SA) analysis of particulate matter and gaseous pollutants thanks to the PSAT source apportionment algorithm. The SA was defined by the European parliament in the last air quality directive, as one of the assessment instrument to define environmental policies. Currently, this analysis could be made by receptor models (RMs), an array of techniques which detects the contributions of specific source categories after particulate matter measurement campaign. The chemical characterization of emission profiles and PM collected are fundamental to apportion correctly total concentrations.

The WRF-CAMx combination was applied over 2 nested domain, the wider domain covering Northern Italy and the Po Valley (580x400 $km^2$ area, 5 km grid step) the inner domain covering the metropolitan area of Milan (85x85 $km^2$ area, 1.7 km grid step) The SA was evaluated at an urban receptor point located in Milan city centre near Duomo cathedral for primary and secondary pollutants: fine particle ($PM_{2.5}$), elemental carbon (EC), nitrate particulate ($NO_3^-$) and nitrogen dioxide ($NO_2$). CAMx v6.30, the new version of the chemical and transport model implemented within the modeling chain, is able to track the emission categories effects combined with the source regions contributions.

Source apportionment for $PM_{2.5}$ showed an unbalanced distribution of contribution between the areas. Regional background emissions contribute for more than half of total $PM_{2.5}$ level in Milan urban receptor (53%), while regional and local sources contribute for the other 47%. In particular, local sources (AUS region) generate the 8% of total estimated concentration. Focusing on emission categories, long range transport (3.8 $\mu g/m^3$ – 21%) prevails within regional emission sources while between urban background emission sources, the transports (3 $\mu g/m^3$ – 17%) was the most impacting. For local sources, biomass burning (2.5 $\mu g/m^3$ – 3%) and transports (2.5 $\mu g/m^3$ – 3%) were the most important emission categories. The primary and secondary behavior of fine particles explained by source apportionment analysis detected $PM_{2.5}$ urban pollution as a regional problem. Local actions could not reduce significantly the ambient level of $PM_{2.5}$.

Conversely, EC source apportionment analysis showed a pronounced primary behavior. 60% (2.1 $\mu g/m^3$) of total contribution was originated from regional background areas, while local sources produced a relevant contribution (0.4 $\mu g/m^3$) equal to 13% of total concentration level. Regional background emissions generated 0.9 $\mu g/m^3$ in Duomo receptor, corresponding to the 26% of total concentration. The highest contribution was represented by transport sector enclosed within urban background area, producing 1.3 $\mu g/m^3$ equal to the 40% of final concentration. At opposite of EC, $NO_3^-$ presented a regional distribution of effects, which accounted for 2.8 $\mu g/m^3$ (86%). Urban backgrounds sources generated only 0.44 $\mu g/m^3$, equal to the 14% of final concentrations, while local sources contributed for a negligible value (< 1 %). The large part of contribution derived from transports (1.4 $\mu g/m^3$ - 44%) with their emission of gaseous precursors, originated principally from regional background regions. As a consequence, local area did not affect the final nitrate level with remarkable contributions. In fact, all sources located within

local and urban background areas affected for just 0.45 µg/m$^3$ nitrate total level. The source apportionment analysis conducted for a gas ($NO_2$) produced remarkable results. Local and urban background sources affected total concentration for 16.8 ppb (80%), with a clear predominance of vehicular traffic sources (15.4 ppb - 74%). As well as for local and urban background areas, within regional area the traffic sources were predominant. More than half of total estimation of $NO_2$ derived from traffic sources located in the urban background region, generating 10 ppb over the total 21 ppb.

CAMx/PSAT outputs were compared with $PM_{2.5}$ chemical speciation data and source apportionement results from the AIRUSE+ project (Amato et al, 2016) at Milan urban background site. PSAT reconstruction provided good results. Notwithstanding a lack of secondary organic aerosols (SOA) processes within CAMx, other species fit quite well measures. Primary organic aerosols (POA) estimated by CAMx contributed for 4.6 µg/m$^3$ while the measure reached 4 µg/m$^3$; total secondary inorganic aerosols (SIA) contributed for a similar concentration, 9.6 µg/m$^3$ for AIRUSE+ and 8.2 µg/m$^3$ for PSAT. However, the clear underestimation of $PM_{2.5}$ annual mean concentration could be ascribed almost totally to SOA concentrations, which are largely diffuse over Po valley region as confirmed by (Parfil 2008, Lonati 2008, Gilardoni 2011, Perrone 2012, Pietrogrande 2016), and partially to WRF underestimation of low dispersion conditions during the winter period which influenced performance of regional scale model. The final part of this work illustrated the second tier of validation of CAMx/PSAT methodology through comparison of source apportionment analysis developed by both approaches. In spite of the different approaches, CAMx/PSAT and PMF factors were in good agreement, both for absolute concentrations and percentage distributions. The positive results of the comparison between CAMx and PMF in AIRUSE states, first of all, that also CTMs can represent an affordable tool to estimate source contribution of the different emission categories to PM concentration at a specific receptor. A second important outcome is that CMTs can represent a powerful tool to provide additional information on source apportionment, particularly concerning the geographical origin of source contribution, the role of sources contributing to secondary PM, the contribution estimates for other pollutants, such as $NO_2$.

Notwithstanding, during this work CAMx/PSAT showed some limitations which concerned lack of SOA and other processes that reduced the feasibility of comparison with PMF results. In conclusion, improvements are needed in order to increase

performance of CAMx and future work will focus on optimization of secondary organic aerosols contribution, resuspension process characterization and further analysis of WRF underestimation of stagnation events during winter periods. Finally, further analysis are required in order to evaluate the reliability of CTM estimates with respect to the geographical origin of pollutants, secondary PM fraction and gaseous pollutants like $NO_2$.

# 6. Acknowledgements

This work has been financed by the Research Fund for the Italian Electrical System under the Contract Agreement between RSE S.p.A. and the Ministry of Economic Development - General Directorate for Nuclear Energy, Renewable Energy and Energy Efficiency in compliance with the Decree of March 8, 2006. The authors would like also to acknowledge ARPA Lombardia for air quality and meteorological observations data, necessary to evaluate HMS and the models which composed it. Authors wish also to thank JRC that through EBAS platform shares observed data collected at Ispra (Italy) EMEP site.

# 7. References

Amato F., Alastuey A., Karanasiou A., Lucarelli F., Nava S., Calzolai G., Severi M., Becagli S., Gianelle V., Colombi C., Alves C., Custodio D., Nunes T., Cerqueira M., Pio C., Eleftheriadis K., Diapouli E., Reche C., Minguillon M. C., Manousakas M., Maggos T., Vratolis S., Harrison R. M. Querol X., 2016. AIRUSE-LIFE+: a harmonized PM speciation and source apportionment in five southern European cities. Atmospheric Chemistry and Physics 16, 3289-3309.

Appel K.W., Pouliot G.A., Simon H., Sarwar G., Pye H.O.T., Napelenok S.L., Akhtar F., Roselle S.J., 2013. Evaluation of dust and trace metal estimates from the Community Multiscale Air Quality (CMAQ) model version 5.0. Geoscientific Model Development 6, 883-899.

Arvani B., Bradley Pierce R., Lyapustin A.I., Wang Y., Ghermandi G., Teggi S., 2016. Seasonal monitoring and estimation of regional aerosol distribution over Po Valley,

northern Italy, using a high-resolution MAIAC product. Atmospheric Environment 141, 106-121.

Bedogni, M., Pirovano, G., 2011. Source apportionment technique: inorganic aerosol 502 transformation processes in the Milan area. International Journal of Environment and 503 Pollution, 47, 167–183

Belis, C.A., Karagulian, F., Larsen, B.R., Hopke, P.K., Critical review and meta-analysis of ambient particulate matter source apportionment using receptor models in Europe, Atmospheric Environment, Volume 69, 2013, Pages 94-108, ISSN 1352-2310,

Belis, C.A., Larsen, B.R., Amato, F., El Haddad, I., Favez, O., Harrison, R.M., Hopke, P.K., Nava, S., Paatero, P., Prevot, A., Quass, U., Vecchi, R., Viana, M., 2014. European Guide on Air Pollution Source Apportionment with Receptor Models. JRC Reference Report EUR 26080. Luxemburg Publication Office of the European Union, ISBN 978-92-79-32514-4. http://dx.doi.org/10.2788/9332.

Buonocore J.J., Dong X., Spengler J.D., Fu J.S., Levy J.I., 2014. Using the Community Multiscale Air Quality (CMAQ) model to estimate public health impacts of $PM_{2.5}$ from individual power plants. Environmental International 68, 200-208.

Ciarelli G., Aksoyoglu S., El Haddad I., Bruns E.A., Crippa M., Poulain L., Äijäkä M., Carbone S., Freney E., O'Dowd C., Baltensperger U., Prévôt A.S.H., 2017. Modelling winter organic aerosol at the European scale with CAMx: evaluation and source apportionment with a VBS parameterization based on novel wood burning smog chamber exeperiments. Atmospheric Chemistry and Physics 17, 7653-7669. https://doi.org/10.5194/acp-17-7653-2017

Curier R.L., Kranenburg R., Sergers A.J.S., Timmermans R.M.A., Schaap M., 2014. Synergistic use of OMI $NO_2$ tropospheric columns and LOTOS-EUROS to evaluate the $NO_x$ emission trends across Europe. Remote Sensing of Environment 2014, 58-69.

ENVIRON, 2016. CAMx (Comprehensive Air Quality Model with extensions) User's Guide Version 6.3. ENVIRON International Corporation, Novato, CA.

European Commission, (2011). Laying down rules for Directives 2004/107/EC and 2008/50/EC of the European Parliament and of the Council as regards the reciprocal exchange of information and reporting on ambient air quality

Gilardoni S., Massoli P., Paglione M., Giulianelli L., Carbone C., Rinaldi M., Decesari S., Sandrini S., Costabile F., Gobbi G.P., Pietrogrande M.C., Visentin M., Scotto F., Fuzzi

S., Facchini M.C., 2016. Direct observation of aqueous secondary organic aerosol from biomass-burning emissions. PNAS, XXX

Hamm N.A.S., Finley A.O., Schaap M., Stein A., 2015. A spatially varying coefficient model for mapping $PM_{10}$ air quality at European scale. Atmospheric Environment 102, 393-405.

INEMAR, Inventario Emissioni in Atmosfera: emissioni in Regione Lombardia nell'anno 2012 - revisione pubblica. ARPA Lombardia Settore Monitoraggi Ambientali)

Karamchandani P., Long Y., Pirovano G., Balzarini A., Yarwood G., 2017. Source-sector contributions to European ozone and fine PM in 2010 using AQMEII modeling data. Atmospheric Chemistry and Physics 17, 5643-5664. doi:10.5194/acp-17-5643-2017

Lenschow P., Abraham H.-J., Kutzner K., Lutz M., Preuß J.-D., Reichenbächer W., 2001. Some ideas about the sources of $PM_{10}$. Atmospheric Environment 35, S23-S33

Meroni A., Pirovano G., Gilardoni S., Lonati G., Colombi C., Gianelle V., Paglione M., Poluzzi V., Riva G.M., Toppetti A., 2017. Investigating the role of the chemical and physical processes on organic aerosol modeling with CAMx in the Po Valley during a winter episode. Atmospheric Environment 171, 126-142.

Mues A., Kuenen J., Hendriks C., Manders A., Segers A., Scholz Y., Hueglin C., Builtjes P., Schaap M., 2014. Sensitivity of air pollution simulations with LOTOS-EUROS to the temporal distribution of anthropogenic emissions 14, 939-955.

Pepe N., Pirovano G., Lonati G., Balzarini A., Toppetti A., Riva G.M., Bedogni M., 2016. Development and application of a high resolution hybrid modelling system for the evaluation of urban air quality. Atmospheric Environment 141,297-311.

Pernigotti D., Thunis P., Cuvelier C., Georgieva E., Gsella A., De Meij A., Pirovano G., Balzarini A., Riva G.M., Carnevale C., Pisoni E., Volta M., Bessagnet B., Kerschbaumer A., Viaene P., De Ridder K., Nyiri A., Wind P., 2013. POMI: a model inter-comparison exercise over the Po Valley. Air Quality Atmosphere Health 6, 701-715.

Perrone M.G., Larsen B.R., Ferrero L., Sangiorgi G., De Gennaro G., Udisti R., Zangrando R., Gambaro A., Bolzacchini E., 2011. Sources of high $PM_{2.5}$ concentrations in Milan, Northern Italy: Molecular marker data and CMB modelling. Science of the Total Environment 414, 345-355.

Pietrogrande M.C., Bacco D., Ferrari S., Ricciardelli I., Scotto F., Trentini A., Visentin M., 2016. Characteristics and major sources of carbonaceous aerosols in $PM_{2.5}$ in Emilia

Romagna Region (Northern Italy) from four-year observations. Science of the Total Environment 553, 172-183.

Pirovano, G., Balzarini, A., Bessagnet, B., Emery, C., Kallos, G., Meleux, F., Mitsakou, C., Nopmongcol, U., Riva, G.M., Yarwood, G., 2012. Investigating impacts of chemistry and transport model formulation on model performance at European scale. Atmospheric Environment, Volume 53, 2012, Pages 93-109, ISSN 1352-2310, https://doi.org/10.1016/j.atmosenv.2011.12.052.

Pirovano, G., Colombi, C., Balzarini, A., Riva, G.M., Gianelle, V., Lonati, G., 2015. $PM_{2.5}$ source apportionment in Lombardy (Italy): Comparison of receptor and chemistry-transport modelling results. Atmospheric Environment, Volume 106, 2015, Pages 56-70, ISSN 1352-2310, https://doi.org/10.1016/j.atmosenv.2015.01.073.

Sandrini S., Fuzzi S., Piazzalunga A., Prati P., Bonasoni P., Cavalli F., Bove M.C., Calvello M., Cappelletti D., Colombi C., Contini D., de Gennaro G., Di Gilio A., Fermo P., Ferrero L., Gianelle V., Giugliano M., Ielpo p., Lonati G., Marinoni A., Massabò D., Molteni U., Moroni B., Pavese G., Perrino C., Perrone M.G., Perrone M.R., Putuad J., Sargolini T., Vecchi R., Gilardoni S., 2014. Spatial and seasonal variability of carbonaceous aerosol across Italy. Atmospheric Environment 99, 587-298.

Skamarock, W.C., Klemp, J.B., Dudhia, J., Gill, D.O., Barker, D.M., Duda, M.G., Huang X.-Y., Wang, W., Powers, J.G., 2008. A Description of the Advanced Research WRF Version 3, NCAR Technical Note NCAR/TN-475+STR, Boulder, Colorado.

Squizzato S., Cazzaro M., Innocente E., Visin F., Hopke P., Rampazzo G., 2017. Urban air quality in a mid-size city – $PM_{2.5}$ composition, sources and identification of impact areas: From local to long range contributions. Atmospheric Research 186, 51-62.

UNC, 2013. SMOKE v3.5 User's manual. Available at: http://www.smoke-model.org/index.cfm

Wang Y, Bao S., Wang S., Hu Y., Shi X., Wang J., Zhao B., Jiang J., Zheng M., Wu M., Russell A.G., Wang Y., Hao J., 2017. Local and regional contributions to fine particulate matter in Beijing during heavy haze episodes. Science of the Total Environment 580, 283-296.

WHO, (2016). European Detailed Mortality Database, update July 2016, Copenhagen, WHO Regional Office for Europe (http://data.euro.who.int/dmdb/).

Yarwood, G., Morris, R.E., Wilson, G.M., 2004. Particulate matter source apportionment technology (PSAT) in the CAMx photochemical grid model. In: Proceedings of the 27th NATO/CCMS International Technical Meeting on Air Pollution Modeling and Application. Springer Verlag.

Zhang H., Chen G., Hu J., Chen S., Wiedinmyer C., Kleeman M., Ying Q., 2014. Evaluation of seven-year air quality simulation using the Weather Research and Forecasting (WRF)/Community Multiscale Air Quality (CMAQ) models in the eastern United States. Science of the Total Environment 473-474, 275-285.

# 8. Supplemental Material

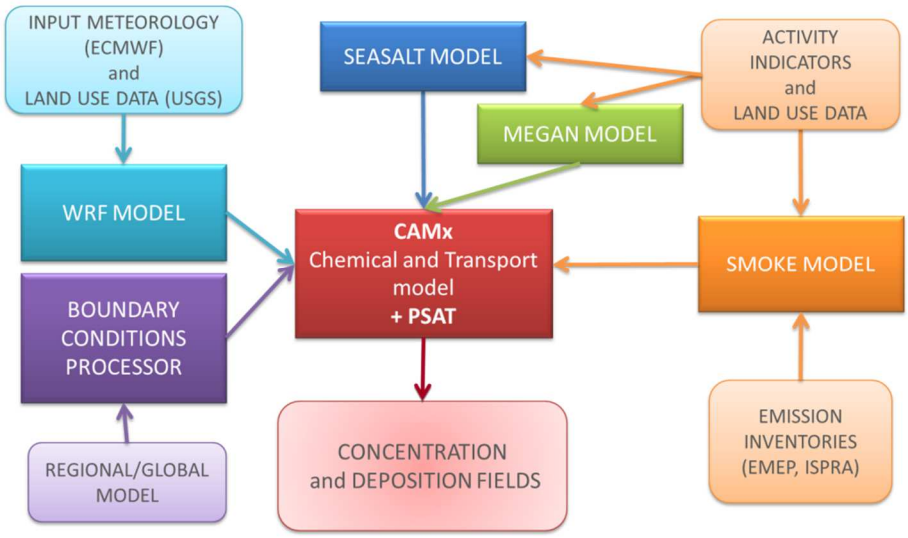


**Figure S 3. Modeling chain setup**

**Table S 2. Lambert Conformal coordinates for nested domains in WRF and CAMx model**

| | *WRF CAMx (Po Valley)* | | *WRF CAMx (Milan area)* | |
|---|---|---|---|---|
| SW X corner [km] | -439.5 | -429.5 | -249.7 | -246.2 |
| SW Y corner [km] | -108.5 | -98.5 | 66.8 | 69.8 |
| NE X corner [km] | 160.5 | 150.5 | -164.7 | -167.8 |
| NE Y corner [km] | 311.5 | 301.5 | 151.8 | 148.2 |
| DX-DY [km] | 5 | 5 | 1.7 | 1.7 |
| N cells X [n] | 120 | 116 | 51 | 47 |
| N cells Y [n] | 84 | 80 | 51 | 47 |

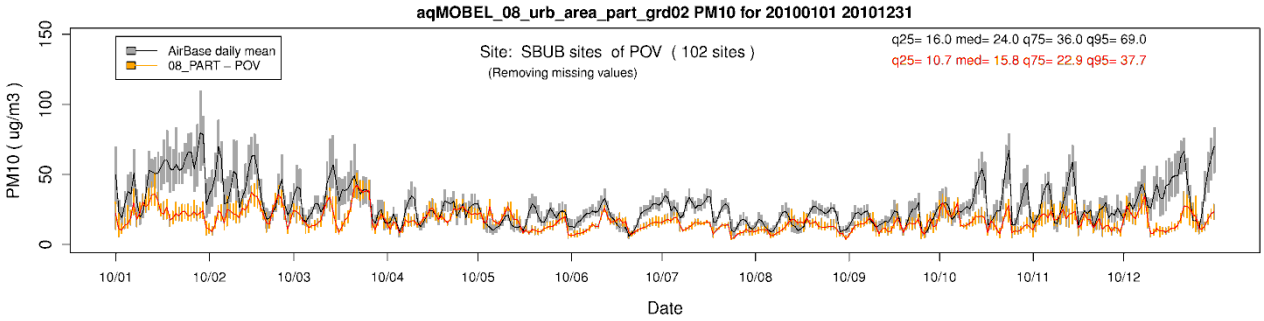


**Figure S 4. Time series of the box and whisker plots for the daily distribution of the observed (black/grey) and computed (red/orange) values of $PM_{10}$ concentrations at 102 ARPA sites, computed over the POV domain for 2010. Bars show the interquartile range (IR), lines the median values, dashed vertical bars (25th – 1.5 · IR) and the (75th + 1.5 · IR) value. Values for the 25th, 50th , 75th, and 95th quantiles of the whole yearly time series are reported too**

**Table S 3. Comparison of stand-alone CAMx model performance for $PM_{10}$ hourly concentrations computed for 2010 at Urban and Suburban AQ stations of Po Valley and Milan area domain**

| | *Po Valley* | | *Milan area* | |
|---|---|---|---|---|
| | Observations | Model | Observations | Model |
| Mean [µg/m$^3$] | 29.2 | 18.0 | 34.2 | 20.3 |
| Standard Deviation [µg/m$^3$] | 19.1 | 10.1 | 22.3 | 10.9 |
| Number Observations [-] | 34123 | | 6555 | |
| Correlation [-] | 0.44 | | 0.42 | |
| Mean Bias [µg/m$^3$] | -11.2 | | -13.9 | |
| Mean Error [µg/m$^3$] | 14.3 | | 17.2 | |
| Index_of_Agreement [-] | 0.56 | | 0.54 | |
| RMSE [µg/m$^3$] | 20.5 | | 24.6 | |

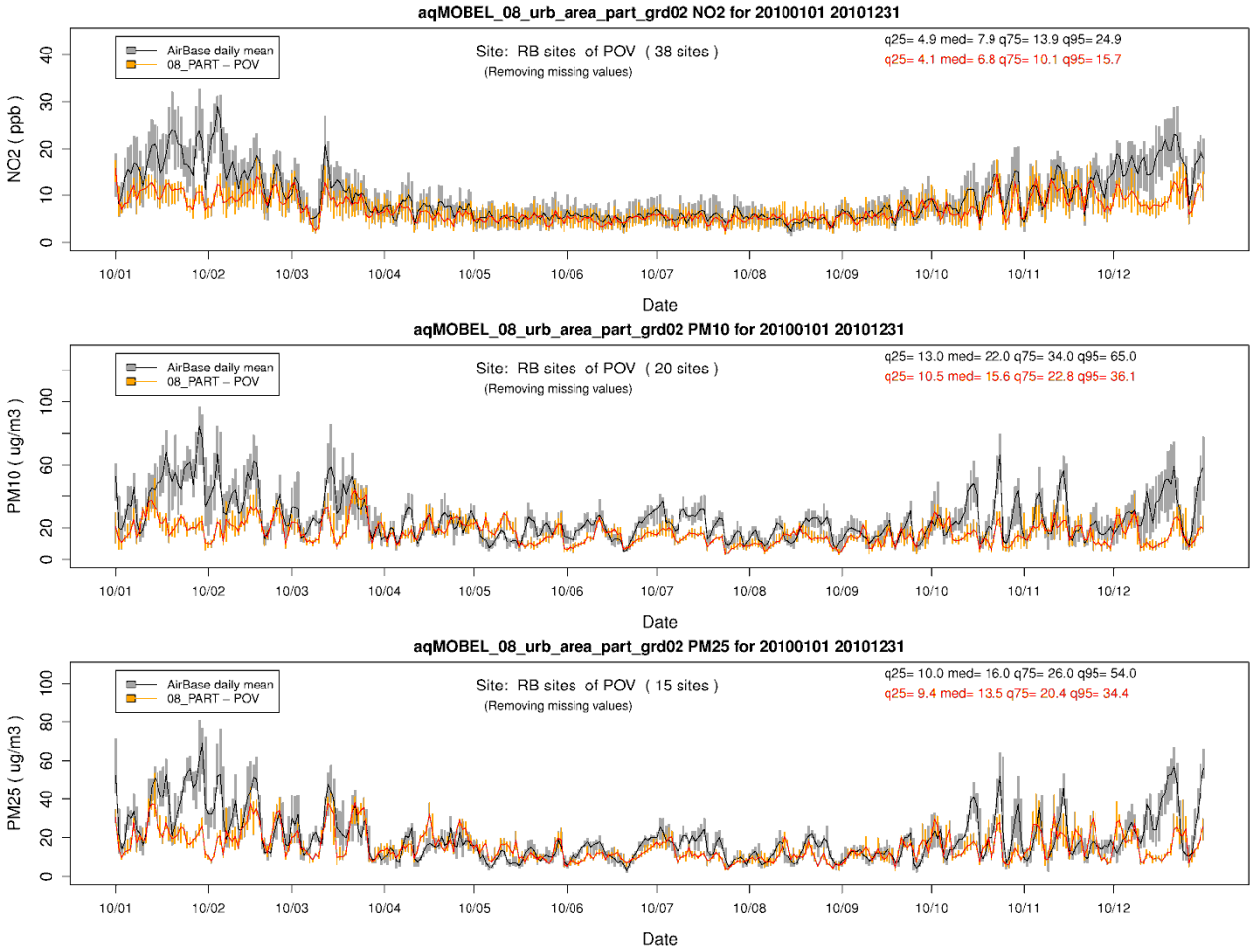


**Figure S 5. Time series of the box and whisker plots for the daily distribution of the observed (black/grey) and computed values of $NO_2$ (ppbV), $PM_{10}$ ($\mu g/m^3$) and $PM_{2.5}$ ($\mu g/m^3$) concentrations at Rural monitoring sites of the Po Valley domain for 2010. CAMx results at 5 km resolution are displayed in red/orange. Bars show the interquartile range, lines the median values. Values for the 25th, 50th, 75th, and 95th quantiles of the whole monthly time series are reported too.**

**Table S 4. Comparison of stand-alone CAMx model performance for $NO_2$ hourly concentrations computed for 2010 at rural AQ stations of Po Valley and Milan area domain**

| | *Po Valley* | | *Milan area* | |
|---|---|---|---|---|
| | Observations | Model | Observations | Model |
| Mean [ppbV] | 10.3 | 7.6 | 14.4 | 9.7 |
| Standard Deviation [ppbV] | 8.6 | 6.2 | 9.8 | 8.3 |
| Number Observations [-] | 304300 | | 32239 | |
| Correlation [-] | 0.42 | | 0.30 | |
| Mean Bias [ppbV] | -2.7 | | -4.7 | |
| Mean Error [ppbV] | 6.0 | | 8.6 | |
| Index_of_Agreement [-] | 0.62 | | 0.56 | |
| RMSE [ppbV] | 8.7 | | 11.7 | |

**Table S 5. Comparison of stand-alone CAMx model performance for $PM_{10}$ hourly concentrations computed for 2010 at rural AQ stations of Po Valley and Milan area domain**

| | *Po Valley* | | *Milan area* | |
|---|---|---|---|---|
| | Observations | Model | Observations | Model |
| Mean [µg/m$^3$] | 26.5 | 17.5 | 34.7 | 18.7 |
| Standard Deviation [µg/m$^3$] | 18.5 | 9.7 | 20.2 | 10.3 |
| Number Observations [-] | 6392 | | 1032 | |
| Correlation [-] | 0.4 | | 0.29 | |
| Mean Bias [µg/m$^3$] | -9 | | -16.1 | |
| Mean Error [µg/m$^3$] | 13.3 | | 18.9 | |
| Index_of_Agreement [-] | 0.55 | | 0.49 | |
| RMSE [µg/m$^3$] | 19.3 | | 25.5 | |

**Table S 6. Comparison of stand-alone CAMx model performance for $PM_{2.5}$ hourly concentrations computed for 2010 at rural AQ stations of Po Valley and Milan area domain**

| | *Po Valley* | | *Milan area* | |
|---|---|---|---|---|
| | Observations | Model | Observations | Model |
| Mean [µg/m$^3$] | 20.9 | 16 | 31.0 | 19.1 |
| Standard Deviation [µg/m$^3$] | 15.4 | 9.1 | 21.6 | 9.4 |
| Number Observations [-] | 5075 | | 346 | |
| Correlation [-] | 0.45 | | 0.42 | |
| Mean Bias [µg/m$^3$] | -4.9 | | -11.9 | |
| Mean Error [µg/m$^3$] | 9.8 | | 15.6 | |
| Index_of_Agreement [-] | 0.61 | | 0.53 | |
| RMSE [µg/m$^3$] | 14.7 | | 23.0 | |

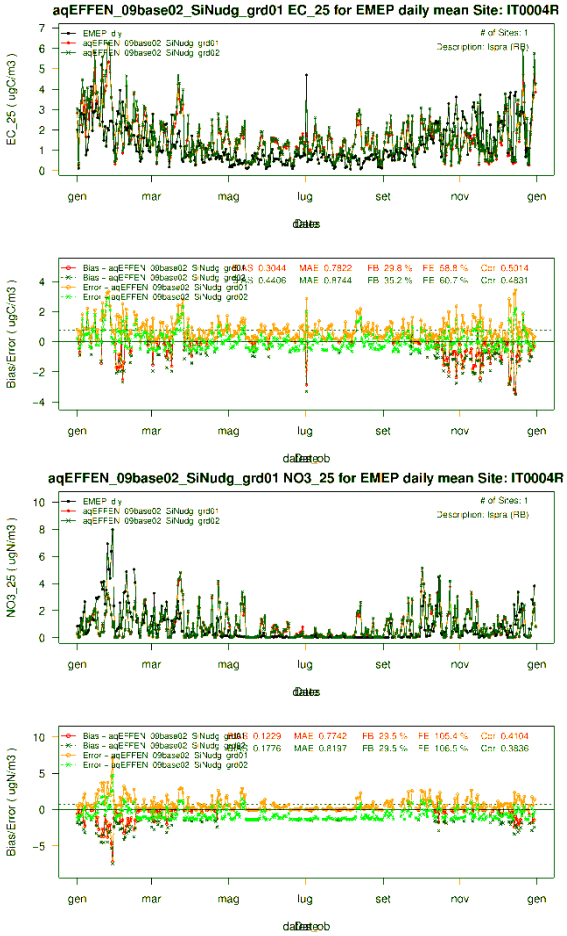


**Figure S 6. Time series of the mean of the observed (black line) and computed (green line) values of EC (top-left) and $NO_3^-$ (top-right) concentrations at ISPRA monitoring site for 2006. Bias and error time series for both pollutants are illustrated in the bottom graphs. Values of bias, Mean Absolute Error (MAE), Fractional bias (FB), Fractional Error (FE) and Correlation (Corr) are reported too.**

The simulation provided gridded concentration levels over the two domains (Po Valley and Milan domain). The pollutants considered by CAMx are both gaseous and particulate matter as well as primary and secondary PM. Furthermore, a particulate matter chemical speciation implemented within CAMx allows to evaluate the complex particles composition and their origin. The source apportionment simulation provided two types of results:

- Gridded output over the nested domains
- Time series at receptor points located everywhere over the nested domains

The gridded maps are available only for particulate matter species. In particular PSAT uses multiple tracer families to track the fate of primary and secondary PM:

- PS4 Particulate sulfate from primary emissions plus secondarily formed sulfate
- PN4 Particulate ammonium
- PN3 Particulate nitrate from primary emissions plus secondarily formed nitrate
- PEC Primary elemental carbon
- POA Primary organic aerosols
- PFN Other fine particulate
- PFC Fine crustal PM
- PCC Coarse crustal PM
- PCS Other coarse particulate

- PM2.5 = PS4 + PN4 + PN3 + PEC + POA + PFN + PFC
- PPM2.5 Primary PM2.5 = PEC + POA + PFN + PFC
  However, the time series evaluation is based on a larger number of pollutants if compared with the map analysis. Additionally to the previous case we have:
- SO2
- NIT Nitric oxide (NO) and nitrous acid (HONO)
- RGN Nitrogen dioxide (NO2), nitrate radical (NO3) and dinitrogen pentoxide (N2O5)
- TPN Peroxyl acetyl nitrate (PAN), analogues of PAN and peroxy nitric acid (PNA)
- NTR Organic nitrates (RNO3)
- HN3 Nitric acid (HNO3)
- NH3 ammonia
- P10 (total)
- P25 (total)
- SPM secondary particulate matter
  PPM2.5 is not included into the time series pollutants

# 6. Conclusions

The three years-thesis period was divided into 3 main parts: the first one that could be called “training”, was focused on studying the regional scale modeling chain adopted within RSE system research. The modeling chain was composed principally by the meteorological model WRF and the chemical and transport model CAMx. This modeling system was the first step for developing the new modeling chain able to reconstruct air quality concentration levels within urban context. AUSTAL2000 was the local scale model fixed for the development of the new hybrid modeling system (HMS). During the first period, AUSTAL2000 source code was studied and modified making it suitable for the the new system. The second period called “developing and testing”, was focused on the evaluation of the method linking regional and local scale model. The analysis of NOx levels over the high-resolution local domain within Milan city center was the first attempt. The third and last period of PhD, that could be appointed as “experimenting”, was characterized by two parallel main arguments: source apportionment analysis applications by CAMx model and HMS system and experimental activities about PM traffic resuspension. The main goal of the first activity was deepen knowledge about source apportionment analysis over Po Valley region through “standard” application of CAMx and its new tools (e.g. emissive regions definition, $NO_2$ source apportionment). Likewise, source apportionment analysis over the Milan local domain was performed by HMS and compared with standard approach performed by CAMx discovering pro and cons. Paralleling, two different PM traffic resuspension experimental campaigns were performed detecting road dust load recovery after rainy events and the influence of two vehicular traffic variables: speed and type of vehicles.

The development of the HMS and the application over the Milan local domain allowed to avoid emissions double counting, an error that occurred when dispersion models were coupled. However, HMS improved considerably the diffusion and the dispersion of pollutants within an urban context. With a 20m grid step size resolution, NOx concentation fields computed over the local domain were quite similar to reality. Hot spots were detected near congested cross-roads and the difference between main and secondary arches were emphasized. Notwithstanding absence of chemical reactions

treatment within local scale model, HMS application improved overall NOx performances over the urban domain. Comparison between air quality observations at Verziere and Senato stations and HMS modeling outcomes showed a good agreement considering all statistical values (e.g. bias, correlation, index of agreement). Similarly, comparison between CAMx stand-alone and HMS approaches evidenced higher performances for the new modeling system, able to capture NOx peaks during the day and to locate them properly. Finally, HMS application showed an interesting feature about urban air quality levels; urban and regional background NOx concentrations, namely concentrations generated by all sources located outside the urban local domain, prevaild largely respect to contribution generated by sources inside local domain (more than 70% of total estimated concentration at two monitoring stations was composed by background contribution).

Source apportionment analysis, included within European air quality Directive (2008/50/EC), represents a valid method in order to discover causes of excedancees or to assess sources contributions when air quality monitoring stations are absent. Despite a wide air quality station network, Po Valley region was investigarted. Source apportionment analysis performed by CAMx v6.30, and in particular PSAT algorithm, introduced two important features: this method was extended from particulate matter to gaseous pollutants and the emissive regions definition allowed to evaluate contributions not only relied on source categories but also on areas. Focusing on an urban receptor located near Duomo square, PM2.5, EC, NO3- and NO2 were evaluated considering 11 source emission categories (e.g. traffic, agriculture and residential heating) and 5 emissive regions (Po Valley, Lombardy region, Metropolitan area of Milan, Municipality of Milan and a small area covering the city center of Milan). Firstly, results showed properly the nature of each pollutant through their spatialization. Starting from EC, local and urban background sources prevailed strongly to the final concentration. Almost 70% of EC level was generated by sources located within Metropolitan area of Milan boundaries, confirming its primary nature, and traffic sector represented the most impactful source. Conversely, urban nitrate levels were affected mainly by regional background sources located outside metropolitan area of Milan; more than 75% was produced far away from urban receptor point. The highest impact could be attributed to transports that generated almost 45% of total concentrantion. Since that source apportionment analysis was

perfomed for each primary and secondary component of particulate matter, PM2.5 results pointed both primary and secondary nature. In fact, areal contributions were distributed homogenously over the domain as well as source categories. Tracking the contribution of each category, residential heating, in particular biomass burning, and transports resulted the principal sources generating fine particles. Focusing on $NO_2$, source apportionment analysis showed that highest contributions derived from local and urban background sources and, as expected, transports sector was the main source. CAMx/PSAT application over an urban domain produced interesting results discovering principal sources and their spatial origin. Such methodology pointed out causes of pollutants supporting municipalities during air quality plans assessment. Despite modeling systems need further improvements and constant updates, these methodologies could help to understand the complexity of atmospheric processes diffusing the importance of cooperation between cities in order to improve human exposure to atmospheric pollution.

Once tested HMS over urban domain, the new modeling system was applied for source apportionment analysis, notwithstanding only CAMx estimated secondary pollution. The main purpose of our last application was a detailed description of causes of pollutions over the urban local domain, however considering all contributions generated within outer areas. As a matter of fact, HMS application increased the concentrations variability over the local domain given the local scale model intergration within the modeling chain. As could be seen from results obtained at three different urban receptors (park, residential area and traffic site) for PM2.5 and EC, the differences of air quality levels were ascribed essentially to local sources contributions. While park and residential site showed similarities for both total concentration level and sources contributions, traffic site presented higher concentration values and distribution of sources contributions quite different from the others during winter and summer. As expected during March, results showed a strong influence of transport at traffic site, with a marginal role of residential heating. However, this ratio changed at park and residential receptors where sources produced similar contributions. During summer, the contribution of residential heating decreased largely and traffic was the most impactful source everywhere over the local domain. HMS application detected a fundamental aspect over urban areas, namely that the human exposition to pollution is largely different, considering both regional and local

scale effects, and could be estimate in order to assess locally the environmental impact of one of the emission categories.

Parallely to modeling applications, experimental campaigns discovering PM traffic resuspension were conducted thanks to collaboration of IDAEA Barcelona institute, in particular Fulvio Amato, one of the best researchers about road dust. Given that PM underprediction over Po Valley represents an important issue, in particular during winter months and at urban and suburban air quality stations, the traffic resuspension was identified as one the missed process. Lacking information about this phenomenon over city of Milan, its characterization resulted an important step. The first campaign's goal was the recovery rate estimation of dust load after rainy events for a correct time modulation of the relative emission. Following studies over other European cities, in particular Utrecht and Barcelona, our preliminaries results confirmed the exponential law detected by Amato and fixed the equilibrium point after almost 1 day. This value relied on climatological conditions and site-dependent features as type of asphalt (material, porosity, wear). Unfortunately, problems occurred during campaign did not allow to repeat four times the experiment, as expected. Second campaign focused on the link between the vertical profile of PM resuspended mass and two traffic-related variables (speed and vehicular fleet composition) in order to estimate a specific emission factor. The experimental campaign relied on passive sampler installation near 3 different roads within Milan for an exposition period of two weeks, before and after speed cameras mounting. Even though this activity was carried out during the last period of PhD, first results showed a reduction of PM mass resuspended at lower layer due to overall reduction of speed, while at higher part of vertical profile no changes were observed. Unfortunately, link between resuspended mass and types of vehicles and estimation of final emission factor were not possible for lacking of time, but will be addressed as soon as possible after the end of PhD period.

Modeling applications by CAMx stand-alone or HMS approach and experimental activities were exclusively designed in order to improve the knowledge of connection between atmospheric pollution and human actions. The proper assessment of environmental scenarios that plan a reduction of air pollution and, consequently, impact on human health is actually a big issue and these instruments are necessary to tackle it.

However, both models and experimental techniques, need constantly further improvements for implementing solutions closer to the reality that answer to updating environmental regulations.

# 7. Presentations in scientific meetings

Hybrid Modeling System methodology as well as results were presented in some national and international conferences in form of oral and poster presentations.

Pepe N., Pirovano G., Balzarini A., Riva G.M., Toppetti A., Lonati G., Bedogni M.. '*A high resolution hybrid modelling system for the evaluation of urban concentrations*' EAC2015 -European Aerosol Conference, 2015, Milan – Italy, 6-11 September. Oral presentation

Pirovano G., N. Pepe, A. Balzarini, A. Toppetti, M. Riva, G. Lonati, M. Bedogni. '*Stima dei livelli urbani di NOx e PM10 con un sistema modellistico ibrido*', PM2016 – VII convegno nazionale sul particolato atmosferico, 2016, Rome – Italy, 17-20 May. Oral presentation.

Pepe N., Pirovano G., Balzarini A., Riva G.M., Toppetti A., Lonati G., Bedogni M. '*A hybrid modeling system for the evaluation of urban concentrations: case study for Milan area*' AQ2016 – 10$^{th}$ International conference on air quality – science and application, 2016, Milan – Italy, 14-18 March. Poster presentation

Pepe N., G. Lonati, G. Pirovano, M. Bedogni. '*PMx traffic resuspension traffic estimation over a Milan area domain*', TAP2016 – International transport and air pollution conference, Lyon - France, 24-26 May. Poster presentation

# 8. Other publications

**Amicarelli A., G. Leuzzi, P. Monti, N. Pepe, G. Pirovano. '*Lagrangian micromixing modelling of reactive scalar statistics: surface pollutant sources in decaying grid turbulence*'. International Journal of Environment and Pollution. Accepted 9th December 201**

# 9. Bibliography

Amato F., Alastuey A., Karanasiou A., Lucarelli F., Nava S., Calzolai G., Severi M., Becagli S., Gianelle V., Colombi C., Alves C., Custodio D., Nunes T., Cerqueira M., Pio C., Eleftheriadis K., Diapouli E., Reche C., Minguillon M. C., Manousakas M., Maggos T., Vratolis S., Harrison R. M. Querol X., 2016. AIRUSE-LIFE+: a harmonized PM speciation and source apportionment in five southern European cities. Atmospheric Chemistry and Physics 16, 3289-3309.

Amato F., Bedogni M., Padoan E., Querol X., Ealo M., Rivas I., 2017. Characterization of road dust emissions in Milan: impact of vehicle fleet speed. Aerosol and Air Quality Research, 17, 2438-2449.

Amato F., Karanasiou A., Moreno T., Alastuey A., Orza J.A.G., Lumbreras J., Borge R., Boldo E., Linares C., Querol X., 2012. Emission factors from road dust resuspension in a Mediterrean freeway. Atmospheric Environment, 61, 580-587.

Amato F., Pandolfi M., Viana M., Querol X., Alastuey A., Moreno T., 2009. Spatial and chemical patterns of PM10 in road dust deposited in urban environment. Atmospheric Environment, 43, 1650-1659.

Amato F., Schaap M., Denier van der Gon H.A.C., Pandolfi M., Alastuey A., Keuken M., Querol X., 2012. Amtospheric Environment, 62, 352-358

Appel K.W., Pouliot G.A., Simon H., Sarwar G., Pye H.O.T., Napelenok S.L., Akhtar F., Roselle S.J., 2013. Evaluation of dust and trace metal estimates from the Community Multiscale Air Quality (CMAQ) model version 5.0. Geoscientific Model Development 6, 883-899.

Arvani B., Bradley Pierce R., Lyapustin A.I., Wang Y., Ghermandi G., Teggi S., 2016. Seasonal monitoring and estimation of regional aerosol distribution over Po Valley, northern Italy, using a high-resolution MAIAC product. Atmospheric Environment 141, 106-121.

Batterman, S., Chambliss, S., Isakov, V., 2014. Spatial resolution requirements for traffic-related air pollutant exposure evaluations. Atmospheric Environment 94, 518-528.

Bedogni, M., Pirovano, G., 2011. Source apportionment technique: inorganic aerosol 502 transformation processes in the Milan area. International Journal of Environment and 503 Pollution, 47, 167–183

Beevers, S.D., Kitwiroon, N., Williams, M.L., Carslaw, D.C., 2012. One way coupling of CMAQ and a road source dispersion model for fine scale air pollution predictions. Atmospheric Environment 59, 47-58.

Belis, C.A., Karagulian, F., Larsen, B.R., Hopke, P.K., Critical review and meta-analysis of ambient particulate matter source apportionment using receptor models in Europe, Atmospheric Environment, Volume 69, 2013, Pages 94-108, ISSN 1352-2310,

Belis, C.A., Larsen, B.R., Amato, F., El Haddad, I., Favez, O., Harrison, R.M., Hopke, P.K., Nava, S., Paatero, P., Prevot, A., Quass, U., Vecchi, R., Viana, M., 2014. European Guide on Air Pollution Source Apportionment with Receptor Models. JRC Reference Report EUR 26080. Luxemburg Publication Office of the European Union, ISBN 978-92-79-32514-4. http://dx.doi.org/10.2788/9332.

Buonocore J.J., Dong X., Spengler J.D., Fu J.S., Levy J.I., 2014. Using the Community Multiscale Air Quality (CMAQ) model to estimate public health impacts of $PM_{2.5}$ from individual power plants. Environmental International 68, 200-208.

Chen, F., Dudhia, J., 2001. Coupling an advanced land-surface/hydrology model with the Penn State/NCAR MM5 modelling system. Part I: model description and implementation. Monthly Weather Review 129, 167-196.

Ciarelli G., Aksoyoglu S., El Haddad I., Bruns E.A., Crippa M., Poulain L., Äijäkä M., Carbone S., Freney E., O'Dowd C., Baltensperger U., Prévôt A.S.H., 2017. Modelling winter organic aerosol at the European scale with CAMx: evaluation and source apportionment with a VBS parameterization based on novel wood burning smog chamber exeperiments. Atmospheric Chemistry and Physics 17, 7653-7669. https://doi.org/10.5194/acp-17-7653-2017

Curier R.L., Kranenburg R., Sergers A.J.S., Timmermans R.M.A., Schaap M., 2014. Synergistic use of OMI $NO_2$ tropospheric columns and LOTOS-EUROS to evaluate the $NO_x$ emission trends across Europe. Remote Sensing of Environment 2014, 58-69.

Denby, B., Cassiani, M., de Smet, P., de Leeuw, F., Horálek, J., 2011. Sub-grid variability and its impact on European wide air quality exposure assessment. Atmospheric Environment 45, 4220-4229.

EEA, 2015. EEA technical report 1. No 1/2006. Air pollution at street level in European cities. Available at: http://www.eea.europa.eu/publications/technical_report_2006_1. (accessed 17.06.15).

ENVIRON, 2011. CAMx (Comprehensive Air Quality Model with extensions) User's Guide Version 5.4. ENVIRON International Corporation, Novato, CA.

ENVIRON, 2016. CAMx (Comprehensive Air Quality Model with extensions) User's Guide Version 6.3. ENVIRON International Corporation, Novato, CA.

Escrig A., Amato F., Pandolfi M., Monfort E., Querol X., Celades I., Sanfélix V., Orza J.A.G., 2011. Simple estimates of vehicle-induced resuspension rates. Journal of Environmental Management 92 (10), 2855-2859.

European Commission, 2011. Laying down rules for Directives 2004/107/EC and 2008/50/EC of the European Parliament and of the Council as regards the reciprocal exchange of information and reporting on ambient air quality

Federal Ministry of Environment, Nature Conservation and Nuclear Safety, 2002: Technical instructions on air quality control – TA Luft, Germany

Gilardoni S., Massoli P., Paglione M., Giulianelli L., Carbone C., Rinaldi M., Decesari S., Sandrini S., Costabile F., Gobbi G.P., Pietrogrande M.C., Visentin M., Scotto F., Fuzzi S., Facchini M.C., 2016. Direct observation of aqueous secondary organic aerosol from biomass-burning emissions. Proceedings of the National Academy of Sciences U.S.A. (PNAS).

Grell, G.A., Devenyi D., 2002: A generalized approach to parameterizing convection combining ensemble and data assimilation techniques. Geophys. Res. Lett., 29(14), Article 1693.

Hamm N.A.S., Finley A.O., Schaap M., Stein A., 2015. A spatially varying coefficient model for mapping $PM_{10}$ air quality at European scale. Atmospheric Environment 102, 393-405.

Hellison, R.B., Greaves, S. P., Hensher, D.A., 2013. Five years of London's low emission zone: Effects on vehicle fleet composition and air quality. Transportation Research Part D 23, 25-33.

Hong, S.-Y., Noh Y., Dudhia J., 2006: A new vertical diffusion package with an explicit treatment of entrainment processes. Mon. Wea. Rev., 134, 2318–2341.

Iacono, M.J., Delamere, J.S., Mlawer E.J., Shephard M.W., Clough S.A., Collins W.D., 2008: Radiative forcing by long-lived greenhouse gases: Calculations with the AER radiative transfer models, J. Geophys. Res., 113, D13103.

INEMAR - Arpa Lombardia (2015), INEMAR, Emission Inventory: 2012 emission in Region Lombardy - public review. ARPA Lombardia Settore Aria. Available at: http://www.inemar.eu/

INEMAR, Inventario Emissioni in Atmosfera: emissioni in Regione Lombardia nell'anno 2012 - revisione pubblica. ARPA Lombardia Settore Monitoraggi Ambientali)

INERIS, 2006. Documentation of the chemistry-transport model CHIMERE [version V200606A]. Available at: http://euler.lmd.polytechnique.fr/chimere/

Isakov, V., Arunachalam, S., Batterman, S., Bereznicki, S., Burke, J., Dionisio, K., Garcia, V., Heist, D., Perry, S., Snyder, M., Vette, A., 2014. Air quality modeling in support of the near-road exposures and effects of urban air pollutants study (NEXUS). International Journal of Environmental Research and Public Health 11, 8777-8793.

Isakov, V., Irwin J.S., Ching J., 2007. Using CMAQ for exposure modelling and characterizing the subgrid variability for exposure estimates. Journal of applied meteorology and climatology 46, 1354-1371.

Isakov, V., Lobdell, D.T., Palma, T., Rosenbaum, A., Özkaynak, H., 2009. Combining regional- and local-scale air quality models with exposure models for use in environmental health studies. Journal of the Air & Waste Management Association 59, 461-472.

Janicke Consulting, 2014. AUSTAL2000. Program description of Version 2.6, 2014-02-24. Technical report. Federal Environmetal Agency, Janicke Consuluting, Germany.

Karamchandani P., Long Y., Pirovano G., Balzarini A., Yarwood G., 2017. Source-sector contributions to European ozone and fine PM in 2010 using AQMEII modeling data. Atmospheric Chemistry and Physics 17, 5643-5664. doi:10.5194/acp-17-5643-2017

Kim Y., Sartelet K., Raut J.C., Chazette P., Influence of an urban canopy model and PBL schemes on vertical mixing for air quality modeling over Greater Paris, Atmospheric Environment, Volume 107, April 2015, Pages 289-306, ISSN 1352-2310, http://dx.doi.org/10.1016/j.atmosenv.2015.02.011.

Lefebvre, W., Van Poppel, M., Maiheu, B., Janssen, S., Dons, E., 2013. Evaluation of the RIO-IFDM-street canyon model chain. Atmospheric Environment 77, 325-337.

Lefebvre, W., Vercauteren, J., Schrooten, L., Janssen, S., Degraeuwe, B., Maenhaut, W., de Vlieger, I., Vankerkom, J., Cosemans, G., Mensink, C., Veldeman, N., Deutsch, F., Van Looy, S., Peelaerts W., Lefebre, F., 2011. Validation of the MIMOSA-AURORA-IFDM model chan for policy support: Modeling concentrations of elemental carbon in Flanders. Atmospheric Environment 45, 6705-6713.

Lenschow P., Abraham H.-J., Kutzner K., Lutz M., Preuß J.-D., Reichenbächer W., 2001. Some ideas about the sources of $PM_{10}$. Atmospheric Environment 35, S23-S33

Lonati, G., Pirovano, G., Sghirlanzoni, G.A., Zanoni, A., Speciated fine particulate matter in Northern Italy: A whole year chemical and transport modelling reconstruction, Atmospheric Research, Volume 95, Issue 4, March 2010, Pages 496-514.

Martins, H., 2012. Urban compaction or dispersion? An air quality modelling study. Atmospheric Environment 54, 60-72.

Meroni A., Pirovano G., Gilardoni S., Lonati G., Colombi C., Gianelle V., Paglione M., Poluzzi V., Riva G.M., Toppetti A., 2017. Investigating the role of the chemical and physical processes on organic aerosol modeling with CAMx in the Po Valley during a winter episode. Atmospheric Environment 171, 126-142.

Monin, A. S. and Obukhov, A. M..: 1954, 'Basic Laws of Turbulent Mixing in the Ground Layer of the Atmosphere', Trans. Geophys. Inst. Akad. Nauk. USSR 151, 163–187.

Morfeld, P., Groneberg, D.A., Spallek, M.F., 2014. Effectiveness of Low Emission Zones: large scale of changes in environmental NO2, NO and NOx concentrations in 17 German cities. Plos One 9,8.

Morrison, H., Thompson, G., Tatarskii, V., 2009: Impact of Cloud Microphysics on the Development of Trailing Stratiform Precipitation in a Simulated Squall Line: Comparison of One- and Two-Moment Schemes. American Meteorological Society, 137, 991- 1007.

Mues A., Kuenen J., Hendriks C., Manders A., Segers A., Scholz Y., Hueglin C., Builtjes P., Schaap M., 2014. Sensitivity of air pollution simulations with LOTOS-EUROS to the temporal distribution of anthropogenic emissions 14, 939-955.

Nenes, A, Pilinis, C., Pandis, S.N., 1998, ISORROPIA: A New Thermodynamic Model for Multiphase Multicomponent Inorganic Aerosols. Aquatic Geochemistry, 4, 123-152.

O'Brien, J.J., 1970. A note on the vertical structure of the eddy exchange coefficient in the planetary boundary layer. Journal of the atmospheric science 27, 1213-1215.

Orza J.A.G., Cabello M., Lidòn V., Martinez J., 2009. Simple passive methods for the assessment of the directional and vertical distributions of wind-blow particulates. In: Advances in Studies on Desertification, Int. Conf. of Desertification in Memory of Professor John B. Thornes, 16-18 September 2009, Murcia, Spain, 367-370.

Pasquill F., 1962. Atmospheric Diffusion. D. Van Nostrand, Princeton, NJ.

Pepe N., Pirovano G., Lonati G., Balzarini A., Toppetti A., Riva G.M., Bedogni M., 2016. Development and application of a high resolution hybrid modelling system for the evaluation of urban air quality. Amtospheric Environment, 141, 297-311.

Pernigotti D., Thunis P., Cuvelier C., Georgieva E., Gsella A., De Meij A., Pirovano G., Balzarini A., Riva G.M., Carnevale C., Pisoni E., Volta M., Bessagnet B., Kerschbaumer A., Viaene P., De Ridder K., Nyiri A., Wind P., 2013. POMI: a model inter-comparison exercise over the Po Valley. Air Quality, Atmopshere & Health, 6, 701-715.

Perrone M.G., Larsen B.R., Ferrero L., Sangiorgi G., De Gennaro G., Udisti R., Zangrando R., Gambaro A., Bolzacchini E., 2011. Sources of high $PM_{2.5}$ concentrations in Milan, Northern Italy: Molecular marker data and CMB modelling. Science of the Total Environment 414, 345-355.

Pietrogrande M.C., Bacco D., Ferrari S., Ricciardelli I., Scotto F., Trentini A., Visentin M., 2016. Characteristics and major sources of carbonaceous aerosols in $PM_{2.5}$ in Emilia Romagna Region (Northern Italy) from four-year observations. Science of the Total Environment 553, 172-183.

Pirovano, G., Balzarini, A., Bessagnet, B., Emery, C., Kallos, G., Meleux, F., Mitsakou, C., Nopmongcol, U., Riva, G.M., Yarwood, G., 2012. Investigating impacts of chemistry and transport model formulation on model performance at European scale. Atmospheric Environment, Volume 53, 2012, Pages 93-109, ISSN 1352-2310, https://doi.org/10.1016/j.atmosenv.2011.12.052.

Pirovano, G., Colombi, C., Balzarini, A., Riva, G.M., Gianelle, V., Lonati, G., 2015. $PM_{2.5}$ source apportionment in Lombardy (Italy): Comparison of receptor and chemistry-transport modelling results. Atmospheric Environment, Volume 106, 2015, Pages 56-70, ISSN 1352-2310, https://doi.org/10.1016/j.atmosenv.2015.01.073.

Sandrini S., Fuzzi S., Piazzalunga A., Prati P., Bonasoni P., Cavalli F., Bove M.C., Calvello M., Cappelletti D., Colombi C., Contini D., de Gennaro G., Di Gilio A., Fermo P., Ferrero L., Gianelle V., Giugliano M., Ielpo p., Lonati G., Marinoni A., Massabò D., Molteni U., Moroni B., Pavese G., Perrino C., Perrone M.G., Perrone M.R., Putuad J.,

Sargolini T., Vecchi R., Gilardoni S., 2014. Spatial and seasonal variability of carbonaceous aerosol across Italy. Atmospheric Environment 99, 587-298.

Skamarock, W.C., Klemp, J.B., Dudhia, J., Gill, D.O., Barker, D.M., Duda, M.G., Huang X.-Y., Wang, W., Powers, J.G., 2008. A Description of the Advanced Research WRF Version 3, NCAR Technical Note NCAR/TN-475+STR, Boulder, Colorado.

Squizzato S., Cazzaro M., Innocente E., Visin F., Hopke P., Rampazzo G., 2017. Urban air quality in a mid-size city – $PM_{2.5}$ composition, sources and identification of impact areas: From local to long range contributions. Atmospheric Research 186, 51-62.

Stein, A.F., Isakov, V., Godowitch, J., Draxler, R R., 2007. A hybrid modeling approach to resolve pollutant concentrations in an urban area. Atmospheric Environment 47, 9410-9426.

Stocker J., Hood C., Carruthers D., Seaton M., Johnson K., The development and evaluation of an automated system for nesting adms-urban in regional photochemical models. 13th Annual CMAS Conference, Chapel Hill, NC, October 27-29, 2014

Torras Ortiz, S., Friedrich, R., 2013. A modelling approach for estimating background pollutant concentrations in urban areas. Atmospheric Pollution Research 4, 147-156.

UNC, 2013. SMOKE v3.5 User's manual. Available at: http://www.smoke-model.org/index.cfm.

Wagner J., Leith D., 2000. Passive aerosol sampler. 1: Principle of operation. Aerosol Science and Technology, 34, 186-192.

Wang Y, Bao S., Wang S., Hu Y., Shi X., Wang J., Zhao B., Jiang J., Zheng M., Wu M., Russell A.G., Wang Y., Hao J., 2017. Local and regional contributions to fine particulate matter in Beijing during heavy haze episodes. Science of the Total Environment 580, 283-296.

Wawda Y., Harrison R.M., Nicholson K.W., Colbeck I., 1990. Use of surrogate surfaces for dry deposition measurements. Journal of Aerosol Science, 21, S201-S204.

WHO, (2016). European Detailed Mortality Database, update July 2016, Copenhagen, WHO Regional Office for Europe (http://data.euro.who.int/dmdb/).

Yarwood, G., Morris, R.E., Wilson, G.M., 2004. Particulate matter source apportionment technology (PSAT) in the CAMx photochemical grid model. In: Proceedings of the 27th NATO/CCMS International Technical Meeting on Air Pollution Modeling and Application. Springer Verlag.

Yarwood, G., Rao, S., Yocke, M., Whitten, G., 2005. Updates to the Carbon Bond Chemical mechanism: CB05, report, Rpt. RT-0400675, US EPA, Res. Tri. Park.

Zhang H., Chen G., Hu J., Chen S., Wiedinmyer C., Kleeman M., Ying Q., 2014. Evaluation of seven-year air quality simulation using the Weather Research and Forecasting (WRF)/Community Multiscale Air Quality (CMAQ) models in the eastern United States. Science of the Total Environment 473-474, 275-285.